THE UNIVERSITY
of EDINBURGH

This thesis has been submitted in fulfilment of the requirements for a postgraduate degree (e.g. PhD, MPhil, DClinPsychol) at the University of Edinburgh. Please note the following terms and conditions of use:

This work is protected by copyright and other intellectual property rights, which are retained by the thesis author, unless otherwise stated.
A copy can be downloaded for personal non-commercial research or study, without prior permission or charge.
This thesis cannot be reproduced or quoted extensively from without first obtaining permission in writing from the author.
The content must not be changed in any way or sold commercially in any format or medium without the formal permission of the author.
When referring to this work, full bibliographic details including the author, title, awarding institution and date of the thesis must be given.

Colloidal Dispersions in Active and Passive Liquid Crystalline Fluids: A Simulation Study

Giulia Foffano

A thesis submitted in fulfilment of the requirements
for the degree of Doctor of Philosophy
to the
University of Edinburgh
October 2013

Abstract

In this thesis we study the physics of colloidal dispersions in active and passive liquid crystals by computer simulations. Liquid crystals are materials that exhibit long-range orientational order, with characteristics intermediate between the ones of simple, isotropic fluids and the ones of crystalline solids. Active fluids are suspensions of particles that continuously stir their ambient fluid. Like liquid crystals, active fluids undergo phase transitions to orientationally ordered phases. The framework that we apply here to describe them extends hydrodynamic equations for liquid crystals to the active case, in which their constituent particles exert local stresses on the simple fluid in which they are embedded.

Studying systems of colloids embedded in these materials can be done with multiple aims. Here we use colloids as probe particles to investigate the rheological properties of active nematics. To do so we apply a constant force to a spherical particle embedded therein and define an effective viscosity, which we determine by measuring the velocity in steady state. We find an important dependence of the effective viscosity on the size of the particle, and a regime characterised by a steady state of negative drag.

We also consider collective properties for systems of many colloids and analyse how they are affected by activity. We find that spontaneous flow can either hinder or favour colloidal aggregation, depending mainly on whether a fixed orientation of the liquid crystal is imposed close to the colloidal surface. This remains true independently of the initial condition chosen for the liquid crystal, which only affects the transition to spontaneous flow.

Lay Summary

Suspensions of microorganisms such as bacteria and algae, and the cytoskeleton, which constitutes the external structure of cells, are all examples of active fluids. The particles they consist of are able to absorb energy from their surroundings and to use it in order to stir their ambient fluid. The study of their mechanical properties is crucial to our understanding of the physics of the cell and of systems of microorganisms.

Due to the elongated nature of their constituents (bacteria or cytoskeletal filaments like actin) these systems share several properties with passive liquid crystalline fluids, which form the basis of liquid crystal display (LCD) monitors. While we now understand quite well the physics of passive liquid crystals, active systems are still a widely unexplored territory, but their similarities are a starting point for the modelling and the understanding of active systems. Two important questions that physicists and scientists are trying to answer regarding active fluids are: "How does activity affect the mechanical properties of liquid crystals?", and "how can we exploit activity to synthesise new materials with desired properties?". Here we address both of these questions by studying the dynamics of colloidal particles within such fluids. Colloids here are spheres of micrometrical size. Such particles are easily available and modern techniques allow to manipulate them with ease. We performed simulations where a spherical particle is dragged through active and passive liquid crystals. This is what experimentalists currently do in order to probe complex fluids. Our results are not only counterintuitive, but also they would be forbidden by fundamental principles of physics in the case of passive systems. We then embedded several colloids in active and passive liquid crystals, and studied their collective properties. We found that activity can either contrast or favour their aggregation.

Declaration

Except where otherwise stated, the research undertaken in this thesis was the unaided work of the author. Where the work was done in collaboration with others, a significant contribution was made by the author.

G. Foffano
October 2013

Acknowledgements

I would like to thank all the people that helped me during this PhD, and with whom I spent these three years.

I thank my supervisors, Davide and Mike, for their guidance and supervision, and for having carefully read this thesis.
Davide, for his constant support, and for his helpful hints and continuous suggestions. During these three years his door was always open, to welcome any doubt or naïf question. His ideas and enthusiasm were a continuous source of motivation, and his approach to physics, as well as his encouraging attitude, contributed to making this an enriching experience, from the scientific and from the personal point of view. Thank you Davide, working with you was a great pleasure!
Mike, whose intuitions gave major contributions to the work presented in this thesis, and were of great help to drive my reasearch towards most interesting directions. It has been an honour for me to work with you, Mike. Thanks!

What is presented here would not have been possible without the work and the patient help of Juho, who showed me the 'tricks of the trade' and helped me whenever I had a problem. Him and Kevin implemented most of the features of lattice Boltzmann that I used for my simulations, thus taking the pain, and leaving me with all the fun of my research. Thank you both! I also thank Alexander Morozov for his contribution to Chapter 4, and Chantal Valeriani for her suggestions on Chapters 6 and 7.

I thank my office mates, for keeping me company every day for three years. Alys introduced me to celidhs and to the highlands; she thought me a lot about

British culture and was very patient with my poor English when I first arrived. She also tried to instill into me some passion for climbing, without success so far, but I enjoyed looking at her many pictures from adventurous weekends. Matt helped me to fight the Scottish winter melancholia with his surprise hugs, his fake Italian accent and his pictures of Eli. Fred and Steve beared my stubborn long days in the office. I will miss you all!

I had the priviledge to be part of the European network COMPLOIDS, which was a wonderful experience. I shared with the COMPLOIDS fellows some of the most beautiful moments of this PhD. Thank you all, COMPLOIDS people!
I thank COMPLOIDS (ITN-COMPLOIDS, FP7-234810) also for having funded my PhD and all the work that is presented in this thesis.

If I can now call Edinburgh my second home, it is also thanks to all my Italian friends in Edinburgh, both within and outside the Physics department: Dario, Chiara, Adriano, Alberto, Giovanni, Nadia, Viviana, and Francesca. Thanks!
Thank you also to all the people in corridor 15XX, and more in general to all the coffee drinkers that made it alive during the last two years, and to my many flatmates during these three years.

This is also probably the best occasion to thank Enzo, who showed me how Physics can be fun, and who introduced me to soft matter, a few years ago. I would not be here without his support.

Thanks to my friends from university, especially Chiara, Francesca, Guglielmo, Stefano and Filippo, who somehow shared this experience with me, from different corners of Europe; and to my very old friends who are always ready for a chat, no matter for how long we have been far, and how different our lives ended up to be: Helga, Selena, Isa, Francesca, Enrico and Marco, thank you!

Thanks to my family: my parents and my brother Gianluca, (but also all the cousins and aunts and uncles and grandparents) for their love and their continuous support.

Contents

Abstract i

Lay Summary ii

Declaration iii

Acknowledgements iv

Contents vi

List of figures viii

List of tables xxiii

1 Introduction 1
- 1.1 Aim and Scope of the Thesis . . . 1
- 1.2 Liquid Crystals . . . 3
  - 1.2.1 What Are Liquid Crystals? . . . 3
  - 1.2.2 Modelling Liquid Crystals: Order Parameters . . . 5
  - 1.2.3 Topological Defects . . . 7
  - 1.2.4 Topological Charge . . . 9
  - 1.2.5 Liquid Crystals as an Example of Complex Fluids . . . 10
- 1.3 Active Fluids . . . 12
  - 1.3.1 Characterisation of Active Systems . . . 12
  - 1.3.2 Giant Number Fluctuations . . . 13
  - 1.3.3 Long Range Orientational Order . . . 14
  - 1.3.4 Role of Hydrodynamic Interactions . . . 15
  - 1.3.5 Instabilities of Long Range Ordered Active Suspensions . . . 19
- 1.4 Colloids in Complex Fluids . . . 21
  - 1.4.1 What Are Colloidal Particles? . . . 22
  - 1.4.2 Uses of Colloids in Soft Matter . . . 23
  - 1.4.3 Colloids as Probes of Soft Matter . . . 23
  - 1.4.4 Colloids as Building Blocks for New Materials . . . 24

2 Model **26**
2.1 Modelling Liquid Crystals: The Free Energy 27
2.1.1 Elastic Free Energy 27
2.1.2 Bulk Free Energy Density and Isotropic-to-Nematic Phase Transition 28
2.1.3 Surface Free Energy 30
2.2 Modelling Liquid Crystals: Hydrodynamic Description 30
2.2.1 Beris-Edwards Equation for the Evolution of the Order Parameter 31
2.2.2 Navier-Stokes Equation 32
2.3 Modelling Active Fluids: Hydrodynamic Equations 32

3 Methods **36**
3.1 Lattice Boltzmann Method for Simple Fluids 36
3.1.1 Lattice Boltzmann Equation 37
3.1.2 The BGK Approximation 39
3.1.3 Equivalence between LB Equation and the Navier-Stokes . 39
3.1.4 Equilibrium Distribution Function 40
3.1.5 Body Force 42
3.1.6 Implementation of Lattice Boltzmann Method 43
3.1.7 Contact with a Fixed Solid Surface 44
3.1.8 Contact with a Moving Solid Surface 44
3.1.9 Simulating Colloids 45
3.2 Lattice Boltzmann Method for Liquid Crystals and Active Fluids 47
3.2.1 Colloids in Liquid Crystals: Implementing Anchoring Conditions 47
3.2.2 Spurious Velocities 48

4 Bulk and Micro-Rheology of Active Fluids **50**
4.1 Background and State of the Art 51
4.1.1 Rheology of Liquid Crystals 51
4.1.2 Rheology of Active Fluids 53
4.2 Methodology 56
4.2.1 Choice of Parameters and Mapping to Physical Systems . 59
4.3 Results 60
4.3.1 Microrheology in Passive Nematics 60
4.3.2 Macrorheology of Active Nematics 61
4.3.3 Microrheology of Active Nematics 65
4.4 Discussion and Conclusions 77

5 Negative drag **81**
5.1 Estimate for the Extra Active Force Term 82
5.2 Comparison with Numerical Data 84

5.3 The 'Negative Drag' State 85
5.4 Discussion and Conclusions 90

6 Collective Behaviour of Colloids in Active Fluids 93
6.0.1 Self-Assembly of Colloids in Liquid Crystals 95
6.1 Simulations Details and Limitations 98
6.2 Results 99
6.2.1 Spontaneous Flow in Quasi-2D Active Liquid Crystals . . 99
6.2.2 Colloids Affect the Transition to Spontaneous Flow 105
6.2.3 Spontaneous Flow Promotes Large Fluctuations in the Number of Colloids when $w = 0$ 121
6.2.4 Spontaneous Flow Hinders Colloidal Clustering when $w > 0$ 127
6.3 Discussion and Conclusions 139

7 Dependence on Initial Conditions: Performing a Quench 142
7.1 Stability and Characteristics of the Flow 142
7.2 Morphology of Spontaneous Flow 144
7.3 Aggregation Properties 155
7.4 Discussion and Conclusions 167

8 Discussion and Conclusions 170

A Hasimoto Corrections To The Effective Viscosity 175

B Macrorheology in Active Fluids: Analytical Predictions in One Dimension 176

C How Colloids Affect Spontaneous Flow: The Case of Planar Anchoring 178

Bibliography 182

Publications 187

List of Figures

1.1 Defect structure close to a colloidal particle embedded in a nematic liquid crystal: in the case of planar anchoring two boojums appear (a), while for normal anchoring we see the formation of a Saturn ring disclination (b). In both cases the bulk director orientation is horizontal. Adapted from [1] with permission. 8
1.2 Sketch of typical defects that can be found in liquid crystals and with half-integer charge. The defect on the left has charge $+1/2$, the charge of the one on the right is $-1/2$. Since these two defects have equal charges but with opposite sign, they can annihilate. . . 9
1.3 Diagram explaining the concepts of strain and of stress for a sheared material. A force F is applied parallel to the top surface, having area A. The shear stress in $\sigma = F/A$. This external force generates a strain $\gamma = \Delta x/L$, where Δx is the displacement along F. 10
1.4 Active particles can be modelled as force dipoles. Extensile particles exert forces that are directed outwards along their main axis (a), and important examples are bacteria such as *E.coli* (b). Contractile particles exert forces on their ambient fluid that are directed inwards along their main axis (c) and important examples are algae such as *Alga Chlamydomonas* (d). 18
1.5 Instabilities in extensile nematics arise due to deformations in the nematic pattern. The panel on the left shows the case of a splay deformation (the blue horizontal line specifies the director orientation in the bulk), which is responsible for a net force acting on the fluid directed according to the red arrow. This originates a flow that contrasts the deformation and tends to recover nematic order: extensile nematics are stable with respect to splay. The panel on the right illustrates the case of a bending deformation. In this case the net force exerted by active particles on the fluid (red arrow) generates a flow that enhances the deformation: extensile nematics are unstable with respect to splay. 20

2.1 Deformations that can be encountered in nematic liquid crystals: panel (a) shows a typical splay deformation, panel (b) refers to bending and (c) to twist. 27
2.2 Behaviour of $\mathcal{F}_{bulk}$ for some representative values of the temperature T: when $T > T^{**}$ $\mathcal{F}_{bulk}$ only has one minimum at $S = 0$, corresponding to the isotropic phase. Reducing the temperature results into the appearance of a secondary minimum at $S > 0$, which becomes equivalent to the one in $S = 0$ when the temperature T_{IN} is reached. For temperatures between T_{IN} and T^*, $S = 0$ is only a secondary minimum, while for $T \geq T^*$, there is only one minimum, at $S > 0$. 28
2.3 This figure explains the notation used in the derivation of the active stress. 33

4.1 Sketch of the system considered in [2] to measure the viscosity of nematic liquid crystals: an external magnetic field (here denoted as $\vec{B}$) is used in order to maintain a fixed orientation of the liquid crystal with respect to the direction of shear. 51
4.2 Effective shear viscosity in active nematics: due to the orientation of active nematogens with respect to the shear direction the effective viscosity of extensile nematics (left) is smaller with respect to the one of their passive counterpart, while the effective viscosity of contractile nematics (right) is larger with respect to the one of passive nematics for an infinite system. 54
4.3 Typical shear stress - strain rate curves for extensile (left, [3]) and contractile (right) nematics. 55
4.4 Cartoons of the setting used in simulations. The one on the left refers to macrorheology simulations and the one on the right to microrheology ones. 56
4.5 Dependence of the effective viscosity on the probe's radius R for passive nematic liquid crystals (double-logarithmic scale). Empty and solid symbols allow to distinguish between motion orthogonal and parallel to the far field respectively. Circles were chosen for the planar anchoring, squares for normal anchoring and triangles for the case of a uniform director field ($w = 0$). Here – and in what follows – η_{eff} is expressed in simulation units, that were clarified at the beginning of the chapter. 58

4.6 Dependence of η_{eff} on system size L in the case of contractile active nematics with planar (a) and normal (b) anchoring, and an extensile active fluid with planar (c) and normal (d) anchoring at the walls. Legend on the left refers to both graphs in the same line. The inset in (d) shows the behaviour for $\zeta = 0.0003$ more in detail. Points here refer to numerical results, while solid lines are theoretical predictions obtained through Eq. B.8. 63
4.7 Dependence of the particle velocity, measured in steady state, on the external force for a particle of fixed radius $R = 11.3$, and different ζ (see legend). (a) refers to a contractile and (b) to an extensile active gel. We used (periodic) cubic simulation box of volume $V = 128^3$. 65
4.8 Dependence of η_{eff} on R for a contractile (a) and for an extensile (b) active fluid. Different symbols refer to different values of ζ (see legend). Filled and open symbols correspond to pulling along and perpendicular to the far field director respectively and dashed lines are to guide the eye. We used (periodic) cubic simulation box of volume $V = 128^3$. 66
4.9 (a) Sketch of the director orientation close to the surface of a spherical particle in the case of planar anchoring. Deformations of the nematic profile are responsible for a net force exerted by active particles on their ambient fluid, whose direction depends on the contractile or extensile character of particles. Panel (b) shows the net force that a group of contractile splayed particles exerts on the ambient fluid, while panel (c) refers to extensile particles. In order to understand this each particle has to be thought of as a force dipole. A larger force density is associated to the internal part of the splay, where the particles are closer together, than in its external part, and this gives rise to a net force. 67
4.10 Planar anchoring generates a splay deformation close to the colloidal surface, along the average orientation of active particles in the bulk (horizontal in these figures). This is the type of deformation that plays a role when the colloid is dragged parallel to the director. These deformations are responsible for net forces exerted by active particles on the fluid and ultimately acting on the colloid, that are directed as in panel (a) for a contractile nematic liquid crystal and as in panel (b) for an extensile one. The direction of forces can be understood on the basis of panels (b) and (c) of Fig. 4.9. These sketches refer to the case of a colloid that is not moving, so that the deformations on both sides of the particle are the same and the forces that they generate do counterbalance. . . 68

4.11 Planar anchoring at the colloidal surface is responsible for a bending deformation close to the particle surface in the direction orthogonal to the director orientation in the bulk. Due to their dipolar character, bent groups of active particles exert forces that are directed towards the colloid in the contractile case (a), and outside in the case of extensile particles (b). 68
4.12 Sketch of the splay and bend deformation when the colloidal particle is dragged parallel to the far-field director orientation, for a contractile fluid (a) or orthogonally to it, for an extensile fluid (b). Blue arrows represent active forces, while the red one refers to the external force. The sketch is further discussed in the text. . 69
4.13 Sketch of the director field deformation for normal anchoring, and for a probe pulled along the far field director. As before, blue arrows refer to the active forces, while the red one represents the external force. 71
4.14 (a) Dependence of the measured effective viscosity on radius for normal anchoring of the director field on the colloidal probe surface, at various ζ (see legend). The dragging direction is orthogonally to the far field director. Other parameters are as in Fig. 4.8. (b) Velocity versus time for $F = 0.12$, $R = 9.3$ in the case of dragging along the far field director. The symbols are chosen according to the legend shown in (a). (c) shows the velocity of a particle of radius $R = 9.3$ pulled through an extensile gel ($\zeta = 0.0001$) as a function of time for three different values of the external force F, which are given in the legend. Note the presence of a non-zero 'yield force' further discussed in the text. As in the previous cases, we used (periodic) cubic simulation box of volume $V = 128^3$. 72
4.15 Flow field patterns close to a moving particle of radius $R = 11.3$ subject to a force $F = 0.12$, in a passive nematic liquid crystal (a,b), in a contractile active fluid (c,d), and in an extensile active fluid (e,f). In all cases there is normal anchoring of the director field at the particle surface. In (a,c,e) the pulling direction is perpendicular to the far field director, whereas in (b,d,f) the colloid is dragged paralled to the far field. 74
4.16 Dependence of the effective viscosity on particle size for no anchoring, and different ζ (see legend). (a) and (b) describe a contractile and extensile active fluid respectively. As previously, filled and open symbols correspond to pulling along and perpendicular to the far field director respectively and we used (periodic) cubic simulation box of volume $V = 128^3$. 75

4.17 Dependence of η_{eff} on R for (a) contractile and (b) extensile fluids, with particle anchoring as in Fig. 4.8, but with strong homogeneous anchoring of the director field at the wall of the container. The anchoring determines in this case the far field director profile. All parameters are as in Fig. 4.8, apart from the system size which is 64 along the direction orthogonal to the walls, and 128 in the other two directions. Empty and filled symbols refer to particles pulled orthogonally and parallel to the far-field director respectively. . . 76
4.18 Dependence of the effective viscosity on particle size with $\mathsf{Q} = 0$ on its surface, and different values of ζ (see legend). (a) and (b) refer to a contractile and extensile active fluid respectively. As previously, filled and open symbols correspond to pulling along and perpendicular to the far field director respectively and we used (periodic) cubic simulation box of volume $V = 128^3$. 77

5.1 Plot of $1/\eta_{\text{eff}}$ on R^2, for a contractile (left) and for an extensile (right) nematic, yielding an approximately linear dependence in agreement with Eq. 5.5. 84
5.2 Snapshots of a colloid having radius $R = 30$ embedded in a contractile nematic liquid crystal having $\zeta = -0.002$ and dragged by a constant force $F = 0.8$ oriented horizontally, along the director, towards the right. Colours in the background refer to the x component of the director, going from red ($\mathrm{n}_x = 1$) to blue ($\mathrm{n}_x = 0$). The frames are taken at times $t = 5000$, 40000, 90000, 175000, as indicated. A red dot is used as a reference point for the starting position of the colloid. Note that, already from the second snapshot, the asymmetry between the deformations at the front and at the back of the colloid is evident. 85
5.3 Dependence of the external force (step functions, axis on the right) and of the particle velocity (axis on the left) on time for two different 'experiments'. In both cases a force $F = 0.8$ is initially applied to the particle and turned off. Then a smaller force is applied along the direction of particle motion: the blue dotted line and the red dot-dashed one give the values of the external force in the two cases. The correspondent particle velocities are given by the black solid and green dashed lines respectively. The dynamics is discussed in the text. In the sketches arrows on the fluid refer to the active force direction, the arrow on the colloid represents the external force, while that above the particle shows the actual direction of motion. 87
5.4 Velocity fields for the case of a quiescent particle (left panel) and of a particle moving to the left (panel on the right), opposite to the applied force (red arrow). 88

5.5 $v(F)$ curve for a case with negative drag ($R = 30, \zeta = -0.002$). Black circles and red squares refer to simulations in which the force is applied to a quiescent and moving colloid respectively. 89

6.1 Stability curve for active nematics in a $128 \times 128 \times 16$ simulation box, in the absence of colloids; the inset shows a zoom-in in the region of small $|\zeta|$. The liquid crystal is initially in the nematic phase, with the director along the x-axis, and a tilt of about 10° is introduced along the xy-plane to trigger the instability. 100

6.2 Velocity and director profiles developing in extensile nematics in a regime of spontaneous flow, for ζ between 0.0002 and 0.0005 and in the absence of colloids. For the velocity profile we show only the xy plane and use colours to quantify the z component: the colour goes from red, denoting the largest positive component along the z axis, to blue, denoting the smallest negative z-component. For the director profile we show 2D maps for each of the components, where the colours go from blue (denoting that that component is equal to zero) to red (that component is equal to one). These snapshots refer to time $t = 160000$. 101

6.3 Velocity and director profiles developing in extensile nematics (without colloids) in a regime of spontaneous flow, for ζ between 0.001 and 0.01. The colour coding for both the velocity and the director is as in Fig. 6.2. These snapshots refer to time $t = 160000$. 102

6.4 Velocity and director profiles developing in contractile nematics in a regime of spontaneous flow, and without colloids, for ζ between -0.009 and -0.02. The colour coding for both the velocity and the director is as in Fig. 6.2. These snapshots refer to time $t = 160000$. 104

6.5 The average modulus of the fluid velocity is studied as a function of ζ for extensile ($\zeta > 0$) and contractile ($\zeta < 0$) active nematics, without colloids (right triangles) and in the case of a colloidal volume fraction (vf) of 15% (up triangles), when no anchoring condition is imposed at the colloidal surface. The inset shows a zoom-in on the data at small $|\zeta|$. These data were averaged over a range of times at steady state. 105

6.6 Velocity and director profiles developing in extensile nematics, with a 15% colloidal volume fraction, in a regime of spontaneous flow, for ζ between 0.0002 and 0.001. Here $w = 0$. The colour coding for both the velocity and the director is as in Fig. 6.2. These snapshots refer to time $t = 160000$. 107

6.7 Velocity and director profiles developing in extensile nematics, with a 15% colloidal volume fraction, for the case of $w = 0$, in a regime of spontaneous flow, for ζ between 0.002 and 0.005. The colour coding for both the velocity and the director is as in Fig. 6.2. These snapshots refer to time $t = 160000$. 108
6.8 Snapshots for the velocity profile of an extensile nematic at $\zeta = 0.0003$ without (left column) and with (right column) colloids. The colloidal volume fraction is 15% and the adimensional anchoring strength is $w = 0$. Cartesian axes here are directed as in Fig. 6.2. 110
6.9 Snapshots for the velocity profile of an extensile nematic at $\zeta = 0.003$ without (left column) and with (right column) colloids. The colloidal volume fraction is 15% and the adimensional anchoring strength is $w = 0$. Cartesian axes here are directed as in Fig. 6.2. 111
6.10 Velocity and director profiles developing in contractile nematics, with a 15% colloidal volume fraction, in a regime of spontaneous flow, for ζ between -0.007 and -0.009, and $w = 0$. The colour coding for both the velocity and the director is as in Fig. 6.2. These snapshots refer to time $t = 160000$. 112
6.11 Velocity and director profiles developing in contractile nematics, with a 15% colloidal volume fraction, in a regime of spontaneous flow, for ζ between -0.01 and -0.02, and $w = 0$. The colour coding for both the velocity and the director is as in Fig. 6.2. These snapshots refer to time $t = 160000$. 113
6.12 The average fluid velocity is studied as a function of ζ for extensile and contractile active nematics with 15% colloids volume fraction and different anchoring conditions: normal anchoring, when a Saturn ring disclination accompanies the colloid (left), and planar anchoring (right). 114
6.13 Snapshots referring to a system of 771 colloids in extensile (top) and contractile (bottom) nematics, with normal anchoring at time $t = 160000$ (same as in Fig. 6.22). We show some level surfaces corresponding to a range of fluid velocities for that system (different in the two cases). Different colours correspond to different values of the fluid velocity, going from red – denoting the highest of the values considered – to blue, chosen for the smallest value in our range. The topology is completely different at different $|\zeta|$: for $\zeta = 0.0001$ and $\zeta = -0.001$ (panels on the left), the level surfaces corresponding to highest velocitis are localised close to the colloids and are hidden by more extended curves corresponding to smaller velocities. At $\zeta = 0.01$ and $\zeta = -0.02$ (panels on the right) high fluid velocity is found also in those regions where the density of colloids is smaller and are not localised close to the colloidal surface. 115

6.14 Snapshots referring to a system of 771 colloids in extensile (top) and contractile (bottom) nematics, with planar anchoring at time $t = 160000$ (same as in Fig. 6.22). We show some level surfaces corresponding to the highest velocities for that system (different in the two cases). Different colours refer to different fluid velocities, going from red – denoting the highest of the values considered – to blue, chosen for the smallest value in our range. The left panels refer to the case of small activities (here $\zeta = 0.0001$ – top – and $\zeta = -0.001$ – bottom) these are localised near the colloids, while for higher $|\zeta|$ (shown in the right panels: $\zeta = 0.005$ – top – and $\zeta = -0.02$ – bottom) highest velocity level surfaces are found also in those regions where the density of colloids is smaller. 116

6.15 Velocity and director profiles developing in extensile nematics, with a 15% colloidal volume fraction, in a regime of spontaneous flow, for ζ between 0.001 and 0.005. The anchoring is normal. The colour coding for both the velocity and the director is as in Fig. 6.2. These snapshots refer to time $t = 160000$. 118

6.16 Velocity and director profiles developing in contractile nematics, with a 15% colloidal volume fraction, in a regime of spontaneous flow, for ζ between -0.0002 and -0.015. The anchoring is normal. The colour coding for both the velocity and the director is as in Fig. 6.2. These snapshots refer to time $t = 160000$. 119

6.17 Two snapshots referring to a system in steady state with 15% colloidal volume fraction, with $w = 0$ and in the case when the liquid crystal (active or passive) is initialised in the ordered nematic phase. On the left $\zeta = 0$, the particles are homogeneously distributed and there is no flow. The box on the bottom right shows a section of the director profile. The homogeneous red colour means that the x component of the director is uniformly equal to one, as for an ordered nematic. The figure on the right refers to $\zeta = 0.005$. The fluid is spontaneously flowing and doing so it disrupts the orientational order as shown in (d). There the colour-coding refers to the x component of the director, which can go from zero (blue) to one (red). We coloured in green the colloids that belong to the largest aggregate, where an aggregate is defined by choosing a fixed binding radius r_b slightly larger than the range of the repulsive potential. Panel (c) displays the corresponding pair correlation functions: the main effect of spontaneous flow is the one of shifting the position of the first peak towards smaller distances. 122

6.18 Pair distribution function for a system of colloids (15% volume fraction) embedded in a (contractile) nematic liquid crystal. The case of $\zeta = 0$ is compared to the one of $\zeta = -0.02$, where spontaneous flow is present. 123
6.19 Number fluctuations for a system of colloids embedded in extensile (left) and contractile (right) nematics in the case of $w = 0$. Note that in the contractile case all the curves corresponding to ζ between 0 and -0.006 are superposed due to the absence of flow that does not allow a reorganisation of the particles and the initial configuration was the same in all cases. 124
6.20 Inhomogeneities in the distribution of colloids can be described in terms of large number fluctuations (a). These correlate very well with the appearance of a macroscopic flow (b), but not with the defect density, studied as a function of ζ (c). This rules out the hypothesis that large number fluctuations are related to the tendency of colloids to gather in regions of large distortions, i.e. of high elastic energy. Instead, these graphs suggest that colloids are pushed together by the flow. 125
6.21 Mean squared displacement for a system of colloids embedded in extensile (left) and contractile (right) nematics in the case of $w = 0$.126
6.22 Two snapshots referring to a system with 15% colloidal volume fraction, with normal anchoring and in the case when the extensile active liquid crystal is initialised in the ordered nematic phase. In panel (a) $\zeta = 0$, the particles are homogeneously distributed, and there is no flow. Figure (c) refers to $\zeta = 0.01$. Panels (b) and (d) show the director (background) and the flow profile (blue arrows). The fluid is spontaneously flowing and disrupts the orientational order. The colour-coding refers to the x component of the director, which can go from zero (blue) to one (red). We coloured in green the colloids that belong to a cluster of average size. For both the systems we considered the last configuration in our simulations (which refers to time $t = 160000$). 128
6.23 Pair distribution function referring to a system of colloids embedded in an extensile (left) and for a contractile (right) nematic liquid crystal that is initialised in the nematic phase. Normal anchoring at the colloidal surface is imposed, which corresponds to the presence of a Saturn-ring disclination. Curves for different values of ζ are shown: for small values of ζ spontaneous flow does not affect colloidal structures significantly, while smearing out the signatures of structure at high ζ. The curves were obtained by averaging over 60 configurations taken from time $t = 100000$ and $t = 160000$. 129

6.24 Time evolution of the average number of colloids in a cluster (including at least two colloids) in the case of normal anchoring for extensile (left) and contractile(right) nematics. Each point is the average over ten different snapshots and the error bars are the associated standard deviations. The significant noise at large times is due to the onset of spontaneous flow, that tends to break the largest clusters in smaller parts, and then push them together again. 130
6.25 This graph shows the correlation between instabilities in the active liquid crystals and the decrease of the average size of a cluster with ζ: spontaneous flow tends to break colloidal structures forming at $\zeta = 0$ and to favour a more homogeneous distribution of colloids. This graph refers to normal anchoring. 131
6.26 Mean squared displacement for a system of colloids embedded in extensile (left) and contractile (right) nematics in the case of normal anchoring. 131
6.27 Two snapshots of a system in steady state with 15% colloidal volume fraction, with planar anchoring and in the case when the extensile active liquid crystal is initialised in the ordered nematic phase. In panel (a) $\zeta = 0$, the particles are homogeneously distributed, and there is no flow. Figure (c) refers to $\zeta = 0.01$. Panels (b) and (d) show the director and the flow profile. The fluid is spontaneously flowing and disrupts the orientational order. The colour-coding refers to the x component of the director, which can go from zero (blue) to one (red). We highlighted in green a number of colloids equal to the average cluster size. 133
6.28 Pair distribution function of a system of colloids embedded in an extensile (left) and a contractile (right) nematic liquid crystal that is initialised in the nematic phase. Planar anchoring at the colloidal surface is imposed. Curves for different values of ζ are shown: for small values of ζ spontaneous flow does not affect colloidal structures significantly, while smearing out the signatures of structure at high ζ. 134
6.29 Angular pair distribution function for a system of colloids in passive and in contractile ($\zeta = -0.005$) nematics, with planar anchoring. The angle θ is measured in radians and goes from 0 to π. 134
6.30 Time evolution of the average number of colloids in a cluster (including at least two colloids) in the case of planar anchoring for extensile (left) and contractile (right) nematics. Each points is the average over ten different snapshots and the errors are the associated standard deviations. 135

6.31 This graph shows the correlation between instabilities in the active liquid crystals and the decrease of the average size of a cluster with ζ in the case of planar anchoring. 135
6.32 Screenshots taken from our simulations of a system of two colloids in active nematics, at $\zeta = 0.005$ and $\zeta = -0.01$ for extensile and contractile nematics respectively. 137
6.33 Mean squared displacement for a system of colloids embedded in extensile (left) and contractile (right) nematics in the case of planar anchoring. 138

7.1 Time evolution for a system of colloids embedded in passive (a) and extensile (b) nematics when a quench is performed: in passive liquid crystals the system relaxes to an ordered nematic through the formation of defect lines. Colloids are attracted by defects whose shrinking drives colloidal clustering. At (b) $\zeta = 0.005$, and spontaneous flow hinders relaxation: regions of disorder in the director profile continuously form due to the chaotic character of the flow. 143
7.2 The average modulus of the fluid velocity as a function of ζ for active nematics in the absence of colloids, and with 15% colloids volume fraction, at $w = 0$, with normal and planar anchoring (see legend). Averages are computed over a range of configurations once steady state has been achieved. The stability curve is not significantly affected by the presence of colloids, nor by the type of anchoring when $|\zeta| \gtrsim 0.003$. 144
7.3 Velocity and director profiles in contractile nematics at $\zeta = -0.005$, for all the cases considered in Fig. 7.2. The similarities between their director and velocity profiles are evident. 145
7.4 Velocity and director profiles in extensile nematics, without colloids, in a regime of spontaneous flow, for ζ between 0.0002 and 0.001. The colour coding for the director profile is as in the legend, while for velocity the colour gives information about the z component: dark blue and dark red refer respectively to the minimum (and therefore negative) and the maximum (positive) component of the velocity field along z. 147
7.5 Velocity and director profiles in extensile nematics, with a 15% colloidal volume fraction, in a regime of spontaneous flow, for ζ between 0.002 and 0.005. The colour coding for the director profile is as in the legend, while for velocity the colour gives information about the z component: dark blue and dark red refer respectively to the minimum (and therefore negative) and the maximum (positive) component of the velocity field along z. . . . 148

7.6 Velocity and director profiles in contractile nematics, with a 15% colloidal volume fraction, in a regime of spontaneous flow, for ζ between -0.0002 and -0.003. The colour coding for the director profile is as in the legend, while for velocity the colour gives information about the z component: dark blue and dark red refer respectively to the minimum (and therefore negative) and the maximum (positive) component of the velocity field along z. . . . 149
7.7 Time evolution of the quantity $\langle \vec{v} \rangle$ for extensile (left) and contractile (right) nematics, in the absence of colloids, and for $|\zeta| < 0.005$. 150
7.8 Time evolution of $\langle |\vec{v}| \rangle$ for extensile (left) and contractile (right) nematics with a colloidal volume fraction of 15%, in the case of $w = 0$. 151
7.9 Velocity and director profiles in extensile nematics, with a 15% colloidal volume fraction, in a regime of spontaneous flow, for ζ between 0.001 and 0.005. The colour coding for the director profile is as in the legend, while for velocity the colour gives information about the z component: dark blue and dark red refer respectively to the minimum (and therefore negative) and the maximum (positive) component of the velocity field along z. . . . 152
7.10 Velocity and director profiles in extensile nematics, with a 15% colloidal volume fraction, in a regime of spontaneous flow, for ζ between 0.001 and 0.005. The colour coding for the director profile is as in the legend, while for velocity the colour gives information about the z component: dark blue and dark red refer respectively to the minimum (and therefore negative) and the maximum (positive) component of the velocity field along z. . . . 153
7.11 Velocity and director profiles in contractile nematics, with a 15% colloidal volume fraction, in a regime of spontaneous flow, for ζ between -0.009 and -0.015. The colour coding for the director profile is as in the legend, while for velocity the colour gives information about the z component: dark blue and dark red refer respectively to the minimum (and therefore negative) and the maximum (positive) component of the velocity field along z. . . . 154
7.12 Comparison between the pair distribution functions that are obtained with different anchoring conditions, at $\zeta = 0$, in the case of $w = 0$, of normal anchoring and of planar anchoring. The $g(r)$ in the case of a liquid crystal initially in the nematics phase, has been obtained by averaging over the time interval between the times $t = 100000$ and $t = 160000$; for the quench we averaged over the time interval between $t = 200000$ and $t = 260000$. 156

7.13 Screenshots referring to a system of 771 colloids in extensile nematics at $\zeta = 0$ (a,b) and at $\zeta = 0.005$ (c,d). Aggregates can be found by defining a binding radius, even though what takes place at $w = 0$ is not actual clustering but rather the dynamic formation of inhomogeneities. Here we highlight in green the largest aggregate, defined through a binding radius $r_b = 6.15$. In panels (b) and (d) we show also the director field (background) and the velocity profile (blue arrows). The velocity profile is omitted in panel (b) since relaxation has not been completed yet. 157
7.14 Comparison between the pair distribution function for a passive and for a spontaneously flowing nematic liquid crystal in the case of $\zeta > 0$ (left panel) and of $\zeta < 0$ (right panel). 158
7.15 Number fluctuations in the cases of an extensile (left) and of a contractile (right) nematic liquid crystal, for $w = 0$ when a quench is performed. 158
7.16 Aggregation properties in passive and extensile nematics when normal anchoring is imposed, and a Saturn ring surrounds each spherical colloid. Panels (a) and (c) show the colloidal configurations, and the distribution of defects for a passive system and for an extensile liquid crystal, at $\zeta = 0.005$, respectively. Panels (b) and (d) show the corresponding director (background) and velocity profiles (blue arrows). The colour coding for the director profile is as in the legend, while for velocity the colour gives information about the z component: dark blue and dark red refer respectively to the minimum (and therefore negative) and the maximum (positive) component of the velocity field along z. The flow profile in not shown in panel (b), since it is small and it stems from incomplete relaxation. 160
7.17 Comparison between the pair distribution function for extensile (left) and contractile (right) nematics at different ζ, for normal anchoring. 161
7.18 Time evolution for the average fraction of colloids in a cluster in the case of extensile (left) and of contractile (right) nematics, for normal anchoring, when a quench is perfomed. 161

7.19 Screenshots for passive and extensile nematics when planar anchoring is imposed. Panels (a) and (c) show the colloidal configurations, and the distribution of defects for a passive system and for an extensile liquid crystal, at $\zeta = 0.005$ respectively. Panels (b) and (d) show the corresponding director (background) and velocity profiles (blue arrows). The colour coding for the director profile is as in the legend, while for velocity the colour gives information about the z component: dark blue and dark red refer respectively to the minimum (and therefore negative) and the maximum (positive) component of the velocity field along z. The flow profile is not shown in panel (b), since it is small and it stems from incomplete relaxation. 162
7.20 Comparison between the pair distribution function for extensile (left) and contractile (right) nematics at different ζ, for planar anchoring. 163
7.21 Time evolution for the average fraction of colloids in clusters, in the case of extensile (left) and of contractile (right) nematics, for planar anchoring, when a quench is perfomed. 163
7.22 The relative average number of colloids in a cluster is studied as a function of ζ for active nematics in the case of 15% colloids volume fraction with normal and planar anchoring (see legend). When no anchoring is imposed ($w = 0$) the quantity to be considered is instead the number fluctuation (ΔN), for which the scale of reference is on the right. A quench is performed and the values showed refer to the steady state. Contrary to the stability of the fluid, the aggregation properties are still affected by the type of anchoring. 164
7.23 Mean squared displacement for a system of colloids embedded in extensile (left) and contractile (right) nematics in the case of $w = 0$.165
7.24 Mean squared displacement for a system of colloids embedded in extensile (left) and contractile (right) nematics in the case of normal anchoring. 166
7.25 Mean squared displacement for a system of colloids embedded in extensile (left) and contractile (right) nematics in the case of planar anchoring. 166

C.1 Velocity and director profiles developing in extensile nematics, with a 15% colloidal volume fraction, in a regime of spontaneous flow, for ζ between 0.001 and 0.005. The anchoring is planar. The color coding for both the velocity and the director is as in Fig. 6.2. These snapshots refer to time $t = 160000$. 179

C.2 Velocity and director profiles developing in contractile nematics, with a 15% colloidal volume fraction, in a regime of spontaneous flow, for ζ between -0.009 and -0.015. The anchoring is planar. The color coding for both the velocity and the director is as in Fig. 6.2. These snapshots refer to time $t = 160000$. 180

List of Tables

4.1 Average values of the effective viscosity for a nematic liquid crystal, for the direction parallel and orthogonal to the far-field director orientation. Data were obtained by simulating the drag of a spherical colloid through the liquid crystal [4], and they are expressed as the ratio of our measured viscosity to the one of the simple fluid in which mesogens are embedded. 60

Chapter 1

Introduction

1.1 Aim and Scope of the Thesis

Imagine you were not able to see and you needed to walk in an environment you are not familiar with. What would you do? You would probably use a stick to explore your surroundings by moving it around. The kind of response you get would give you information about how the place in which you are is structured. Moreover, you could guess how hard or soft the obstacles you encounter are, by touching them directly, or with an object. This however should have the right size. A stick that you could easily handle, and whose size were comparable with the length scale you needed to scan, would be appropriate, but a needle would not be as useful, as it would be too small.

This is how we usually proceed whenever we want to understand the mechanical properties of a system: we look at its structure by probing it on the scale that is most significant for the use that we want to make of it. In the first part of this thesis we simulate the use of spherical beads, ideally micron-sized colloidal particles, to investigate the properties of active fluids and liquid crystals.

When many of these particles lie in a medium, they can affect its physical properties, in the same way as the medium can affect the way in which they interact. This can be studied and exploited, since it can lead to new materials, with interesting and useful properties. Two chapters of this thesis will be devoted to studying how the properties of passive and active liquid crystals change in the presence of dispersed spherical particles, that can then be used as constituents of a new composite material, made out of the fluid and of the colloids.

Simulations can bridge theory and experiments by easing the comparison between abstract models, where many of the complexities of the real world are neglected, and experiments. The use of colloids has been largely enhanced by the introduction of modern techniques, such as optical tweezers, that allow for the manipulation of single micron-sized colloids. A numerical study of the phenomenology of colloids in active fluids can provide both a deeper insight into current models and a characterisation of active fluids more similar to the one accessible through experiments. In particular, we will focus on the use of colloids as probe particles through simulations of microrheology experiments in active fluids, and as building blocks for new materials. Precisely, we will consider how the collective properties of colloids are affected by activity.

Active fluids constitute a novel type of out-of-equilibrium system and one that has been drawing the interest of a wide part of the soft matter community, for the last decade. They consist of particles that use energy from their surroundings in order to do work, and are therefore intrinsically out of equilibrium. Main examples are suspensions of microorganisms, such as bacteria or algae, and solutions of biopolymers and molecular motors, such as actin and myosin. Like particles constituting liquid crystals, active particles can be associated with a preferential direction in space and can therefore be found, like liquid crystals, in orientationally ordered phases, for example with all the particles aligned along the same direction.

In all these cases hydrodynamics plays a key role, since the constituent particles are suspended in a fluid. We describe active fluids and liquid crystals through a similar continuum model which follows the evolution of flow field and orientational order. During the last decades liquid crystals have been described thoroughly theoretically, experimentally, and through simulations, and understanding the role played by activity in this framework cannot disregard a comparison with their passive analogues.

In the rest of this chapter, we will summarise the basics of active systems. A more detailed discussion on the aspects we are most interested in will be presented in the following chapters. Finally, we will describe some of the uses of colloids in soft matter, with particular reference to the ones on which we will focus later on.

In Chapter 2 we will introduce the model that we applied to describe active and passive liquid crystals, while in Chapter 3 we will review the lattice

Boltzmann method, which we applied to solve the equations presented in Chapter 2.

In Chapters 4 and 5 we will present our results on microrheology simulations, where a spherical particle is dragged through active (and passive) nematics. While in Chapter 4 systematic results concerning different anchoring and boundary conditions will be presented (and compared with simulations and analytical predictions on macrorheology), in Chapter 5 we will propose a theoretical correction to the effective viscosity accounting for the results of Chapter 4 in the case of strong anchoring, and investigate further the case of contractile fluids, when planar anchoring is considered, for which our model predicts the existence of a regime of negative drag.

In Chapters 6 and 7 we will study a suspension of spherical colloids in active nematics, and analyse both the impact of colloids on the onset of spontaneous flow, and how the latter affects their collective properties. In Chapter 6 we will consider the case of a liquid crystal initialised in the nematic phase, while in Chapter 7 we will perform a quench from the isotropic to the nematic phase. We will discuss our results and present our conclusions in Chapter 8.

1.2 Liquid Crystals

Here we will present the essential background to the results that will be shown in the following chapters. For all the reasons explained above, a discussion on active fluids requires an introduction to liquid crystals. Particularly, the hydrodynamic model used to describe active fluids throughout this thesis is a slight variation of that used for liquid crystals, accounting for the continuous stirring exerted by active particles on their ambient fluid. In this framework, we will often refer to active fluids as to active liquid crystals. Understanding how the additional terms affect the physical behaviour of the system is made easier by a parallel study of the corresponding passive system.

1.2.1 What Are Liquid Crystals?

Liquid crystals are materials that can experience a phase transition from the isotropic phase, where the orientation of molecules is not ordered, to a long range

orientationally ordered phase, characterised by a broken rotational symmetry, while translational symmetry is preserved, or broken only along specific directions. The microscopic structure of liquid crystals is therefore intermediate between the one of isotropic liquids and the one of crystalline solids. The former are both isotropic and homogeneous. This is what leads to the fluid character of these materials. In crystalline solids instead, both rotational and translational symmetries are broken and their structure is invariant only under a discrete set of translations and point-group operations. A system of particles in a liquid-crystalline phase usually has only some restricted rotational degrees of freedom, but translation by arbitrary quantities is allowed at least along one direction.

Particles that constitute liquid crystals, usually referred to via the term *mesogens*, are anisotropic, i.e. either they have a non-spherical shape or they interact non-isotropically. The main cases are the ones of rod-like and of discotic (i.e. with the shape of a disc or flat cylinder) particles. Onsager showed for a system of rod-like particles that this shape is enough to determine an entropy-driven phase transition from an isotropic to an orientationally ordered phase, where all the particles are oriented, on average, along the same direction, upon increasing concentration [5]. When this is the case liquid crystals are said to be *lyotropic*, while when the transition takes place through a decrease of temperature, they are said to be *thermotropic*.

A fundamental characteristic of nematic liquid crystalline phases is the absence of local average polarity. This means that, when averaging over a locally ordered domain, the system is head-tail symmetric. This can be either associated to the head-tail symmetry of constituent particles, or to an equal average number of particles pointing in different directions. The *director* is an headless vector associated to the local average orientation of mesogens. We will define it formally later on.

The Nematic Phase

There are different possible ways in which orientational order can be introduced in a system of anisotropic particles, thus giving origin to several possible ordered phases. For simplicity we will focus here on rod-like particles.
The simplest case is the one in which they are aligned on average along the same direction. The headless vector that identifies this average direction is the *director*.

This phase is called *nematic* and mesogens organised in a nematic phase are also called *nematogens*. In this phase constituent particles are allowed to translate along all directions, and therefore they form a homogeneous anisotropic fluid. This is the liquid-crystalline phase that has been studied more in detail so far, and it is the one we will refer to in this thesis since main examples of active fluids have been observed in orientationally ordered phases where all the particles are oriented on average along the same direction.

1.2.2 Modelling Liquid Crystals: Order Parameters

Here we will start introducing the model that we used to describe liquid crystals through the definition of the order parameters that capture the main features of liquid crystalline phases. The free energy terms that describe these systems at equilibrium and the equations for their evolution towards the free-energy minimum will be introduced in Chapter 2.

Director

The description of orientationally ordered phases requires the choice of significant parameters able to describe the phase transition from a disordered to an ordered phase, and that also allow for the characterisation of the system in the ordered phase. Understanding what these parameters are is probably easier when considering the nematic phase. In the nematic phase all the particles are aligned on average along the same direction. It is therefore natural to introduce a vector that identifies that direction in space. However, the head-tail symmetry that characterises orientational order in liquid crystals requires to opt for a unit headless vector, i.e. a vector $\hat{\mathrm{n}}$ that is head-tail symmetric: $\hat{\mathrm{n}} \leftrightarrow -\hat{\mathrm{n}}$; $\hat{\mathrm{n}}$ is called the *director* and it is chosen so that $|\hat{\mathrm{n}}| = 1$.

A constant director is enough to provide a complete description of the nematic phase, in the case of a perfectly aligned liquid crystal. Other phases have a more complicated structure and the local orientation varies in space. Moreover, liquid crystals are never perfect and an exhaustive description needs to take into account local deformations. That is why a director field $\hat{\mathrm{n}}(\vec{x})$ can be defined as the coarse-grained average of the head-tail symmetric unit vectors $\hat{\nu}_i$, each of which points along the symmetry axis of the i-th particle.

Scalar Order Parameter

In order to describe the transition from the isotropic to an orientationally ordered phase it is necessary to define a local degree of order, which quantifies how much the orientation of single particles differs from the one of the local director. This can be done by introducing a scalar order parameter field, usually defined as:

$$S(\vec{x}) = \frac{1}{2}\langle 3(\hat{\nu}_i \cdot \hat{\mathrm{n}}(\vec{x}))^2 - 1\rangle = \frac{1}{2}\langle 3\cos^2\theta_i(\vec{x}) - 1\rangle, \tag{1.1}$$

where $\hat{\nu}_i$ is defined as above and $\langle\cdot\rangle$ here denotes an average over the microscopic volume that is identified by the vector $\vec{x}$ and with associated local director $\hat{\mathrm{n}}(\vec{x})$ [6]. According to this definition, S is maximum and equal to 1 in the case of a perfect aligned nematic liquid crystal. Smaller values of S are associated to a certain degree of disorder, while the case of $S = 0$ is associated to the isotropic phase. A negative S corresponds to a *discotic* type of allignment, where the normals to $\hat{\mathrm{n}}$ are all aligned on average along the same direction.

Tensorial Order Parameter

The director field and the scalar order parameter only allow for a partial description of liquid crystals. In particular, as will be described later, an elastic free-energy density that describes defect-free liquid crystals deep in the nematic phase can be written solely in terms of $\hat{\mathrm{n}}(\vec{x})$. On the other hand, the phase transition from the isotropic to the nematic phase can be described in a Landau approach by writing an effective free-energy that only depends on S. However, a more global and complete description of liquid crystals can be achieved through the introduction of a single, but tensorial, order parameter $Q_{\alpha\beta}$, defined in terms of the vectors $\{\hat{\nu}_i\}$ associated to each of the mesogens constituting the liquid crystal:

$$Q_{\alpha\beta}(\vec{x}) = \frac{V}{N}\langle\sum_i \left(\nu_\alpha^i \nu_\beta^i - \frac{1}{3}\delta_{\alpha\beta}\right)\delta(\vec{x} - \vec{x}^i)\rangle, \tag{1.2}$$

where $\langle\cdot\rangle$ is defined as above, while V denotes the volume of the sample and N the total number of particles. The normalisation factor V/N makes $Q_{\alpha\beta}$ dimensionless. Moreover, it is a symmetric tensor and, since $\hat{\nu}$ is a unit vector, $\mathrm{Tr}\,\mathsf{Q} = 0$. Here, as in the rest of the thesis, greek indices denote cartesian

coordinates, while latin indices are used to denote particles. $\mathsf{Q}(\vec{x})$ can be diagonalised by choosing a reference frame in which one of the axis is parallel to the average molecular alignment:

$$\mathsf{Q} = \begin{pmatrix} \frac{2}{3}S & 0 & 0 \\ 0 & -\frac{1}{3}S - \lambda & 0 \\ 0 & 0 & -\frac{1}{3}S + \lambda \end{pmatrix}. \tag{1.3}$$

According to this definition, the order parameter S is directly proportional to the highest eigenvalue of Q, and the director $\hat{\mathrm{n}}$ is its associated eigenvector [6]. Note that Q is not defined in terms of $\hat{\mathrm{n}}$ and of S, and in general the relation between the three cannot be written in simple terms. Non-zero values of λ indicate biaxiality, where nematic order is found along two of the three cartesian axes. When $\lambda = 0$, the liquid crystal is uniaxial, and Q can be easily related to $\hat{\mathrm{n}}$ and to S:

$$Q_{\alpha\beta} = S\left(n_\alpha n_\beta - \frac{1}{3}\delta_{\alpha\beta}\right). \tag{1.4}$$

Despite the fact that most nematic liquid crystals are uniaxial, and hydrodynamic equations can be written in terms of $\hat{\mathrm{n}}$ and S, this description is insufficient to our purpose. We will need to deal with $Q_{\alpha\beta}$ in our description of active and passive liquid crystals, in order to be able to study the dynamics of defects that necessarily form when colloids are introduced in a liquid-crystalline system.

1.2.3 Topological Defects

In materials with long range order there can be regions where order is destroyed and the order parameter is not defined. Within defects the characteristic symmetry of the material is broken. Crystalline solids are invariant with respect to a discrete set of translations. Defects in this case are called *dislocations*. In the case of liquid crystals, defect lines are likely to form, which are called *disclinations* [7]. Defects are regions of high elastic stress, since the constituent particles are away from the equilibria of the elastic free energy. As a consequence, the mechanical properties of materials are strongly affected by defects [8].

Disclinations in liquid crystals can be present in the bulk. This is the case of blue phases, for example, that are characteristically permeated by an – ordered or amorphous – network of disclinations [9]. In general bulk disclinations appear

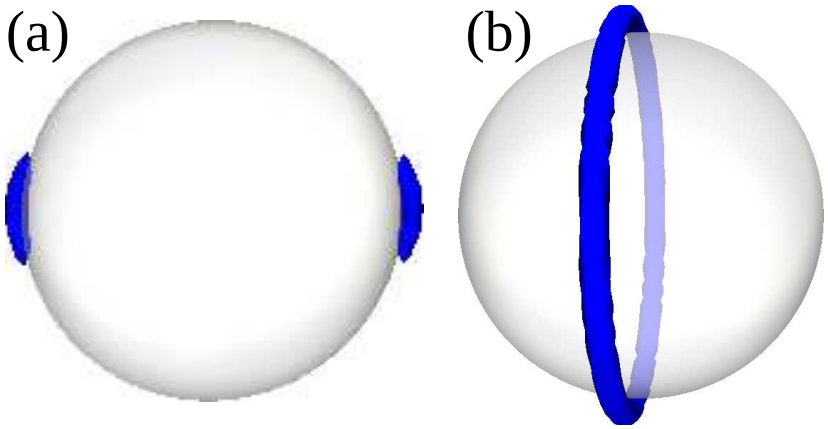

Figure 1.1: Defect structure close to a colloidal particle embedded in a nematic liquid crystal: in the case of planar anchoring two boojums appear (a), while for normal anchoring we see the formation of a Saturn ring disclination (b). In both cases the bulk director orientation is horizontal. Adapted from [1] with permission.

naturally in experimental systems, mainly due to unavoidable impurities.

The case we will be mostly interested in is the one of defects that appear close to a surface, because of boundary conditions imposed by the interaction between the liquid crystal and the material at the boundary. Interaction with a solid surface in real systems determines the local reorientation of mesogens. This can typically take place in two ways: either particles align orthogonally, on average, to the contact surface, or parallel. We will refer to the first case as to *normal* or *homeotropic* anchoring, and to the second case as to *planar* or *homogeneous* anchoring [10].

Along the whole thesis we will consider colloids embedded in (active or passive) liquid crystals. Because of the anchoring condition, defects develop close to the colloidal surface. The kind of defects appearing depends on the type of anchoring, on the anchoring strength, and on the system size. What is general is that they can importantly affect the colloidal motion through the liquid crystal, as we will describe in detail when studying the microrheology of passive and active nematics.

According to whether normal or planar anchoring is imposed on the particle surface, three different scenarios can present. The case of planar anchoring is characterised by two surface defects called boojums (see Fig. 1.1(a)), that are placed at the antipodes, along the far-field director. In the case of normal

Figure 1.2: Sketch of typical defects that can be found in liquid crystals and with half-integer charge. The defect on the left has charge $+1/2$, the charge of the one on the right is $-1/2$. Since these two defects have equal charges but with opposite sign, they can annihilate.

anchoring instead, the arrangement of the director profile, due to the need of recovering a far-field nematic order, can either be characterised by a "hyperbolic hedgehog" that tightly binds to the particle, thus forming a *dipole*, or by a disclination ring that encircles the particle at its equator (Saturn ring). This last case is represented in Fig. 1.1(b) and it is the only one we will consider in our simulations with normal anchoring [11],[12],[13].

1.2.4 Topological Charge

Let us consider an orientationally ordered two-dimensional system, with a point defect at the origin. In general the ordered system will be described by an order parameter $\vec{s}(\vec{x})$, which in a two-dimensional system can be written as: $\vec{s}(\vec{x}) = |\vec{s}|(\cos\theta(\vec{x}), \sin\theta(\vec{x}))$, and is a periodic function of θ:

$$\vec{s}(\vec{x}) = \vec{s}(r, \theta) = \vec{s}(r, \theta + 2\kappa\pi). \tag{1.5}$$

The parameter κ represents the number of full 360° rotations that the order parameter $\vec{s}$ has to perform around the origin in order to go back to its initial orientation. As a convention κ is negative when the rotation of nematogens is opposite to the rotation of the path around the origin, and positive in the other cases. The parameter κ is the *topological charge* of the defect. When $\vec{s}$ is a vector, with an associated polarity, κ can only be an integer. In the case of liquid

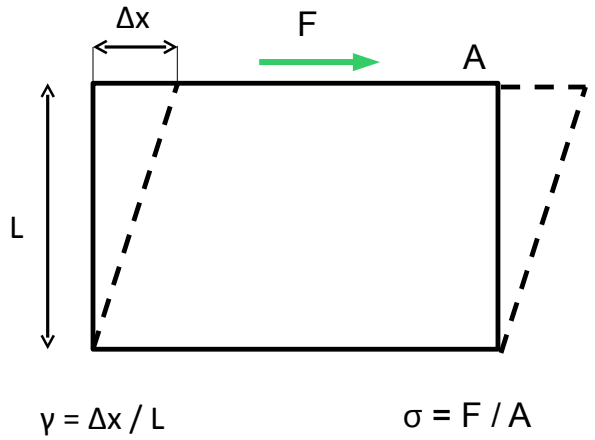

Figure 1.3: Diagram explaining the concepts of strain and of stress for a sheared material. A force F is applied parallel to the top surface, having area A. The shear stress in $\sigma = F/A$. This external force generates a strain $\gamma = \Delta x/L$, where Δx is the displacement along F.

crystals, $\vec{s}$ is identified with the director $\hat{\mathrm{n}}$, which is headless. Because of this head-tail symmetry, the topological charge of defects in liquid crystals can also be half-integer. Typical examples of defects that can be found in liquid crystals are the ones sketched in Fig. 1.2.4. Charges are additive and defects having charges of opposite sign attract each other and annihilate. This is what happens, for example for the two defects shown in Fig. 1.2.4.

1.2.5 Liquid Crystals as an Example of Complex Fluids

The fact that the characteristic structure of liquid crystals is intermediate between the one of liquids and the one of a crystalline solid, is reflected in their macroscopic properties. Materials in the solid-crystalline state usually show elastic properties: when they are sheared (i.e. when a force is applied parallel to their surface), they deform by a quantity proportional to the applied force and go back to their initial shape when shear is stopped. The shear stress, σ_{el}, is the external force parallel to the surface per unit area, while the strain, denoted with γ, is the deformation parallel to the external force. Elementary definitions are given in Fig. 1.3. In

elastic solids the shear stress is directly proportional to the strain:

$$\sigma_{el} = \epsilon\gamma, \tag{1.6}$$

where the proportionality costant ϵ is called elastic modulus. Perfectly elastic solids, that by definition behave according to Eq. 1.6 are also called *Hookean* solids, since they follow Hooke's law, stating the proportionality between the elastic force and the displacement for an ideal spring. Ideal solids can be considered as materials with an infinite memory: as soon as the external force is stopped, the initial shape is restored. This can be seen from Eq. 1.6: when $\sigma_{el} = 0$, necessarily $\gamma = 0$. From the energetic point of view elastic materials do not dissipate any of the energy that is introduced in the system when the external force is applied to produce the deformation.
Fluids, on the other side, typically display a different behaviour: they are viscous. When sheared, they deform gradually and the shear stress, σ_{visc}, is proportional to the shear rate $\dot{\gamma}$, i.e. the ratio of the variation in the fluid velocity parallel to the force in the direction orthogonal to it, to the distance between the two confining walls (measured in s^{-1}):

$$\sigma_{visc} = \eta\dot{\gamma}. \tag{1.7}$$

The proportionality constant, η, is the *shear viscosity* of the fluid. Fluids that display a purely viscous behaviour, by obeying Eq. 1.7, are called *Newtonian*. Oppositely with respect to elastic solids, viscous fluids do not have memory of their initial state: when the external stress is stopped, the fluid stops flowing, but deformation is maintained. All the energy introduced in the system is dissipated, as a consequence of the dependence of the stress on the shear rate (on velocity) rather than on the deformation.

Real materials are never either perfect elastic solids nor perfect viscous fluids. However, for most of them either Eq. 1.6 or Eq. 1.7 are good approximations. There are materials for which this is not the case, and these are usually called *viscoelastic* fluids. They are examples of complex fluids (i.e. fluids that do not obey Eq. 1.7). Among these are liquid crystals in their orientationally ordered phases. The branch of physics that studies the response of materials to external

stresses, i.e. their deformation and flow properties, is called *rheology*. The rheological properties of liquid crystals will be discussed in detail in Chapters 4 and 5, where we will present an overview of the current state of the art on the topic. Later on in this chapter we will describe how colloids can be used in order to infer the rheological properties of the fluid in which they are embedded (microrheology), as an alternative to more traditional experimental techniques where the relation between the stress and the strain or the shear rate is studied.

1.3 Active Fluids

Active particles absorb energy from their surroundings, or from an internal tank, to do work [14]. This definition includes a wide spectrum of systems, among which flocks of birds and schools of fish are maybe the ones we are more familiar with. Attempts have been made to build up non-biological active systems, that display the main properties predicted so far, for example through the vertical vibration of rods lying on a plane [15] or by synthesising self-propelled particles that are driven in a certain direction by local gradients [16, 17]. Scientific interest in this type of system, especially from the statistical physics community, comes mainly from the observation of recurring behaviours in systems of living creatures, characterised by a common tendency to aggregate in flocks and to display collective motion [14]. Some of these properties are universal and appear at different length scales. However, we are mostly interested in those systems that can be labelled as "soft materials" and whose characteristic length scale is the micrometre.

1.3.1 Characterisation of Active Systems

The general definition of active matter that we have just provided will be clarified here, with a short summary of the way in which active particles can be classified. Some of the surprising implications of the novel character of active systems will be also introduced.

A Novel Way of Staying Out of Equilibrium

Most of the systems that we encounter in our everyday life are out of equilibrium. The ones we are more familiar with involve an external field that keeps the

system out of equilibrium. This is what happens for the tungsten filament in a light bulb: a time-dependent electric potential difference between the two ends maintains an alternate current of electrons along the filament. In other cases equilibrium is not reached despite the absence of external forces. This is the case of glasses, where relaxation takes place on a time scale that is very long in comparison to the observation time. These are all systems that statistical physics has been trying to describe for a long time and for which an effective framework is now well established. The case of active systems is completely different: active particles are intrinsically out of equilibrium, since they continuously use their internal energy, usually stocked in the form of ATP, to do work, which might include self propulsion or the simple stirring of an ambient fluid. Differently from most of the systems that we are used to, active systems keep themselves out of equilibrium without the need of any external field. This is responsible for a range of counterintuitive behaviours, among which are the appearance of anomalous giant fluctuations of the number of particles, the existence of long range ordered phases also in two dimensions, and instabilities related to a regime of spontaneous flow. All of these will be introduced in the following sections.

1.3.2 Giant Number Fluctuations

One of the pillars which equilibrium statistical mechanics far from critical points relies on, is that number fluctuations $\Delta N = \sqrt{\langle N^2 \rangle - \langle N \rangle^2}$ at equilibrium grow with the square root of the number of particles, so that the relative number fluctuations:

$$\frac{\Delta N}{N} \sim \frac{1}{\sqrt{\langle N \rangle}} \to 0 \text{ when } N \to \infty, \tag{1.8}$$

and the relative fluctuations in the number density ρ grow with $1/\sqrt{V}$, becoming negligible in the thermodynamic limit. This makes the number density a well defined quantity, which for large enough systems is independent of the system size. What the first models for active systems predicted [18], and successive experiments on a system of vibrated granular rods proved true [15], is that this does not hold for active systems. What happens in that case is that large number fluctuations are found, with $\Delta N \sim N^\alpha$, where $\alpha > 0.5$. In two dimensions *giant number fluctuations* have been found, with $\alpha = 1$ and ΔN which grows like N [15]. The number density is therefore ill defined, $\Delta\rho/\rho$ growing with the system

size. This phenomenon is a mere consequence of the intrinsic out of equilibrium character of active systems. Giant number fluctuations are associated with large scale inhomogeneities in the distribution of particles, that are responsible for their characteristic flocking. This behaviour is taken into account in models where the concentration of active particles is allowed to vary in space. We note here that this is not the case of the model that we are going to introduce, where we assume a constant density of mesogenic particles and neglect variations in the concentration, which would require the introduction of a concentration field that should be coupled to the fluid and to the tensor Q. The systems that we aim at modelling are suspensions of active particles at a density high enough to allow for a continuum description. We expect that at such a high density variations in the particle density are negligible.

1.3.3 Long Range Orientational Order

We have already anticipated in this chapter that active systems tend to form orientationally ordered phases due to the intrinsic anisotropy of active particles, which can always be associated with a specific direction in space. This is where the analogy with liquid crystals comes from. However, the out-of-equilibrium character of active systems has important implications on the possibility to form orientationally ordered phases, which we will discuss here.

Polar and Apolar Particles

Active particles are always associated with a certain direction in space. This is usually the direction along which they move or exert forces on their ambient fluid. Some distinctions here are in order. Active particles can have well defined head and tail, i.e. they can be *polar*. *Apolar* active particles, that are head-tail symmetric, can also be found. Among apolar particles there are melanocytes [19], which distribute pigment in the skin, while most of the main examples of active fluids consist of polar particles. This is the case of bacteria and of actomyosin in the cytoskeleton. The difference between polar and apolar particles was pointed out by Gruler in [19]. Both polar and apolar particles can form both polar and apolar phases [14]. The former are in general characterised by a collective motion of all the particles in the same direction, so that the system has a non-zero drift velocity, while the latter can be represented e.g. by particles moving collectively

in rows but with opposite directions, so that the average velocity of the system is zero. If in a fluid, active particles continuously stir it, even when they do not self propel. This is the case of apolar particles, that for this reason are also called *shakers*, as opposed to *movers*, that are instead polar [20]. As we will see later, when presenting the model for active fluids in more detail, at least at a first order approximation, there is no difference between the effect of polar and apolar particles on a simple fluid as far as the Navier-Stokes equation is concerned [21]. This means that on a macroscopic scale the two should behave in the same way and active fluids should display the same rheological properties, independently of the polarity of their constituents. In this thesis we will deal with a model for apolar active fluids, but in principle this argument allows us to extend our conclusions also to the study of important biological systems.

Long Range Order in Two Dimensions

For systems at equilibrium, the Mermin-Wagner theorem [22] states that long range ordered phases where continuous symmetries are broken are forbidden in less than three spatial dimensions. For active systems instead, long range orientational order was predicted to show up also in two dimensions. This first came from the simple Vicsek model [23], where each particle is associated with a constant velocity whose direction is updated according to a local rule, depending on the average direction of motion of the neighbour particles, with some angular tolerance meant to account for thermal and active noise. Experiments performed later on a system of vibrated granular apolar rods seemed to confirm these results [15].

1.3.4 Role of Hydrodynamic Interactions

The attention of the soft active matter community has recently mainly been addressed towards two types of systems. On one side there are biological systems consisting either of microbial (e.g. bacterial or algal) suspensions, or of long filaments activated by motor proteins, such as the actomyosin solution or the recently synthesised suspension of microtubules and kinesin described in [24]. On the other side, synthetic colloidal particles able to exploit the existence of gradients in the environment for their motion, try to mimic living systems [16, 17]. In both cases active particles are usually embedded in a fluid whose

presence is responsible for the propagation of the continuous forces that active particles exert on the ambient fluid itself. These hydrodynamic interactions typically decay with powers of the inverse distance between two particles and therefore affect the dynamics in a non-negligible way. The questions that we want to address, concerning the study of colloidal systems in active fluids, are inherently raised on the basis of a model where active suspensions are considered as a continuum system. For such a coarse grained, continuum description, hydrodynamic interactions are in order and a distinctive feature.

Dry and Wet Systems

At this point of the discussion, we need to distinguish between "*dry*" and "*wet*" active systems. In the former active particles usually interact with a momentum sink, such as a substrate, the friction with which determines a loss of momentum for the system [25]. This is the case of vibrated granular rods [15]. On the other hand, *wet* active systems are such that the total momentum is conserved. This is usually the case when active systems are considered in the bulk. The condition that momentum is globally conserved makes hydrodynamic interactions play a key role in the dynamic evolution of the system. However hydrodynamic interactions can be important also for "dry" systems, for example in the case of vibrated rods, where despite the friction with the substrate there can be fluid-mediated long range interactions among the particles [25].
First theoretical studies of active matter ([23, 18, 26, 27]) considered self-propelled particles as moving on an inert frictional substrate, while [28] did not examine fluid flow, despite considering viscosity as a source of friction. These models neglect momentum conservation, and are therefore reliable for systems of particles on a substrate, as those considered in the experiments presented in [19]. Here we will focus on modelling bulk properties of suspensions of micro-organisms such as bacteria or algae, and of the actomyosin solution, and therefore we will need to impose momentum conservation in the system. Suspensions of active particles will be described as a continuum fluid and far-field hydrodynamic interactions are determinant (while near-field ones are ignored, as it will be explained later on). Other than for dense bacteria and algae suspensions, this model is suitable also for recently synthesised active fluids such as the ones described in [24].

Systems at Low Reynolds Number

When dealing with hydrodynamic systems, the characteristics of the flow depend strongly on the Reynolds number (Re). This is an adimensional quantity defined as the ratio between inertial and viscous forces: $Re = av\rho/\eta$, where ρ and η are respectively the density and the viscosity of the fluid. For a body moving through the fluid, one should consider a as the size of the body, and v as its velocity in the fluid. The active particles we are most interested in, e.g. bacteria, are usually embedded in aqueous solutions. Considering the viscosity and density of water (respectively $\eta = 10^{-3}$ Pa $\cdot$ s and $\rho = 10^3$ kg/m^3), with typical sizes of 1 μm and velocities of about 30 μm/s, one obtains $Re \sim 10^{-5}$. Microorganisms therefore live at very low Reynolds numbers and for them inertia plays no role. This has enormous implications in the swimming mechanisms available to these organisms [29], as it can easily be understood when considering that the Reynolds number for a human being in water is around 10^6. At low Re a force exerted on the fluid instantaneously results on velocity, rather than on acceleration, and organisms need to continuously stir their ambient fluid in order to propel.
In this thesis we will not be concerned with the understanding of swimming mechanisms since we aim at a coarse-grained description, where the flow field associated to each particle is looked at only from a large distance, and the way particles exert forces on the fluid is taken for granted. However, the fact of considering a regime of low Re still affects our description and our understanding of the physics behind the systems that we aim at modelling, particularly its instabilities, as will be discussed in the following paragraph.

Active Particles as Force Dipoles: Extensile and Contractile Particles

Once the goal of describing hydrodynamic interactions between active particles has been settled, it is important to characterise the way in which a single particle interacts with its surroundings. How do active particles exert forces on their ambient fluid? A better understanding of the modelling of active particles in a hydrodynamic framework comes from looking at examples of self propelled particles that are found in biology. These are micro-organisms such as bacteria, algae or protozoa, that self-propel in the absence of any external force. The flow profile close to their body is very complex. It can be described analytically e.g. in the case of organisms covered with many protrusions called *cilia*, which are

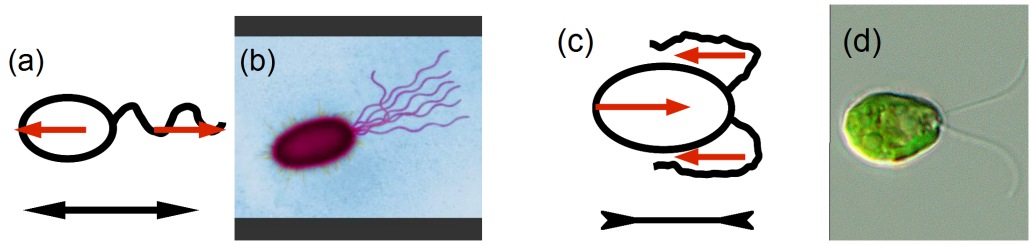

Figure 1.4: Active particles can be modelled as force dipoles. Extensile particles exert forces that are directed outwards along their main axis (a), and important examples are bacteria such as *E.coli* (b). Contractile particles exert forces on their ambient fluid that are directed inwards along their main axis (c) and important examples are algae such as *Alga Chlamydomonas* (d).

very short with respect to flagella, and whose synchronal motion generates a flow able to propel the particle. The model in this case is the one of a squirmer [30], for which the flow profile close to the surface, in the approximation of a spherical shape, is known.

However, what we want to capture, is the collective behaviour of a dense suspension of many of these organisms, interacting hydrodynamically. For such a description, the detailed flow profile close to the surface of each one of them is not relevant, since the important length scale in a hydrodynamic, coarse-grained description is much larger than the size of the single particles. At these distances all that we need to consider is that self-propulsion does not require any external action and therefore active particles cannot be associated with a monopolar force, which would require an external action in order to be counterbalanced. The minimal approximation requires to consider each active particle as a force dipole. Direct measurements of the flow close to bacterium *E.coli* have been performed through the use of fluorescent tracer nanoparticles [31] and have confirmed that this is a good approximation, at least in this case. In a coarse-grained description active particles are therefore modelled as objects that, in order to move in a fluid, pull it or push it along one main axis. In such framework we distinguish between extensile and contractile active fluids. Examples of the former are suspensions of bacteria, such as *E. coli*, characterised by a main body and a bundle of flagella at their back, allowing the bacterium to propel forewards. Also the solution of microtubules and kinesin described in [24] constitutes an example of extensile fluid. Extensile particles push the fluid along their axes, i.e. the forces that they

exert on the fluid are directed out of each particle centre, along their axis, on both sides, and are therefore also called "*pushers*". Contractile particles (or "*pullers*") pull the fluid along their axes, which means that the flow that each particle creates is directed towards its own centre, from both sides along its axis. One example is provided by *Alga Chlamydomonas*, which consists of a main body with two flagella at the front, that are pushed backwards during propulsion [32, 33], as illustrated in Fig. 1.4. The actomyosin solution is also an example of contractile fluid. Contractility in striated muscles relies on the organisation of actin filaments in ordered structures called sarcomeres. In the lack of sarcomeric organisation the buckling of actomyosin bundles has been recently suggested as a mechanism inducing contractility [34].

Extremely different behaviours have been predicted for extensile and contractile particles, as will be presented in more detail in Chapter 4, where the rheological properties of these systems will be discussed.

1.3.5 Instabilities of Long Range Ordered Active Suspensions

Active systems have been proved to be characterised by a wide range of instabilities. In order to understand what their mechanisms are, we will focus here on our case of interest, i.e. a system of apolar particles that are interacting hydrodynamically. Apolar active particles do not self propel but still stir their ambient fluid by continuously applying forces on it. When they are in a perfectly aligned nematic phase, the local flow generated by each particle is cancelled by those of its neighbours, so that there is no net macroscopic flow. Distortions in the nematic pattern are at the origin of instabilities. Similar, but different mechanisms take place in contractile and extensile suspensions, as a consequence of the interplay between deformations, flow and active stresses.

The deformations at the origin of instabilities are the ones sketched in Fig. 1.5: the panel on the left shows a splay and the one on the right a bending deformation. Splay and bending will be defined formally in the next chapter, when the expression for the elastic free energy of the liquid crystal will be introduced. Fig. 1.5 is enough to illustrate the mechanism for instability for an extensile fluid. While in a perfectly ordered suspension active forces cancel out locally, in

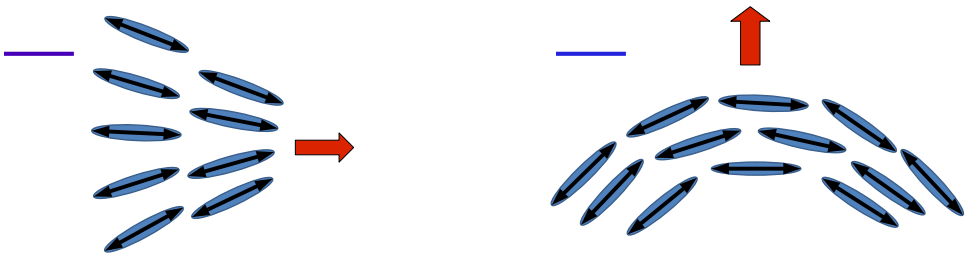

Figure 1.5: Instabilities in extensile nematics arise due to deformations in the nematic pattern. The panel on the left shows the case of a splay deformation (the blue horizontal line specifies the director orientation in the bulk), which is responsible for a net force acting on the fluid directed according to the red arrow. This originates a flow that contrasts the deformation and tends to recover nematic order: extensile nematics are stable with respect to splay. The panel on the right illustrates the case of a bending deformation. In this case the net force exerted by active particles on the fluid (red arrow) generates a flow that enhances the deformation: extensile nematics are unstable with respect to splay.

the presence of a splay deformation in Fig. 1.5 (left) local stesses add up to give a non-zero net force on the fluid, that is directed as in the figure (red arrow) and therefore generates a local flow that works so as to re-establish order. One can find out the direction of this flow by considering the extensile character of dipolar forces (black arrows) [35]. The opposite happens in the case of bending (see right panel in Fig. 1.5): now the net active force generates a local flow that enhances the deformation. Extensile nematics are therefore *stable* with respect to splay and *unstable* with respect to bending. Similar reasonings apply in the case of contractile nematics, where the forces are directed opposite with respect to the case of extensile particles and the fluid is stable with respect to splay, but unstable with respect to bending. This explanation relies on the hypothesis of a regime of low Reynolds numbers, which allows for an instantaneous and global response of the system to the net active forces that originate from deformations.

These instabilities were predicted in early theoretical work [36] and were later supported by experiments [37] and investigated through simulations [38]. They are strongly connected to what is probably the most striking feature of these systems: the appearance of a regime of *spontaneous flow*. Particularly,

experiments have shown that phenomena of turbulence can take place in bacterial suspensions and a macroscopic flow is observed despite the complete absence of external forces [37, 39].

Long range ordered bulk active fluids are always unstable to fluctuations of the order parameter Q. Introducing boundaries with suitable anchoring conditions was found to stabilise these systems [38]. Particularly, for extensile fluids, it is possible to define a critical activity ζ_c such that for $|\zeta| > \zeta_c$ the fluid becomes unstable. As shown in detail in [38], the threshold for the onset of spontaneous flow is set by the product ζL^2. Therefore, for a fixed choice of parameters, ζ_c decreases with the system size, as $1/L^2$ [38]. For contractile systems the appearance of an instability is more difficult to characterise. Particularly, in a quasi one-dimensional system, stability is maintained in a very wide range of activities if the perturbation to the order parameter is chosen as small enough [20] (with quasi one-dimensional we mean a system that is translationally invariant along two directions).

Simulations presented in [38],[3], and [40] analysed the flow pattern arising for different values of activity. For example it was found that in a quasi one-dimensional slab, for $\zeta > \zeta_c$ a spontaneous Poiseuille flow develops, which breaks the symmetry and results in a fluid flow parallel to the confining walls [38]. Larger activities give rise to even more surprising flow patterns, such as a shear banded flow, where layers of fluid with different shear rates are found. Simulations performed in a quasi two-dimensional geometry on extensile systems also showed that for low enough activities above the critical threshold a stationary unstable flow, characterised by the presence of vortices arises. In a regime of larger ζ instead the flow becomes chaotic. What is observed in this case is very similar to what is described in [37, 39].

1.4 Colloids in Complex Fluids

The last step for the description of the systems we are interested in, is the one of embedding colloids in liquid crystals and active suspensions. The topic of colloidal systems is broad and covers a large part of soft matter. Here we will focus on those aspects that are directly relevant to the systems we study. Particularly, the colloidal particles that we consider in our simulations are modelled as hard

spheres that interact with the solvent just (a) by momentum exchange, and (b) by a boundary condition on the liquid-crystalline alignment at the colloid surface. In this section we will provide an essential characterisation of colloidal systems and describe their uses in soft matter, as probe particles and as building blocks for the synthesis of new materials. These two uses will be studied in this thesis for the cases of passive and active liquid crystals.

1.4.1 What Are Colloidal Particles?

The term *colloid* is here used to indicate a broad category of particles whose size is approximately between 100 nm and 10 μm, therefore several orders of magnitude larger than the one of atoms and molecules, but small enough not to be seen without the use of a microscope. (This is usually the range of sizes of the particles that are used in experiments such as the ones that we describe in this thesis, particularly for what concerns Chapters 4 and 5.) Thus the label of "colloid" can be attached to many different objects, such as solid particles, bubbles, droplets, micelles, etc. More precisely, colloids are usually encountered in suspensions where one substance is found in microscopic units, the ones called *colloidal particles*, dispersed in another substance.

Colloidal particles are subject to thermal fluctuations. Brownian motion, discovered during the first half of the nineteenth century by the Scottish botanist Robert Brown, is the characteristic random motion performed by microscopic particles due to the continuous collisions with the much smaller molecules that constitute the fluid in which they are embedded. The dynamics of a system of colloids in a simple fluid is dominated by Brownian motion, which allows the system to explore the phase space. We note here, and will discuss later on, that in this thesis we neglect thermal fluctuations when studying the collective properties of a system of many colloids embedded in passive or active nematics. This is because liquid crystal mediated interactions between colloids, that dominate the dynamics at short distances, are of the order of hundreds or thousands of k_BT. Moreover, we studied the role of spontaneous flow, where the Péclet number, i.e. the ratio of advection to diffusion rates, is large and the dynamics is dominated by the former.

1.4.2 Uses of Colloids in Soft Matter

One of the fundamental characteristics of soft matter is complexity [41]: the macroscopic behaviour of these materials stems from their mesoscale constituents, which can be polymers, colloidal grains, droplets, etc., rather than from their atomic or molecular structure. Colloids are fundamental constituents of soft matter, that modern technology allows us to manipulate relatively easily. They are therefore both ideal probes and constituents of existing and potentially new soft materials. Here we will discuss both these uses of colloidal particles.

1.4.3 Colloids as Probes of Soft Matter

The value of colloids as probes of soft matter stems primarily from their size. Colloids are large enough to make quantum effects negligible in most cases, so that their motion follows Newton's laws, provided that thermal fluctuations are taken into account. Moreover, position and velocities can be measured through optical tracking and the forces they are subject to can be inferred.

Microrheology

In microrheology the motion of colloidal particles is studied in order to infer the viscoelastic properties of the complex fluid in which they are embedded. Viscoelasticity relates to the way the material stores and dissipates energy. These properties have traditionally been studied using rheometers, that allow to apply stresses to the whole fluid and to measure its global response. Embedding particles in a fluid allows to study the storage and dissipation of mechanical energy at a microscopic scale (micrometer or sub-micrometer). These techniques have several advantages with respect to bulk macrorheology. In particular they do not require the use of large samples of materials that could be expensive and difficult to get, especially in the case of biological systems. Moreover they allow to minimise the risk of damage caused during the measurement, and they require equipment that is usually available in a soft matter lab. Agreement between such a microscopic characterisation and bulk measurements has been found for a subset of complex fluids, but this is not always the case. This is importantly affected by the size of inherent heterogeneities with respect to the one of the probe particles. When these two length scales are comparable, the probes' dynamics,

and therefore the properties that are measured, depend strongly on their position. This does not allow to infer bulk properties from the motion of small particles, but it proves that microrheology constitutes a useful tool for the characterisation of local properties that are not accessible through rheometers.

In *passive* microrheology the Brownian motion of probe particles is visualised and tracked with optical microscopy in order to measure their diffusion coefficient. The classical way of interpreting these experiments is through the fluctuation-dissipation theorem which, for a spherical particle having radius R, subject to thermal fluctuations, can be written in the form of the Stokes-Einstein law, relating the diffusion coefficient D to the fluid viscosity η:

$$D = \frac{k_B T}{6\pi\eta R}, \tag{1.9}$$

where k_B is the Boltzmann constant and T the temperature. In *active* microrheology the motion of probe particles subject to external fields is studied. One way of doing that is through optical tweezers. These exploit the radiation pressure of light to trap a colloid at the focus of a laser beam and to apply forces on it. Particle tracking is then done by measuring the light scattered by the particle. When e.g. a constant force is applied to the particle, the latter experiences a drag force that is related to the viscosity η of the fluid through Stokes' law:

$$F = 6\pi\eta R v, \tag{1.10}$$

where v is the velocity of the colloid at steady state.

1.4.4 Colloids as Building Blocks for New Materials

Physicists have for long tried to understand the molecular self-assembly of complex and hierachical materials, e.g. molecular crystals, viral capsids, and lipid bilayers, such as the ones that constitute the cell membrane [42]. One way of understanding the self-organisation of such systems consists of modelling single molecules as patchy particles, i.e. as particles with highly directional interactions [43]. This framework has then been directly exported to soft matter, where colloidal particles with characteristics very similar to the ones of simple coarse-grained models for molecular systems can now be easily synthesised [43, 44]. An

important goal of soft matter has been to design new materials with desired structure by means of colloidal particles whose interactions we can now easily tune. A whole zoo of particles is now available (see e.g. [45, 46, 47]). DNA-coated patchy particles attract each-other thanks to sticky ends that allow for selective and strongly directional interactions [43]. Polyhedra self-assemble into ordered structures driven by entropy maximisation, which is enhanced by the presence of flat facets [48]. Depletion interaction between particles with complementary shapes allows for a lock-key selective recognition mechanism [49]. What is common to all these examples is anisotropy of the interactions, induced through a wise design of the particles. One can alternatively consider the case where perfectly spherical hard particles are embedded in an anisotropic fluid. The defects that form close to the colloidal surface due to colloid-liquid crystal interactions resemble long range attractive patches and can drive colloidal assembly [50, 51, 52]. In this thesis we will be interested in the case of active liquid crystals used as ambient fluids, both in their quiescent and in their spontaneously flowing regimes. We will study both the impact of colloids on the phase transition to a spontaneous flow, and the role of the latter on the collective behaviour of colloids.

Chapter 2

Model

In this chapter we will introduce the model applied to describe liquid crystals and active fluids. In both cases we want to take into account hydrodynamic interactions between the particles and will use a continuous description. The case of active fluids is obtained from the one of liquid crystals by considering each particle as a force dipole. It is possible to show [21], and we will review the full phenomenological derivation here, that the only effect is an additional stress term in the equation for the conservation of momentum.
We will first present the model for liquid crystals, starting from introducing the free-energy terms that are needed to describe the nematic phase and the transition from the isotropic one. We will also present the free energy term that models contact with a surface.
We will then introduce hydrodynamic equations for liquid crystals, that are obtained by coupling the Navier-Stokes and the continuity equations, for the conservation of momentum and mass, with the Beris-Edwards equation, that describes the relaxation of a system towards the minimum of the free-energy [53].
At the end of the chapter we will introduce the active stress with which the Navier-Stokes for liquid crystals has to be corrected in order to account for the dipolar character of active forces.

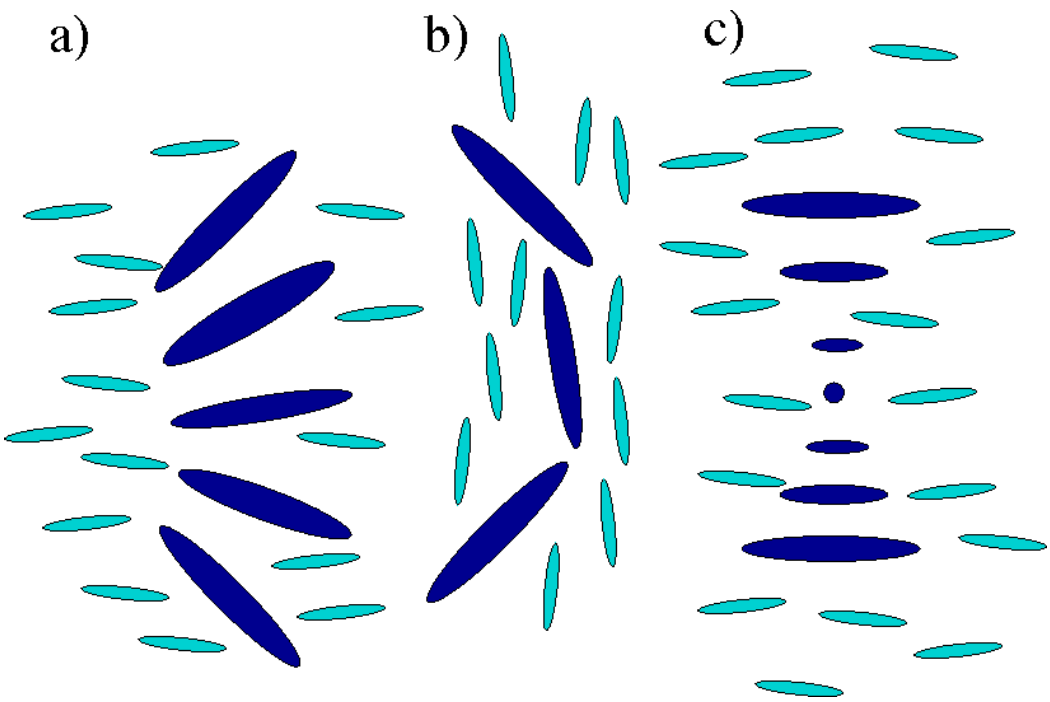

Figure 2.1: Deformations that can be encountered in nematic liquid crystals: panel (a) shows a typical splay deformation, panel (b) refers to bending and (c) to twist.

2.1 Modelling Liquid Crystals: The Free Energy

We will now present the two fundamental contributions to the effective free energy that are necessary to describe the physics of liquid crystals. We will focus on the nematic and the cholesteric phases, even though the final form, written in terms of Q is general.

2.1.1 Elastic Free Energy

It took a long time to physicists to find the form of the free energy that was able to describe equilibrium properties of nematic liquid crystals. Frank eventually wrote an equation for the elastic contribution that describes distortions of the ordered phase [54]. Such deformations are unfavoured with respect to the ordered liquid crystals and can be divided into splay, bend and twist (described in Fig. 2.1.1), leading to the following free-energy density:

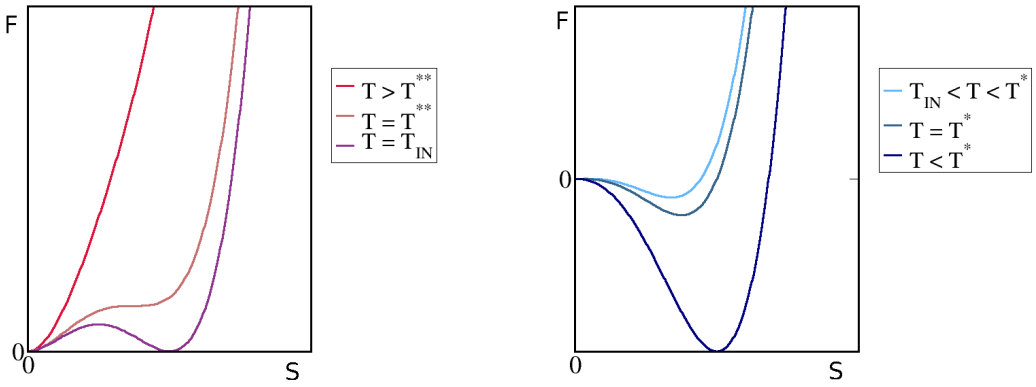

Figure 2.2: Behaviour of $\mathcal{F}_{bulk}$ for some representative values of the temperature T: when $T > T^{**}$ $\mathcal{F}_{bulk}$ only has one minimum at $S = 0$, corresponding to the isotropic phase. Reducing the temperature results into the appearance of a secondary minimum at $S > 0$, which becomes equivalent to the one in $S = 0$ when the temperature T_{IN} is reached. For temperatures between T_{IN} and T^*, $S = 0$ is only a secondary minimum, while for $T \geq T^*$, there is only one minimum, at $S > 0$.

$$\mathcal{F}_{el} = \frac{K_{11}}{2}(\vec{\nabla} \cdot \hat{n})^2 + \frac{K_{33}}{2}(\hat{n} \times (\vec{\nabla} \times \hat{n}))^2 + \frac{K_{22}}{2}(\hat{n} \cdot (\vec{\nabla} \times \hat{n}))^2. \tag{2.1}$$

In particular, the term proportional to K_{11} describes splay, the one in K_{22} describes twist, and finally the term with K_{33} describes bending deformations. It is common, especially among theoreticians, to consider $K = K_{ii}$, $i = 1, 2, 3$. This is referred to as *one elastic constant approximation* and does not compromise the qualitative physical picture of the system. We will adopt it in our description. Within this approximation $\mathcal{F}_{el}$ can more generally be written in terms of Q:

$$\mathcal{F}_{el} = \frac{K}{2}(\vec{\nabla}\mathsf{Q})^2. \tag{2.2}$$

2.1.2 Bulk Free Energy Density and Isotropic-to-Nematic Phase Transition

The elastic free energy density describes nematic liquid crystals only far from the isotropic-nematic transition T_{IN}, at $T \ll T_{IN}$ (i.e. deep in the ordered phase).

The symmetry breaking can be captured through a classic Landau approach,

by writing an effective free energy on the basis of the characteristic symmetries of the system, and by stopping at a high enough order to describe a phase transition. In the case of nematic liquid crystals we require that $\mathcal{F}_{bulk}$ is invariant under all rotations. Since tensors and vectors are not invariant under rotations, we need to consider scalar quantities that can be built out of Q. These are the traces $\mathrm{Tr}\ \mathsf{Q}^p$, $p \in \{2, 3, \dots\}$ since $\mathrm{Tr}\ \mathsf{Q} = 0$. The bulk free-energy density, up to fourth order, is:

$$\mathcal{F}_{bulk} = \frac{a}{2}\mathrm{Tr}\ \mathsf{Q}^2 - \frac{b}{3}\mathrm{Tr}\ \mathsf{Q}^3 + \frac{c}{4}(\mathrm{Tr}\ \mathsf{Q}^2)^2, \tag{2.3}$$

where a, b and c are constants; a is proportional to $T - T^*$, where T^* is the *spinodal* temperature (smaller than T_{IN}) below which the isotropic phase stops being a metastable secondary minimum. The discontinuity of the order parameter as a function of the temperature is allowed by the third order term[1]. It can be shown that, since Q is a 3×3 traceless and symmetric matrix, $\mathrm{Tr}\ \mathsf{Q}^4$ is strictly proportional to $(\mathrm{Tr}\ \mathsf{Q}^2)^2$, so that we can include only the latter in $\mathcal{F}_{bulk}$ [55]. [2]

Eq. 2.3 describes a phase transition characterised by a critical temperature T_{IN}, below which the absolute minimum of the free energy goes from $S = 0$ to a non-zero value, corresponding to the nematic phase.

The presence of a third order term allows for the appearance of asymmetries in $\mathcal{F}_{bulk}$, so that secondary minima develop, corresponding to metastable states. In particular, there are the spinodal temperature T^*, below T_{IN}, as explained above, and a temperature T^{**} above which the nematic phase stops being a metastable phase. The functional dependence of $\mathcal{F}_{bulk}$ on S is displayed in Fig. 2.2.

The existence of metastable states and the whole phenomenology of the isotropic-to-nematic phase transition is important for understanding the physics of liquid crystals and will be important later on in this thesis to understand our choice of parameters in simulations.

It is worth mentioning here that we rewrite Eq. 2.3 as:

$$\mathcal{F}_{bulk} = \frac{A_0}{2}\left(1 - \frac{\gamma}{3}\right)\mathrm{Tr}\ \mathsf{Q}^2 - \frac{A_0\gamma}{3}\mathrm{Tr}\ \mathsf{Q}^3 + \frac{A_0\gamma}{4}(\mathrm{Tr}\ \mathsf{Q}^2)^2, \tag{2.4}$$

where γ is related to the temperature or to the concentration according to whether

[1] The latter would not be there in a system described by a vectorial order parameter, and in that case the transition would be second order instead of first order.

[2] According to Eq. 1.3 the traces that appear in Eq. 2.3 are proportional to powers of S, so that $\mathcal{F}_{bulk}$ can be rewritten only in terms of the scalar order parameter S, that is enough to describe the isotropic-nematic phase transition.

thermotropic or lyotropic liquid crystals are considered.

2.1.3 Surface Free Energy

Another term needs to be taken into account when the liquid crystal is in contact with a surface. In that case there are usually two possible types of anchoring: normal (or homeotropic) anchoring, when the rodlike particles are directed orthogonally to the surface, and planar (or homogeneous) anchoring, when they lie parallel to it. This can be either *degenerate* or *fixed*. In the first case all possible orientations in the plane are allowed, in the second case a specific direction along the plane is imposed. The surface free-energy density term is:

$$\mathcal{F}_s = \frac{1}{2} W (Q_{\alpha\beta} - Q^0_{\alpha\beta})^2, \tag{2.5}$$

where W is the parameter controlling the anchoring strength, and Q^0 denotes the order parameter at the surface. In the case of normal anchoring and of fixed planar anchoring a director $\hat{n}^0$ can be defined at the colloidal surface, so that: $Q^0_{\alpha\beta} = S_0(n^0_\alpha n^0_\beta - \frac{\delta_{\alpha\beta}}{3})$, where S_0 quantifies the degree of order on the surface. This is the expression that we will use to model the anchoring of the liquid crystal at the surface of a colloid. In that case it is useful to define an adimensional anchoring strength:

$$w = \frac{WR}{K}, \tag{2.6}$$

where R denotes the radius of the colloid. For $w \ll 1$ the system is characterised by *weak* anchoring, while *strong* anchoring corresponds to $w > 1$.

2.2 Modelling Liquid Crystals: Hydrodynamic Description

Hydrodynamic equations for liquid crystals need to describe the time evolution of the fluid density, of the fluid momentum and of the order parameter for liquid crystals, by taking into account the coupling of the fluid flow with the liquid crystal elastic properties.

2.2.1 Beris-Edwards Equation for the Evolution of the Order Parameter

The hydrodynamic equation for the evolution of the order parameter is:

$$(\partial_t + \vec{u} \cdot \vec{\nabla})\mathsf{Q} - \mathsf{S}(\nabla \mathsf{u}, \mathsf{Q}) = \Gamma \mathsf{H}, \tag{2.7}$$

where Γ is a collective rotational diffusion coefficient. The second term of Eq. 2.7 describes the advection of the order parameter. The latter being a tensor, it can be associated to an ellipsoid and therefore it can not only be advected, but also rotated and stretched by the fluid; these actions are described by $\mathsf{S}(\nabla \mathsf{u}, \mathsf{Q})$, where $\nabla \mathsf{u}$ is the velocity gradient tensor $\partial_\beta u_\alpha$. The complete expression for S is:

$$\begin{aligned} \mathsf{S}(\nabla \mathsf{u}, \mathsf{Q}) = &(\xi \mathsf{D} + \Omega)\left(\mathsf{Q} + \frac{\mathsf{I}}{3}\right) + \left(\mathsf{Q} + \frac{\mathsf{I}}{3}\right)(\xi \mathsf{D} - \Omega) \\ &- 2\xi \left(\mathsf{Q} + \frac{\mathsf{I}}{3}\right) \mathrm{Tr}(\mathsf{Q} \nabla \mathsf{u}), \end{aligned} \tag{2.8}$$

where $\nabla \mathsf{u}$ is the velocity gradient tensor $\partial_\alpha u_\beta$, $\mathsf{D} = (\partial_\alpha u_\beta + \partial_\beta u_\alpha)/2$, and $\Omega = (\partial_\alpha u_\beta - \partial_\beta u_\alpha)/2$. The parameter ξ is related to the aspect ratio of nematogens [56] and to the *flow tumbling* or *flow aligning* nature of the liquid crystals. Flow-aligning nematogens (obtained e.g. for $\xi > 0.6$ when $\gamma = 3$, or large enough ξ) assume a fixed angle with respect to the flow direction (Leslie angle), while flow-tumbling ones (e.g. $\xi \leq 0.6$ for $\gamma = 3$, or small enough ξ) continuously change their orientation, in a chaotic way. Hereon we will refer only to flow aligning particles, since a flow tumbling behaviour would introduce a more complex scenario on top of the one determined by activity [20].

The right-hand side of Eq. 2.7 describes the relaxation of the order parameter towards an equilibrium configuration. The tensor H is called the *molecular field* and it is obtained by taking the symmetric and traceless part of the functional derivative of the free energy $F = \int d^3x \mathcal{F}(\vec{x})$ with respect to the order parameter $Q_{\alpha\beta}$:

$$H_{\alpha\beta} = -\frac{\delta F}{\delta Q_{\alpha\beta}} + \frac{\delta_{\alpha\beta}}{3} \mathrm{Tr} \frac{\delta F}{\delta \mathsf{Q}}. \tag{2.9}$$

2.2.2 Navier-Stokes Equation

The equation for the fluid density ρ is simply the continuity equation:

$$\partial_t \rho + \partial_\alpha \rho u_\alpha = 0. \tag{2.10}$$

We note that here, as in the remainder of this thesis, we adopted Einstein's convention, according to which summation over repeated indices is understood. The evolution of momentum for an incompressible fluid ($\partial_\alpha u_\alpha = 0$) is described by a modified Navier-Stokes equation where new stress terms are introduced:

$$\rho(\partial_t + u_\beta \partial_\beta) u_\alpha = \eta \partial_\beta (\partial_\beta u_\alpha + \partial_\alpha u_\beta) + \partial_\beta \Pi^p_{\alpha\beta}. \tag{2.11}$$

Here $\Pi^p_{\alpha\beta}$ is the liquid crystal *stress tensor* whose detailed full expression is [53]:

$$\begin{aligned} \Pi^p_{\alpha\beta} = &- P\delta_{\alpha\beta} + 2\xi \left(Q_{\alpha\beta} + \frac{1}{3}\right) Q_{\gamma\epsilon} H_{\gamma\epsilon} \\ &- \xi H_{\alpha\gamma} \left(Q_{\gamma\beta} + \frac{1}{3}\delta_{\gamma\beta}\right) - \xi \left(Q_{\alpha\gamma} + \frac{1}{3}\delta_{\alpha\gamma}\right) H_{\gamma\beta} \\ &- \partial_\alpha Q_{\gamma\nu} \frac{\delta \mathcal{F}}{\delta \partial_\beta Q_{\gamma\nu}} + Q_{\alpha\gamma} H_{\gamma\beta} - H_{\alpha\gamma} Q_{\gamma\beta}. \end{aligned} \tag{2.12}$$

In the case of a simple fluid $\Pi^p_{\alpha\beta} = -P\delta_{\alpha\beta}$, where P is the isotropic pressure.

2.3 Modelling Active Fluids: Hydrodynamic Equations

Since active particles often have an elongated shape, they tend to form long range orientationally ordered phases when their concentration is large enough [5]. In our description this is considered as an inherent property of the system, captured just by considering it as a liquid crystal, whose behaviour, if at equilibrium, would be described through the Landau - de Gennes free energy and whose dynamics in the absence of activity, would be captured by the hydrodynamic equations that were introduced in the previous sections. In that framework the countinuous stirring of the ambient fluid by active particles is taken into account through some extra terms.

Ramaswamy *et al.* examined the role of the fluid flow and its coupling with

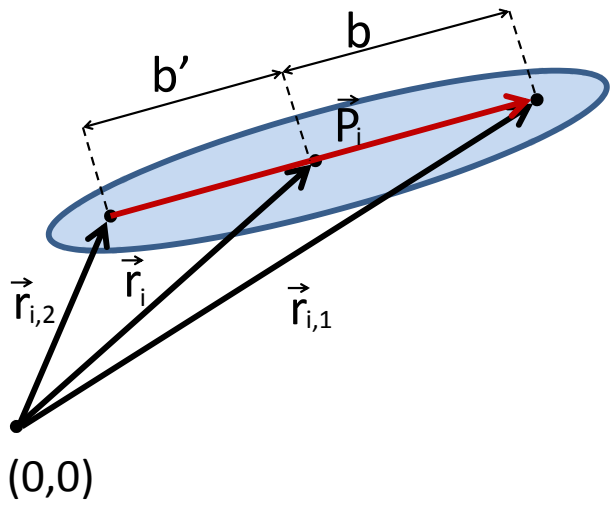

Figure 2.3: This figure explains the notation used in the derivation of the active stress.

activity and with liquid crystals elastic properties in [57], where a correction to the stress tensor in the Navier-Stokes equation, as a consequence of the stirring exerted by active particles on the fluid, is proposed. The same hydrodynamic equations were derived by Liverpool *et al.* in [58], starting from a specific microscopic model.

Hydrodynamic equations for active matter are obtained from Eq. 2.7, 2.10 and 2.11, by correcting the latter with an additional stress term that takes into account the forces that active particles exert on the fluid. This description is continuous, i.e. we will not resolve the motion of single particles, but rather describe an active fluid as a continuum.

Let us consider a system of N active particles at a fixed time t and let $\vec{r}_i$ be the centre of the i-th particle, which is represented in Fig. 2.3. Let $\vec{P}_i$ be the unit vector that connects the head of the particle to its tail. The particle being a force dipole, it will have point forces of equal magnitude f directed along $\pm\vec{P}_i$ and applied in points $\vec{r}_{i,1} = \vec{r}_i + b\vec{P}_i$ and $\vec{r}_{i,2} = \vec{r}_i - b'\vec{P}_i$, where b and b' are the distances of the points where the active forces are applied from the particle centre, as sketched in Fig. 2.3. For apolar particles $b = b'$, while $b \neq b'$ implies that the particles are polar (even though a particle can be polar and still have

its centre of mass placed in the middle). The total force density $\vec{f_i}$ exerted by the i-th particle on the fluid is $\vec{f_i} = \vec{f_{i,1}} + \vec{f_{i,2}}$, where $\vec{f_{i,1}}$ and $\vec{f_{i,2}}$ are the force densities acting respectively on $\vec{r}_{i,1}$ and $\vec{r}_{i,2}$:

$$\vec{f_i} = f\vec{P_i}\left(\delta(\vec{r} - \vec{r_i} - b\vec{P_i}) - \delta(\vec{r} - \vec{r_i} + b'\vec{P_i})\right). \tag{2.13}$$

The total force density exerted globally on the fluid can be obtained by summing over all the particles. Since we are interested in hydrodynamic effects, which are long range, we can consider that the size of active particles is negligible with respect to the space scale we are looking at ($|\vec{r} - \vec{r_i}| \gg b, b'$). In that case we can make an expansion of the total force density in terms of b and b', and stop at the first non-zero term, as follows:

$$\vec{f^a} \sim f \sum_{i=1}^{N} \vec{P_i}(\delta(\vec{r} - \vec{r_i}) - b\vec{P_i} \cdot \vec{\nabla}\delta(\vec{r} - \vec{r_i}) - \delta(\vec{r} - \vec{r_i}) - b'\vec{P_i} \cdot \vec{\nabla}\delta(\vec{r} - \vec{r_i})), \tag{2.14}$$

so that the α-th component of $\vec{f^a}$ is:

$$f^a_\alpha = -(b + b')f \sum_{i=1}^{N} P_{i,\alpha} P_{i,\beta} \partial_\beta \delta(\vec{r} - \vec{r_i}). \tag{2.15}$$

$\vec{P_i}$ is independent of $\vec{r}$ and it is therefore possible to include $P_{i,\alpha}$ and $P_{i,\beta}$ inside the partial derivative. This allows to express the total active force as the divergence of a tensor, that represents the active contribution to the stress tensor. In the case of large N, the quantity $\sum_{i=1}^{N} P_{i,\alpha} P_{i,\beta} \delta(\vec{r} - \vec{r_i})$ can be considered as a coarse-grained average of $P_{i,\alpha} P_{i,\beta}$, times the average concentration of particles ϕ [21], whose derivative is equal to that of $\phi Q_{\alpha\beta}$ (see Eq. 1.2), so that:

$$f^a_\alpha = -\zeta \partial_\beta Q_{\alpha\beta}, \tag{2.16}$$

where $\zeta = f(b + b')\phi$ is the *activity coefficient* of the active fluid; it has the dimension of a stress and it is therefore measured in Pa. Contractile dipoles are directed inwards along $\vec{P_i}$ ($f < 0$), while extensile dipoles are directed outwards in that same direction ($f > 0$). Therefore ζ is negative in the contractile case

and positive for extensile active fluids.

The force density $\vec{f}^a$ is the correction that has to be included in the right side of the Navier-Stokes equation (Eq. 2.11) in order to take into account activity. That term can be written as the divergence of a stress tensor with the form:

$$\Pi^a_{\alpha\beta} = -\zeta \left(Q_{\alpha\beta} + \frac{1}{3}\delta_{\alpha\beta} \right). \tag{2.17}$$

It is important to point out here that, at first order, the active stress tensor only depends on $b+b'$ and not on $b-b'$. This means that polar and apolar active fluids should display similar rheological properties. With this in mind, in our simulations we will always consider equations for nematic active liquid crystals, without taking polarity into account[3].
The complete form of Navier-Stokes equation in the case of an active fluid becomes therefore:

$$\rho(\partial_t + u_\beta \partial_\beta) u_\alpha = \eta \partial_\beta (\partial_\beta u_\alpha + \partial_\alpha u_\beta) + \partial_\beta \Pi^p_{\alpha\beta} + \partial_\beta \Pi^a_{\alpha\beta}. \tag{2.18}$$

This equation is coupled to Eq. 2.7 for the evolution of the order parameter Q.

[3]Most of the biologically interesting systems, such as suspensions of bacteria and the cytoskeleton, consist of polar particles. The reason for considering an apolar theory is that, as just explained, the stress tensor to lowest order (Eq. 2.17) is the same.

Chapter 3

Methods

3.1 Lattice Boltzmann Method for Simple Fluids

After having presented the physics behind our study, we will now explain the numerical technique that we used in our simulations. Lattice Boltzmann (LB) methods represent a powerful numerical tool that exploits the equivalence between the Boltzmann equation, and the Navier-Stokes and the continuity equations, which avoids the need to deal with numerical second-order partial differentiation. We will now describe this method for a simple fluid, and say briefly how this is applied to our case. A review with the description of some applications to complex fluids can be found in [59].

The most general case of a compressible fluid, which is described by the Navier-Stokes equation in the form:

$$\rho\left(\partial_t + u_\beta \partial_\beta\right) u_\alpha = -\partial_\beta P_0 \delta_{\alpha\beta} + \partial_\beta \left[\eta(\partial_\alpha u_\beta + \partial_\beta u_\alpha) + \left(\mu - \frac{2}{3}\right)\partial_\gamma u_\gamma \delta_{\alpha\beta}\right], \quad (3.1)$$

where μ is the *bulk viscosity* and describes the response to compression. The evolution in time of the fluid density is simply decribed by the continuity equation (Eq. 2.10).

The Boltzmann equation describes the approach to equilibrium of the distribution function $f(\vec{x}, \vec{v}, t)$, which is proportional to the probability of finding a fluid particle at point $\vec{x}$, at time t, with velocity $\vec{v}$ and therefore gives a mesoscopic description of the system. Its complete form is:

$$\left(\frac{\partial}{\partial t} + \vec{v}\frac{\partial}{\partial \vec{x}} + \vec{a}\frac{\partial}{\partial \vec{v}}\right) f(\vec{x}, \vec{v}, t) = \left(\frac{\partial}{\partial t} f(\vec{x}, \vec{v}, t)\right)_{coll}, \tag{3.2}$$

where the last term represents the variation in time of the probability density $f(\vec{x}, \vec{v}, t)$ due to collisions between particles, and $\vec{a} = \partial\vec{v}/\partial t$.

The equivalence between Eq. 3.2 and Eq. 3.1 can rigorously be shown by defining macroscopic hydrodynamic quantities, such as the fluid local density $\rho(\vec{x}, t)$ and the fluid local velocity $\vec{u}(\vec{x}, t)$, in terms of the first and of the second momenta of $f(\vec{x}, \vec{v}, t)$.

The idea at the basis of LB methods is the one of exploiting the equivalence between the Navier-Stokes equation, which is numerically difficult to solve, and the Boltzmann equation, that is instead much easier to deal with, being a relaxation equation, where only first order derivatives are involved.

We note here that the majority of fluids have a very small compressibility when in the liquid phase, and are better described by the Navier-Stokes equation in the incompressible limit. This leads to a constraint on pressure which is hard to handle numerically. Lattice Boltzmann instead considers a compressible fluid, where $P = \rho c_s^2$, c_s is the speed of sound. Provided that the fluid velocity $\vec{u}$ is everywhere such that $u \ll c_s$[1], compressible effects are negligible.

3.1.1 Lattice Boltzmann Equation

LB methods deal with mesoscopic quantities, but just in order to catch the macroscopic behaviour of the system: an equation for $f(\vec{x}, \vec{v}, t)$ is solved, in order to obtain $\rho(\vec{x}, t)$ and $\vec{u}(\vec{x}, t)$. In LB $\{\vec{x}\}$ is only allowed to vary on a lattice, such that the lattice spacing in all cartesian directions are $\Delta x_\alpha = 1$, and time is discretised. Moreover, since we are not interested in the microscopic picture, approximations at the mesoscopic level (i.e. in the Boltzmann equation) are allowed, as far as it is still possible to maintain the equivalence with the Navier-Stokes equation. It is therefore not necessary to consider all the continuous values that the velocity $\vec{v}$ of a microscopic particle constituting the fluid can assume, and the lattice Boltzmann method is actually based on the choice of a minimal discretised set of velocities $\{\vec{e}_i\}_{i=0,\ldots,N_Q-1}$ in the phase space, where N_Q denotes the number of velocities allowed to a certain particle and $\vec{e}_0$ is the null

[1] In practice $u \lesssim 0.1$ with $c_s = \frac{1}{\sqrt{3}}$ is good enough.

vector. Including also $\vec{e}_0$ is important especially in the case of a fluid close to the limit of incompressibility [59]. The discrete set of velocities is chosen in order to recover the Navier-Stokes and the continuity equations and it has to satisfy some symmetry criteria for that to be possible. Different choices are available at a given dimensionality. The compact notation DdQN_Q is used to identify the scheme used in a certain dimensionality d. In the case of $d = 2$ the usual choice is D2Q9, which includes the following choice of velocities:

$$\vec{e}_0 = (0,0); \tag{3.3}$$

$$\vec{e}_{1,2} = (\pm 1, 0) \tag{3.4}$$

$$\vec{e}_{3,4} = (0, \pm 1); \tag{3.5}$$

$$\vec{e}_{6-8} = (\pm 1, \pm 1). \tag{3.6}$$

In the case of a three dimensional system the most stable schemes are D3Q15 and D3Q19. The code that we used to implement lattice Boltzmann applies the latter. We will use the notation $f_i(\vec{x}, t)$ for the probability density of a certain particle to be at position $\vec{x}$ on the lattice, at time t, with a velocity $\vec{e}_i$ in $\{\vec{e}_j\}_{j=0,\ldots,N_Q-1}$. In this framework, the discretised Boltzmann equation becomes:

$$f_i(\vec{x} + \vec{e}_i \Delta t, t + \Delta t) = f_i(\vec{x}, t) + C_i(f_i^{eq}(\vec{x}, t), f_i(\vec{x}, t))\Delta t, \tag{3.7}$$

where the Euler method for first order differentiation was applied.

The relations between the mesoscopic function f_i and the macroscopic functions $\rho(\vec{x}, t)$ and $\vec{u}(\vec{x}, t)$, which at the end will allow a complete description of the fluid, are:

$$\rho(\vec{x}, t) = \sum_{i=0}^{N_Q-1} f_i(\vec{x}, t); \tag{3.8}$$

$$\rho(\vec{x}, t)\vec{u}(\vec{x}, t) = \sum_{i=0}^{N_Q-1} \vec{e}_i f_i(\vec{x}, t). \tag{3.9}$$

In general, the collision term on the right-hand side of Eq. 3.2 can be very complicated and it is based on the microscopic description of the system. The advantage of the LB method is that it can be chosen as having a very

simple form, that allows to easily solve the Boltzmann equation numerically, still maintaining the equivalence with the exact Navier-Stokes equation. This is possible because we only need to care about being accurate at the macroscopic scale. A suitable choice is to consider C_i in Eq. 3.7 to be a linear collision operator: $C_i = L_{ij}(f_j(\vec{x},t) - f_j^{eq}(\vec{x},t))$. The lattice Boltzmann equation takes therefore the form:

$$f_i(\vec{x} + \vec{e}_i\Delta t, t + \Delta t) = f_i(\vec{x},t) + L_{ij}\left(f_i(\vec{x},t) - f_i^{eq}(\vec{x},t)\right)\Delta t. \tag{3.10}$$

3.1.2 The BGK Approximation

In most cases it is possible to simplify the collision operator even further. Particularly one can consider that all the N_Q propagation modes are characterised by the same relaxation time τ. In this hypothesis L_{ij} is diagonal and equal to $-\delta_{ij}/\tau$. This is called *single relaxation time* or BGK (Bhatnagar-Gross-Krook) approximation [60], and it is the one applied in the code that we used. The lattice Boltzmann equation in this case becomes:

$$f_i(\vec{x} + \vec{e}_i\Delta t, t + \Delta t) = f_i(\vec{x},t) + \frac{f_i^{eq}(\vec{x},t) - f_i(\vec{x},t)}{\tau}\Delta t. \tag{3.11}$$

Despite the fact that the BGK approximation might give some numerical-stability problems, it allows to simplify significantly the study of a fluid flow: the LB equation becomes now a very simple linear relaxation equation, which is much less computationally costly than Eq. 3.1, while the equivalence with the latter can be maintained by imposing specific conditions on f_i^{eq}. Moreover it is a local equation, which makes it very easy to parallelise codes that implement the method.

3.1.3 Equivalence between LB Equation and the Navier-Stokes

Imposing the equivalence between Eq. 3.1 and Eq. 3.11 is done through the Chapman-Enskog expansion of the probability density function f_i around f_i^{eq} [59]. Here we will just summarise the key aspects, needed to understand how the method works.

- The Chapman-Enskog expansion results into four constraints to be imposed on $f_i^{eq}(\vec{x},t)$, which are the following:

$$\sum_i^{N_Q-1} f_i^{eq}(\vec{x},t) = \rho \tag{3.12}$$

$$\sum_i^{N_Q-1} f_i^{eq}(\vec{x},t)e_{i,\alpha} = \rho u_\alpha \tag{3.13}$$

$$\sum_i^{N_Q-1} f_i^{eq}(\vec{x},t)e_{i,\alpha}e_{i,\beta} = \rho u_\alpha u_\beta - p\delta_{\alpha\beta} \tag{3.14}$$

$$\sum_i^{N_Q-1} f_i^{eq}(\vec{x},t)e_{i,\alpha}e_{i,\beta}e_{i,\gamma} = \rho c_s^2(u_\alpha\delta_{\beta\gamma} + u_\beta\delta_{\gamma\alpha} + u_\gamma\delta_{\alpha\beta}), \tag{3.15}$$

  where the last condition uses the equation of state $P = \rho c_s^2$.

- When verifying that Eq. 3.15 holds, it is possible to notice that the BGK approximation requires to impose a relation between the shear viscosity η and the bulk viscosity μ: $\mu = 2/3\eta$. This is a condition coming from the choice of a single relaxation time.

- The relaxation time τ is related to the fluid viscosity through a relation that depends on the integration scheme chosen when discretising the Boltzmann equation in 3.7. Having chosen the Euler scheme, we find that η depends on Δt, which is the integration step for the time variable. In particular:

$$\eta = c_s^2\rho\left(\tau - \frac{\Delta t}{2}\right). \tag{3.16}$$

3.1.4 Equilibrium Distribution Function

Eqs. 3.12-3.15 do not depend on the choice of the lattice, while f_i^{eq} is lattice-specific and it has to be computed for every choice of dimensionality and velocity set $\{\vec{e}_i\}$, and every time new terms are introduced in Eq. 3.1.

We will now perform the calculation in the simplest case of D2Q9, just to give a hint of the procedure followed. The case of D3Q19 that applies to us can be repeated in the same way. We consider the set of velocities in Eqs. 3.3 - 3.6. In order to simplify the analysis, it is convenient to group the elements of that

set into three subsets, which will be denoted with the index $s(i)$, related to their squared modulus: $s(i) = \vec{e}_i \cdot \vec{e}_i$. If in the continuum, and in the absence of body forces acting on the fluid, the equilibrium distribution function would simply be the Maxwell-Boltzmann distribution. In the case of a discrete phase space we can build an ansatz for f_i^{eq} by writing it as an expansion in terms of the fluid velocity. It is useful to calculate the moments associated to the velocity set in Eqs. 3.3-3.6. It can be shown, through direct calculation, and based on symmetry considerations, that:

$$\sum_i e_{i,\alpha}^{(s)} = \sum_i e_{i,\alpha}^{(s)} e_{i,\beta}^{(s)} e_{i,\gamma}^{(s)} = ... = 0 \text{ for all odd moments.} \tag{3.17}$$

In this notation, s is used as a shortening of $s(i)$ and refers to the subset which each velocity vector belongs to. Second and fourth moments are:

$$\sum_i e_{i,\alpha}^{(s)} e_{i,\beta}^{(s)} = \begin{cases} 0 & \text{if } s = 0; \\ 2\delta_{\alpha\beta} & \text{if } s = 1; \\ 4\delta_{\alpha\beta} & \text{if } s = 2. \end{cases} \tag{3.18}$$

$$\sum_i e_{i,\alpha} e_{i,\beta} e_{i,\gamma} e_{i,\epsilon} = \begin{cases} 2\delta_{\alpha\beta\gamma\epsilon} & \text{if s} = 1; \\ 4\left(\delta_{\alpha\beta}\delta_{\gamma\epsilon} + \delta_{\alpha\gamma}\delta_{\beta\epsilon} + \delta_{\alpha\epsilon}\delta_{\beta\gamma} - 2\delta_{\alpha\beta\gamma\epsilon}\right) & \text{if } s = 2. \end{cases} \tag{3.19}$$

Here $\delta_{\alpha\beta\gamma\epsilon}$ is defined as follows:

$$\delta_{\alpha\beta\gamma\epsilon} = \begin{cases} 1 & \text{if } \alpha = \beta = \gamma = \epsilon; \\ 0 & \text{otherwise.} \end{cases} \tag{3.20}$$

Knowing that all odd moments are zero, the only terms that we need to include in the expansion are even-order terms, which we consider up to the fourth order:

$$f_i^{eq} = A_{s(i)} + B_{s(i)} e_{i,\alpha} u_\alpha + C_{s(i)} u^2 + D_{s(i)} e_{i,\alpha} e_{i,\beta} u_\alpha u_\beta. \tag{3.21}$$

The coefficients $A_{s(i)}$, $B_{s(i)}$, $C_{s(i)}$, and $D_{s(i)}$ need to be determined so that Eqs. 3.12-3.15 are satisfied. A suitable solution for $f_i^{eq}(\vec{x}, t)$ is the following[2]:

[2]This is in general not unique.

$$f_i^{eq}(\vec{x},t) = w_i\rho(\vec{x},t)\left(1+\frac{e_{i,\alpha}u_\alpha}{c_s^2}+\frac{u_\alpha u_\beta(e_{i,\alpha}e_{i,\beta}-c_s^2\delta_{\alpha\beta})}{2c_s^4}\right), \tag{3.22}$$

which defines the weights $\{w_i\}_{i=0,\ldots,N_Q-1}$ associated to each direction of propagation.

3.1.5 Body Force

Eq. 3.1 refers to a fluid where the only sources of force are the isotropic pressure and the internal friction. In the most general case a body force $\vec{F}(\vec{x},t)$ acts on the fluid. When this is the case Eq. 3.1 has to be corrected with a term $F_\alpha(\vec{x},t)$ on the right hand side. This case is very relevant to us, because we are interested in solving hydrodynamic equations for liquid crystals and active fluids, where elastic and active forces have to be included in the equation for momentum conservation, as is done in Eq. 2.11. To take it into account, Eq. 3.11 has to be corrected with an additional term:

$$f_i(\vec{x}+\vec{e}_i\Delta t, t+\Delta t) = f_i(\vec{x},t)+\frac{f_i^{eq}(\vec{x},t)-f_i(\vec{x},t)}{\tau}\Delta t + p_i(\vec{x},t)\Delta t, \tag{3.23}$$

where p_i must be related to F_α through the relations:

$$\sum_i^{N_Q-1} p_i = 0; \tag{3.24}$$

$$\sum_i^{N_Q-1} e_{i,\alpha}p_i = F_\alpha. \tag{3.25}$$

$$\tag{3.26}$$

Note that when an external force acts on the system mass is conserved, but not momentum. It is worth mentioning here that when choosing the Euler integration scheme, as done so far, and imposing a body force on the system, the Chapman-Enskog expansion does not allow to get the continuity equation, but instead:

$$\partial_t\rho + \partial_\alpha(\rho u_\alpha) + \frac{1}{2}\partial_\alpha F_\alpha = 0, \tag{3.27}$$

from which the continuity equation can be recovered by redefining the velocity:

$$u_\alpha^* = u_\alpha + \frac{\Delta t}{2\rho} F_\alpha. \tag{3.28}$$

The Chapman-Enskog expansion also imposes a constraint on the second moment of the distribution $p_i(\vec{x}, t)$:

$$\sum_i p_i e_{i,\alpha} e_{i,\beta} = \left(1 - \frac{1}{2\tau}\right) \left(u_\alpha^* F_\beta + u_\beta^* F_\alpha\right). \tag{3.29}$$

3.1.6 Implementation of Lattice Boltzmann Method

One of the most important advantages of lattice Boltzmann methods is that Eq. 3.11 is very easy to solve. This is done in two separate steps: *collision* and *propagation*, that can be implemented in either order.

- *Collision.* The existing distribution $f_i(\vec{x}, t)$ is substituted by the post-collision distribution $f_i^*(\vec{x}, t)$, calculated as follows:

  $$f_i^*(\vec{x}, t) = f_i(\vec{x}, t) + \frac{f_i^{eq}(\vec{x}, t) - f_i(\vec{x}, t)}{\tau} \Delta t. \tag{3.30}$$

  Doing this requires to compute the equilibrium distribution function $f_i^{eq}(\vec{x}, t)$, that depends on the local density and velocity of the fluid, which can be computed by applying Eq. 3.8. It becomes very clear now what is the big advantage of working in a small and discretised phase space: the recovery of macroscopic quantities (the local density and momentum of the fluid) requires a summation over the whole velocity phase space, that would be very demanding and time consuming if it were continuous.

- *Propagation.* The distribution at point $\vec{x} + \vec{e}_i \Delta t$ is substituted with the post-collisional distribution $f_i^*(\vec{x}, t)$:

  $$f_i(\vec{x} + \vec{e}_i \Delta t, t + \Delta t) = f_i^*(\vec{x}, t). \tag{3.31}$$

  This step needs to be performed differently for different boundary conditions. In the next section we will show how to implement contact with a solid surface. Here we will show the case of periodic boundary conditions for

a D1Q3 lattice. The set of velocities in this case is simply $e_0 = 0$, $e_1 = 1$, $e_2 = -1$. Let us consider a system of size L, such that the coordinate x belongs to the one-dimensional lattice $\{1, 2, ..., L\}$. Periodic boundary conditions require $f_i(1,t) = f_i(L+1,t)$ and $f_i(L,t) = f_i(0,t)$ at all i, t.

3.1.7 Contact with a Fixed Solid Surface

The general problem in lattice Boltzmann when dealing with solid surfaces is that the probability density function f_i is not defined on those lattice sites that belong to the solid, and it is therefore necessary to find a criterion that allows to update its value on a site immediately out of the wall and to implement the desired boundary condition, also taking into account the exchange of momentum between the fluid and the solid. The contact surface between the fluid and the solid could either be placed right on the lattice nodes or at some point between two of them. It has been shown that computational error on the no-slip condition is minimised when the boundary is placed at half-way between a solid and a fluid node [61]. When the solid surface is not moving, one way to implement the case of zero relative velocity of the fluid close to the boundary with respect to the wall (no-slip condition), is to impose the reflection of f at the surface (*bounce-back* boundary conditions). To implement this, one has to identify all the 'outgoing' links $\{b\}$, such that $\vec{x}$ is in the fluid region but $\vec{x} + \vec{e}_b\Delta t$ is in the solid. Then the post-collision distribution at point $\vec{x}$, $f_b^*(\vec{x}, t)$, is computed exactly as in the absence of a boundary (fluid sites only are involved in this step). But in the propagation step close to the wall the 'outgoing' distribution $f_b^*(\vec{x}, t + \Delta t)$ has to be replaced by an incoming one $f_{b'}^*(\vec{x}, t + \Delta t)$, going in the opposite direction, i.e. such that $\vec{e}_{b'} = -\vec{e}_b$. Note that in this way mass is conserved, but the fluid transfers some momentum to the fixed solid wall, which does not move and therefore acts as a momentum sink.

3.1.8 Contact with a Moving Solid Surface

When considering a moving boundary, it is necessary to correct the reflected probability density function by a term that is proportional to the velocity with which the sites immediately inside it are moving. The easiest case to deal with is the one in which the solid is just a flat wall that moves parallel to the contact

surface, with a velocity $\vec{u}_b$. Note that $\vec{u}_b$ is the relative velocity of the wall with respect to the lattice, and not to the fluid. The condition that the fluid be close to the incompressible limit imposes a constraint on $\vec{u}_b$: $|\vec{u}_b| \ll c_s$. When moving, the solid trasfers some momentum to the fluid. This is taken into account by imposing that the propagation step after the collision is done as follows:

$$f^*_{b'}(\vec{x}, t + \Delta t) = f^*_b(\vec{x}, t) - \frac{2w_b\rho_0\vec{u}_b \cdot \vec{e}_b}{c_s^2}, \tag{3.32}$$

where w_b is the weight associated with the direction $\vec{e}_b$ and ρ_0 is the average density. Note that ρ_0 is used instead of the local density since it makes calculations much faster by introducing a negligible error on the total fluid mass. In this way, the fluid velocity is updated in order to take into account the change in the fluid momentum due to the interaction with the solid surface. Note that in the case of a surface that is not flat movement would imply the need to eliminate and to reintroduce fluid nodes as the surface moves.

3.1.9 Simulating Colloids

Important constituents of the systems that we want to describe are colloids. The description of the basic theory to simulate colloids within a lattice Boltzmann method can be found in [61] and [62, 63]. Here we will review some of the most important aspects. We consider a colloid as a hard sphere having a radius a and placed at a random position $\vec{r}_a$, not necessarily belonging to the lattice. Good enough representations of spheres in a discrete lattice are obtained when $a > 2$ [62]. The rule to update the distribution f^* (after collision-step) is now analogous to the one in Eq. 3.32, where now $\vec{u}_b$ is the total velocity of the colloid, including a translational and a rotational component, respectively $\vec{U}_c$ and $\vec{\Omega}$:

$$\vec{u}_b = \vec{U}_c + \vec{\Omega} \times \vec{r}_c, \tag{3.33}$$

where $\vec{r}_c = \vec{r}_b - \vec{r}_a$. Here $\vec{r}_b = \vec{x} + \frac{1}{2}\vec{c}_b\Delta t$.

Two conditions on the discrete colloid are in order, to guarantee mass conservation:

$$\sum_b w_b \vec{e}_b = 0 \tag{3.34}$$

$$\sum_b w_b (\vec{r}_b - \vec{r}_a) \times \vec{e}_b = 0. \tag{3.35}$$

It is possible to see that when these two conditions are satisfied the total fluid mass is conserved ($\sum_i f_i(\vec{x}, t) = \rho(\vec{x}, t)$ for each $\vec{x}$ in the lattice):

$$\begin{aligned}\sum_b \left(-2w_b\rho_0 \frac{\vec{u}_b \cdot \vec{e}_b}{c_s^2}\right) &= -\frac{2\rho w_b}{c_s^2} \sum_b (\vec{U}_c + \vec{\Omega} \times (\vec{r}_b - \vec{r}_a)) \cdot \vec{e}_b \\ &= -\frac{2\rho}{c_s^2} \left(\vec{U}_c \cdot \sum_b w_b \vec{e}_b + \vec{\Omega} \cdot \sum_b w_b (\vec{r}_b - \vec{r}_a) \times \vec{e}_b\right) \\ &= 0.\end{aligned} \tag{3.36}$$

Additionally, momentum is transferred from the fluid to the colloid, which results in a force for each link b equal to:

$$\frac{\Delta p}{\Delta t} = \vec{F}_b(\vec{x}, t) = \frac{\Delta x^3}{\Delta t} \left(2f_b^*(\vec{x}, t) - 2w_b\rho_0 \frac{\vec{u}_b \cdot \vec{e}_b}{c_s^2}\right). \tag{3.37}$$

Likewise, the torque exerted by the fluid on the colloid at link b is:

$$\vec{T}_b = \vec{r}_c \times \vec{F}_b. \tag{3.38}$$

The total force that the fluid exerts on the colloid is $\vec{F} = \sum_b \vec{F}_b$, and the total torque $\vec{T} = \sum_b \vec{T}_b$. These quantities allow to update the linear and angular velocity of the colloid, as one would do in a molecular dynamics scheme, treating the particle as a sphere. We note here that, rather than by the fixed radius a, the hydrodynamics of the colloid is described by the *hydrodynamic radius* a_h, that is defined according to Stokes' law: $\vec{F} = 6\pi\eta a_h \vec{U}_c$, and that changes according to the exact position of the particle on the lattice due to its discretised shape.

3.2 Lattice Boltzmann Method for Liquid Crystals and Active Fluids

This procedure allows to simulate a simple Newtonian fluid and to reproduce quite well its expected behaviour. The lattice Boltzmann method was shown to work well also for complex fluids. In the case of liquid crystals, it is necessary to modify the code that solves Eq. 3.10 in order to include in Eq. 3.1 the elastic stress terms referred to the liquid crystal (as in Eq. 2.11). The case of active fluids additionally requires to add the active stress term (see Eq. 2.17). Moreover, the equation for the evolution of the Q tensor needs to be solved. First applications of this method to liquid crystals applied the LB method also to the equation for the order parameter [64]. However, this technique was soon substituted by a hybrid lattice Boltzmann algorithm, in which the equation for the order parameter is solved through a standard finite-difference method, while for the Navier-Stokes equation the LB method is still applied. This hybrid algorithm revealed to have many advantages with respect to a full lattice Boltzmann approach, that would require a much larger memory storage and is theoretically cumbersome [20].

To solve Eq. 2.7, the distribution functions $f_i(\vec{x}, t)$, updated according to the lattice Boltzmann scheme, are used at each time step to compute the local velocity of the fluid. The latter is needed to calculate the tensor $\mathsf{S}(\nabla \mathsf{u}, \mathsf{Q})$ and the advective fluxes appearing in Eq. 2.7. For the latter, an upwind scheme is used, as a standard discretisation method for hyperbolic partial differentiation [65]. The tensor Q is then updated according to Eq. 2.7 via an Euler forward step.

3.2.1 Colloids in Liquid Crystals: Implementing Anchoring Conditions

The complication of introducing colloids in liquid crystals stems from the need to impose a specific orientation of the order parameter at the surface. The free-energy density describing interaction with a surface is described by Eq. 2.5. This expression for the surface free energy density has a minimum in Q^0, that needs to be fixed. Suitable choices of Q^0 allow therefore to implement conditions of homeotropic or planar anchoring, where the director is aligned along a certain

specific direction. This approach was followed in [1] for both normal and planar anchoring. Alternatively it is possible to consider a *degenerate* planar anchoring at the surface, where only the scalar order parameter is fixed at the interface between the colloid and the liquid crystal and the director is allowed to assume any direction in the plane tangent to the surface. An expression for the surface free energy density favouring this condition was presented in [66]. The aim is to write a free energy whose minima are placed at $Q_{\alpha\beta} = S_0(n_\alpha n_\beta - \frac{1}{3}\delta_{\alpha\beta})$, where $\hat{n}$ is a unit vector lying parallel to the colloidal surface and S_0 is fixed. To do that the tensors: $\tilde{Q}_{\alpha\beta} = Q_{\alpha\beta} + \frac{1}{3}S_0\delta_{\alpha\beta}$ were defined and the following form for the surface free energy density was proposed:

$$\mathcal{F}_{s,deg} = W_1 \left(\tilde{Q}_{\alpha\beta} - \tilde{Q}^{\perp}_{\alpha\beta}\right)\left(\tilde{Q}_{\alpha\beta} - \tilde{Q}^{\perp}_{\alpha\beta}\right) + W_2 \left(\tilde{Q}_{\alpha\beta}\tilde{Q}_{\alpha\beta} - S_0^2\right)^2. \tag{3.39}$$

Here $\tilde{\mathsf{Q}}^{\perp}$ denotes the projection of $\tilde{\mathsf{Q}}$ on the plane tangent to the colloidal surface. Moreover $W_1, W_2 > 0$. This is the expression that we used to implement planar anchoring in our simulations.

3.2.2 Spurious Velocities

When a particle is embedded in a liquid crystal and a certain anchoring is imposed at the surface, a non-physical flow develops close to the particle as a discretisation error related to the coupling of the Navier-Stokes and of the Beris-Edwards equations. An explanation for the case of a binary fluid is given in [67], while a similar calculation for the case of liquid crystals was done in [68]. In the Beris-Edwards equation the evolution of the order parameter Q is driven by the molecular field. Similarly, in the Navier-Stokes equation the forcing term $\partial_\beta \Pi^p_{\alpha\beta}$ is related to the gradient of H. However, due to discretisation, the identity between $\partial_\beta \Pi^p_{\alpha\beta}$ and its expression in terms of H holds only approximately. This is at the origin of spurious velocities.

One way to remove spurious velocities is to substitute $\partial_\beta \Pi^p_{\alpha\beta}$ with its expression in terms of H directly, in the Navier-Stokes. This has some important drawbacks: (i) now the discretised version of the forcing term in the Navier Stokes equation cannot be written as the divergence of a stress tensor any more. As a consequence, momentum is conserved only approximately; (ii) this substitution

originates numerical instabilities that can be removed only at the price of adding artificially some viscosity terms [67]. Spurious velocities are more important where there are large distortions in the order parameter – since these are related to a non-zero gradient of Q [68] and we observe them whenever dealing with a colloid in a liquid crystal, and $w > 0$, since defects form close to the colloidal surface. Spurious velocities do not play an important role in our microrheology simulations, since the flow generated by the motion of the colloid is always significantly larger than spurious velocities. In most cases there are about three orders of magnitude between the two. However, spurious velocities might be important when many colloids are embedded in a liquid crystal and interact at close distances. We believe that they hinder relaxation in the case of many colloids embedded in a passive liquid crystal. However, what we will be interested in, in that case, is the role of spontaneous flow, which is dominant ($\gtrsim 10^{-3}$ while spurious velocities are $\lesssim 10^{-5}$ – expressed in simulation units, that will be introduced in the chapters that follow). This will be discussed further in Chapters 6 and 7.

Chapter 4

Bulk and Micro-Rheology of Active Fluids

Introduction

Active fluids represent a broad category of materials, whose properties are novel and, to a big extent, still to be investigated. Main examples of active fluids, such as bacterial suspensions and the cytoskeleton (see Chapter 1) can be found in biology and understanding how these materials behave when they are subject to external forces might give important insight into their macroscopic behaviour and their potential.

Here we will present a study on the viscoelastic properties of active fluids where we simulate both macrorheology and microrheology experiments, with particular focus on the latter. The key paradigm for interpretation of microrheology experiments, independently of whether the Brownian motion of colloids is tracked or an external, constant force is applied, is Stokes' law. According to the latter the resistance that a micron-size particle experiences when dragged through the fluid (*local* property) is related to the viscosity, which is a *global* property, traditionally measured by shearing the fluid between two surfaces.

The fluctuation-dissipation theorem states the strong connection between the response of a system at or close to equilibrium to external forcing and its thermal fluctuations. Stokes' law allows to re-write the fluctuation-dissipation theorem for a spherical particle having radius R that performs Brownian motion, in terms of the Stokes-Einstein relation. Passive microrheology applies the latter

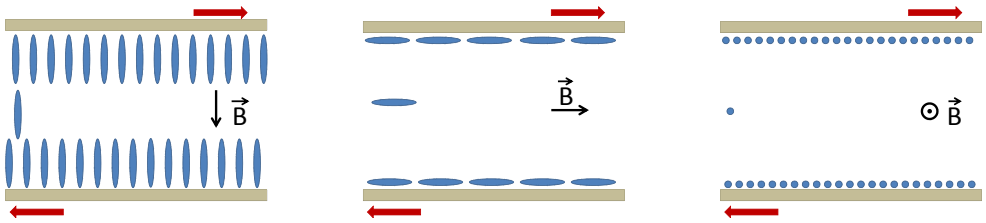

Figure 4.1: Sketch of the system considered in [2] to measure the viscosity of nematic liquid crystals: an external magnetic field (here denoted as $\vec{B}$) is used in order to maintain a fixed orientation of the liquid crystal with respect to the direction of shear.

to determine the diffusion coefficient of a particle by tracking its random motion in the absence of external forces.
On the other hand, the simplest experiment that one can think of in active microrheology, is based on the application of a constant force and on the measurement of the equilibrium velocity. This is the analogous, on a microscopic scale, of what happens in the 'falling ball' experiment, where a small sphere subject to gravity moves through a fluid. In the hypothesis of small Reynold's numbers, measuring the colloid limit velocity gives the viscosity of the fluid, to which it is related through Stokes' law.

In this chapter, after a brief review of the theoretical and experimental state of the art, we will present numerical results where the rheological behaviour of passive nematic liquid crystals is compared to the one of both extensile and contractile nematics, at different values of the activity coefficient ζ.

4.1 Background and State of the Art

4.1.1 Rheology of Liquid Crystals

Nematic liquid crystals are characterised by an intrinsic anisotropy that reflects on their rheological properties: shear stress and shear rate are related through a viscosity tensor with five independent components, that reduce to three in the case of an incompressible fluid [7]. When a liquid crystal is sheared between two planes, the measured viscosity depends on the shear direction with respect to the nematic far field (bulk director orientation) and on the anchoring at the walls.

Moreover, the flow generated by the shearing tends to reorient the nematogens at an angle to the direction of shear, and the resistance to shearing can therefore be affected by the shear rate. Macrorheology experiments in nematic liquid crystals taking this into account were performed by Miesowicz [2], who used a magnetic field to impose a certain director orientation, independently of the shear flow. In this way the measured viscosity only depends on the relative orientation between the shear velocity and the director. There are three possibilities, according to whether the director is parallel or orthogonal to the shearing walls and to the shear velocity, that are sketched in Fig. 4.1.

Microrheology experiments are affected by the colloid/liquid crystal interaction. In a way, this makes it difficult to characterise liquid crystals through microrheology experiments, but understanding how the viscous force acting on a particle at the micron-scale can vary according to the specific type of interaction between the particle and the liquid crystal can be very important for applications. For instance such studies can help the understanding of the biological dynamics in the cell membranes, which are examples of biological liquid crystals. They consist of phospholipids whose tails can acquire orientational order. Membrane proteins are free to diffuse inside the membrane. Understanding how small particles behave when moving through liquid crystals could help to shed light on the functioning of these proteins, which are vital to the survival of organisms.

In microrheology the measured viscosity depends on the type of anchoring and on the adimensional anchoring strength, w, a parameter that we defined in Eq. 2.6. In principle the dependence of the drag force on the particle radius for colloids in liquid crystals might not be linear, in contrast with Stokes' law. Experiments and simulations ([69],[70]), have proved that Stokes' law can be extended to nematic liquid crystals, subject to the definition of two independent viscosity coefficients associated to the directions with respect to the bulk director orientation (parallel or orthogonal). In particular, the ratio of the viscous force acting on a particle that is dragged orthogonally to the bulk director orientation, to the one on a particle dragged parallel to that direction, is in general larger than one. Passive microrheology experiments where the two independent diffusion coefficients for the directions parallel and orthogonal to the director were measured, confirmed this scenario [69], at least for particles of size $\gtrsim 1\mu$m. Different anchoring types are associated to different topological defects,

that importantly influence the flow in the vicinity of the particle, and therefore the drag force. Different topologies were shown to be related to different drag coefficients and to different ratios between the drag force parallel and orthogonal to the director orientation. The latter is also affected by the anchoring strength. Simulations (e.g. [13, 71]) and experiments [69] in the past focused on the case of normal anchoring, where both a dipolar and a ring defect can be observed, depending on the size of the particle and on the anchoring strength. In [71] numerical results relative to these two topologies were compared to the case when the director field is uniform (no anchoring condition).

It is worth noting that it is still slightly controversial whether this scenario holds for nano-particles. Skarabot *et al.* in [72] peformed diffusion experiments where the inverse proportionality between the diffusion coefficient and the particle size is proved to saturate for particles whose radius is $\approx$ 300nm. This result however was not reproduced by simulations and experiments in [73], which considered probes of size $\gtrsim$ 190 nm. Interestingly cholesteric liquid crystals lead to a different scenario, where the apparent viscosity depends on the ratio R/p, where p is the cholesteric pitch, when the probe is dragged parallel to the cholesteric helical axis [74].

4.1.2 Rheology of Active Fluids

Bulk rheological properties of active fluids have been investigated, theoretically [21, 75], with simulations [3, 40], and through experiments [76, 77]. Theoretical studies and simulations, mainly based on a lattice Boltzmann method, were focussed on solving Eqs. 2.18 in quasi-one and quasi-two dimensions[1]. A systematic numerical study of the bulk rheological properties of active fluids in three dimensions has been performed in [4, 78]. This chapter and the following one present results that were published there.

These studies were mainly focused on the stress/shear rate relation, that can either be derived analytically from Eq. 2.18 in the linear approximation, or be measured from direct simulations. The shear rate is the ratio of the difference between the fluid velocities at the walls (where no-slip boundary conditions are applied), to their distance. An effective viscosity can be defined as the ratio

[1]By quasi-one dimensional system we mean a system that is translationally invariant along two directions.

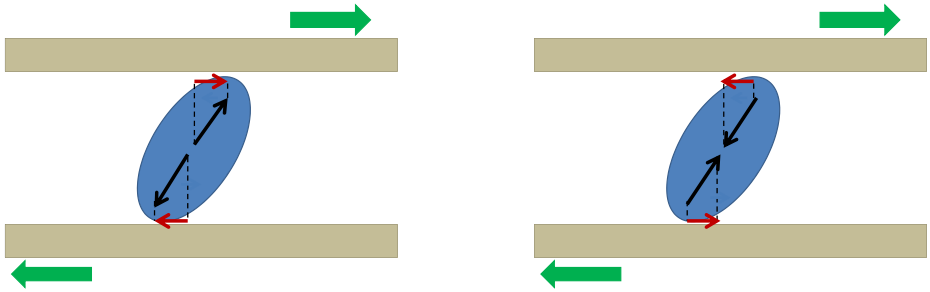

Figure 4.2: Effective shear viscosity in active nematics: due to the orientation of active nematogens with respect to the shear direction the effective viscosity of extensile nematics (left) is smaller with respect to the one of their passive counterpart, while the effective viscosity of contractile nematics (right) is larger with respect to the one of passive nematics for an infinite system.

of the measured shear stress to the applied shear rate. The scenario predicted by Eq. 2.18 changes considerably according to whether a negative or a positive value of ζ is considered, especially in comparison with passive nematics, and the important effects of activity on the rheology of a fluid are due to their inherent out-of-equilibrium character.

The active stress tensor allows for a non-zero macroscopic stress even in the absence of externally applied forces [21]. According to [21, 75], in the isotropic phase activity contributes to the viscosity with a term $\delta\eta = -\zeta\tau$, τ being a characteristic correlation time in the active fluid. Negative values of ζ, corresponding to contractile fluids, determine a greater resistance to being sheared than their passive counterpart, while for positive ζ (extensile fluids), the shear viscosity is smaller. These predictions have been widely confirmed, both by simulations in quasi-one [38] and quasi-two dimensional systems [3] and by experiments, that were performed on suspensions of bacteria [77] and algae [76]. In [77] both a macro- and a micro-rheology technique were applied to measure the viscosity of a diluted bacteria suspension and agreement was found between them. In [76] diluted suspensions of alive and dead algae at different volume fractions were sheared: the viscosity was found to be systematically larger for the former and a shear thinning behaviour was observed.

For very concentrated active suspensions, where a nematic order is found, this behaviour can be understood on the basis of the definition of pullers and pushers

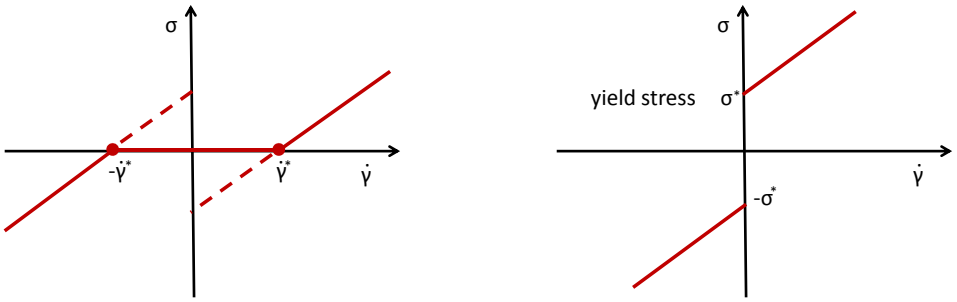

Figure 4.3: Typical shear stress - strain rate curves for extensile (left, [3]) and contractile (right) nematics.

and of the deformations of a sheared nematic liquid crystal induced by the flow [21], as depicted in Fig. 4.2. The orientation of sheared active rods with respect to the walls (independently of the anchoring condition) determines a local flow whose direction either opposes or favours the shear flow, according to whether they are contractile or extensile particles respectively. In particular, an extensile particle exerts forces on the fluid that are directed outwards along its main axis. Their orientation is such that they favour the external shear, which results in a smaller resistance to flow (see Fig. 4.2 (left)). The opposite happens in the case of contractile particles (Fig. 4.2 (right)).

According to the model described in [21, 75], the viscosity of a contractile fluid diverges at the isotropic-nematic transition [3], as is typical of a liquid-solid transition, where traslational order is introduced, rather than of a transition where the fluid goes from an isotropic to an orientationally-ordered phase.

Fig. 4.3 shows the stress/shear rate plot for extensile (left) and for contractile nematics (right). Eqs. 2.18 predict a region of "negative viscosity" for extensile nematics, that simulations [3] proved to be substituted by shear banding and the observation of non-zero strain rates in the absence of any external stress ('superfluid'). Differently, for contractile nematics, a minimum finite non-zero value of the external stress, called yield stress, is necessary to induce a non-zero shear rate in contractile nematics (panel on the right), as is typical of solids.

The shear viscosity of a passive nematic decreases for increasing shear rate: passive nematic liquid crystals are shear thinning. Activity affects also this property. In particular, in contractile nematics, when a shear stress larger than

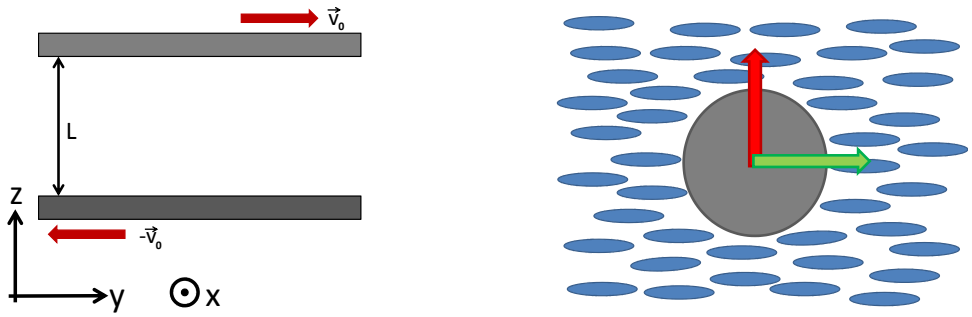

Figure 4.4: Cartoons of the setting used in simulations. The one on the left refers to macrorheology simulations and the one on the right to microrheology ones.

the yield stress is applied, the increase in viscosity with respect to the passive counterpart is more important the higher the shear rate, and leads to a shear thickening effect. In extensile fluids, on the other hand, the shear thinning is enhanced by activity.

Microrheology experiments, where the simple diffusion of colloids through the cytoskeleton was observed, and active microrheology performed by driving particles through the cytoskeleton [79, 80] or through bacterial suspensions [81], have so far mainly focused on studying the limits of validity of the fluctuation-dissipation theorem, that was proved not to hold for this category of out-of-equilibrium systems. A systematic numerical study of the local rheological properties of active fluids in three dimensions has been presented in [4], and will be reported in this chapter. In [78] we focused on the case of contractile nematics and presented unintuitive results that point out once again the completely novel character of active fluids. These will be treated thoroughly in the next chapter.

4.2 Methodology

Macrorheology (quasi-1D) simulations were performed by choosing a simulation box that was $1 \times 1 \times L$ large. Walls are introduced along the z direction, at a distance L from each other. Both the cases of normal and planar anchoring at the walls were considered, and a fixed, costant velocity (v_0 and $-v_0$) was imposed to the external walls, along the y direction. A cartoon of this setting is shown in the left panel of Fig. 4.4. We measured the shear stress in the right-hand side of

Eq. 2.18, and we studied this as a function of the average shear rate $\dot{\gamma} = 2v_0/L$.

Microrheology simulations are performed by applying a constant force to a single colloid embedded in passive and active nematic liquid crystals, along the two possible directions, parallel and orthogonal to the bulk average director orientation (see right panel of Fig. 4.4). The applied force F was small enough to cause a linear dependence of the drag force on the particle velocity v, in a regime of small Reynolds numbers. Another important adimensional quantity for liquid crystals is the *Ericksen number*, defined as the ratio of the viscous to the elastic forces: $Er = \gamma_1 Rv/K$, where $\gamma_1 = 2S^2/\Gamma$. (Here R and v are the radius and the velocity of the colloid, K the elastic constant, S the scalar order parameter and Γ is the collective rotational diffusion coefficient appearing in Eq. 2.7.) We chose Er to be small enough so that the fluid flow does not importantly affect the director field – and therefore the topology of defects. A drag coefficient ξ_0 can then be defined as $\xi_0 = F/v$. According to Stokes' law, in a simple fluid ξ_0 is directly proportional to the particle size R, and to the fluid viscosity η, $\xi_0 = 6\pi\eta R$. Complex fluids, for which in general Stokes' law does not hold, can be assigned an effective viscosity:

$$\eta_{\text{eff}} = \xi_0/6\pi R. \tag{4.1}$$

We studied the dependence of η_{eff} on R, for planar and normal anchoring conditions, and in the case of a uniform director field, which can be thought of as the limit of a very low anchoring strength.

For most simulations we chose periodic boundary conditions. This means that the flow and the director fields are effectively the ones of an infinite system, but the drag force that we measured is necessarily affected by the interaction of the probe particle with its own copies in neighbouring cells of the periodic simulation box. This effect cannot be neglected, because of the long range character of hydrodynamic interactions. Analytical corrections due to periodic boundary conditions for the drag coefficient in the case of a simple fluid were computed by Hasimoto in [82], but to our knowledge nothing has been done so far in the case of a liquid crystal, where not only hydrodynamic but also elastic forces have to be taken into account. Hasimoto corrections allow to remove important probe-size dependencies that would otherwise emerge in the effective viscosity of a simple fluid, defined as in Eq. 4.1. Even though they do not take into account

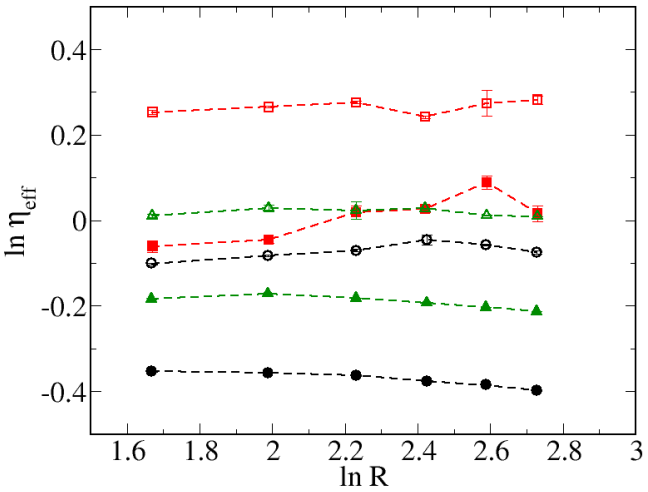

Figure 4.5: Dependence of the effective viscosity on the probe's radius R for passive nematic liquid crystals (double-logarithmic scale). Empty and solid symbols allow to distinguish between motion orthogonal and parallel to the far field respectively. Circles were chosen for the planar anchoring, squares for normal anchoring and triangles for the case of a uniform director field ($w = 0$). Here – and in what follows – η_{eff} is expressed in simulation units, that were clarified at the beginning of the chapter.

director-mediated interactions, they still allow to partially correct for the fluid flow, also in our case. Plotting the values of η_{eff} as a function of R for a passive nematic liquid crystal, in a double-logarithmic scale, corrected as in [82], showed negligible dependence on R (within an error of 0.05 for the drag coefficient, see Fig. 4.5). Since an effective viscosity independent of the size of the colloid is in agreement with experimental results in [72] and simulations from [73], we conclude that for our purposes elastic long range interactions between different images of the system are negligible, in a regime of low Er. Hence all results for η_{eff} in the following were only corrected as according to [82], as described in detail in Appendix A.

4.2.1 Choice of Parameters and Mapping to Physical Systems

In our simulations we applied the following choice of parameters. The viscosity of the simple fluid was set to 0.6. For the bulk free energy, whose expression is given in Eq. 2.4, we chose $A_0 = 1$ and $\gamma = 3$. Note that this value of γ corresponds to the spinodal temperature, at which the isotropic phase stops being a minimum of $\mathcal{F}_{bulk}$. This choice gives an ordered nematic phase. For the elastic constant K we chose $K = 0.05$, and for the constant W appearing in Eq. 2.5, and in Eq. 3.39 (where we put $W_1 = W_2$), we chose $W = 0.05$, unless differently specified, which corresponds to a regime of strong anchoring. The parameter Γ appearing in Eq. 2.7 was chosen to be equal to 0.3, while $\xi = 0.7$, which corresponds to a flow-aligning regime.

It should be noted here that in all our simulations we took care of working in a regime of low Reynolds numbers, as it is relevant for colloids. Particularly, for the values of R that we chose, and considering the velocities assumed by the particles when dragged through the (passive or active liquid crystal) we worked at $Re \sim 10^{-2}$. Similarly, one can estimate that $Er \sim 10^{-2}$.

To convert simulation units into physical ones, relevant e.g. for the actomyosin solution, we consider that, for typical cytoskeletal gels, $K \sim 1.25$ nN and $\Gamma \sim 10$ kPa/s [83]. Our units for force, length, and time are mapped onto 25 nN, 0.5 μm, and 10 ms respectively. Note that the mapping to a different system, e.g. a bacterial suspension, would be significantly different. In the large majority of the simulations that will be presented in this chapter, we will consider colloids

	planar	normal	$w = 0$
$\eta_\perp$	0.931 ± 0.018	1.30 ± 0.02	1.019 ± 0.009
$\eta_\parallel$	0.689 ± 0.012	1.01 ± 0.06	0.826 ± 0.013

Table 4.1: Average values of the effective viscosity for a nematic liquid crystal, for the direction parallel and orthogonal to the far-field director orientation. Data were obtained by simulating the drag of a spherical colloid through the liquid crystal [4], and they are expressed as the ratio of our measured viscosity to the one of the simple fluid in which mesogens are embedded.

having radii between ∼5 and 15, corresponding to the range between 2.5 and 7.5 μm, and will apply forces between 0.002 and 0.02, corresponding to F between 50 and 500 pN, which is in the range accessible by optical tweezers.

4.3 Results

In what follows we present and discuss numerical results obtained through the application of an hybrid lattice Boltzmann method, as described in Chapter 3.

4.3.1 Microrheology in Passive Nematics

In this chapter we will show results of microrheology simulations in nematic liquid crystals that constitute a systematic study where the role of anchoring conditions and of the size of colloids are investigated with a lattice Boltzmann method. They partly complement previous research in [70] on normal anchoring and uniform director field (that is obtained in the hypothesis of no interaction between the nematic liquid crystal and the surface of the colloid), by including the case of planar anchoring and hydrodynamic interactions. Moreover, they address the question of the role played by the particle size, which recent experiments [72] and simulations [74] have shown to be a partly unexplored ground that can still reveal nontrivial behaviour. Beyond that, our investigation of passive nematics in this chapter mainly aims at providing a term of comparison with the case of active nematics, that will be presented later on in the chapter. This will help to emphasise and point out the novel contributions of activity.

Fig. 4.5 shows the dependence of η_{eff} on the radius of the dragged colloid, R, in a double-logarithmic scale. It is worth mentioning here that the values of

η_{eff} and of R here are expressed in simulation units, as all the other meaningful quantities throughout this thesis. The mapping to meaningful physical systems must be done as explained in the previous paragraph.

Here we find that data lie approximately on a straight horizontal line, thus indicating no dependence of η_{eff} on R, in agreement with Stokes' law. This allows to average over different R's, to compute $\eta_{\parallel}$ and $\eta_{\perp}$. The values are presented in Table 4.1 for the three different types of anchoring considered. In agreement with [70] we find that η_{eff} is larger in the case of normal anchoring than in the uniform case. This was explained in [70] as the result of an effective larger size of the particle, when disclinations are there. However, we find that for planar anchoring, the resistance of the fluid to the particle motion is remarkably lower. We do not have a clear explanation for that, but these results show that the complex interplay between the local orientation of nematogens close to the surface of the colloid and the flow is not taken into account simply by a larger effective extent of the particle, that would give a viscosity larger than the one obtained for $w = 0$.

4.3.2 Macrorheology of Active Nematics

In this section and in the next we present a systematic numerical study of the rheological properties of active fluids, which we investigated both globally, through shear experiments (in a quasi-one dimensional geometry, as used in [3]), and locally, through microrheology experiments where a spherical particle is dragged by a constant force.

We compare the local and the global description to verify whether an effective viscosity, η_{eff}, exists. To be a useful quantity, η_{eff} should be independent of the experimental technique used to measure it. In particular, results of macro- and micro-rheology experiments should agree. Moreover, a well defined η_{eff} should be independent of the size of the system. The effective viscosity for the bulk rheology simulations is defined as the ratio between the measured shear stress and the applied shear rate. For microrheology in the linear regime $F = \xi_0 v$, with ξ_0 the friction coefficient. In analogy with simple fluids, and with previous discussion on passive liquid crystals, the effective viscosity is defined as $\eta_{\text{eff}} = \xi_0/6\pi R$. As we will see, in the case of active nematics these definitions lead to a strong dependence of η_{eff} on the size of the system.

We performed simulations for different anchoring conditions on the walls and for different system sizes, and considered a range of values for the activity coefficient ζ. Macrorheology simulations show that η_{eff} depends on the anchoring condition, as in the passive case, because of the anisotropic nature of nematics. Furthermore, activity is responsible for an important dependence of η_{eff} on the system size L, that is not present in the passive case, and that can be analytically predicted through a linearisation of the system equations. This was done by A. Morozov, as published in [4]; the linearised equations and their solutions are specified in Appendix B. As will be discussed further below, the dependence of η_{eff} on L undermines the physical meaning of viscosity for active fluids.

In microrheology simulations we changed the radius of the colloid, R, and studied the dependence of η_{eff} on R. We will first present results for the planar anchoring, which are well explained by the interplay between activity and director deformations. Later on, we will present results for normal anchoring, and for a uniform director field, that confirm predictions based on our argument. To verify the consistency of our results, independently of boundary conditions, we repeated microrheology simulations in the presence of boundary walls in one direction, in the case of planar anchoring, which confirmed previous findings.

To ease connection with future experiments, we also modelled the case when the colloid locally disrupts nematic order, by imposing a zero value of the scalar order parameter at the colloidal surface. We expect this to be the most realistic scenario in the case of active fluids, such as bacterial suspensions, whose constituent particles are micron-sized and therefore on the scale of the colloidal probes used in microrheology experiments. In this case one can expect local disorder, rather than a specific type of anchoring at the surface.

Given the importance of boundary conditions in determining the behaviour of liquid crystalline and active fluids (as found e.g. in [38, 84, 3]), we address here the roles played by the anchoring condition on the walls and by the system size. With this aim in mind, we consider both planar and normal anchoring, as defined previously.

As anticipated, an effective viscosity η_{eff} can be defined as the ratio of the measured stress to the imposed average shear rate, and we measure it for different values of ζ. We highlight that here we are interested in the bulk rheology of active fluids in their quiescent (passive) phase, i.e. when they are not spontaneously

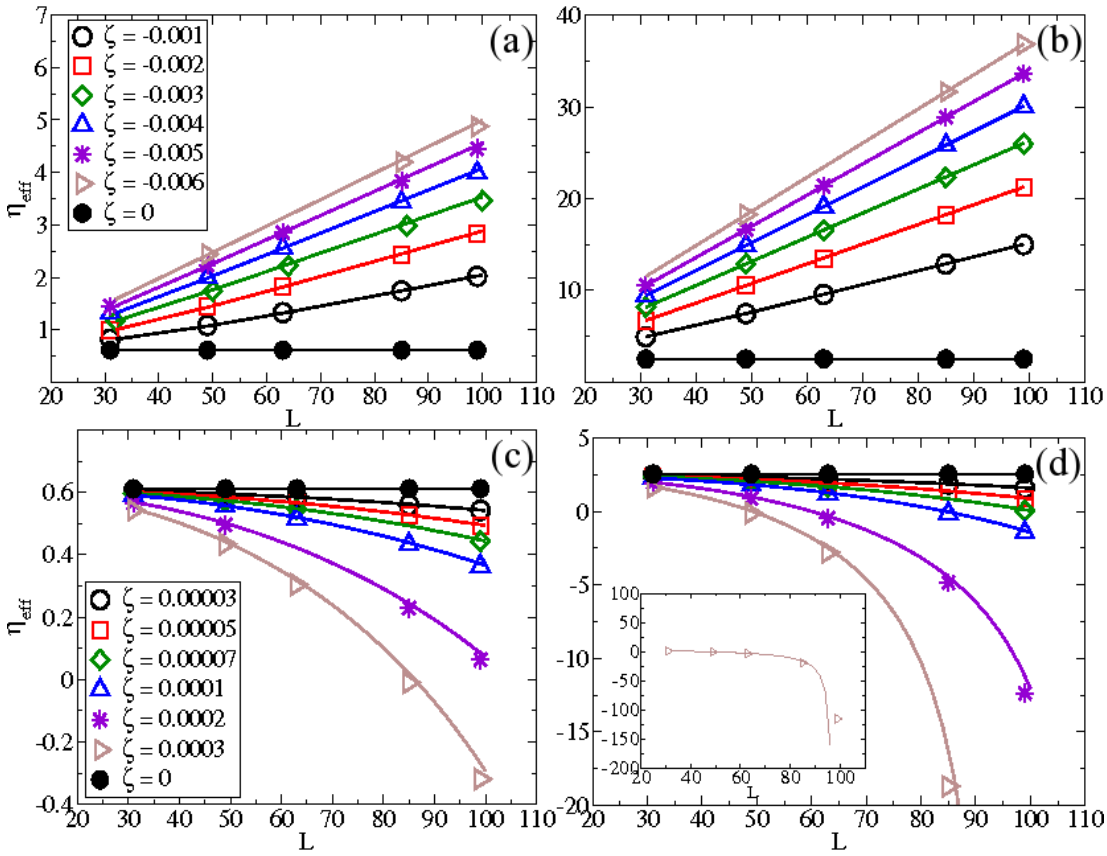

Figure 4.6: Dependence of η_{eff} on system size L in the case of contractile active nematics with planar (a) and normal (b) anchoring, and an extensile active fluid with planar (c) and normal (d) anchoring at the walls. Legend on the left refers to both graphs in the same line. The inset in (d) shows the behaviour for $\zeta = 0.0003$ more in detail. Points here refer to numerical results, while solid lines are theoretical predictions obtained through Eq. B.8.

flowing. We focus for simplicity on the case of a quasi-one-dimensional system, where there is translational invariance in the flow direction, and all quantities only vary along the flow gradient direction, which is z in our notation. This case is already sufficient to describe qualitatively the basic features of the spontaneous flow transition in active fluids [14, 38, 20, 84, 3], that can be avoided by applying a small enough stress.

Fig. 4.6 shows that η_{eff} in the nematic phase in our geometry behaves consistently with previous theoretical estimates [21, 75]: it is higher with respect to the passive isotropic viscosity in the case of contractile active fluids and smaller in the extensile case. Moreover, by analysing its dependence on the system size L, which we define as the distance between the two shearing planes, we find that η_{eff} increases with L in contractile active fluids and decreases with L in extensile ones. As it can be seen from Fig. 4.6, the anchoring of active particles at the walls plays an important role: the difference with the passive viscosity is enhanced for normal anchoring.

An analytical prediction for the apparent viscosity η_{eff} at low shear rates is obtained by linearising the equations of motion, Eqs. 2.7, 2.11. In Fig. 4.6 we compare this analytical prediction (solid lines) with our lattice Boltzmann data (symbols). The results show a very good agreement of the viscosity in the linear regime obtained in our simulations with the predictions in Eq. B.8, except for the case of an extensile fluid with $L = 100$ and $\zeta = 0.0003$, where spontaneous flow sets up in the numerical solution at $\dot{\gamma} = 2 \cdot 10^{-7}$, which introduces non-linear effects invalidating our linearised analytical treatment.

Our main result is that the effective viscosity of active nematics importantly depends on the system size, differently from their passive analogue, as according to what displayed in Fig. 4.6 ($\zeta = 0$), and therefore it is not well-defined in the limit of an infinite system, when the boundary walls are infinitely far apart. Consequently, the viscosity of an active fluid cannot be operationally defined as the ratio between the shear stress and the shear rate, as it usually is in experiments probing the bulk rheology of complex fluids. This is true despite the existence of a linear regime where the shear stress is proportional to the shear rate, as shown in Fig. 4.6, and where the system behaviour is well described by the solution of the linearised equations.

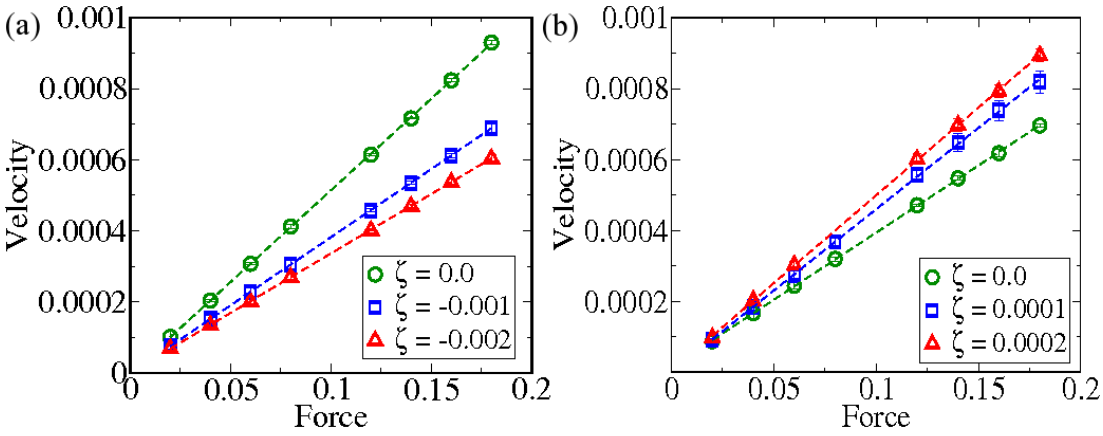

Figure 4.7: Dependence of the particle velocity, measured in steady state, on the external force for a particle of fixed radius $R = 11.3$, and different ζ (see legend). (a) refers to a contractile and (b) to an extensile active gel. We used (periodic) cubic simulation box of volume $V = 128^3$.

4.3.3 Microrheology of Active Nematics

We now turn to the study of local rheological properties of active fluids. We do this by simulating microrheology experiments similar to the one described for passive nematics, where we drag a spherical particle parallel and orthogonally to the orientation of the director far from the particle (bulk director orientation), by applying a constant external force, F. Also here, in a regime of small external forces, we can observe that $F = \xi_0 v$, as shown in Fig. 4.7, and an effective viscosity can therefore be defined as in Section 4.3.1: $\eta_{\text{eff}} = \xi_0/6\pi R$.

As mentioned in Section 4.2, we applied periodic boundary conditions and used Hasimoto corrections [82] to account for the effect of periodic images.

Here we probe the role of system size and of boundary conditions in rheology measurements, by considering colloids of different sizes R and by changing the anchoring at the surface. We will also consider different values of the parameter w (see Eq. 2.6), and will either work in a regime of strong anchoring strength, with $w \gtrsim 5$, or in the limit of very low anchoring, by imposing $w = 0$.

The values of the activity coefficient ζ that were chosen are high enough for activity to play a role in the system behaviour, but small enough to avoid the onset of a regime of spontaneous flow in the bulk. In the case of planar anchoring, we considered $\zeta = -0.001$ and -0.002 for contractile liquid crystals, $\zeta = 0.0001$ and 0.0002 for extensile nematics. In all other cases we focused on only one value

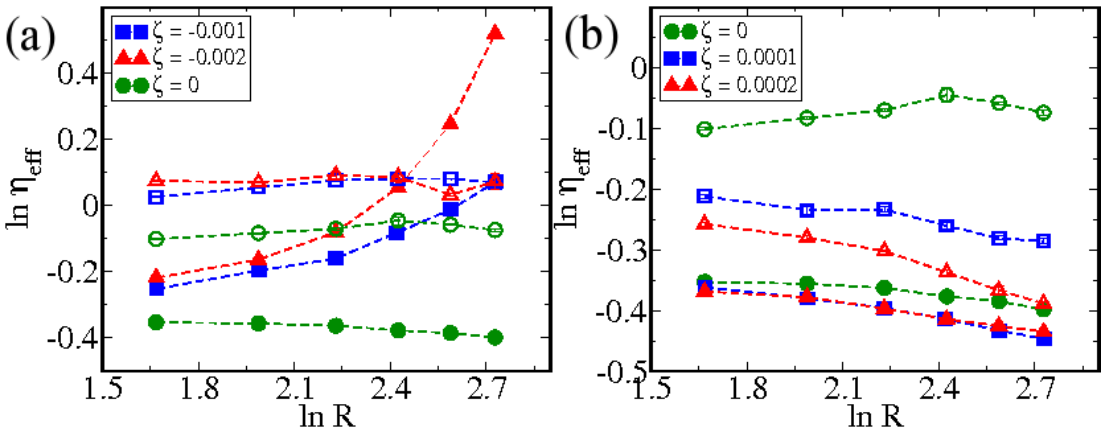

Figure 4.8: Dependence of η_{eff} on R for a contractile (a) and for an extensile (b) active fluid. Different symbols refer to different values of ζ (see legend). Filled and open symbols correspond to pulling along and perpendicular to the far field director respectively and dashed lines are to guide the eye. We used (periodic) cubic simulation box of volume $V = 128^3$.

of ζ (which is -0.001 for contractile nematics and 0.0001 for extensile ones). It is worth noting here that the absolute values of ζ chosen in the contractile case are an order of magnitude larger than the ones chosen for extensile nematics. This is because spontaneous flow shows up at much smaller $|\zeta|$ in extensile than in contractile active fluids. It is also worth mentioning here that the flow developing when the colloid is dragged through the (active) liquid crystal is such that we can exclude the possibility that the motion of the colloid triggers a transition to spontaneous flow at the values of ζ that we considered.

We start by considering the case of planar anchoring of the liquid crystal at the particle surface. Our estimates for η_{eff} are plotted in Fig. 4.8 as a function of R, in a double logarithmic scale. The curves obtained in the active cases are compared to the ones referring to their passive analogues ($\zeta = 0$).

In agreement with the macrorheology results in the previous section, we find here that a negative ζ increases the fluid resistance to the particle motion with respect to the case of $\zeta = 0$, so that η_{eff} in contractile nematics is larger than in passive nematics. The opposite happens for positive ζ. Moreover, we find that, in contractile nematics, differences with the passive case are more relevant when the particle is dragged parallel to the far-field director orientation, while the effect of activity is larger in the orthogonal direction for an extensile fluid.

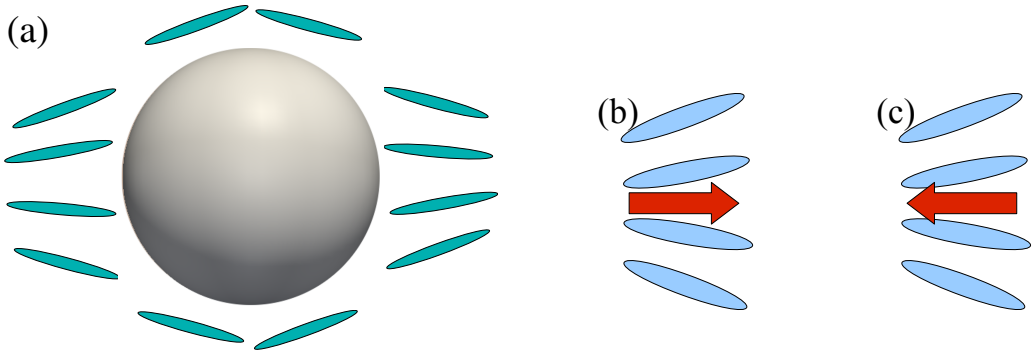

Figure 4.9: (a) Sketch of the director orientation close to the surface of a spherical particle in the case of planar anchoring. Deformations of the nematic profile are responsible for a net force exerted by active particles on their ambient fluid, whose direction depends on the contractile or extensile character of particles. Panel (b) shows the net force that a group of contractile splayed particles exerts on the ambient fluid, while panel (c) refers to extensile particles. In order to understand this each particle has to be thought of as a force dipole. A larger force density is associated to the internal part of the splay, where the particles are closer together, than in its external part, and this gives rise to a net force.

What is most relevant in our results is that as soon as $\zeta \neq 0$, η_{eff} shows a strong dependence on R, that is more important the larger $|\zeta|$. Comparison with the case of $\zeta = 0$ leads to the conclusion that this must be due to the role of activity only. Dependence of η_{eff} on R reveals that ξ_0 does not depend linearly on R, in striking contrast with Stokes' law, that is usually applied in microrheology experiments to infer information on the fluid from the motion of the probe.

Let us focus on Fig. 4.8 (a) first: here η_{eff} rapidly increases with R when the particle is dragged along the director. When an extensile active fluid is considered (Fig. 4.8 (b)) instead, η_{eff} decreases with R, the effect being more visible when the particle is dragged normal to the far field director.

Before going on with the analysis of other anchoring conditions, we will provide a qualitative explanation of what we found in the case of planar anchoring first. We will do this through a heuristic argument, and sketches shown in Fig. 4.9 and following will help us. Active nematogens are particles that continuously exert forces on their ambient fluid. In a perfectly ordered, unperturbed active nematic, all these forces cancel locally. When a spherical particle is embedded in a nematic liquid crystal, interaction between its surface and nematoges determines a local

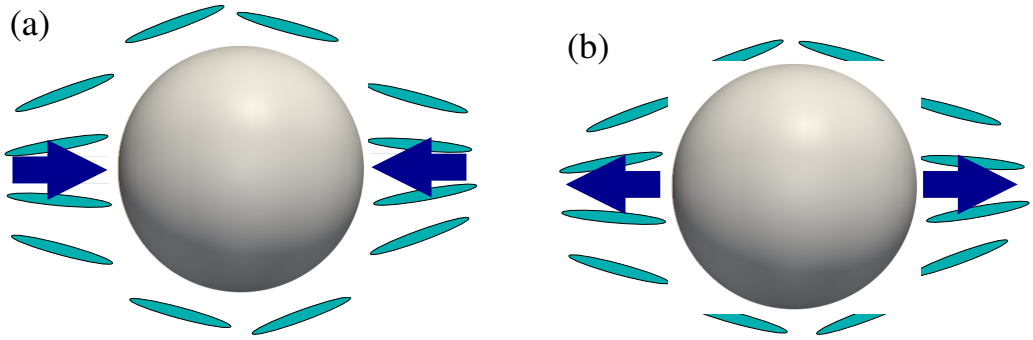

Figure 4.10: Planar anchoring generates a splay deformation close to the colloidal surface, along the average orientation of active particles in the bulk (horizontal in these figures). This is the type of deformation that plays a role when the colloid is dragged parallel to the director. These deformations are responsible for net forces exerted by active particles on the fluid and ultimately acting on the colloid, that are directed as in panel (a) for a contractile nematic liquid crystal and as in panel (b) for an extensile one. The direction of forces can be understood on the basis of panels (b) and (c) of Fig. 4.9. These sketches refer to the case of a colloid that is not moving, so that the deformations on both sides of the particle are the same and the forces that they generate do counterbalance.

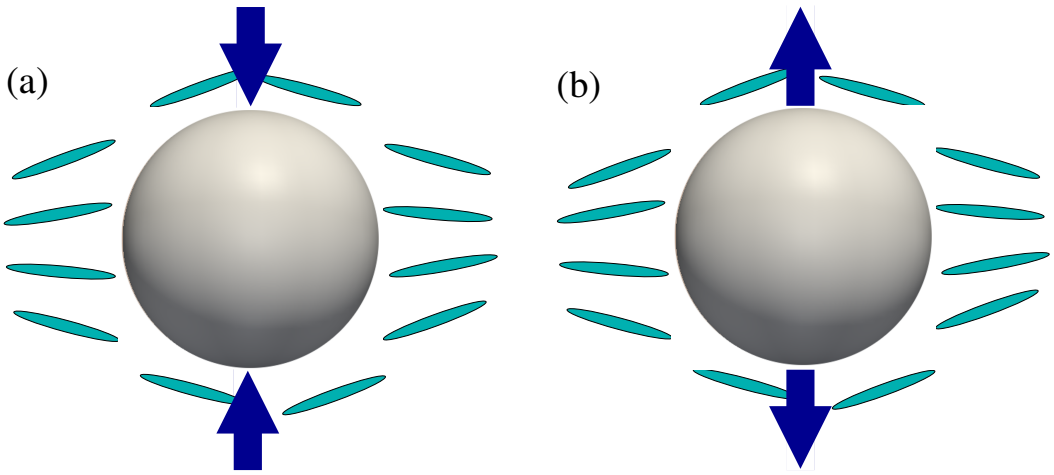

Figure 4.11: Planar anchoring at the colloidal surface is responsible for a bending deformation close to the particle surface in the direction orthogonal to the director orientation in the bulk. Due to their dipolar character, bent groups of active particles exert forces that are directed towards the colloid in the contractile case (a), and outside in the case of extensile particles (b).

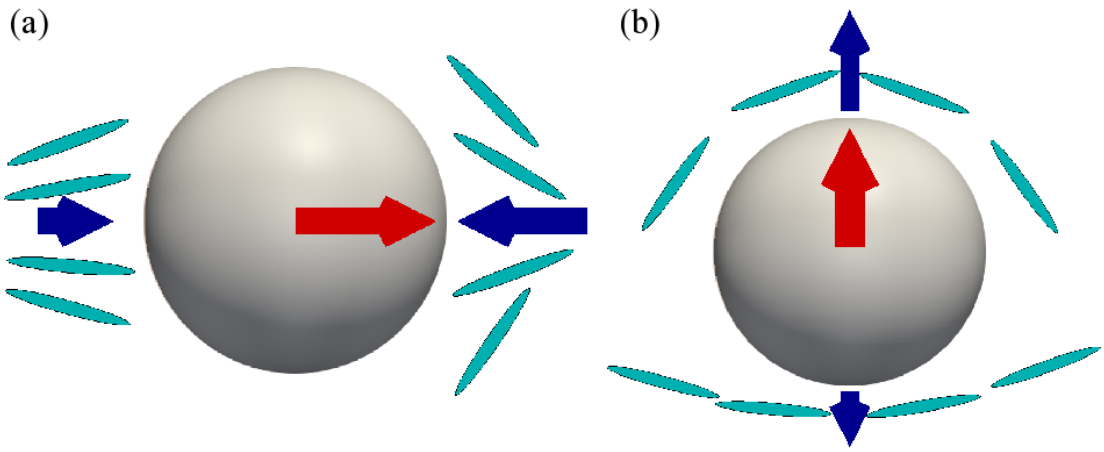

Figure 4.12: Sketch of the splay and bend deformation when the colloidal particle is dragged parallel to the far-field director orientation, for a contractile fluid (a) or orthogonally to it, for an extensile fluid (b). Blue arrows represent active forces, while the red one refers to the external force. The sketch is further discussed in the text.

deformation of the nematic director field, that depends on the anchoring type. In the case of planar anchoring, the situation is like in Fig. 4.9 (a). Because of local deformations, forces exerted by active particles on the fluid do not sum up to zero. A splay deformation, like the one depicted in Fig. 4.9 (b) and (c), gives rise to a net force acting on the fluid. In the case of contractile nematogens, that force is directed as in Fig. 4.9 (b), as one can easily realise by considering each particle as a force dipole directed inwards along its axis, according to the definition of contractile particles. Fig. 4.9 (c) refers to the extensile case. When the colloid is not moving, the director deformations close to its surface are perfectly symmetrical and the forces that active particles exert on the fluid, and therefore on the colloid, cancel out: in Fig. 4.10 the ones acting parallel to the far field director are shown, while Fig. 4.11 refers to the orthogonal direction. In both cases the picture on the left refers to contractile and the one on the right to extensile fluids.

When an external force is applied to the colloid, the particle motion must determine an asymmetry in the deformation, that we expect to be as in Fig. 4.12 (a), in the case when the particle is dragged along the director: the splay in front of the particle is larger than the one at the back. This generates

a net force that, in the case active particles are contractile, opposes the external one and is responsible for the larger viscosity measured in this situation. When instead the fluid is extensile, the forces acting on the colloid are in the opposite direction and therefore favour the motion of the colloid, which explains why the colloid experiences a smaller resistance in this case, as according to our simulations. The fact that a larger effect is observed when the colloid is dragged parallel to the far field director in contractile fluids can be explained by their instability with respect to splay, that was explained in Chapter 1: the forces that contractile particles exert on their ambient fluid determine a local flow that tends to deform the director field even more. This does not happen instead when a splay deformation is introduced in extensile nematics, which are stable with respect to splay. Finally, the R dependence must come from the need to integrate the local stresses over the whole colloidal surface. A more quantitative description of the extra force term that must intervene in the force balance for the system will be provided in Chapter 5.

When the colloid is dragged orthogonally to the director, the asymmetry in the director field generated by its motion involves a bending deformation. Again, we expect the latter to be larger at the front of the particle, than at the back. This generates a net force ultimately acting on the colloid, that opposes the external force in the contractile case, and favours it in extensile nematics (see Fig. 4.11 (a) and (b)), in agreement with our results on η_{eff}. Similarly to the previous case, the effect is now larger for extensile nematics, since they tend to bend more easily than their passive counterpart, while contractile nematics are more resistant to bending.

This argument explains our results for planar anchoring in Fig. 4.8. It further suggests that a key role is played by the director orientation at the particle surface. In order to shed light on how the anchoring condition can affect microrheology measurements we repeated our simulations with different types of anchoring: we considered also the case of normal anchoring and the one in which no anchoring condition is imposed. Despite not being very realistic, since the presence of a colloid in liquid crystals is very unlikely not to affect the local orientation, the latter case is a useful limiting case that clarifies the role of local deformations.

Before analysing results for normal anchoring at the colloid surface, let us apply our argument, to predict what we expect from our simulations. This can

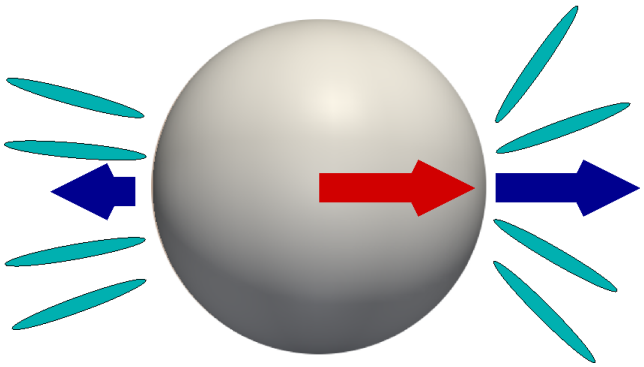

Figure 4.13: Sketch of the director field deformation for normal anchoring, and for a probe pulled along the far field director. As before, blue arrows refer to the active forces, while the red one represents the external force.

be more easily done when the external force is along the far field director. This case is sketched in Fig. 4.13, for a colloid in a contractile namatic. As in the case of a planar anchoring, the deformation involved is a splay, but this time it is reversed, so that the net force acting on the colloid is now expected to favour the particle motion, instead of hindering it, as in the planar case. Analogously, we expect an extensile fluid to oppose the external force.

Results concerning both the contractile and the extensile case are presented in Fig. 4.14. In Fig. 4.14 (b) we show the evolution of the velocity of the colloid when dragged along the director: results for a passive nematic are presented as comparison. In agreement with our predictions, the velocity of the colloid is larger, when it moves through a contractile liquid crystal, and smaller through an extensile fluid. Interestingly, the inset shows that in the latter case we found evidence of a yield force, that prevents the motion of the colloid when a small external force is applied. This 'yield force' may be seen as a microrheological analog of the yield stress in bulk rheology experiments. Note that in this case we preferred to show the dependence of the colloid velocity on time, rather than computing the effective viscosity. The presence of a yield force is equivalent to the absence of a linear regime which is why we do not report estimates for η_{eff} for this pulling mode.

In the case of particles pulled orthogonal to the director, we computed η_{eff} as a function of R, as shown in Fig. 4.14 (a). In this case predictions based on our argument are more difficult, since in this direction both a bending and

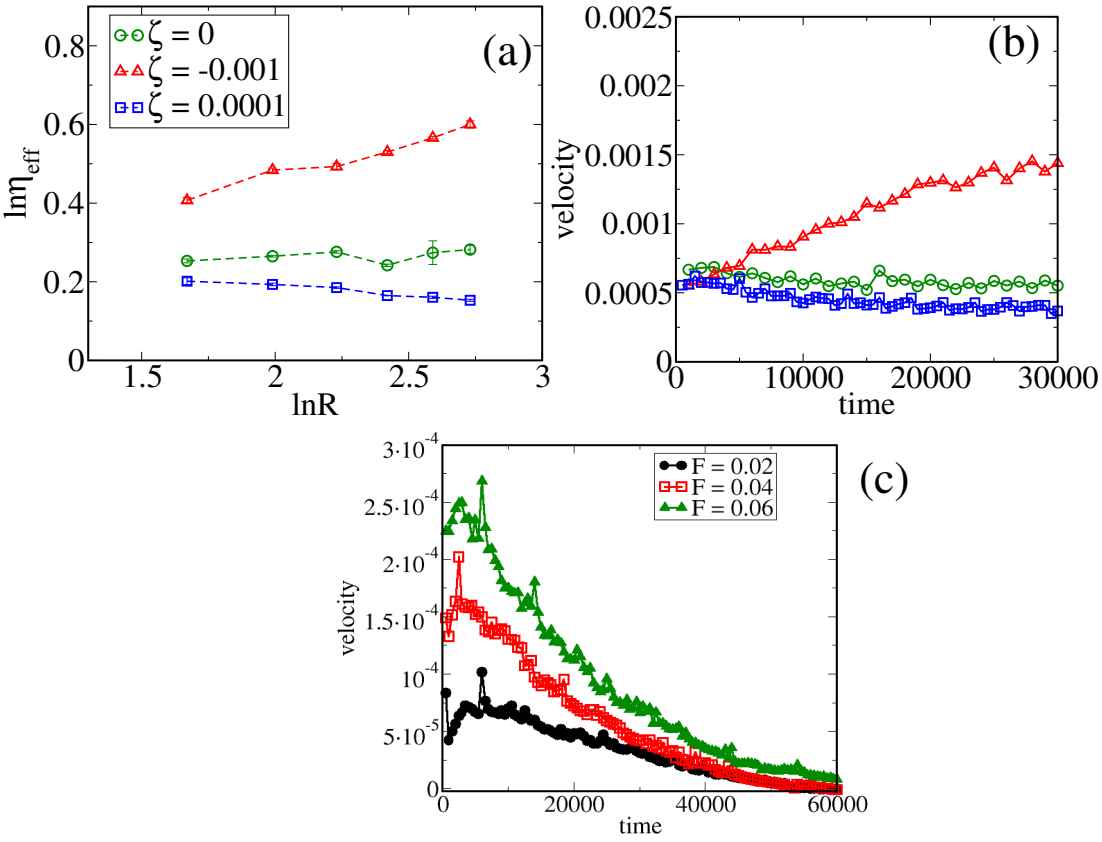

Figure 4.14: (a) Dependence of the measured effective viscosity on radius for normal anchoring of the director field on the colloidal probe surface, at various ζ (see legend). The dragging direction is orthogonally to the far field director. Other parameters are as in Fig. 4.8. (b) Velocity versus time for $F = 0.12$, $R = 9.3$ in the case of dragging along the far field director. The symbols are chosen according to the legend shown in (a). (c) shows the velocity of a particle of radius $R = 9.3$ pulled through an extensile gel ($\zeta = 0.0001$) as a function of time for three different values of the external force F, which are given in the legend. Note the presence of a non-zero 'yield force' further discussed in the text. As in the previous cases, we used (periodic) cubic simulation box of volume $V = 128^3$.

a splay deformation might play a role, with opposite effects. Fig. 4.14 shows agreement with results on planar anchoring and with macrorheology: η_{eff} is larger for contractile fluids than in the passive case, while it is smaller for extensile nematics.

The scenario that we hypothesised is fully confirmed by the flow profiles that we present in Fig. 4.15. All the figures refer to normal anchoring. Orthogonal drag is depicted in the panels on the left, and the right panels concern parallel drag. The cases of passive, of contractile and of extensile nematics are compared. In particular, from panel (d), and with comparison to (b), it is possible to see how in the contractile case the fluid flow is larger at the front of the particle than at the back. This is in agreement with the presence of a larger splay deformation at the front of the particle, pushing the fluid away from it and favouring the external force. Consistently, panel (f) shows that the opposite happens when an extensile fluid is considered.

Results for normal anchoring are very important, especially for the reduction of resistence to the particle motion in contractile nematics. This case provided us with further confirmation of our interpretation of results for planar anchoring. Most importantly, it pointed out how the thickening and thinning effects of activity in contractile and extensile environments respectively, which were measured in shear experiments and supported by our simulations of microrheology for planar anchoring, are strongly affected by the anchoring condition on the colloid surface in the case of microrheology, rather than being an intrinsic property of the fluid. Again, this provides evidence of a substancial dependence of the fluid resistance to the motion of an embedded particle, on the probe itself. Not only does η_{eff} depend on R, but also the active nature of the fluid might have an opposite (contrasting or favouring) effect on the particle motion depending on the anchoring condition.

Let us now consider the case in which the anchoring strength is equal to zero. There the presence of the colloid does not affect the director profile, at least when it is not moving. This situation can be easily obtained in simulations by setting $W = 0$ in Eq. 2.5, but cannot be easily realised in experiments, since local interactions between the fluid and the colloidal surface cannot be suppressed. It however constitutes an interesting limiting case that can ideally point out

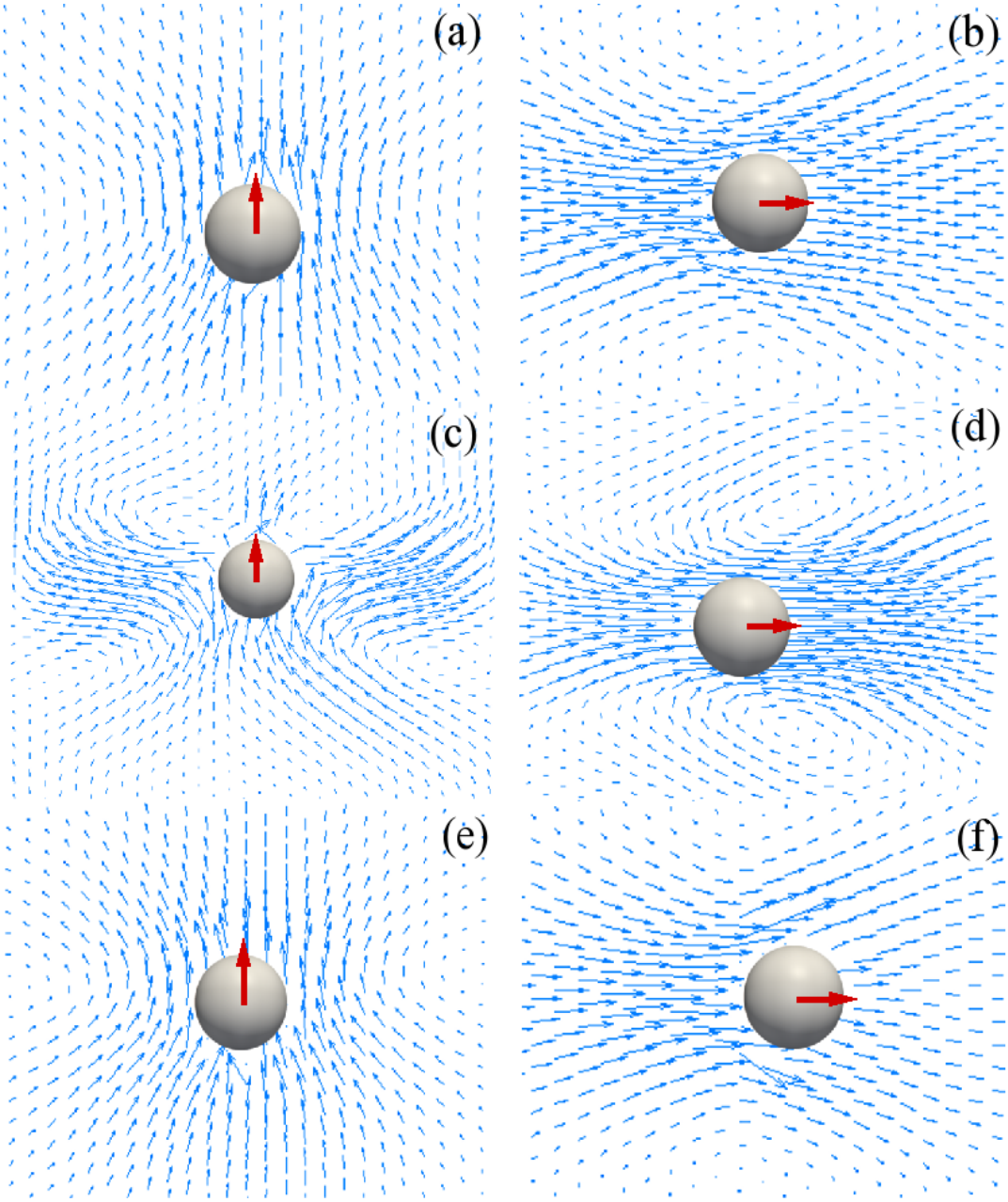

Figure 4.15: Flow field patterns close to a moving particle of radius $R = 11.3$ subject to a force $F = 0.12$, in a passive nematic liquid crystal (a,b), in a contractile active fluid (c,d), and in an extensile active fluid (e,f). In all cases there is normal anchoring of the director field at the particle surface. In (a,c,e) the pulling direction is perpendicular to the far field director, whereas in (b,d,f) the colloid is dragged paralled to the far field.

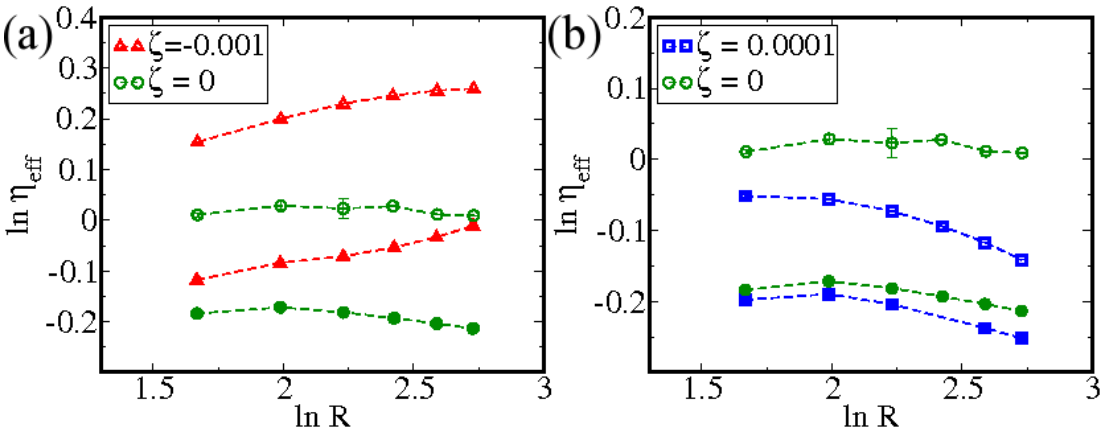

Figure 4.16: Dependence of the effective viscosity on particle size for no anchoring, and different ζ (see legend). (a) and (b) describe a contractile and extensile active fluid respectively. As previously, filled and open symbols correspond to pulling along and perpendicular to the far field director respectively and we used (periodic) cubic simulation box of volume $V = 128^3$.

properties that are intrinsic of the fluid, irrespective of the anchoring[2].

Results referring to this case are presented in Fig. 4.16. The way η_{eff} is affected by activity is similar to the one observed in the case of planar anchoring: it is larger than in the passive case for contractile, and smaller for extensile fluids. The dependence on R is much milder than when anchoring is imposed, probably because now the region of deformation is less affected by the probe size.

All the simulations of microrheology presented so far were performed with periodic boundary conditions. This is an artificial situation that might affect our results. In order to verify that this is not the case, we repeated our measurements with planar anchoring on the colloid, in a system where boundary walls are introduced along one direction. This is a physical way to stabilise the quiescent phase at low activity [14, 20, 38, 84] (although periodic boundary conditions also do that). Hydrodynamic interactions between different images of the particle are still there in the two directions parallel to the wall, however they are no more described by the theory in [82]. We therefore corrected our data through the deviation of the simple fluid viscosity measured in the same conditions, from its theoretical value, which corresponds to an infinite box size parallel to the

[2]Note that the deformations we refer to are only due to the direct interaction between the nematogens and the surface of the colloid, while the director profile will of course be deformed by the flow as soon as the colloid starts moving in the liquid crystal.

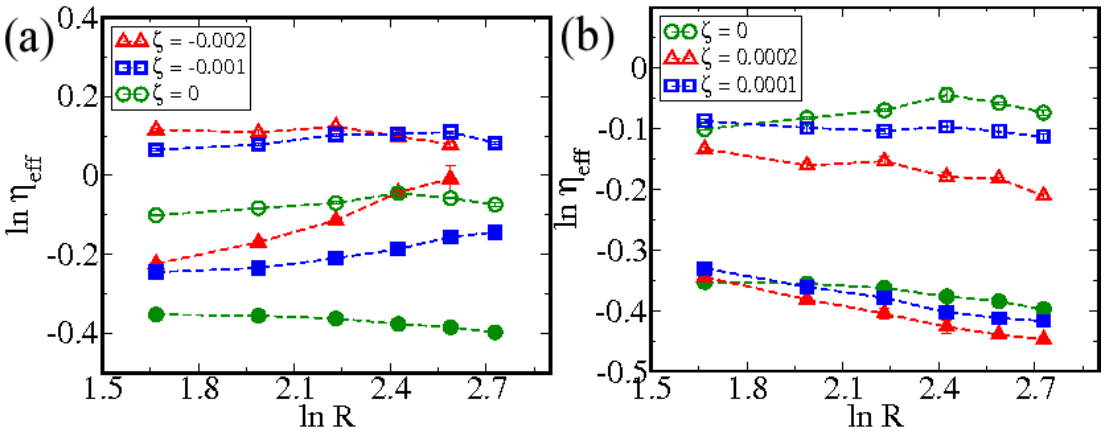

Figure 4.17: Dependence of η_{eff} on R for (a) contractile and (b) extensile fluids, with particle anchoring as in Fig. 4.8, but with strong homogeneous anchoring of the director field at the wall of the container. The anchoring determines in this case the far field director profile. All parameters are as in Fig. 4.8, apart from the system size which is 64 along the direction orthogonal to the walls, and 128 in the other two directions. Empty and filled symbols refer to particles pulled orthogonally and parallel to the far-field director respectively.

boundaries.

Results obtained in this case are presented in Fig. 4.17. They qualitatively confirm what we had obtained for planar anchoring with periodic boundaries: the resistance that active nematics oppose to the motion of the colloid is larger in contractile nematics and smaller in extensile ones, than in their passive counterpart. A significant dependence on R is observed, even though the effect of activity is now milder than with periodic boundaries. This might be because the system is now slightly smaller than in Fig. 4.8 and the director deformation close to the particle might accordingly be slightly less.

Probe particles used in microrheology usually have sizes between 1 and 10μm ([85]), comparable to the ones of typical bacteria (e.g. bacterium *E.coli* has a body whose length is about 2μm long and 1μm wide). Such a small probe would make it difficult to impose a specific orientation of active particles close to the colloidal surface.

Our suggestion is that this situation can be reproduced in simulations by associating a region of disorder to the region close to the particle surface. We did this by imposing a null value of the amplitude S_0 to the order parameter at the

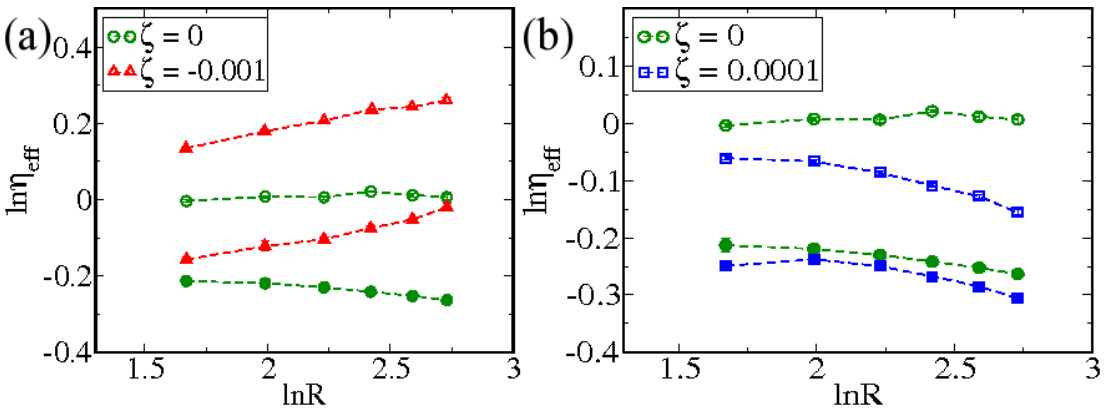

Figure 4.18: Dependence of the effective viscosity on particle size with $\mathsf{Q} = 0$ on its surface, and different values of ζ (see legend). (a) and (b) refer to a contractile and extensile active fluid respectively. As previously, filled and open symbols correspond to pulling along and perpendicular to the far field director respectively and we used (periodic) cubic simulation box of volume $V = 128^3$.

surface of the colloid, Q_0, appearing in Eq. 2.5. We find that the director profile in this case is very similar to the one observed for $w = 0$.

Also the results for this case, which are presented in Fig. 4.18, are very similar to the ones obtained when no anchoring condition was imposed. In particular, we found again that a contractile active fluid imposes a greater resistance to the particle motion than its passive counterpart, and that the opposite happens for extensile nematics. Concerning the dependence on the particle size R, here it is rather mild, and also the shape of the curves showing η_{eff} as a function of R, and not much difference is observed between parallel and orthogonal drag. This is probably bacause imposing $S_0 = 0$ melts the nematic liquid crystal close to the surface, so that local deformations in that region are not much affected by the direction of drag.

4.4 Discussion and Conclusions

In this chapter we have presented numerical results on rheological experiments performed in passive and active nematic liquid crystals. Both the bulk rheology and the microrheology of passive nematics have been studied widely in the past. Our simulations on passive nematics were mainly aimed at providing a benchmark

for our numerical method and a term of comparison for the active counterpart of these systems. We confirmed previous numerical and experimental results on the viscous force acting on a spherical colloid dragged through a nematic liquid crystal, both parallel and orthogonally to the bulk director orientation, by considering the case of normal anchoring of the liquid crystal at the colloidal surface, when a Saturn ring arises, and of a uniform director field (no anchoring). The case of planar anchoring complements the existing literature and shows a behaviour very similar to the one obtained for normal anchoring.

The rheological properties of active nematics on the other hand had so far been addressed only through bulk studies, whose main result was to point out how activity can increase the resistance of a fluid to shear in the case of contractile nematics, and decrease it for extensile ones. We performed simulations of macrorheology experiments on a quasi-one dimensional system consisting of an active liquid crystal confined between two walls, and measured the effective viscosity. We found that the latter depends strongly on both the anchoring condition at the walls and on the system size: particularly, the resistance to shear of contractile nematics increases with the distance between the shearing planes. The opposite is true for extensile nematics. These results were found despite the existence of a linear regime, that can be described by linearising the system equations. We presented solutions for different anchoring and found very good agreement with our numerical results. Our main result on the bulk rheology of active nematics is the dependence of the effective viscosity on the system size, in contrast with what happens for their passive counterpart. A consequence of this is that the effective viscosity of an infinite system diverges.

As a further step in the study of the rheological properties of active fluids, we simulated some microrheology experiments where spherical particles of different sizes are dragged through an active nematic liquid crystal in order to measure an effective voscosity defined according to Stokes' law, as it is usually done in 'falling ball' experiments. In order for this quantity to be a useful one, it should (i) be in agreement with the one measured through macrorheology experiments and (ii) not depend on the characteristics of the probe, particularly on its size. We first presented results for planar anchoring at the particle surface and found that not only does the effective viscosity depend on the anchoring condition (as it does for passive liquid crystals), but it also shows a significant dependence on

the radius of the probe particle, in striking contrast with Stokes' law. This result undermines the physical meaning of the usual definition of the effective viscosity in microrheology experiments, in the case of an active fluid.

Our attempt to understand these results is based on the argument that a key role is played by the deformations of the director field close to the particle and determined by the anchoring condition. The resulting argument explains well the results obtained for planar anchoring and it allows predictions for the case of normal anchoring that are in good agreement with the results we found in this case. What is most important about this last case is that, differently from what obtained in all other simulations, including the ones on macrorheology, here we find that activity favours the external force in the contractile case, while opposing it in extensile fluids. Therefore these results imply a reduction of the effective viscosity in the contractile case with respect to the passive one and an increase of viscosity in extensile nematics. This points out that the effect of activity on the fluid resistance to flow is *not* an intrinsic property of the fluid, as the agreement between bulk rheology and microrheology experiments in the case of planar anchoring would have led us to conclude. Instead, even this effect is importantly affected by the method used to probe the fluid and by the anchoring conditions, i.e. by the specific microscopic interaction between the fluid and the experimental apparatus.

As a further proof of the important role played by the anchoring condition we considered also the case when there is no anchoring of the liquid crystal at the probe's surface. As expected, despite an effect of activity on the viscosity similar to the one seen in the case of planar anchoring, we do not observe a strong dependence on the particle size any more. We believe this is because the deformations in the director profile are now only determined by the flow and the region of the deformation must depend less importantly on the particle size.

To make sure that the effects that we observed were not a mere effect of the choice of periodic boundary conditions, we presented also the case when boundary walls are introduced in one direction (we did this only for the case of a probe particle with planar anchoring at the surface). We found good qualitative agreement with the results obtained without the walls, as a confirmation of the general character of our findings.

Finally, we would hope for microrheology experiments similar to the ones we

simulated, in active fluids such as bacterial suspensions and in the actomyosin solution. Recently active liquid crystals have been produced in experiments by using microtubules [24]. The nematic character of these suspensions, and the good control achieved on them give us confidence that our model of an active fluid gives predictions that should be comparable with experimental results that might be obtained in the future for this type of systems.

At the same time we note that the same experiments performed in a suspension of bacteria could be challenging and that the size of typical bacteria (around 1 μm), very similar to the one of typical probes, might complicate the understanding of the anchoring at its surface. To bridge our simulations to this more realistic situations, we also analysed the case when the amplitude of the liquid crystal order parameter is set to zero at the surface of the colloid. This should ideally break the order in a region surrounding the colloid close to its surface. The results that we found in this case are similar to the ones obtained when no anchoring condition was imposed, again lending credibility to the possibility of directly testing our results with experiments.

Chapter 5

Negative drag

Introduction

In this chapter we will present further results concerning the microrheology of active fluids, particularly of contractile ones. We start from our previous observation (see Fig. 4.6) that, in the case of planar anchoring, the resistence experienced by the particle is larger in contractile and smaller in extensile nematics than in their passive counterparts. Most strikingly, we found a strong dependence of the effective viscosity on the size of the particle and that the effect of activity is considerably more important when the particle is dragged parallel to the far-field director orientation in contractile fluids, while for extensile ones a larger effect is seen orthogonally to the director. In Chapter 4 we presented an argument that explains our findings well, and showed that it successfully predicts the system behaviour in the case of normal anchoring on the colloid, when the latter is dragged parallel to the far-field director orientation. In that case we gave only a qualitative explanation of the size dependence of the effective viscosity. Here we will recap our argument and investigate that dependence more quantitatively. We will provide a theoretical prediction for the extra active term that must intervene in the force balance, based on dimensional analysis. We will derive a correction to the passive viscosity and compare our predictions for the effective viscosity with our simulation results, finding good compatibility in the contractile case where, according to our basic model, the effective viscosity is expected to become *negative* for large enough absolute values of the activity coefficient and of the particle size. We investigated this regime and surprisingly

found a steady state where the particle moves in the direction opposite to the one of the external force. This 'negative drag' state is also characterised by significant memory effects.

We explained our results as due to the interplay between activity, flow, and liquid crystal distortions generated close to the colloid by the anchoring condition. In the case of planar anchoring the orientation of nematogens at the surface is as in Fig. 4.9 (a). The contractile or extensile character of nematogens is responsible for a force exerted by active particles on the fluid and ultimately on the colloid, directed as in Fig. 4.10 and Fig. 4.11. The motion of the colloid when an external force F is applied results in an asymmetry between the deformations at the front and the back of the colloid, that is responsible for a net force. The latter opposes F in contractile nematics and favours it in extensile fluids (see Fig. 4.12).

While these considerations allow for a qualitative explanation of our results, a more quantitative description is desirable. In the next section we will start from suggesting a formula for the extra active term that must contribute to the force balance, on the basis of dimensional analysis, and we will see that, remarkably, it leads to the prediction of the 'negative drag' state which we report in the simulations of this chapter.

5.1 Estimate for the Extra Active Force Term

The anomalous dependence of the effective viscosity on the radius of the probe, R, arises from an active contribution to the force acting on the particle, that must depend on the details of the flow and of the director profile. The latter can be computed only numerically. Nonetheless, an estimate for a correction to the Stokes' law coming from the active nature of the fluid, can be provided on the basis of dimensional analysis.

Since we do not see significant deviation from Stokes' law for passive nematics, we can write for this case a force balance that includes only the external force and the Stokes' viscous term, where the fluid viscosity η is substituted by an effective viscosity $\tilde{\eta}$: $F = 6\pi\tilde{\eta}Rv$. Here $\tilde{\eta}$ assumes a different value according to the direction of the external force. We consider such a force balance as a starting point and expect that the deviations of our results for active nematics from the ones for their passive counterparts must be accounted for by an additional "active" force

term. The extra contribution must be related to the active stress described in Eq. 2.17, that constitutes the main difference between the active and the passive system. The extra stress term is proportional to the activity coefficient ζ. The associated total active force is obtained by integrating it over the colloidal surface and dimensional analysis suggests:

$$F^a = A(F)\zeta R^2, \tag{5.1}$$

where $A(F)$ is an adimensional function depending on the external force F (as the asymmetry in the splay deformation in Fig. 4.12 is larger for larger F). The simplest case is that of $A(F)$ linearly dependent on F. Since when $F = 0$ there is no active force acting on the colloid, it must be $A(0) = 0$, so that $A(F)$ in the simplest case is proportional to F. Moreover, we expect that A relates somehow to the liquid crystal elastic constant K, since it affects the size of deformations in the director profile. On dimensional grounds, and considering that larger values of K are associated to smaller deformations, we can expect that:

$$A(F) = c\frac{F}{K}, \tag{5.2}$$

where c is a positive, dimensionless constant. The active force therefore becomes:

$$F^a = cF\frac{\zeta R^2}{K}. \tag{5.3}$$

The forces acting on the colloid are the external force F, the active force F^a, and an effective viscous force $F^v = -6\pi R\tilde{\eta}v$, that includes also the effect of the liquid crystal. The force balance is therefore:

$$F + cF\frac{\zeta R^2}{K} = 6\pi\tilde{\eta}Rv. \tag{5.4}$$

Remebering that we defined $\eta_{\text{eff}} = F/(6\pi Rv)$, we can find a relation between η_{eff} and $\tilde{\eta}$ as follows:

$$\frac{1}{\eta_{\text{eff}}} = \left(1 + c\frac{\zeta R^2}{K}\right)\frac{1}{\tilde{\eta}}. \tag{5.5}$$

According to Eq. 5.5, $1/\eta_{\text{eff}}$ depends linearly on R^2.

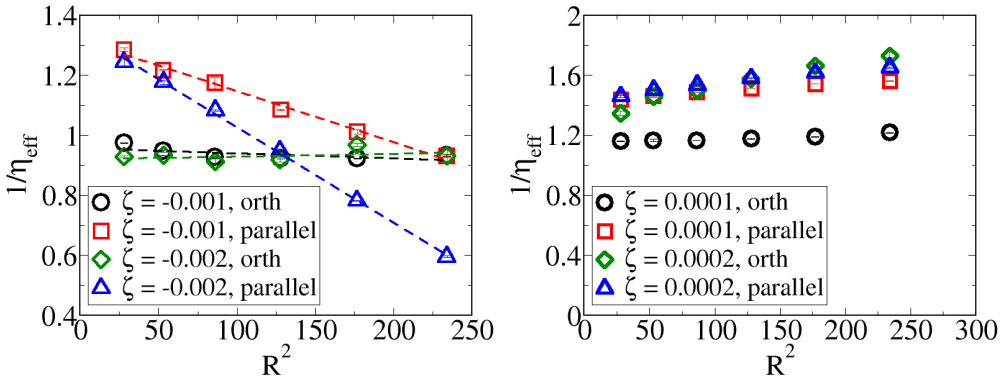

Figure 5.1: Plot of $1/\eta_{\text{eff}}$ on R^2, for a contractile (left) and for an extensile (right) nematic, yielding an approximately linear dependence in agreement with Eq. 5.5.

5.2 Comparison with Numerical Data

We verify this prediction in Fig. 5.1 where we plot $1/\eta_{\text{eff}}$ for an active nematic as a function of R^2, when planar anchoring on the colloid is imposed. Data for contractile nematics are very well fitted by a line, in both the cases of orthogonal and parallel drag force (see Fig. 5.1, left). In particular, in the latter case, we find that the intercept stays the same for both the values of ζ considered, giving $c = 0.06$. This result validates our description of the system that, albeit very approximate, is able to capture its distinctive character.

On the basis of such description, we were able to make further predictions. From a careful look at Fig. 5.1 (left), one realises that at large enough values of R^2 the lines referring to the parallel drag will cross the horizontal axis, thus apparently entering a region of *negative* η_{eff}. A negative bulk or microscopic viscosity is of course not physical for standard, equilibrium systems, and one may therefore expect that for large enough R our description of the system will break down as a sign of an instability. What happens when the region of larger R's in Fig. 5.1 (left) is explored, will be the subject of the next section.

In the case of extensile nematics our data are presented in Fig. 5.1 (right): although a linear behaviour can be recognised, our data do not show very good agreement with theoretical predictions: we find two different values of the constant c for different ζ. The dependence of η_{eff} on R in that case is smaller, and passive contributions to the stress tensor not included in $\tilde{\eta}$ might play an important role there.

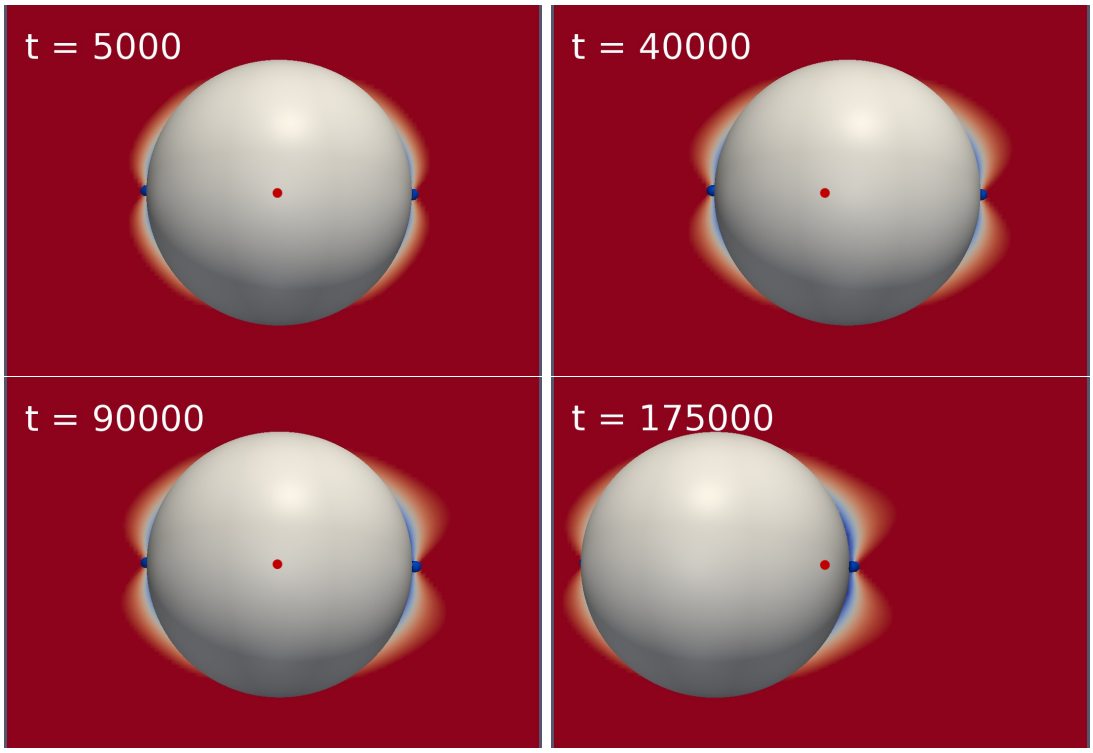

Figure 5.2: Snapshots of a colloid having radius $R = 30$ embedded in a contractile nematic liquid crystal having $\zeta = -0.002$ and dragged by a constant force $F = 0.8$ oriented horizontally, along the director, towards the right. Colours in the background refer to the x component of the director, going from red ($n_x = 1$) to blue ($n_x = 0$). The frames are taken at times $t = 5000$, 40000, 90000, 175000, as indicated. A red dot is used as a reference point for the starting position of the colloid. Note that, already from the second snapshot, the asymmetry between the deformations at the front and at the back of the colloid is evident.

5.3 The 'Negative Drag' State

That our argument predicts a negative viscosity, can be seen directly from Eq. 5.5: when $\zeta < 0$ (i.e. in the contractile case), for large enough values of the ratio $|\zeta|R^2/K$, η_{eff} becomes negative. In particular, for fixed ζ and K there is a critical value R_c of the colloid radius, such that for $R > R_c$ our description of the system predicts a negative value of η_{eff}.

This happens when $c|\zeta|R^2/K > 1$. We explored this regime by keeping K constant and choosing $\zeta = -0.002$. For this choice of parameters, the critical value of the colloid radius defined by $c|\zeta|R_c^2/K = 1$ is $R_c \sim 25$. Here we present

data from simulations performed with a colloid of radius $R = 30$.

We dragged the colloid through a contractile nematic. Fig. 5.2 shows screenshots taken from our simulation at different times. The external force in the figure is directed towards the right and the director in the bulk is directed horizontally. The background refers to its x component, as described in the caption. After an initial time interval where the particle moves forewards, in the direction of F (see first and second frames), the particle stops and starts moving towards the left, i.e. opposite to the external force. Note the asymmetry in the deformation (denoted in blue in the snapshots) of the director profile, which is larger on the right than on the left, in agreement with our description of the system (see Fig. 4.12). Fig. 5.3 was obtained by performing an ideal experiment where different constant external forces were applied to the colloid at different stages. Here we show both the force (dotted and dash-dotted lines) and the velocity of the colloid (continuous and dashed lines) as a function of time: first we applied a force $F = 0.8$ parallel to the bulk director orientation[1]. Strikingly the colloid reaches a steady state of negative velocity(!). This is a novel effect, allowed by the intrinsic out-of-equilibrium nature of active particles.

Imposing planar anchoring on such a large colloid determines large deformations in the liquid crystal. In particular, the local flow generated by active particles is now easily visible in a simple plot of the velocity field, as in Fig. 5.4 (left), which refers to the particle at rest. The flow field close to the particle is in very good agreement with our description of the system. Here the bulk director orientation is horizontal and the director deformation is a splay at the left and at the right side of the particle, while at the bottom and at the top the director bends. As one would expect for a contractile fluid, the local flow is directed towards the colloid in all these directions. The velocity profile around the colloid at steady state is shown in Fig. 5.4 (right): a net flow opposing F (red arrow), which is directed along the far-field director orientation, is clearly visible.

To further investigate this new regime we asked what happened when we turned off F while the particle was moving backwards at steady state. In a passive fluid the particle would have stopped. What we observed is shown in Fig. 5.3, where the reader can see that the velocity at steady state is negative also once

[1]According to our choice of parameters, for cytoskeletal gels this would correspond to a force $F = 20$nN, which is quite large considering that a typical value of K in such system is $K \sim 1.25$nN [83].

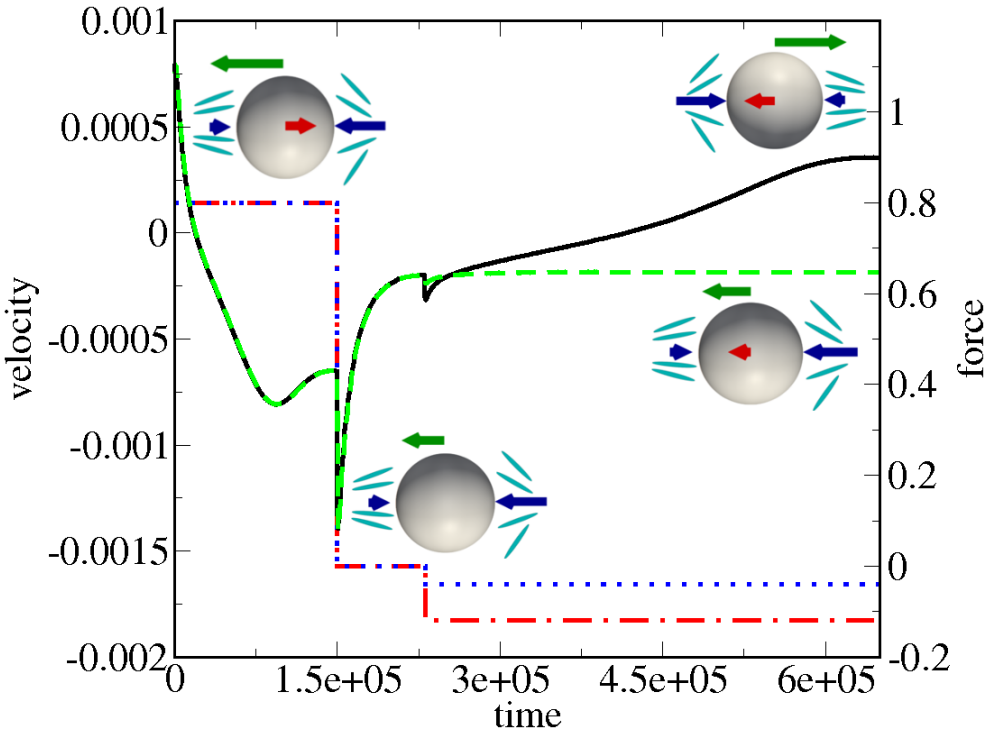

Figure 5.3: Dependence of the external force (step functions, axis on the right) and of the particle velocity (axis on the left) on time for two different 'experiments'. In both cases a force $F = 0.8$ is initially applied to the particle and turned off. Then a smaller force is applied along the direction of particle motion: the blue dotted line and the red dot-dashed one give the values of the external force in the two cases. The correspondent particle velocities are given by the black solid and green dashed lines respectively. The dynamics is discussed in the text. In the sketches arrows on the fluid refer to the active force direction, the arrow on the colloid represents the external force, while that above the particle shows the actual direction of motion.

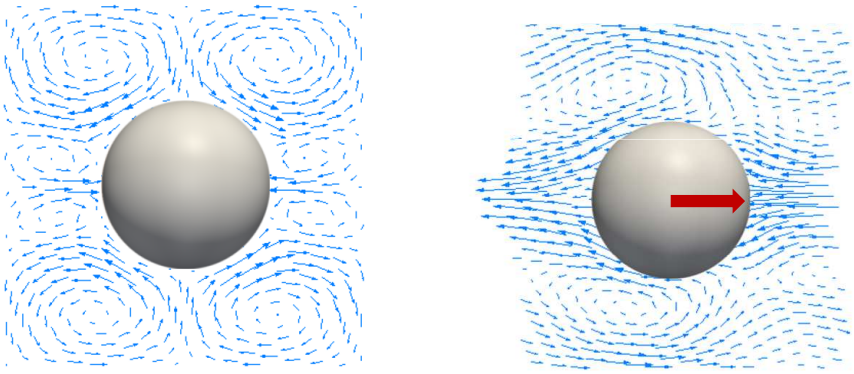

Figure 5.4: Velocity fields for the case of a quiescent particle (left panel) and of a particle moving to the left (panel on the right), opposite to the applied force (red arrow).

the external force has been turned off. This can still be explained through our argument and is the most important evidence of the presence of an instability, different from the well known bulk spontaneous flow, discussed in Chapter 1. In particular, if the colloid keeps on moving with a negative steady state velocity, the head-back asymmetry in the director deformation, responsible for the extra force term, must be maintained even when no external force is applied. This is possible only if a spontaneous local flow is generated. We explain our results conjecturing that, in the regime of large $-\zeta R^2/K$, where we observe the negative drag, the deformation is large enough to generate an instability where the local flow is able to self-sustain the asymmetry in the director deformation, even when the external force is turned off. This is supported by the characteristic instability of contractile nematics with respect to splay. Since no motion is observed when the particle is embedded in the fluid at rest, this effect must be strongly history-dependent. To understand this we continued our simulated experiment by turning on a negative external force, along the direction of motion of the particle. We expected that forcing the particle to move in that direction would have reversed the asymmetry in the director deformation that is responsible for the additional active force opposing F, thus making the particle move in the positive direction now.

This part of our ideal experiment, is plotted in Fig. 5.3. We considered two different values for F: $F = -0.04$ and $F = -0.12$. For small $|F|$ the force we exert on the colloid is not large enough to reverse its velocity, and the particle

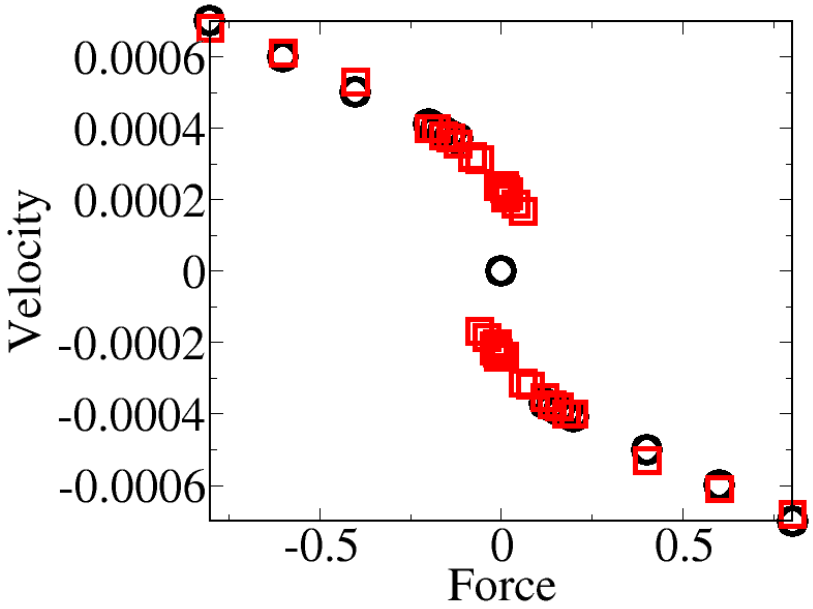

Figure 5.5: $v(F)$ curve for a case with negative drag ($R = 30, \zeta = -0.002$). Black circles and red squares refer to simulations in which the force is applied to a quiescent and moving colloid respectively.

keeps moving with negative velocity, having an absolute value just slightly smaller than the one characterising the steady state at $F = 0$. For larger $|F|$ though, we are able to impose a large enough perturbation to allow the particle to restructure the director profile, and move now in the *positive* direction. As described in the sketches of Fig. 5.3, we find that a large enough external force is able to reverse the asymmetry in the director deformation, so that the net force exerted by active particles on the fluid generates a flow that pushes the particle in the positive direction, once more against F.

A more complete characterisation of the system, as well as an explanation of the seemingly bizarre behaviour shown in Fig. 5.3 is provided in Fig. 5.5, where we plot the steady-state velocity of a colloid having radius $R = 30$, as a function of F. Two different colours are used, according to the initial state: we considered different initial conditions, both at a null external force. Part of the data (black circles) are obtained by starting from a quiescent state, where the particle is not moving, whilst others (red squares) refer to the case when F is applied when the particle is already moving at steady state. The black circle

at the origin refers to a zero force applied to a quiescent colloid: no motion is observed. When the external force is large enough, the particle velocity is always opposite to F, independently of the initial condition (squares and circles superpose), which provides robust confirmation of a regime of negative drag. Concerning data represented with red squares, the ones forming the branch of negative velocity were obtained by starting from the state where the colloid is moving in the negative direction, after the initial, external (positive) force has been turned off. What we find in this case is that there is a whole range of *small* forces that, when applied to the particle, do not allow to reverse its motion so that the direction in which the colloid moves at steady state depends strongly on the initial condition: the same force applied to a particle moving in the opposite (positive) direction would result into a positive velocity. In this sense there is a hystory-dependence in the behaviour of the system, that allows us to talk about hysteresis. The region of small $|F|$'s is characterised by bistability. Note that not all the points were obtained from direct simulations: we instead verified that the graph was symmetric with respect to the origin and then reproduced that symmetry for the missing data.

5.4 Discussion and Conclusions

In this chapter we provided an in-depth analysis of the results on microrheology in active fluids, and on the implications of our argument to explain them, presented in Chapter 4. In particular, we gave a quantitative, if approximate, explanation of the dependence of η_{eff} on the particle size, R, by considering an extra active force term in the force balance, whose form was guessed on the basis of a dimensional analysis. We derived an expression for the effective viscosity of active nematics as a function of the effective viscosity of their passive counterpart, that we could compare with our data. We found good agreement in the case of contractile nematics, which validated our interpretation of numerical results.

We also foresaw the onset of an instability in the regime of large $|\zeta|R^2/K$, where our formula predicts a negative value for the effective viscosity of a contractile nematic. Repeating simulations with a large enough colloid, we actually found evidence of a regime characterised by a steady state of negative drag where the colloid moves opposite to the direction of the external force, at

steady state.

We characterised that state by performing numerical experiments where the external force is first turned off, and then turned on again. We found that the steady state at zero force is characterised again by a small, non-zero negative velocity, which we interpret as an evidence of the existence of a local instability, able to sustain the flow that pushes the particle in the negative direction, and different from the global spontaneous flow that arises at large values of $|\zeta|L^2/K$. The response of the system when an external force is turned on again depends on its intensity. In particular, we performed two ideal experiments, both involving a negative force, by pulling the particle along the current direction of motion. We found that, for small values of the force, the particle continues to move in the negative direction, with a slightly smaller absolute velocity. A large enough negative force instead is able to reverse the asymmetry in the elastic deformation and to lead to a steady state where the colloid moves with a positive velocity.

We noticed that in this regime the system response to an external force strongly depends on the initial state. We studied this characteristic hysteresis by measuring the steady state velocity of a particle that was either quiescent or moving at steady state with no applied force. At large forces we found strong evidence of a stable regime of negative drag. At small forces the system is bistable: there are two steady state velocities that the system achieves depending on the initial condition.

It is worth noting here that all the simulations were performed in a 128^3 lattice, with periodic boundary conditions. In order to reach the region of large $|\zeta|R^2/K$, with ζ and K as in Fig. 5.1, we chose $R = 30$. This means that the size of the colloid is about half the simulation box, and the dynamics is certainly biased by the hydrodynamic interaction with its images in the confining boxes. We therefore believe that simulations concerning such a large colloid are not able to provide a quantitatively accurate description of the dynamics. However, we are confident that the one we obtained is a reliable qualitative portrait, since the prediction of negative drag was obtained from data referring to much smaller colloids, and corrected according to [82] (which was revealed to capture boundary effects well enough, also when liquid crystal elastic effects are introduced, as specified in detail in Chapter 4).

The existence of a steady state with negative drag is, to our knowledge, novel

and restricted to active systems. The simplicity of the experimental setup we have simulated could encourage experiments where spherical colloids are dragged through an active fluid, e.g. by using optical tweezers. These experiments, however, are still challenging at the moment for many reasons. Our results are based on a well-accepted model for active systems, that need to be dense enough and ordered, so to be described with a continuous model for liquid crystals.

This kind of description is in principle suitable for systems such as cytoskeletal gels, but some requirements are needed: in actomyosin macroscopic network clustering, described e.g. in [86], is to be avoided. This can be done e.g. through a suitable choice of parameters. Its contractile nature, and the fact that in specific conditions it is characterised by (polarised) order, make actomyosin ideal to test our predictions. It seems still very difficult to realise a suitable experimental system, for which our model could represent a good description, with bacteria: this would require dealing with a sufficiently dense suspension, where order should be maintained, which seems challenging at the moment. However, new possibilities could come from different systems. Recently, an extensile nematic gel has been synthesised by Dogic *et al.* [24], from biological material extracted from the cell. It is a gel consisting of microtubules, whose activity can be induced and controlled by adding kinesin motors. This system seems promising as relatively easy to control. However, it would not allow to benchmark the existence of a regime of negative drag, which we predict to be peculiar of contractile nematics.

Although directly performing the experiments we suggest is still a difficult task, something analogous to our negative drag has already been observed in contractile active systems. In particular, an accelerated load response was observed in experiments on molecular motors moving along microtubular or actin filaments, where a load force was applied against the unloaded direction of motion [87].

In [88] an experiment is described where an axon is mechanically stimulated through a microneedle. The authors observe that in many cases the axon actively contracts in response to the external stress. This behaviour is similar to the one observed in our simulations since contraction requires a response from the system that opposes the external stimulus. Hence ours is not the only example of an active system whose response to external forcing has the opposite sign to that arising in passive systems.

Chapter 6

Collective Behaviour of Colloids in Active Fluids

Introduction

We now move to a system of several colloids embedded in an active fluid. Colloids have recently been used widely as constituents for new materials. New modes of interaction can be designed in different ways, which usually involve a mechanism that breaks rotational symmetry. This can be done e.g. by imposing an external field [43], by using particles with polyhedral shape [48, 89], or by decorating colloids with attractive patches [90]. Anisotropy can also be introduced at the level of the solvent, as happens when colloids are embedded in liquid crystals, where colloidal interactions depend on the long range liquid crystalline order and on the type of anchoring at the surface, thus giving rise to a variety of structures that result into different macroscopic properties [51, 91]. In the next section we will briefly review the current knowledge on these systems.

Activity opens up a new direction for colloidal particles to self-organise. Large number fluctuations (that were introduced in Chapter 1), flocking and clustering [14] are hallmarks of the collective behaviour of active particles. These properties were initially associated to their anisotropy and tendency to form orientationally ordered phases, but they were later suggested in [92] to be a more general property stemming from the local energy input that is among the defining characteristics of active systems [14]. In particular, when the self-propulsion velocity decreases with density (e.g. due to crowding) clusters or stable patterns can form [93, 94, 95].

These results prove that activity strongly promotes aggregation and can be used as a valuable candidate route towards colloidal self-assembly. Self-propelled colloids have already been predicted to aggregate in the form of glassy [96] and crystalline phases [94, 95, 97], and signs of their crystallisation have been observed for a number of systems [47, 98].

Motivated by these premises, here we aim at shedding light on the collective behaviour of a diluted system of passive spherical colloidal particles embedded in active liquid crystals. Recent studies have considered systems of passive beads in active suspensions, but were mainly focussed on very dilute suspensions of tracers and on the effect of activity on their motion, which can be described as an increase in the diffusion constant, known with the name of *enhanced diffusion* (see e.g. [99]). In [100], a system of beads embedded in a bacterial suspension was considered and it was observed that the active character of the ambient fluid resulted into an effective attraction between the beads, which was interpreted as a result of the run-and-tumble motion of bacteria, coupled to a depletion effect. This makes it difficult to distinguish the actual contribution of activity. Our system is different from that of [100], since we are not taking into account the self-propulsion of active particles. Moreover, since we are using a continuum model, there is no depletion interaction between the passive colloids.

We will consider different activity coefficients and anchoring conditions, with the main purpose of analysing how structure formation can be affected by activity.

Comparison with the case of passive liquid crystals, as ambient fluids, will arise naturally, and major differences will be found in the regime of spontaneous flow, where the peculiarity of active fluids shows up most strikingly. In the previous chapters we have shown that the effective rheological properties of active fluids are importantly conditioned by the system size and by the anchoring, both at the boundary and at the surface of a colloidal probe. One expects that the presence of colloids might similarly affect the transition from the quiescent to the spontaneously flowing phase. For this reason, before analysing how aggregation properties change in response to activity, we study how the presence of colloids influences the onset of spontaneous flow. We do this for different anchoring conditions and our data show that colloids play an important role and also change the character of the transition.

We find that activity can strongly affect colloidal aggregation, in a way that

can be tuned by changing the anchoring strength. We find that in the case where no anchoring condition is imposed, as is likely when colloids are embedded in a dense bacterial suspension, activity is responsible for the dynamic formation of inhomogeneities in the distribution of colloids.
The opposite happens when colloids strongly affect the liquid crystalline order close to their surface and are associated with the presence of defects. In the passive case colloidal aggregates form during the process of liquid crystal relaxation. Activity in this case tends to break clusters, which results into a more homogeneous distribution of colloids in space.

We here focus on the case where the liquid crystal is initialised in the nematic phase (with a small amount of noise to allow the transition to spontaneous flow). In the next chapter we will present results obtained with a different initial condition (a quench from the isotropic to the nematic phase).

6.0.1 Self-Assembly of Colloids in Liquid Crystals

Colloidal structures in liquid crystals strongly depend on the topology of the system. The interaction potential has been described in detail for the nematic case and allows for a good theoretical understanding of experiments.

When colloids are significantly larger than mesogenic particles, the energetic cost of defects and deformations can be described in the framework of a continuum elastic theory [50]. Dimensional analysis suggests that the elastic cost for embedding a colloid in a nematic liquid crystal is of the order of KR, where K is the liquid crystal elastic constant, and R is the colloidal radius. This energy can be several orders of magnitude larger than thermal fluctuations[1] and the equilibrium state for the system is therefore the one of minimum elastic energy, where minimisation is attained through colloidal clustering [50].

Defects are responsible for both an attractive and a repulsive component of the effective interaction potential. In particular, the anchoring condition imposes the presence of a region of paranematic order close to the colloidal surface, where the elastic energy of the liquid crystal is higher. When colloids get closer to each other, their paranematic regions merge, thus contributing to a reduction of the total elastic energy of the system. This leads to a long range attractive

[1] A typical value of K for e.g. 5CB, a commonly used nematic liquid crystal, is 3 pN, while R is typically $\sim 1\mu$m.

component of the effective interaction potential. However, defects belonging to different colloids carry the same topological charge, and cannot annihilate. This is responsible for a short range repulsive potential: defects cannot be removed and the equilibrium distance between pairs of colloids is larger than their diameter.

Most of the work has been focussed on the case of nematic liquid crystals, which we will review briefly, while more recently attention has been addressed to the cases of cholesterics [101, 102] and blue phases [103, 104].

Self-Assembly of Colloids in Nematic Liquid Crystals

The nematic phase of passive liquid crystals already includes a wide spectrum of possible interactions, depending on the type of anchoring. Here we will review current knowledge on the effective interactions between colloids in passive nematics, together with the characteristics of self assembled structures.

Normal anchoring

Hedgehog defect. In the case of spherical colloids embedded in a nematic liquid crystal with normal anchoring, either a hedgehog defect or a Saturn ring defect will form. Experimental results for the former were presented in [50] and in [105]. The presence of a point defect on one side of the particle attributes a preferential direction to the interaction potential and allows for the formation of lines of colloids [50]. The director profile in that case is very similar to a dipolar electric field and colloidal structures forming in this case can be partly explained with this analogy, which can be tested through the direct measurement of the interaction force along the dipolar main axis [72, 105, 106, 107, 108]. At close distances, however, repulsion is observed, since colloids are never seen to touch at equilibrium. Experiments proved that these short-range effects are very complex and cannot simply be explained by including higher order terms in the interaction potential, as the electrostatic analogy might suggest [108].

In [109] large colloidal volume fractions were embedded in an isotropic liquid crystal, which was then quenched to the nematic phase, leading to a material with solid-like properties. Networks of colloids connected by defects were observed and it was suggested that they originated from the trapping of colloids in disordered regions that shrinked during the quench, thus driving colloidal clustering.

Saturn ring. The study of colloidal self-assembly in the case of Saturn rings

was delayed with respect to the one of dipoles. This is mainly for two reasons. On one hand the director deformation pattern in the far field has a quadrupolar symmetry. This means that the interaction between pairs of colloids decays faster as a function of their distance ($\sim r^{-6}$), than it does in the case of a hedgehog ($\sim r^{-4}$), so that this configuration was thought to be less interesting for the purpose of self-assembly. On the other hand, Saturn ring defects are more difficult than hedgehogs to observe in real systems. Simulations predicted that for large particles and sufficiently strong anchoring ($w = WR/K \gg 1$) the dipolar configuration is preferred. The Saturn ring should appear for small w [13, 110, 111]. However, experiments have proved that the dipole is prevalent even for spheres of nanometric size [72]. An easy way to see Saturn rings in experiments is to confine the system in two dimensions [72]. This case drew increasing interest after simulations predicted [52, 112, 113], and experiments performed on pairs of colloids confirmed [113], that, when at close distances, Saturn rings form entangled and more stable configurations than a pair of isolated rings and that the interaction force is significantly larger than in the non-entangled case [113]. Structures of several ($\sim$10) colloids were observed experimentally to be characterised by a "zig-zag" shape [114].

Simulations predicted that in three dimensions sufficiently high colloidal volume fractions ($\sim 15\%$) should lead to the formation of sheets [115] or networks [51], rather than lines. In [51] colloidal volume fractions of up to about 20% were considered. What they saw in experiments is that at volume fractions smaller than $\sim 15\%$ colloids formed isolated clusters, while at larger volume fractions a connected network was observed, associated with macroscopic solid-like behaviour. This was described as a self-quenched glass. Comparison with simulations at similar volume fractions showed that colloids are kept together by a percolating defect network, most probably responsible for such a high material rigidity [51].

Planar Anchoring

In the case of planar anchoring, mesogens lie parallel to the colloidal surface and two boojums form at opposite poles with respect to the far-field director orientation. In the electrostatic analogy, such configuration can be described through a quadrupolar potential. A detailed study of the interaction potential can

be made through the minimisation of the system's elastic and surface free energy [116, 117]. Comparison with the quadrupolar potential shows that nonlinear effects are responsible for a short-range attraction also at angles with the far-field director at which the electrostatic analogy predicts repulsion. This is due to the nonlinear superposition of the distortions in the director field when two colloids are close to each other [116, 117]. Experiments [118] have shown agreement with these theoretical predictions, and the measured preferential orientation between colloids was found at angles of about thirty degrees, in agreement with [116] (but not with [117]).

6.1 Simulations Details and Limitations

The parameters used in this chapter for the liquid crystal are as in the previous chapters (see Section 4.2.1), apart from the parameter γ, appearing in Eq. 2.4, which was here chosen to be equal to 3.1. This choice is motivated by the fact that in Chapter 7 we will compare the results of this chapter with the ones obtained when initialising the liquid crystal in the isotropic phase and performing a quench. In order for that to be possible we chose a value of γ larger than 3 (which according to Eq. 2.4 corresponds to the spinodal temperature), to make sure that an absolute minimum of the free energy was found in the nematic phase.

We point out here that we neglect any thermal fluctuations, which are very small with respect to the liquid crystal elastic energy (as previously mentioned), and therefore do not play a role when colloids are very close to one another. Moreover, in the active phase, when spontaneous flow is present, advection is usually very important and the Brownian motion of colloids is negligible[2]. However, thermal fluctuations could affect colloid-colloid long range interactions, and therefore the way the system reaches equilibrium in the case of small values of the activity parameter ζ (defined in Chapter 2, Section 2.3), particularly when the system is already in the nematic phase.

We focus here on systems of 771 colloids of size $R = 2.3$ lattice sites, in a simulation box of size $128 \times 128 \times 16$, corresponding to a volume fraction of 15%. The colloids are hard spheres that interact with each other through an

[2]The importance of advection with respect to diffusion is quantified by the *Péclet number*, defined as the ratio of the advection rate over the diffusion rate: $Pe = vR/D$, where v is the fluid velocity, R is the size of the colloid, and D its diffusion coefficient.

additional soft potential, acting between their surfaces, whose role is to forbid the colloids from getting too close to one another. In our lattice Boltzmann simulations, ideally there should always be at least one fluid node between two colloids in order to correctly account for hydrodynamic interactions [119]. The soft potential has the form:

$$V(r) = \begin{cases} \epsilon \exp\left[-\left(\frac{r}{\sigma}\right)^{\nu}\right] & \text{for } r \leq r_{\text{cutoff}}, \\ 0 & \text{for } r > r_{\text{cutoff}} \end{cases} \tag{6.1}$$

where r here denotes the distance between the surfaces of colloids. We used the following values of parameters: $\epsilon = 0.004$, $\sigma = 0.8$, $\nu = 6.0$, $r_{\text{cutoff}} = 1.5$, validated from lattice Boltzmann simulations in passive fluids [119]. Since for $w > 0$ the particles attract quite strongly due to the presence of defects, in order for them not to move too fast or to get too close to one another, we had to choose a significantly high value of r_{cutoff} and of σ. Moreover, when $w > 0$ also spurious velocities (introduced in Chapter 3, Section 3.2.2) may play a role. Since they are of the order of 10^{-5} and are localised at the colloidal surface, as the soft potential spurious velocities may affect some details of the bound state configurations at late times and short range, without competing with long range elastic and spontaneous flow effects, which dominate the phase behaviour of the system and on which we focus here. We are confident that our approach gives a good description of the system and of its clustering properties, even though for small ζ, at large timescales the soft potential allows for a broader exploration of the phase space than mere elastic interactions.

6.2 Results

6.2.1 Spontaneous Flow in Quasi-2D Active Liquid Crystals

We start here with a characterisation of the flow that we observe in the absence of colloids. The transition to spontaneous flow for nematic liquid crystals was studied in [3, 38, 40] for quasi-one and quasi-two dimensional systems with walls. In [120] active nematics confined in cylindrical geometries were studied and the onset of a flow was observed as stemming from defects appearing at the boundary

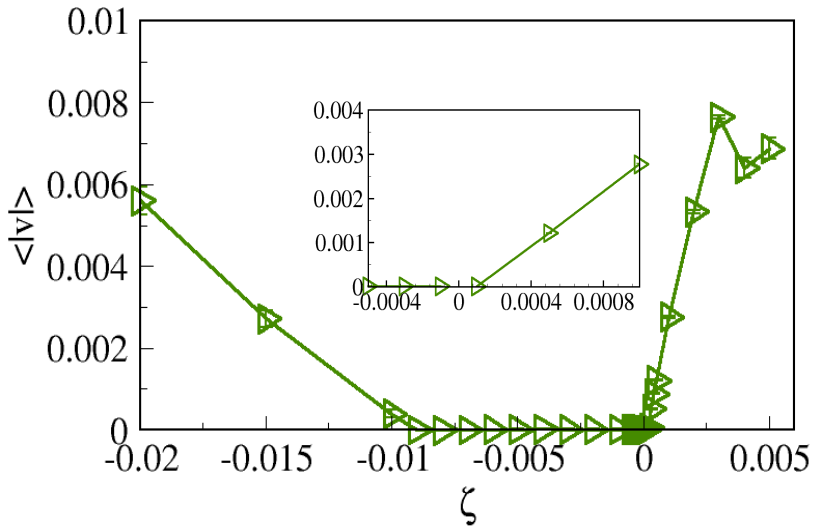

Figure 6.1: Stability curve for active nematics in a $128 \times 128 \times 16$ simulation box, in the absence of colloids; the inset shows a zoom-in in the region of small $|\zeta|$. The liquid crystal is initially in the nematic phase, with the director along the x-axis, and a tilt of about 10° is introduced along the xy-plane to trigger the instability.

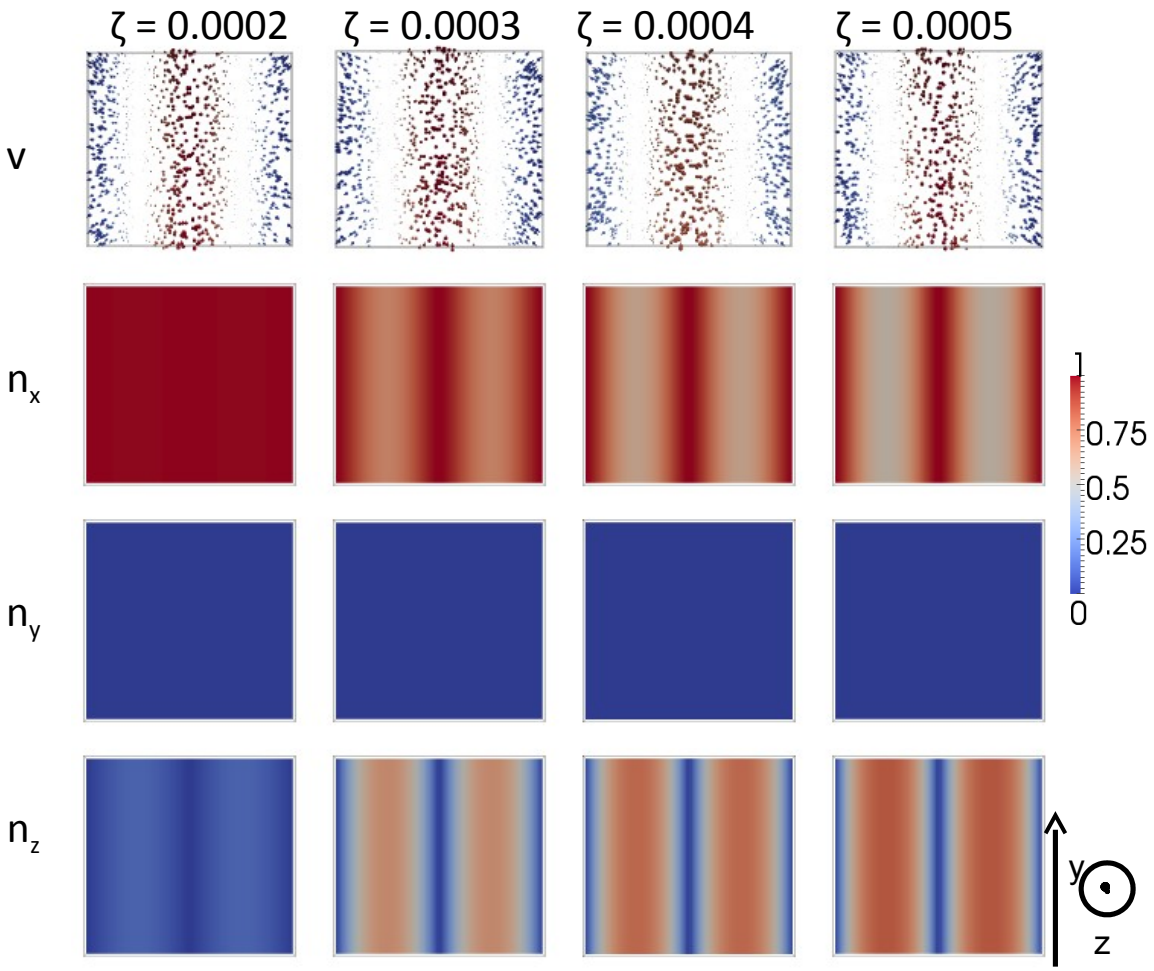

Figure 6.2: Velocity and director profiles developing in extensile nematics in a regime of spontaneous flow, for ζ between 0.0002 and 0.0005 and in the absence of colloids. For the velocity profile we show only the xy plane and use colours to quantify the z component: the colour goes from red, denoting the largest positive component along the z axis, to blue, denoting the smallest negative z-component. For the director profile we show 2D maps for each of the components, where the colours go from blue (denoting that that component is equal to zero) to red (that component is equal to one). These snapshots refer to time $t = 160000$.

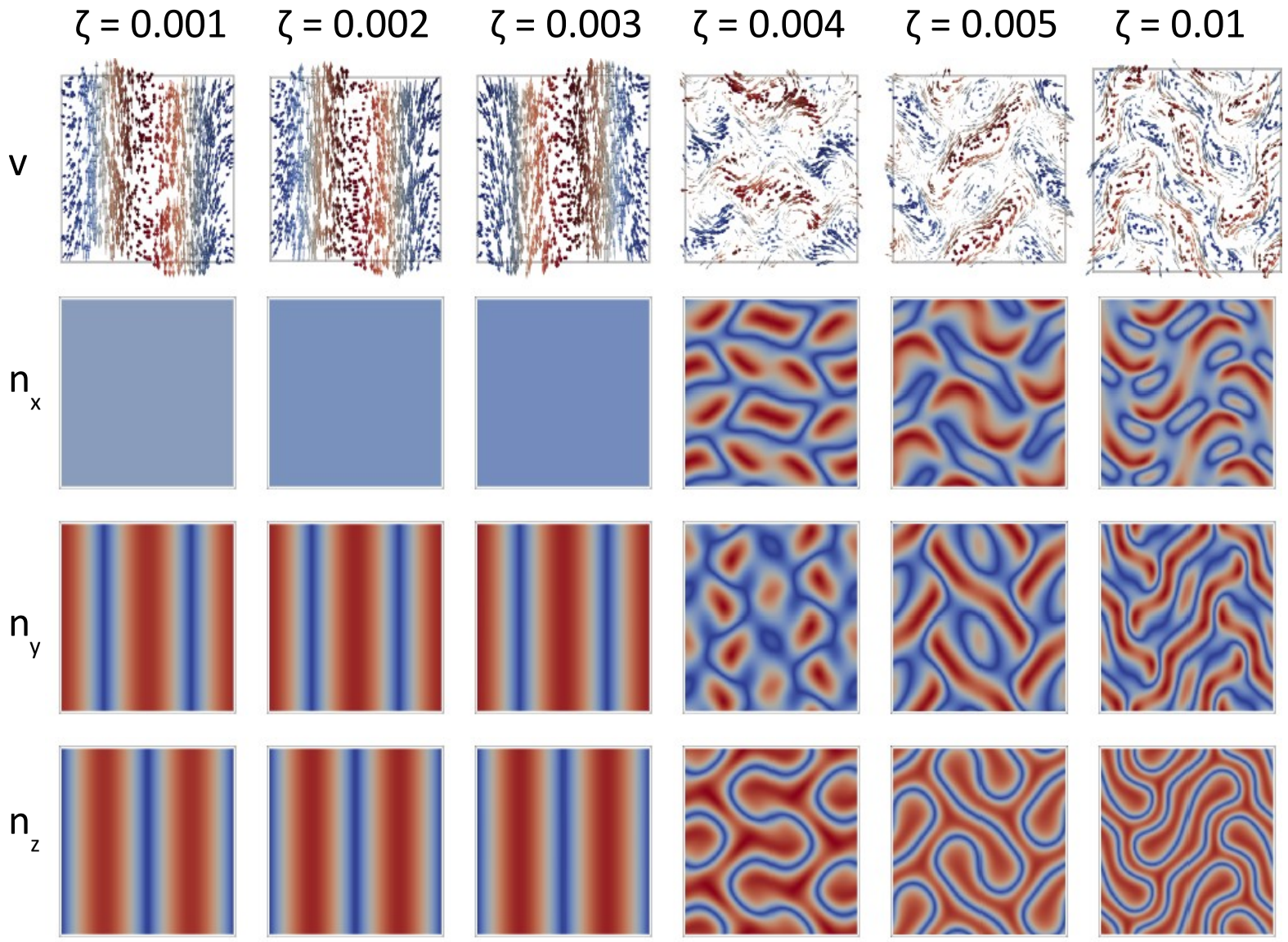

Figure 6.3: Velocity and director profiles developing in extensile nematics (without colloids) in a regime of spontaneous flow, for ζ between 0.001 and 0.01. The colour coding for both the velocity and the director is as in Fig. 6.2. These snapshots refer to time $t = 160000$.

due to the anchoring condition. Active nematics were simulated in [121] to describe the interactions between two defects of opposite charge, which were proposed as a new framework for the interpretation of spontaneous flow.

Here we consider a quasi-two dimensional system[3] with periodic boundary conditions. In this chapter the liquid crystal is initialised in the ordered phase, with the director parallel to the x-axis and we only introduce a 10° tilt of the director along the xy plane as a small perturbation required to trigger the instability (the nematic phase is metastable). As a measure of macroscopic flow, we compute $\langle|\vec{v}|\rangle$ by averaging the modulus of the fluid velocity, here denoted as $\vec{v}$, over the whole lattice. The stability curve is shown in Fig. 6.1. Critical activities $\zeta^0_{c,contr}$ and $\zeta^0_{c,ext}$ can be defined for contractile and extensile nematics respectively, such that spontaneous flow arises for $\zeta > \zeta^0_{c,ext}$ and $\zeta < \zeta^0_{c,contr}$, as it is clear from Fig. 6.1. From our data we see that spontaneous flow develops for $\zeta < -0.008$ and $\zeta > 0.0001$ for contractile and extensile active fluids respectively.

Figures 6.2 and 6.3 show the velocity and the director profiles in case of spontaneous flow for extensile nematics (in the case of $\zeta < \zeta^0_{c,ext}$ there is no flow). From the velocity profiles we see that for small ζ ($\zeta \lesssim 0.0005$) the flow is one dimensional and directed along the z axis. For very small ζ the director profile remains unaffected by the flow (and therefore directed along x), but already at $\zeta = 0.0003$ distortions of nematic order appear where the flow is more intense. For values of ζ between 0.0002 and 0.0005 this scenario stays almost unchanged and larger activities simply correspond to a larger flow (see Fig. 6.2). At $\zeta = 0.001$ the flow becomes two-dimensional by acquiring a significant non-zero component along the y axis. This affects also the director profile: $\hat{\mathrm{n}}$ lies now in the zy-plane and has only a small component along x. At $\zeta = 0.004$ vortices appear and both the flow and the director profiles become fully three-dimensional. Increasing ζ results into the appearance of more and more vortices.

In contractile nematics spontaneous flow arises more abruptly than in extensile ones, in agreement with previous studies [122]. This case is shown in Fig. 6.4 where we show the velocity and the director profiles once spontaneous flow has set in (i.e. for $\zeta \lesssim -0.009$). The characteristics of the flow in this case are completely different: vortices appear already at $\zeta = -0.009$, and they are limited to the xy plane, while the z component of the velocity field is negligible. This

[3]By that here we mean that the simulation box has a size comparable to the one of the colloid along one direction, along which the system is, in practice, translationally invariant.

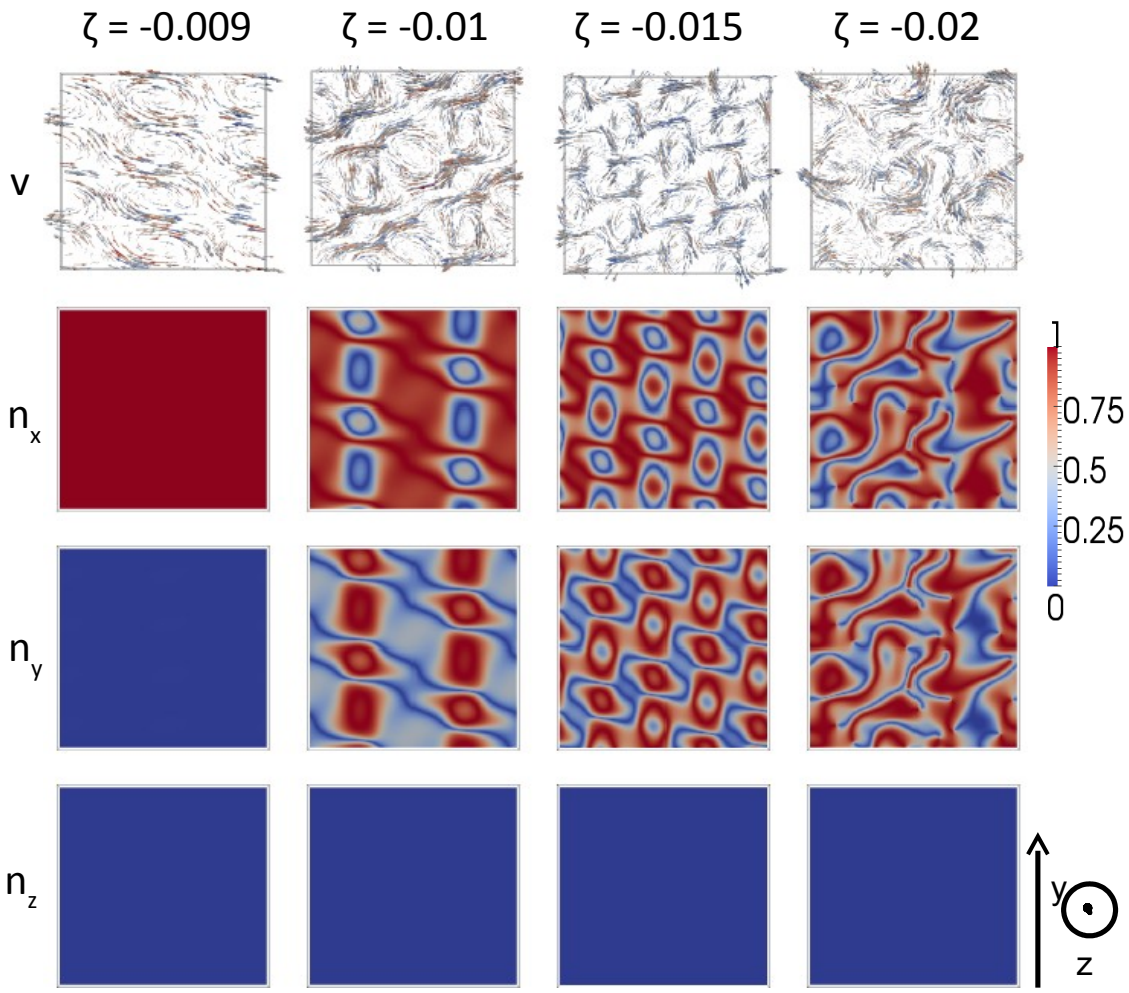

Figure 6.4: Velocity and director profiles developing in contractile nematics in a regime of spontaneous flow, and without colloids, for ζ between -0.009 and -0.02. The colour coding for both the velocity and the director is as in Fig. 6.2. These snapshots refer to time $t = 160000$.

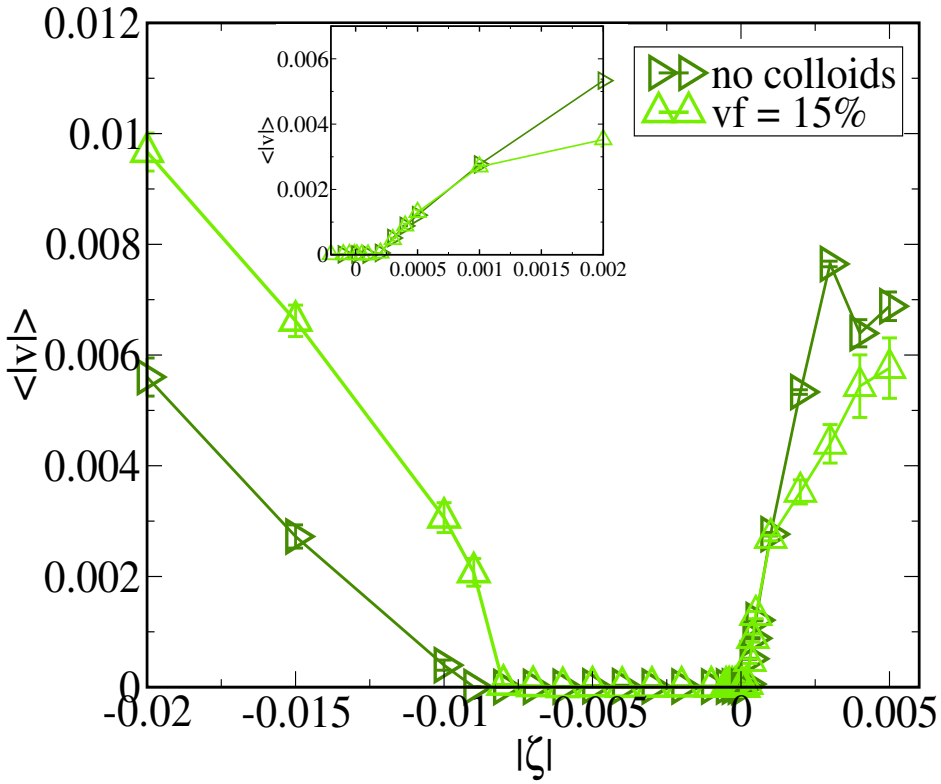

Figure 6.5: The average modulus of the fluid velocity is studied as a function of ζ for extensile ($\zeta > 0$) and contractile ($\zeta < 0$) active nematics, without colloids (right triangles) and in the case of a colloidal volume fraction (vf) of 15% (up triangles), when no anchoring condition is imposed at the colloidal surface. The inset shows a zoom-in on the data at small $|\zeta|$. These data were averaged over a range of times at steady state.

remains true for all the values of ζ that we considered (up to $\zeta = -0.02$). As in the extensile case, more vortices appear when ζ is increased and at $\zeta = -0.02$ the flow is visibly chaotic and even results into the appearance of defects.

6.2.2 Colloids Affect the Transition to Spontaneous Flow

As an aside and necessary preliminary study for the understanding of the way in which activity affects colloidal aggregation, here we analyse how the presence of hard spherical particles impacts on the transition from a quiescent to a spontaneously flowing phase.

Colloids are expected to affect that transition, because of the local distortions

they create when a specific anchoring is imposed at their surface. Further to that, the onset of instabilities was shown to be strongly dependent on the size of the system [38], and could be affected by colloids also when they are not directly associated to the presence of defects (due to the no-slip boundary condition at their surface). We first analyse this case, which is equivalent to working in the limit of very small anchoring strength $w \to 0$, that we obtain in simulations by imposing $w = 0$. The results that we present here and in the next chapter refer to a box size of $128 \times 128 \times 16$ (quasi-two dimensional), with periodic boundary conditions.

In Fig. 6.5, we show the dependence of $\langle|\vec{v}|\rangle$ on ζ, in the case of extensile and contractile nematics, and compare the curve obtained without colloids with the one referring to a 15% volume fraction. Here and in the remainder of this chapter the colloids that we consider have a diameter of 4.6 lattice units. In the case of extensile nematics colloids do not affect the critical activity and the stability curve for small values of ζ, as the inset in Fig. 6.5 shows. However, for $\zeta > 0.001$ the average fluid velocity is reduced in the presence of colloids, as one would expect by considering that a no-slip boundary condition is imposed at the colloidal surface. At negative ζ the value of $|\zeta_{c,contr}|$ at which the spontaneous flow arises is slightly smaller when colloids are present. Moreover, the average fluid velocity at a fixed ζ, when not zero, is always larger in the presence of colloids than in their absence for the range of activities that we considered in our simulations (Fig. 6.5). We conclude that, in the limit of very small anchoring strength, colloids slow down spontaneous flow in extensile nematics, while enhancing in contractile ones. We suggest that this effect is related to the strong instability of contractile nematics with respect to (splay) deformation in the director field, that is also at the origin of the much quicker onset of spontaneous flow with chaotic character than in extensile nematics, as described in [122], and as we have just shown for the case of bare active nematics.

We now look at the velocity and director profiles, in order to characterise the spontaneous flow also in the presence of colloids. In the case of extensile nematics (Figures 6.6 and 6.7) we still observe the same qualitative behaviour as in the absence of colloids, but now the transition from a one-dimensional to a two-dimensional flow takes place between $\zeta = 0.0002$ and $\zeta = 0.0003$, i.e. at significantly smaller ζ. Vortices appear already at $\zeta = 0.002$, at which the flow

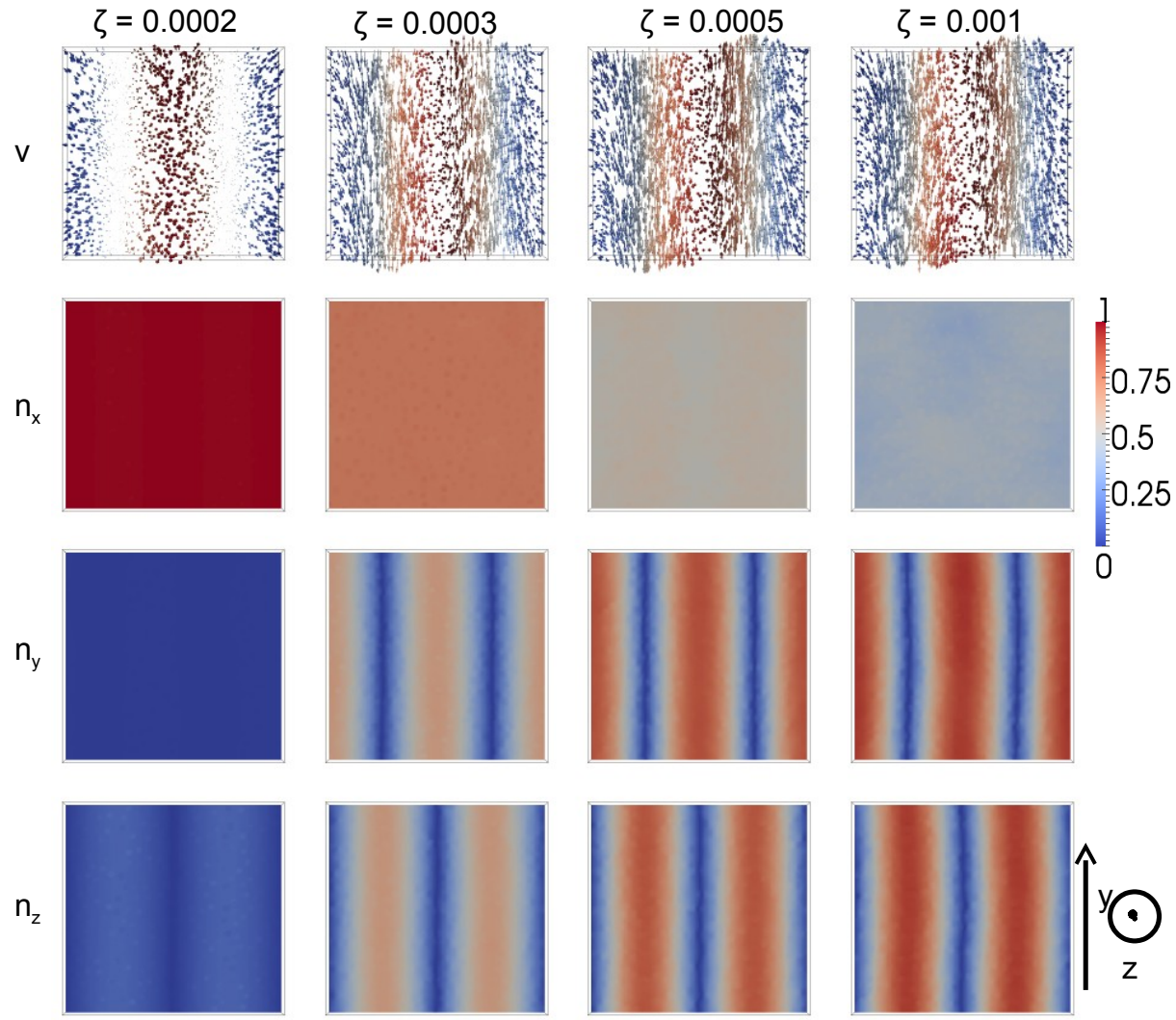

Figure 6.6: Velocity and director profiles developing in extensile nematics, with a 15% colloidal volume fraction, in a regime of spontaneous flow, for ζ between 0.0002 and 0.001. Here $w = 0$. The colour coding for both the velocity and the director is as in Fig. 6.2. These snapshots refer to time $t = 160000$.

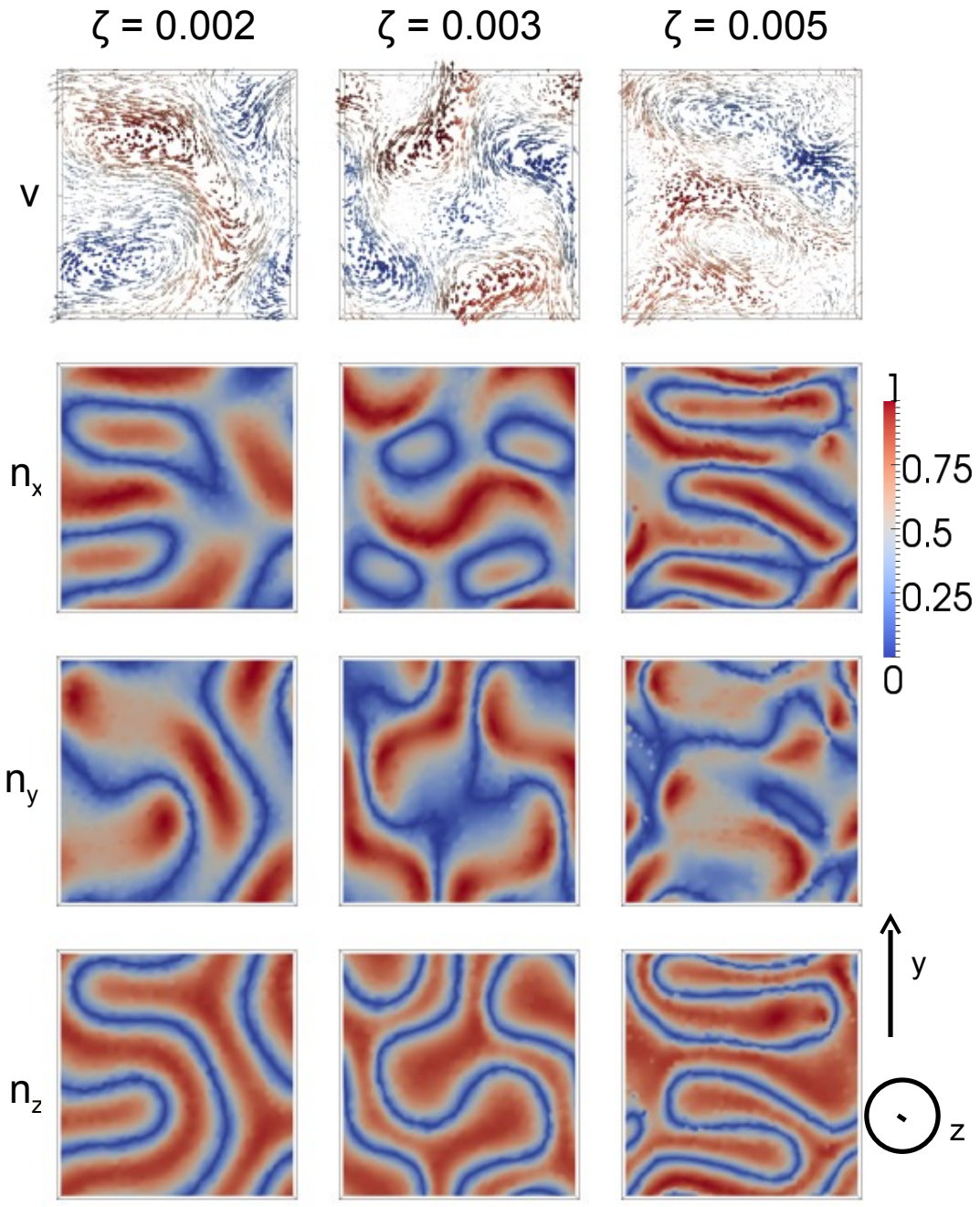

Figure 6.7: Velocity and director profiles developing in extensile nematics, with a 15% colloidal volume fraction, for the case of $w = 0$, in a regime of spontaneous flow, for ζ between 0.002 and 0.005. The colour coding for both the velocity and the director is as in Fig. 6.2. These snapshots refer to time $t = 160000$.

is already fully three-dimensional and chaotic: the flow and the director profile continuously change in time. For $\zeta \gtrsim 0.002$ the role of colloids is dual: they enhance the appearance of a three-dimensional flow characterised by vortices and they disrupt the ordered patterns that we could still see at $\zeta \lesssim 0.01$ in the absence of colloids, thus favouring the onset of a flow with chaotic character.

It is also interesting to look at how the presence of colloids affects the time evolution of the system, which we show in Figs. 6.8 and 6.9, where we compare velocity profiles without (column on the left) and with a 15% volume fraction of colloids (right column) at different times, for $\zeta = 0.0003$ and $\zeta = 0.003$ respectively. The same scaling factor for the velocity was chosen for all snapshots in each case, and one can see that in the presence of colloids the flow is less intense (arrows are smaller), in agreement with what is shown in Fig. 6.5 for extensile fluids. Fig. 6.8 shows that, when colloids are there, the flow is initially along the z axis, as in the case of a bare fluid, but it later develops also along y. The case of $\zeta = 0.003$ is particularly significant. Fig. 6.9 shows that even in the presence of colloids, where at this value of ζ we know that the flow will end up having a three-dimensional, chaotic character (see Fig. 6.7), the velocity profile is initially only one-dimensional, along z as in the absence of colloids, and progressively develops along other directions, first along y and then along x. At this point it is fully chaotic. When colloids are not there the flow is first one-dimensional and directed along z for a long time before reaching the steady state where the flow is two-dimensional and restricted to the zy plane. This happens after the flow in the presence of colloids has already developed a chaotic character.

The case of contractile nematics is presented in Figures 6.10 and 6.11. As we noticed previously spontaneous flow sets in at smaller $|\zeta|$ when colloids are present: a small flow, unable to affect the director profile, is observed already at $\zeta = -0.007$. The flow is again confined in the xy plane and characterised by a regular pattern of vortices. At $\zeta = -0.008$ the flow becomes more intense and deformations in the director profile become visible. At $\zeta = -0.009$ the flow is chaotic and so strong that important deformations develop, affecting only the x and the y component of the director. These characteristics are maintained for all the values of $\zeta < -0.009$ that we considered: larger $|\zeta|$ are simply associated to larger deformations of the director profile, that however is still confined to the xy plane. The time evolution of contractile systems is affected by colloids very

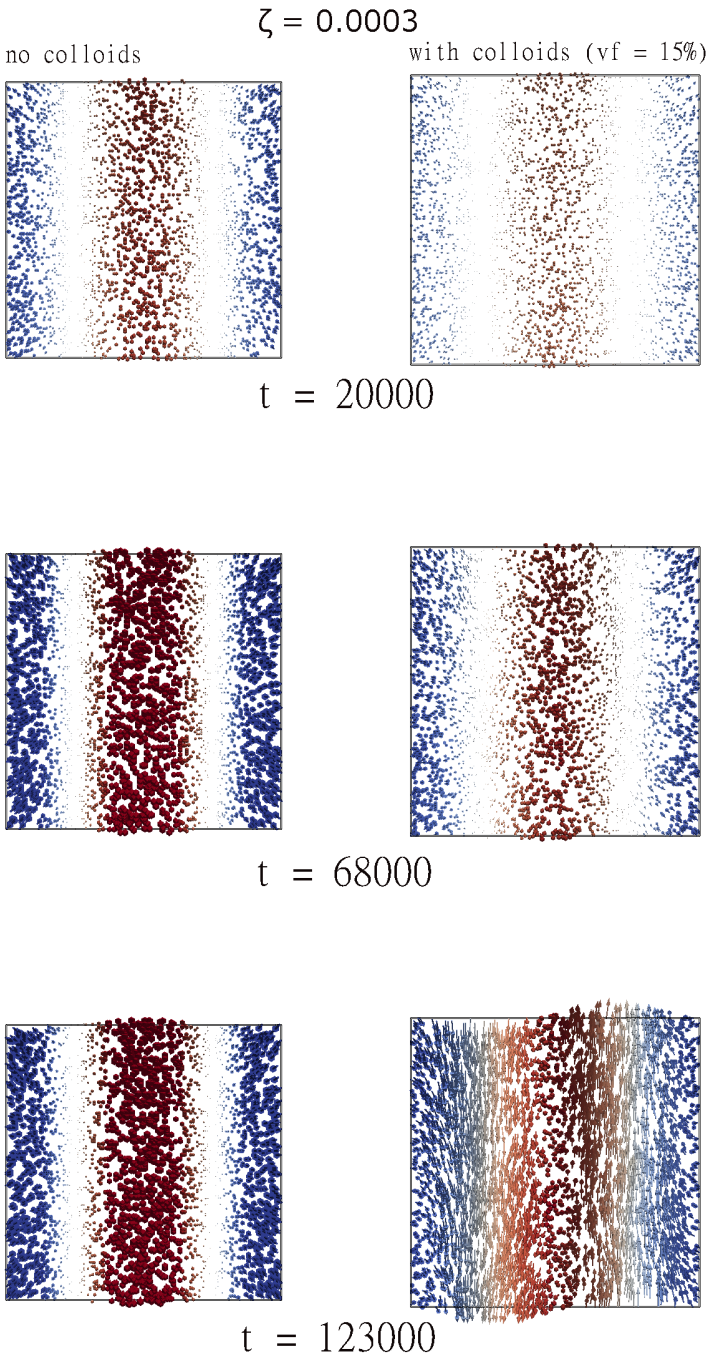

Figure 6.8: Snapshots for the velocity profile of an extensile nematic at $\zeta = 0.0003$ without (left column) and with (right column) colloids. The colloidal volume fraction is 15% and the adimensional anchoring strength is $w = 0$. Cartesian axes here are directed as in Fig. 6.2.

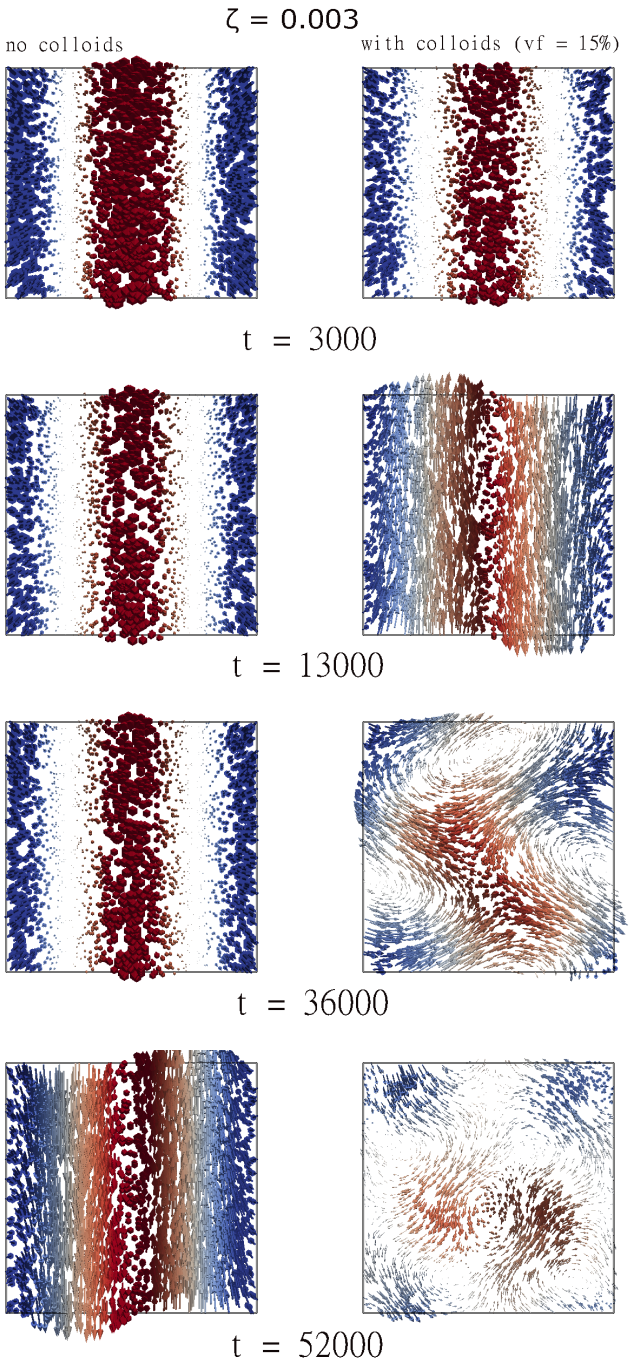

Figure 6.9: Snapshots for the velocity profile of an extensile nematic at $\zeta = 0.003$ without (left column) and with (right column) colloids. The colloidal volume fraction is 15% and the adimensional anchoring strength is $w = 0$. Cartesian axes here are directed as in Fig. 6.2.

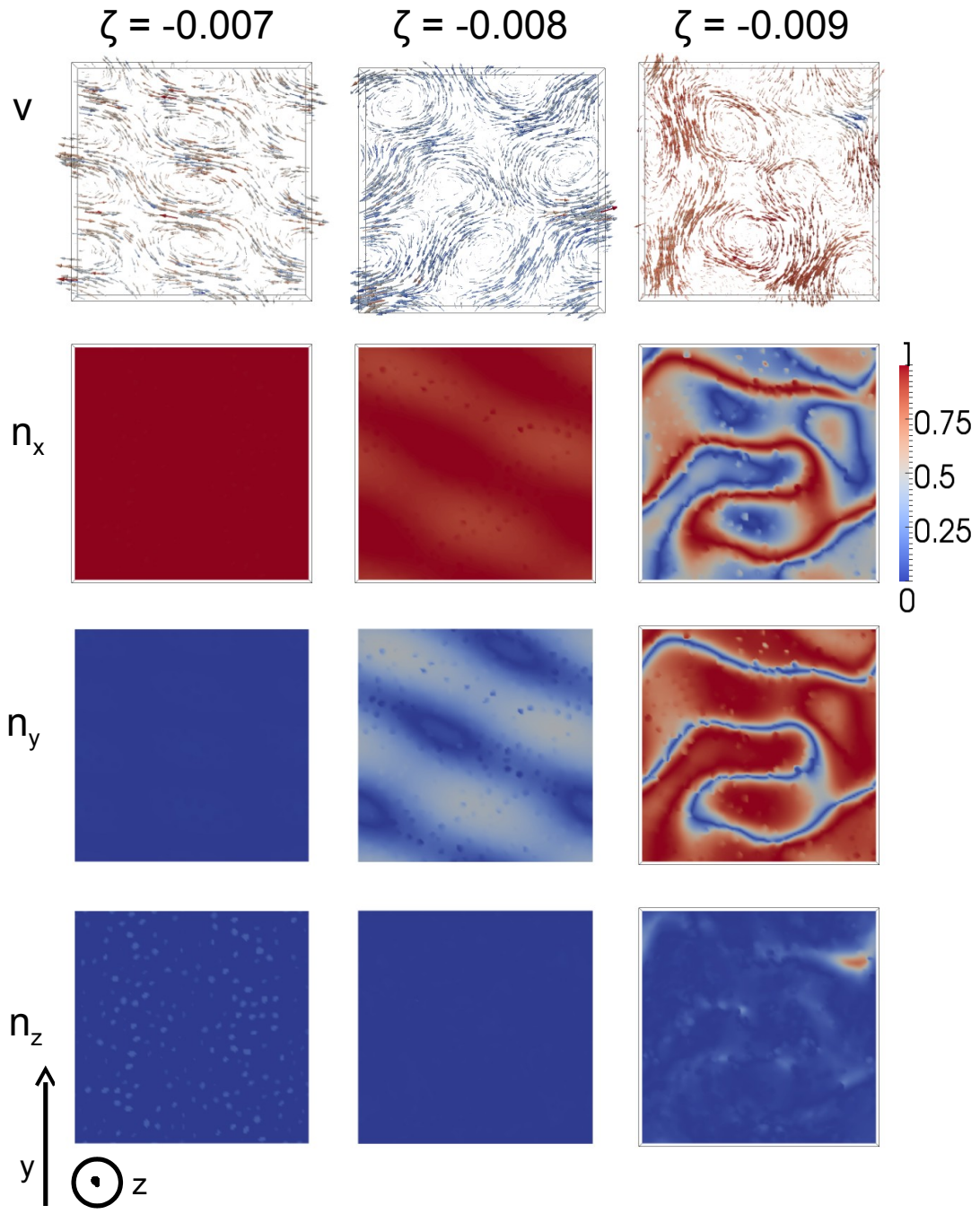

Figure 6.10: Velocity and director profiles developing in contractile nematics, with a 15% colloidal volume fraction, in a regime of spontaneous flow, for ζ between -0.007 and -0.009, and $w = 0$. The colour coding for both the velocity and the director is as in Fig. 6.2. These snapshots refer to time $t = 160000$.

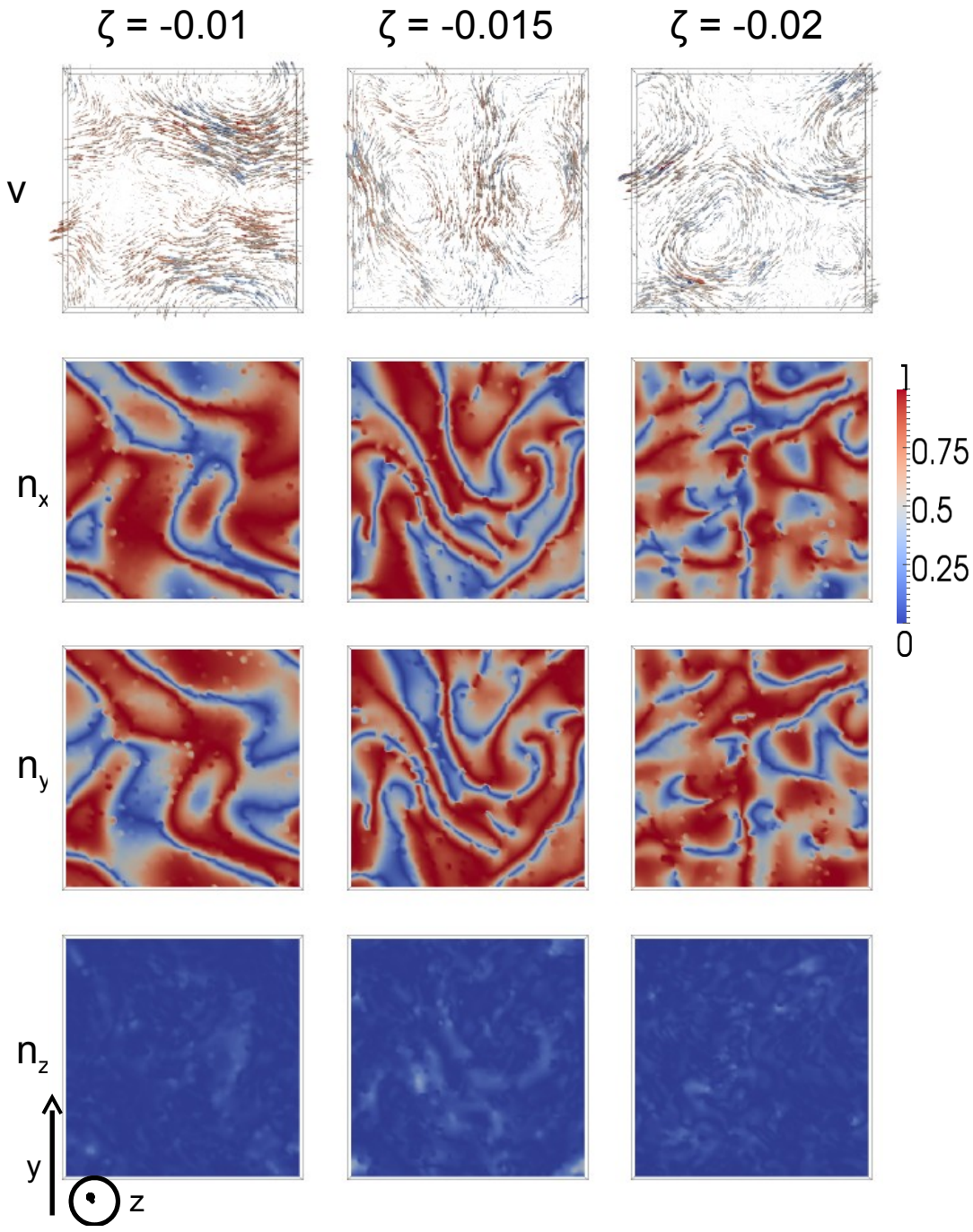

Figure 6.11: Velocity and director profiles developing in contractile nematics, with a 15% colloidal volume fraction, in a regime of spontaneous flow, for ζ between -0.01 and -0.02, and $w = 0$. The colour coding for both the velocity and the director is as in Fig. 6.2. These snapshots refer to time $t = 160000$.

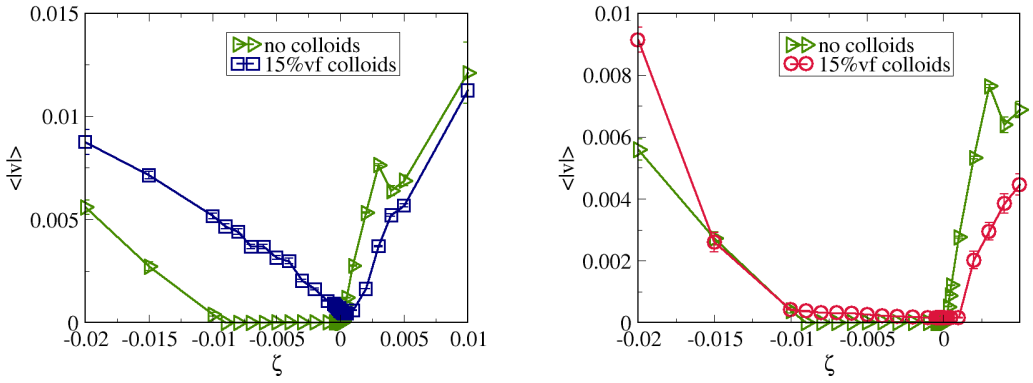

Figure 6.12: The average fluid velocity is studied as a function of ζ for extensile and contractile active nematics with 15% colloids volume fraction and different anchoring conditions: normal anchoring, when a Saturn ring disclination accompanies the colloid (left), and planar anchoring (right).

similarly to the extensile case: the presence of randomly distributed particles accelerates the transition to spontaneous flow.

A fixed director orientation at the colloidal surface ($w > 0$) is responsible for important local distortions in the liquid crystal, which, in the case of $\zeta \neq 0$ are coupled to the appearance of a local flow [14]. The latter is such that in the case of a 15% volume fraction, the stability of the fluid is strongly affected by the type of anchoring. In Fig. 6.12 we present stability curves for both the cases of normal, when a Saturn ring disclination shows up, and of planar anchoring, and always compare them with the corresponding curves referred to the bare fluid.

The average fluid velocity is significantly larger than zero also at very small activities both in the case of planar and of normal anchoring, and is much larger for the latter. In that case, for the range of ζ considered, we do not see the sudden onset of a macroscopic flow, but rather a rapid increase of $\langle|\vec{v}|\rangle$ up to values comparable to the ones observed in the case of planar anchoring and of the bare fluid at the same, large $|\zeta|$. For the case of planar anchoring instead, we see an initial linear regime in the dependence of $\langle|\vec{v}|\rangle$ on $|\zeta|$, where the fluid velocity is relatively small if compared to the one of the spontaneously flowing bare fluid. In this regime the flow generates from defects and is localised close to the colloidal surface. It is only at values of activity larger than the critical activity that a sudden increase in $\langle|\vec{v}|\rangle$ shows up, related to the onset of a more global flow. This observation is clarified by a more detailed study of the flow. Our

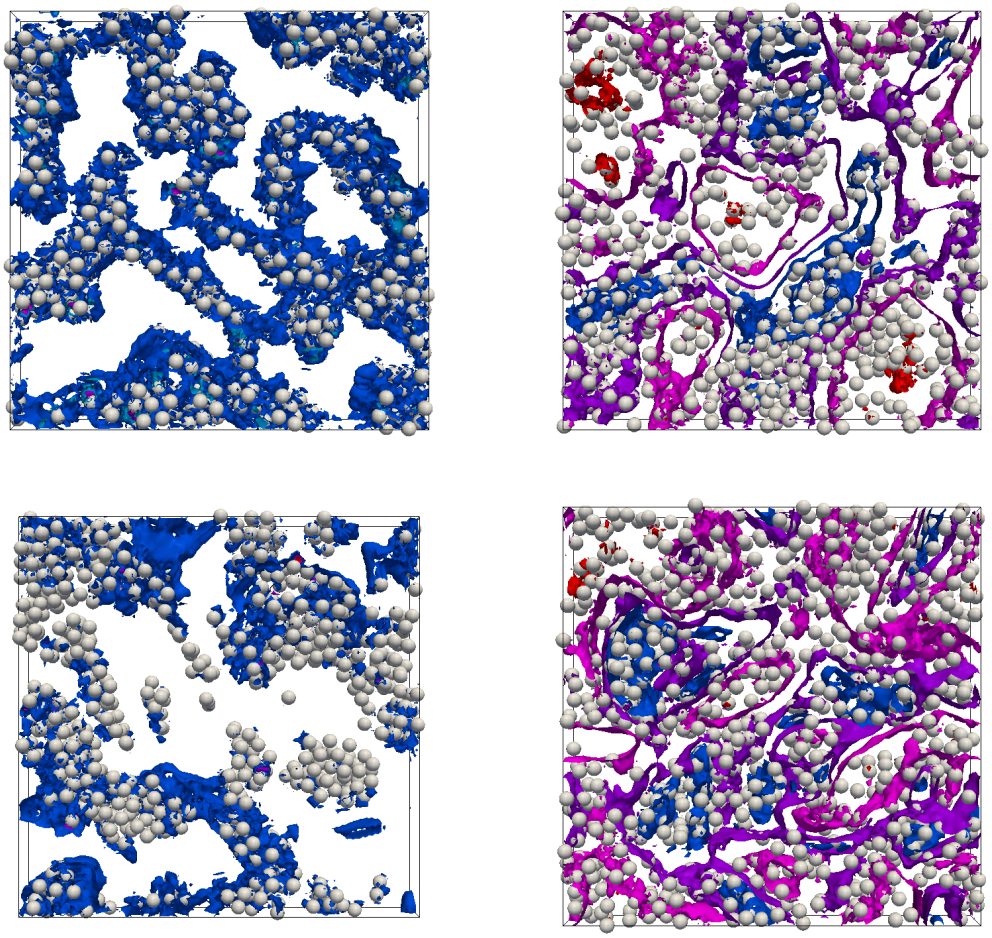

Figure 6.13: Snapshots referring to a system of 771 colloids in extensile (top) and contractile (bottom) nematics, with normal anchoring at time $t = 160000$ (same as in Fig. 6.22). We show some level surfaces corresponding to a range of fluid velocities for that system (different in the two cases). Different colours correspond to different values of the fluid velocity, going from red – denoting the highest of the values considered – to blue, chosen for the smallest value in our range. The topology is completely different at different $|\zeta|$: for $\zeta = 0.0001$ and $\zeta = -0.001$ (panels on the left), the level surfaces corresponding to highest velocitis are localised close to the colloids and are hidden by more extended curves corresponding to smaller velocities. At $\zeta = 0.01$ and $\zeta = -0.02$ (panels on the right) high fluid velocity is found also in those regions where the density of colloids is smaller and are not localised close to the colloidal surface.

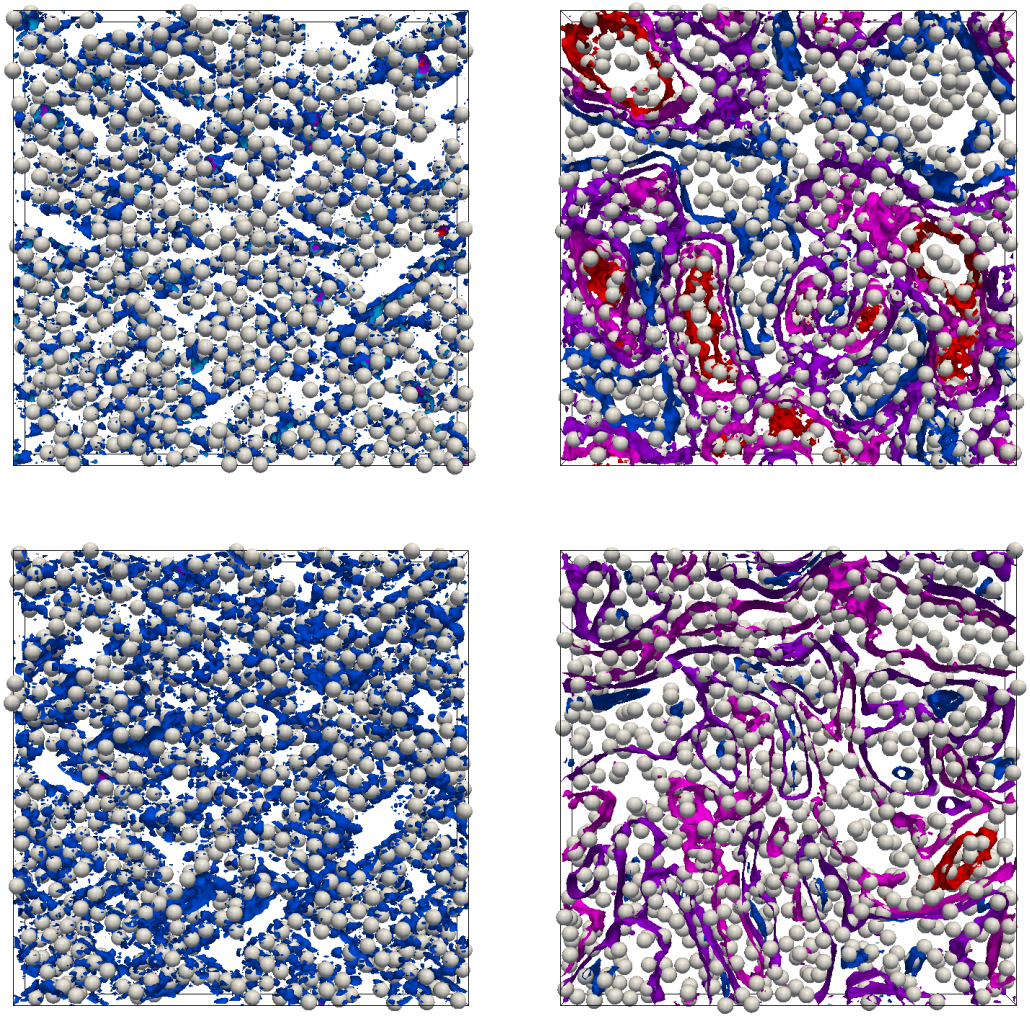

Figure 6.14: Snapshots referring to a system of 771 colloids in extensile (top) and contractile (bottom) nematics, with planar anchoring at time $t = 160000$ (same as in Fig. 6.22). We show some level surfaces corresponding to the highest velocities for that system (different in the two cases). Different colours refer to different fluid velocities, going from red – denoting the highest of the values considered – to blue, chosen for the smallest value in our range. The left panels refer to the case of small activities (here $\zeta = 0.0001$ – top – and $\zeta = -0.001$ – bottom) these are localised near the colloids, while for higher $|\zeta|$ (shown in the right panels: $\zeta = 0.005$ – top – and $\zeta = -0.02$ – bottom) highest velocity level surfaces are found also in those regions where the density of colloids is smaller.

idea is that for small and intermediate values of ζ the flow stems mainly from the defects that accompany colloids, since those are regions of large deformations in the director profile, and therefore large active stress. If activity is small, the flow is mainly localised close to the colloidal surface. For increasing ζ the flow becomes more and more intense and must assume a global character for those values of ζ at which spontaneous flow develops in the absence of anchoring. As a proof of our explanation we show level surfaces corresponding to the highest values of velocities in Fig. 6.13 and Fig. 6.14, for normal and planar anchoring respectively. In Fig. 6.13 the two panels at the top refer to extensile nematics with $\zeta = 0.0001$ (left) and $\zeta = 0.01$ (right). The panels at the bottom are for contractile nematics with $\zeta = -0.001$ (left) and $\zeta = -0.02$ (right). For $\zeta = 0.0001$ and $\zeta = -0.001$ the flow is more intense close to the colloidal surface, while at $\zeta = 0.01, -0.02$ level surfaces corresponding to high velocity are found also for the fluid in those regions where the density of colloids is smaller. This is a sign that spontaneous flow is no longer stemming merely from defects and has a more global character, which is able to disrupt the colloidal structure, as we will see later on. For both extensile and contractile nematics this seems to happen at values of $|\zeta|$ that are slightly larger than $\zeta^0_{c,ext}$ and $|\zeta^0_{c,contr}|$ respectively. But while colloids slow down the flow in extensile nematics, they enhance it in contractile fluids, thus confirming the trend that we observed in the case of $w = 0$. The situation is very similar in Fig 6.14 for the case of planar anchoring.

We now study the characteristics of spontaneous flow by looking at the velocity and director profiles in the case of normal anchoring. A similar analysis for the case of planar anchoring is presented in Appendix C, and is omitted here. In the case of normal anchoring, large deformations are associated with defects as is visible from Fig. 6.15 and 6.16. However, the cases of extensile and contractile nematics are different. In the former at the beginning the flow is not coherent and mainly stems from defects. A transition to a more global and coherent flow can be found between $\zeta = 0.0005$ and $\zeta = 0.001$, where the flow appears to be two dimensional. In this case the presence of anchoring hinders the onset of a coherent flow, despite defects are associated to a local, macroscopic flow also at smaller ζ. In the case of $\zeta < 0$ instead, it is hard to find a critical point: the flow seems to progressively develop a coherent character already at values of $|\zeta|$ that are significantly smaller than the critical activity in the case of $w = 0$

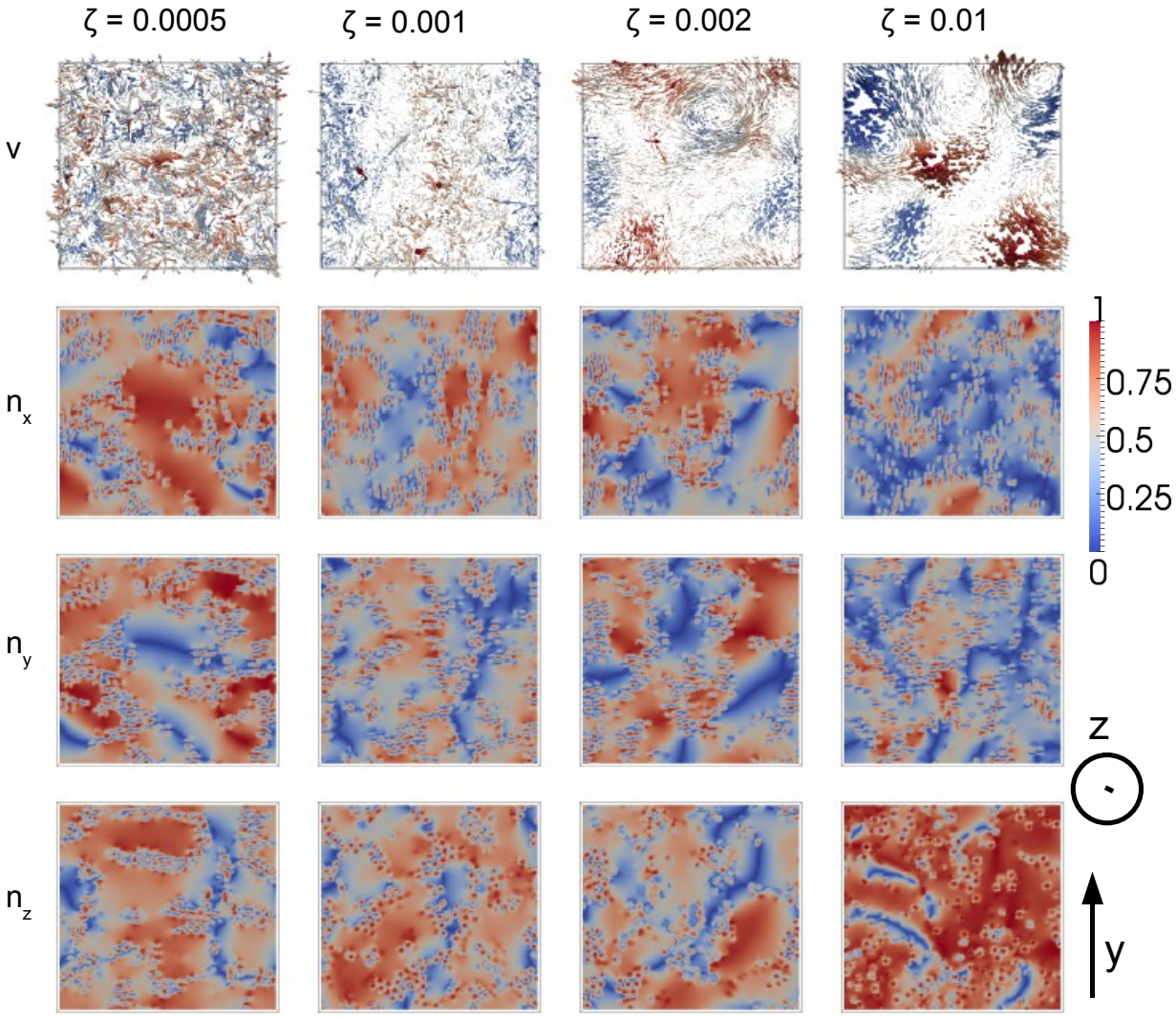

Figure 6.15: Velocity and director profiles developing in extensile nematics, with a 15% colloidal volume fraction, in a regime of spontaneous flow, for ζ between 0.001 and 0.005. The anchoring is normal. The colour coding for both the velocity and the director is as in Fig. 6.2. These snapshots refer to time $t = 160000$.

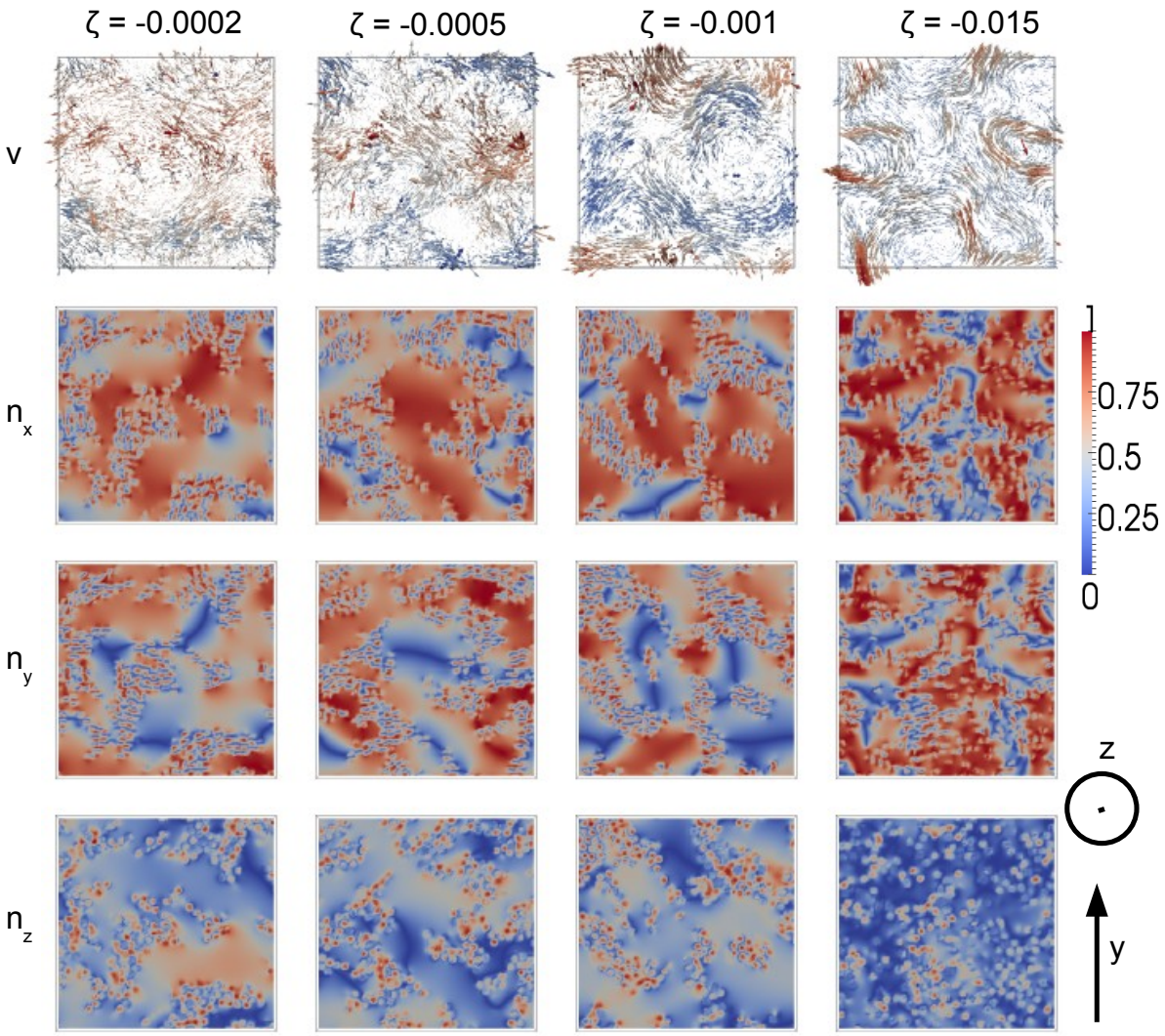

Figure 6.16: Velocity and director profiles developing in contractile nematics, with a 15% colloidal volume fraction, in a regime of spontaneous flow, for ζ between -0.0002 and -0.015. The anchoring is normal. The colour coding for both the velocity and the director is as in Fig. 6.2. These snapshots refer to time $t = 160000$.

($|\zeta_{c,contr}| > 0.007$). This is probably related to the fact that normal anchoring associates to a large splay deformation, all along the Saturn ring, and contractile nematics are strongly unstable with respect to splay.

We conclude that, in the case of extensile nematics the presence of colloids (for $w = 0$, and for planar anchoring) does not affect the critical activity for the onset of a global spontaneous flow, while in the case of normal anchoring, despite the appearance of an important, local flow, associated to the presence of defects, a global flow develops only at ζ larger than $\zeta^0_{c,ext}$. The characteristics of the flow change significantly according to whether colloids are there or not, and to the presence of defects at $w > 0$. In particular, when $w = 0$ spontaneous flow goes through the same phases that are observed in the absence of colloids: it first develops in one dimension, along the z axis, then in two and in three dimensions. While in the absence of colloids the flow in three dimensions is associated to the appearance of steady vortices, colloids break this regular pattern and are responsible for the sudden onset of a chaotic flow. This is even more evident when $w > 0$: for normal anchoring the flow first develops in two dimensions, before a three dimensional flow is observed. In the case of planar anchoring the onset of spontaneous flow is abrupt: a three dimensional, chaotic flow develops as soon as the critical threshold is passed, while being localised close to defects for smaller ζ (as presented in Appendix C).

The case of contractile nematics is similar. Not only the character of the flow, but also the threshold at which a global flow develops, depend strongly on the presence of colloids and on the type of anchoring. In the absence of colloids and when $w = 0$ the onset of spontaneous flow is abrupt and characterised by the appearance of two-dimensional vortices in the xy plane. Colloids break the regular pattern of vortices that form at $\zeta \gtrsim -0.015$ and are responsible for a more chaotic character of the flow as soon as the latter sets in. Also, colloids enhance the onset of spontaneous flow: the critical $|\zeta|$ is smaller than in the case of a bare fluid. Also the type of anchoring has a decisive role at $\zeta < 0$. The presence of defects is responsible for the onset of a local flow also at small $|\zeta|$, both in the case of contractile and of extensile nematics, but while for the latter it is always possible to identify a critical ζ above which the flow acquires a global character, the same is not true at $\zeta < 0$ for the case of normal anchoring, while for planar anchoring such a threshold exists and is much lower than the one

observed at $w = 0$. We can therefore say that for contractile fluids the presence of colloids hinders the onset of spontaneous flow in the case of planar anchoring, while it strikingly favours it when the anchoring is normal. It is remarkable that in contractile nematics a spontaneous, global flow always has a two-dimensional character and never involves the z direction (significantly).

6.2.3 Spontaneous Flow Promotes Large Fluctuations in the Number of Colloids when $w = 0$

We now start analysing how the collective properties of colloids are affected by activity. We first consider the case of $w = 0$ and of a liquid crystal initialised in the nematic phase, with still a small tilt in the xy plane that is meant to be the seed for instabilities. In such a system there is no mechanism favouring colloidal aggregation when spontaneous flow does not set in, but we do observe inhomogeneities in the spatial distribution of colloids when the fluid is spontaneously flowing. Two snapshots referring to the case of a passive liquid crystal ($\zeta = 0$, panel (a)) and of a spontaneously flowing extensile active fluid ($\zeta = 0.005$, panel (b)) are shown in Fig. 6.17. In the absence of activity (or, equivalently, when activity is very low), the distribution of colloids stays almost unchanged after the initial relaxation, with respect to the starting, random one. Moreover, there is no flow at equilibrium and the director field is in the ordered phase (inset in panel (a); the colour-coding is explained in the caption). When activity is high enough for spontaneous flow to set in, regions of higher and smaller colloidal density can be spotted, as is visible in panel (b) of Fig. 6.17, where green spheres denote colloids belonging to the same, largest aggregate (defined by fixing an arbitrary binding radius r_b, larger than the total range of the colloid-colloid repulsive potential, as explained later on). Panel (d) shows the director (background) and the velocity profile (blue arrows) for a section in the xy plane.

A more quantitative comparison between these two pictures comes from the pair distribution function, plotted in panel (c) of Fig. 6.17. Here, as in all other graphs for the $g(r)$, r represents the projection of the actual 3D-distance between two colloids on the xy-plane, and $\sigma = 2R$. We note here that, because the system is quasi-2D, when computing the pair correlation function for one particle, we only considered those colloids for which the distance along the shortest axis

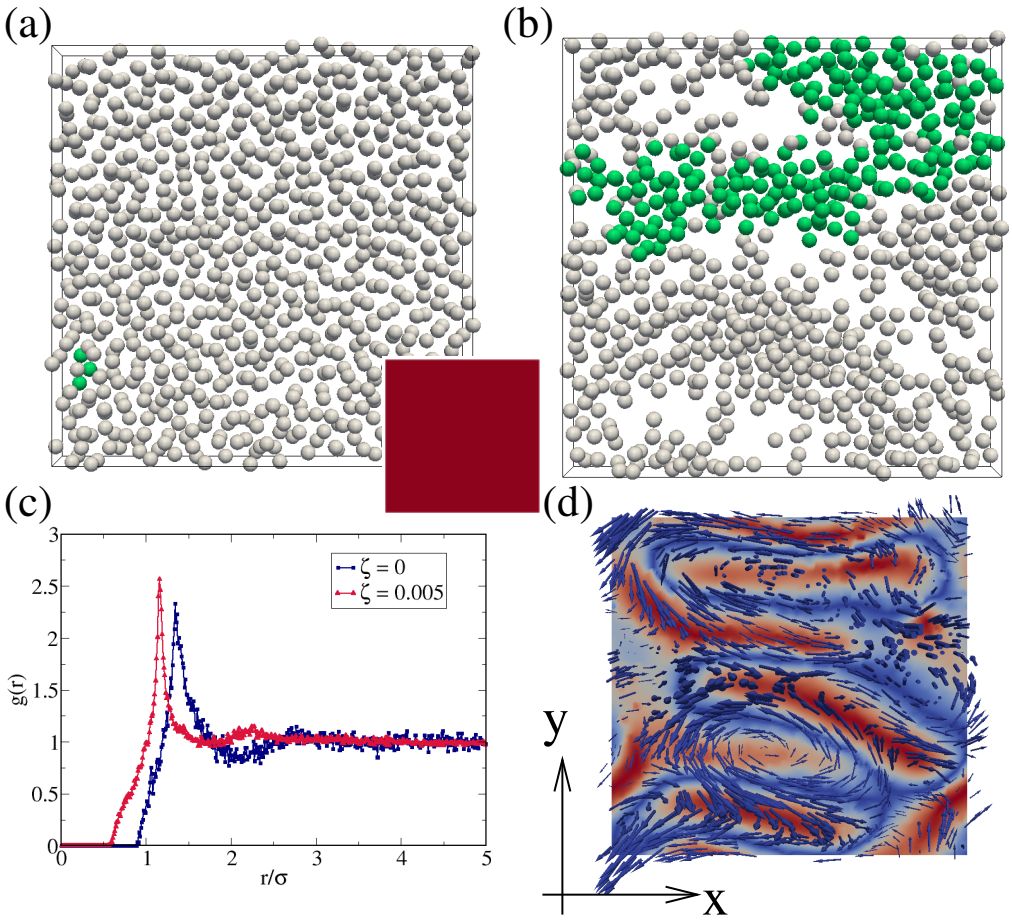

Figure 6.17: Two snapshots referring to a system in steady state with 15% colloidal volume fraction, with $w = 0$ and in the case when the liquid crystal (active or passive) is initialised in the ordered nematic phase. On the left $\zeta = 0$, the particles are homogeneously distributed and there is no flow. The box on the bottom right shows a section of the director profile. The homogeneous red colour means that the x component of the director is uniformly equal to one, as for an ordered nematic. The figure on the right refers to $\zeta = 0.005$. The fluid is spontaneously flowing and doing so it disrupts the orientational order as shown in (d). There the colour-coding refers to the x component of the director, which can go from zero (blue) to one (red). We coloured in green the colloids that belong to the largest aggregate, where an aggregate is defined by choosing a fixed binding radius r_b slightly larger than the range of the repulsive potential. Panel (c) displays the corresponding pair correlation functions: the main effect of spontaneous flow is the one of shifting the position of the first peak towards smaller distances.

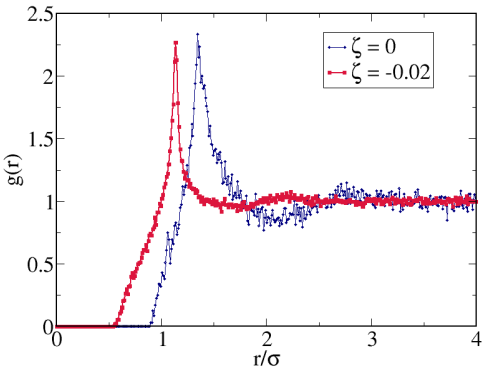

Figure 6.18: Pair distribution function for a system of colloids (15% volume fraction) embedded in a (contractile) nematic liquid crystal. The case of $\zeta = 0$ is compared to the one of $\zeta = -0.02$, where spontaneous flow is present.

was less than a particle diameter. The main effect of spontaneous flow is the one of decreasing the average distance between nearest neighbours, as evident from the shift of the main peak towards shorter distances. This originates the inhomogeneities of Fig. 6.17 (b). A similar effect is found for contractile nematics, for which we only show the pair distribution function in Fig. 6.18.

When looking at the time evolution of the system, once spontaneous flow has set in, what we see is a dynamic gathering of colloids in different regions, while they are advected by the flow. Colloids do not form stable clusters, and the dynamic inhomogeneities that we observe can be described in terms of fluctuations in the number of colloids, rather than as colloidal aggregates.

The number fluctuations for a system at equilibrium, far from criticalities, grow with the square root of the number of particles. This is one of the pillars of equilibrium statistical mechanics, since this property allows for a well-defined number density in the thermodynamic limit. We have already mentioned in the Introduction to this thesis, that systems of active particles display large number fluctuations. Here we observe a similar effect in a system of colloids embedded in an active fluid.

We present the number fluctuations ΔN as a function of N for extensile and contractile nematics in Fig. 6.19 (left and right panels respectively). ΔN was computed by dividing the lattice into boxes of size $l \times l \times 16$, calculating their average number of particles, $\langle N \rangle$, and its fluctuations. Different l's correspond to different $\langle N \rangle$'s, and ΔN can thus be studied as a function of $\langle N \rangle$. From the

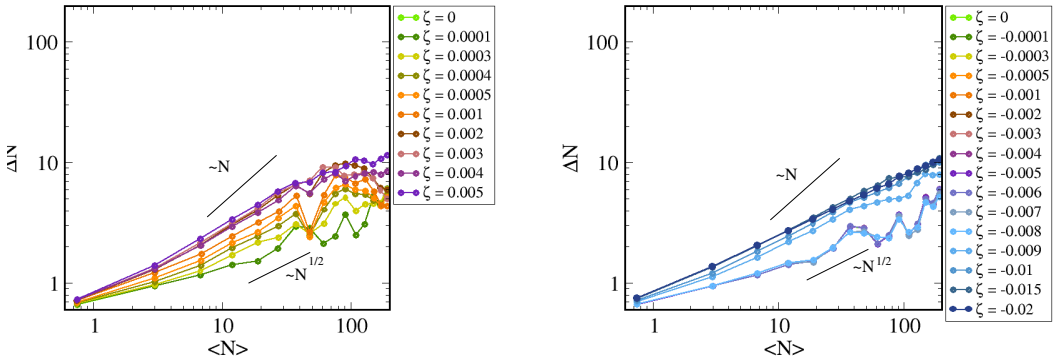

Figure 6.19: Number fluctuations for a system of colloids embedded in extensile (left) and contractile (right) nematics in the case of $w = 0$. Note that in the contractile case all the curves corresponding to ζ between 0 and -0.006 are superposed due to the absence of flow that does not allow a reorganisation of the particles and the initial configuration was the same in all cases.

plots in Fig. 6.19 you can see that in general $\Delta N \sim \langle N \rangle^{\alpha}$. In the passive case a system large enough so that finite size effects are not relevant, would display Gaussian fluctuations, with $\alpha = 1/2$. Instead, the value of α that we find here is slightly smaller (even 0.3 in some cases), as a finite size effect. Note that data in the region of largest $\langle N \rangle$ in Fig. 6.19 are characterised by significant noise due to the small number of boxes over which we could average in order to calculate ΔN. As a consequence, our estimate of α is based on the region of small $\langle N \rangle$, where deviations from the Gaussian behaviour are important. However, what is relevant to our description, is that larger and larger $|\zeta|$ are associated to larger and larger α, up to values around 0.6.

The strong interdependence between the number fluctuation of colloids and the appearance of spontaneous flow is evident from comparing the plots in Fig. 6.20. In panel (a) $\Delta N = \sqrt{\langle N^2 \rangle - \langle N \rangle^2}$ represents the average number fluctuation computed for a box of size 16^3 within the simulation box. This quantity is studied as a function of ζ and should be compared to the stability curve in panel (b): the number fluctuation and the average modulus of the fluid velocity display the same behaviour, when considered as a function of ζ.

Since, in general, colloids are attracted towards the regions of largest disorder, where the elastic energy is highest, the continuous disruption of orientational order produced by spontaneous flow might be considered as an alternative

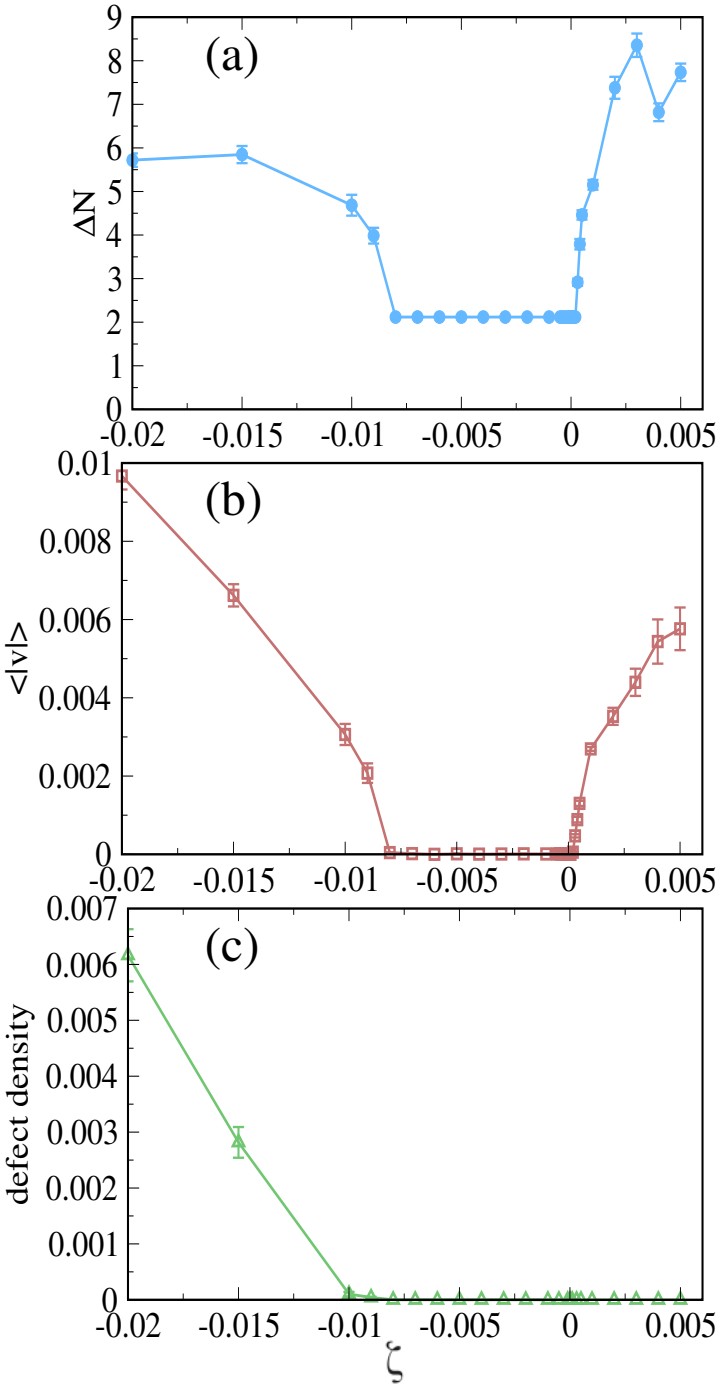

Figure 6.20: Inhomogeneities in the distribution of colloids can be described in terms of large number fluctuations (a). These correlate very well with the appearance of a macroscopic flow (b), but not with the defect density, studied as a function of ζ (c). This rules out the hypothesis that large number fluctuations are related to the tendency of colloids to gather in regions of large distortions, i.e. of high elastic energy. Instead, these graphs suggest that colloids are pushed together by the flow.

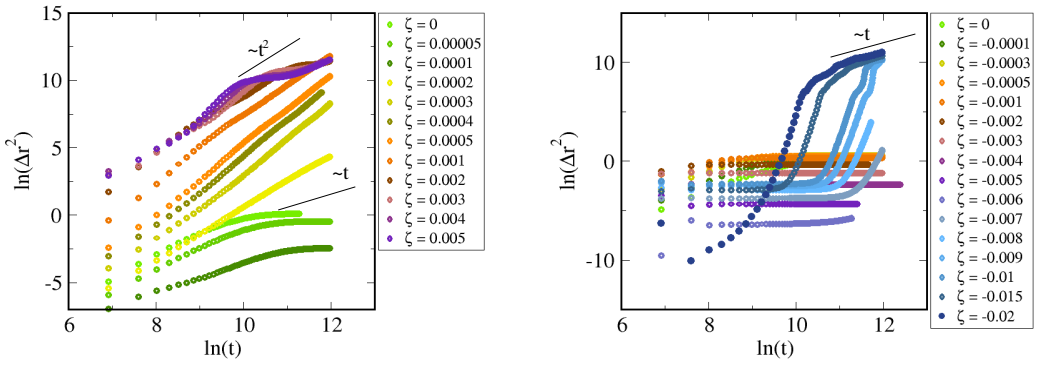

Figure 6.21: Mean squared displacement for a system of colloids embedded in extensile (left) and contractile (right) nematics in the case of $w = 0$.

mechanism at the origin of the observed inhomogeneities. To rule out this possibility, we computed the defect density and studied its dependence on ζ (Fig. 6.20(c)). For the range of activities that we considered, the scalar order parameter never differs significantly from the value corresponding to a perfectly aligned nematic ($S = 0.5$). In Fig. 6.20 (c) we fixed the threshold of the order parameter to $S_t = 0.45$ and defined a defect as a region where $S < S_t$. The defect density computed according to this definition does not show the same high correlation with the number fluctuations as the average fluid velocity does. From this we conclude that it is the appearance of a macroscopic flow that pushes the colloids together and is at the origin of large number fluctuations, while the appearance of disordered regions is more indirectly related to this phenomenon.

To give a more complete description of the system, in Fig. 6.21 we present the mean squared displacement (MSD, Δr^2) of the colloids as a function of time (t), at different activities. Both in the extensile and in the contractile case we can identify two different ranges of ζ. For values of ζ smaller than the critical activity at which spontaneous flow shows up, the particles stop moving once the liquid crystal has relaxed in the nematic phase, and the MSD rapidly saturates. In the spontaneously flowing regime, depending on the value of ζ, the evolution of the MSD is superdiffusive, while for large values of ζ the flow is such that the particles start colliding with each other on a timescale compatible with our observation time, as one can see by noting the decrease in the slope of the curves at large t, large $|\zeta|$ in Fig. 6.21.

6.2.4 Spontaneous Flow Hinders Colloidal Clustering when $w > 0$

So far we have considered the role of spontaneous flow in affecting the aggregation properties of colloids in the limit of $w = 0$, where colloids are not accompanied by defects. We now move to the instance of $w > 0$. Regions of high elastic energy close to the colloidal surface are responsible for an effective attraction between them. As a consequence, a system of spherical particles embedded in a nematic liquid crystal spontaneously tends to form structures whose characteristics are strongly dependent on the anchoring condition, as described in the Introduction to this chapter. We have already described how the presence of defects, associated with colloids, affects the transition to spontaneous flow. In this section we study how activity and the onset of a macroscopic flow affect colloidal aggregation. As in the previous sections, we consider the case when the liquid crystal is initially in the ordered phase.

Normal anchoring. The effect of spontaneous flow on colloidal aggregation can be seen from the snapshots that we presented in Fig. 6.22. There we compare the distribution of colloids in space at different activities, $\zeta = 0$ (a) and $\zeta = 0.01$ (c), where spontaneous flow has already set in. Defects at the colloidal surface are responsible for an effective attraction between colloids which form actual clusters. To quantify aggregation we consider that two colloids are bound when the distance between their centres is smaller than a binding radius r_b, that we chose arbitrarily as being slightly larger than the range of the total colloid-colloid repulsive potential. This includes a hard and a soft component, with range R and r_{cutoff} respectively. We checked that this choice does not affect our results significantly. In the absence of activity colloidal aggregation takes place through the formation of many clusters having on average the same size and separated by large voids. Spontaneous flow tends to oppose colloidal aggregation and is responsible for the more homogeneous distribution of colloids that characterises Fig. 6.22 (c) with respect to Fig. 6.22 (a). The director and velocity profiles are shown in Fig. 6.22 (b) and (d) (colour-coding is as in previous section). It is clear that the flow disrupts nematic order. Regions of disorder in the director field are now present also at $\zeta = 0$, even if in smaller measure, due to defects accompanying colloids. We point out here that in the case of $\zeta = 0$ the flow field in not completely absent (although not showed), despite one would expect so at

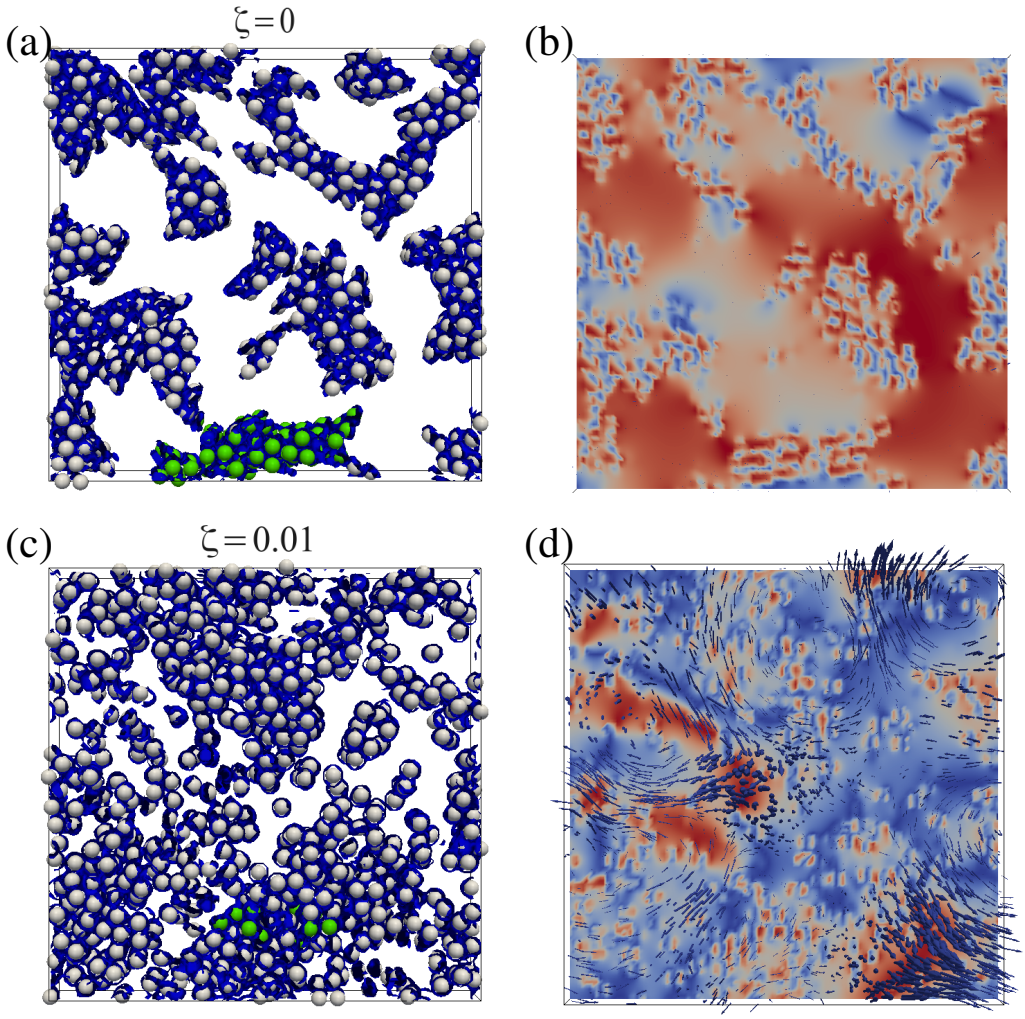

Figure 6.22: Two snapshots referring to a system with 15% colloidal volume fraction, with normal anchoring and in the case when the extensile active liquid crystal is initialised in the ordered nematic phase. In panel (a) $\zeta = 0$, the particles are homogeneously distributed, and there is no flow. Figure (c) refers to $\zeta = 0.01$. Panels (b) and (d) show the director (background) and the flow profile (blue arrows). The fluid is spontaneously flowing and disrupts the orientational order. The colour-coding refers to the x component of the director, which can go from zero (blue) to one (red). We coloured in green the colloids that belong to a cluster of average size. For both the systems we considered the last configuration in our simulations (which refers to time $t = 160000$).

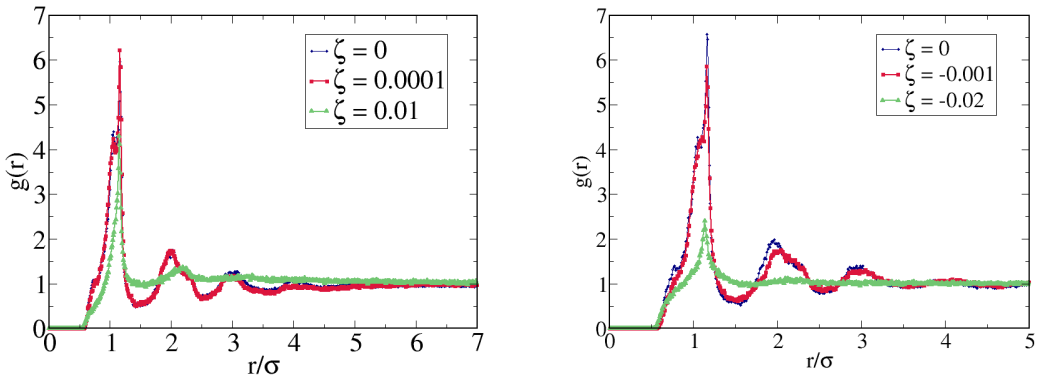

Figure 6.23: Pair distribution function referring to a system of colloids embedded in an extensile (left) and for a contractile (right) nematic liquid crystal that is initialised in the nematic phase. Normal anchoring at the colloidal surface is imposed, which corresponds to the presence of a Saturn-ring disclination. Curves for different values of ζ are shown: for small values of ζ spontaneous flow does not affect colloidal structures significantly, while smearing out the signatures of structure at high ζ. The curves were obtained by averaging over 60 configurations taken from time $t = 100000$ and $t = 160000$.

relaxation completed. As it will be discussed later on, colloids keep on moving (albeit very slowly and locally), for the whole time of our simulations at $\zeta = 0$. This is due to the interplay of spurious velocities (these are numerical artefacts of discretisation, see Chapter 3) and of the soft repulsion at short range.

In order to quantify the effect of activity on colloidal structures, we present the pair distribution function in Fig. 6.23 for the case of an extensile (left) and of a contractile (right) fluid. The effect of activity is striking: at small activities the structures are the same that characterise their passive analogues. The pair correlation function shows that this structure is maintained for a range of activities and disappears when a more intense spontaneous flow sets in: similar behaviours characterise $\zeta = 0$ and $\zeta = 0.0001$, while significant difference is seen at $\zeta = 0.01$. As well described in the snapshots presented in Fig. 6.22(c), for $\zeta = 0.01$ spontaneous flow is responsible for a much more homogeneous distribution of colloids in space, that results in a smoother $g(r)$, where secondary peaks are absent or small. According to our definition of a binding radius r_b, it is still possible to find aggregates, also in this regime (a number of particles equal to the average size of a cluster is highlighted in green in Fig. 6.22) but, on average, they are significantly reduced in size.

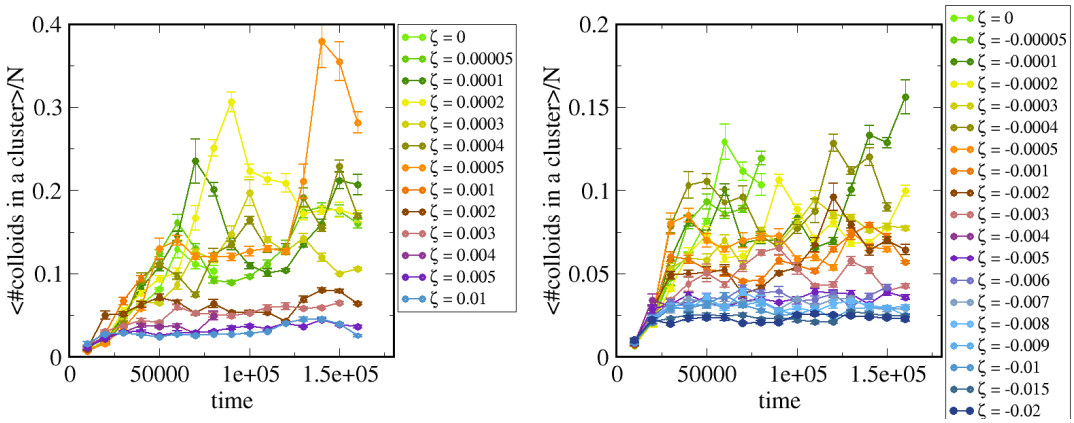

Figure 6.24: Time evolution of the average number of colloids in a cluster (including at least two colloids) in the case of normal anchoring for extensile (left) and contractile(right) nematics. Each point is the average over ten different snapshots and the error bars are the associated standard deviations. The significant noise at large times is due to the onset of spontaneous flow, that tends to break the largest clusters in smaller parts, and then push them together again.

We conclude, from our simulations, that there is an intermediate regime of small, non-zero $|\zeta|$ where spontaneous flow is revealed by a value of $\langle|\vec{v}|\rangle$ larger than the one at $\zeta = 0$ (due to spurious velocities) and growing with $|\zeta|$, but does not have significant effect on the organisation of colloids in space.

The situation is similar in the case of contractile fluids and here we show only the pair distribution function in Fig. 6.23 (right): at small ζ the spontaneous flow is not strong enough to disrupt the colloidal structures that form at $\zeta = 0$.

In Fig. 6.24 we show the time evolution of the average fraction of colloids in a cluster. As one can see, the effect of activity is to reduce the average size of clusters both in extensile and in contractile fluids. In Fig. 6.25 we show the average fraction of colloids in a cluster, computed by averaging over different times at steady state, as a function of ζ. We relate the breaking of clusters to the onset of significant spontaneous flow. The average modulus of the fluid velocity is shown for comparison (squares, scale on the right): the decrease in the size of colloidal clusters correlates with the appearance of a macroscopic flow in the fluid.

Before starting to analyse the case of planar anchoring, we present graphs of the evolution of the mean squared displacement in time in Fig. 6.26. The

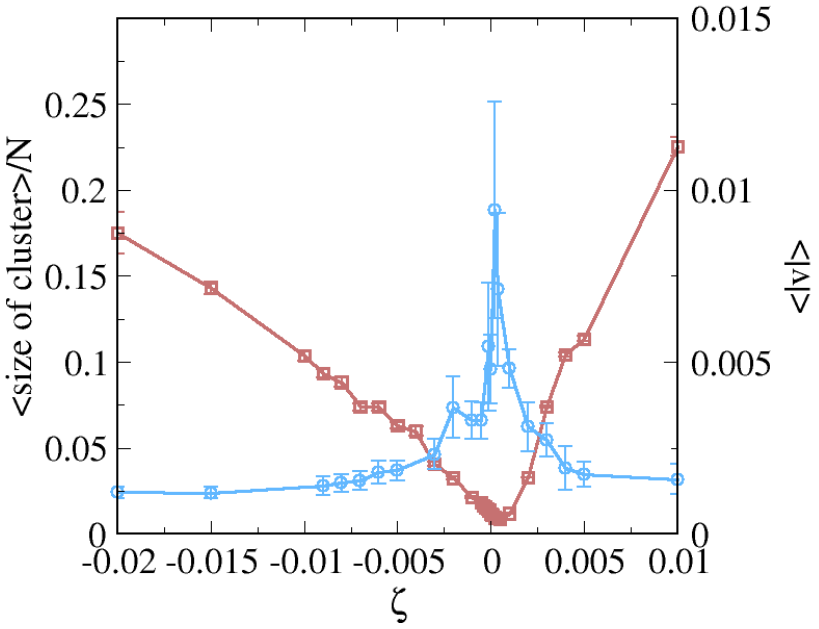

Figure 6.25: This graph shows the correlation between instabilities in the active liquid crystals and the decrease of the average size of a cluster with ζ: spontaneous flow tends to break colloidal structures forming at $\zeta = 0$ and to favour a more homogeneous distribution of colloids. This graph refers to normal anchoring.

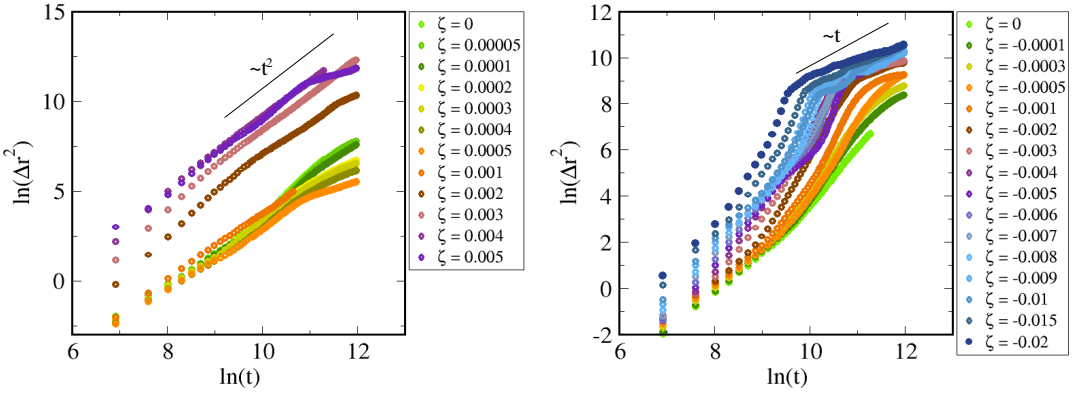

Figure 6.26: Mean squared displacement for a system of colloids embedded in extensile (left) and contractile (right) nematics in the case of normal anchoring.

reader can notice that the colloids do not completely stop moving even at large time scales, also in the case of $\zeta = 0$. This may be a limitation of our simulations that comes from the presence of spurious velocities, or suggest that equilibration requires even longer times. However, this fact does not affect our conclusions on the effects of activity on clustering. Furthermore, the behaviour of the system is not affected by spurious velocities at large ζ, where spontaneous flow dominates. The differences between the extensile (Fig. 6.26, left) and the contractile (Fig. 6.26, right) cases stems mainly from the different character of the flow, that we studied before. In the case of planar anchoring the transition to spontaneous flow is smoother in contractile nematics, where the flow is characterised by vortices from the beginning. In extensile nematics instead the flow is only localised close to the defects for small ζ, before a global and chaotic flow develops at $\zeta = 0.002$. Here we interpret the differences between the behaviour of the MSD in extensile and contractile nematics as a direct effect of the different character of spontaneous flow. Vortices appearing in contractile nematics in the case of normal anchoring (see Fig. 6.15) must be responsible for collisions between colloids, that result in the plateau in their MSD at large $|\zeta|$ and large t. A much larger MSD at $\zeta \gtrsim 0.002$ in the extensile case seems to be associated with the development of a chaotic flow, as one can see from Fig. 6.7. For $\zeta = 0.005$, the MSD shows the signs of collisions between colloids similar to the ones that characterise contractile nematics, at large $|\zeta|$.

Planar anchoring. Similar conclusions apply in this case, where colloids are accompanied by two boojums. Snapshots of the system at the same time, $t = 160000$, for the cases of $\zeta = 0$ and $\zeta = 0.005$, are shown in Fig. 6.27, in panels (a) and (c) respectively, for an extensile nematic. Again, the main role of the flow is the one of opposing colloidal aggregation, as described more quantitatively by the pair distribution function, $g(r)$, and by the angular distribution function, $g(r, \theta)$, that we plot in Fig. 6.28 and Fig. 6.29 respectively, for $\zeta = 0$ (left) and for a contractile fluid at $\zeta = -0.005$ (right). Note that, in agreement with [116, 118], the case of $\zeta = 0$ shows that colloids in passive nematics tend to orient preferentially at 30° with respect to one another (at short distances $g(r, \theta)$ displays two maxima at 30° and at 150°).

In Fig. 6.30 we show the time evolution of the average fraction of colloids in a cluster (including at least two colloids) for extensile (left) and contractile

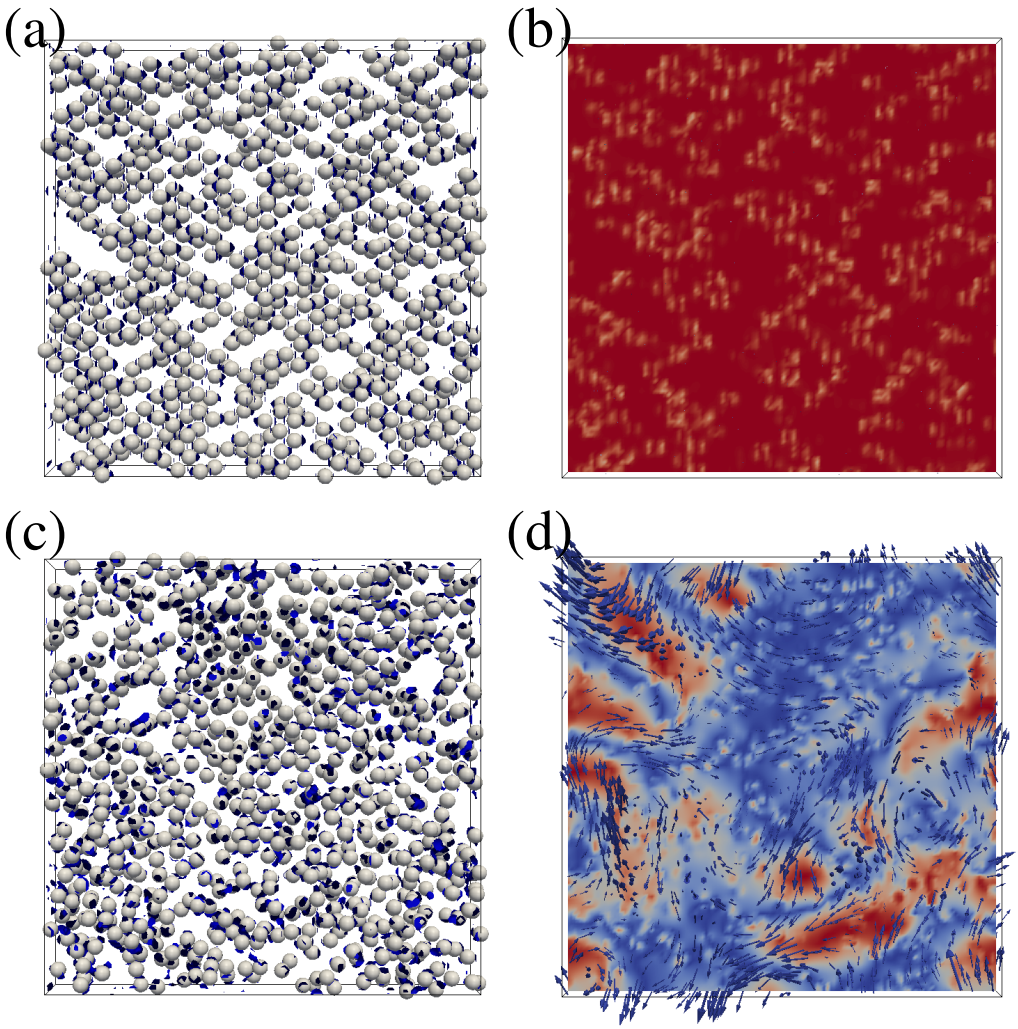

Figure 6.27: Two snapshots of a system in steady state with 15% colloidal volume fraction, with planar anchoring and in the case when the extensile active liquid crystal is initialised in the ordered nematic phase. In panel (a) $\zeta = 0$, the particles are homogeneously distributed, and there is no flow. Figure (c) refers to $\zeta = 0.01$. Panels (b) and (d) show the director and the flow profile. The fluid is spontaneously flowing and disrupts the orientational order. The colour-coding refers to the x component of the director, which can go from zero (blue) to one (red). We highlighted in green a number of colloids equal to the average cluster size.

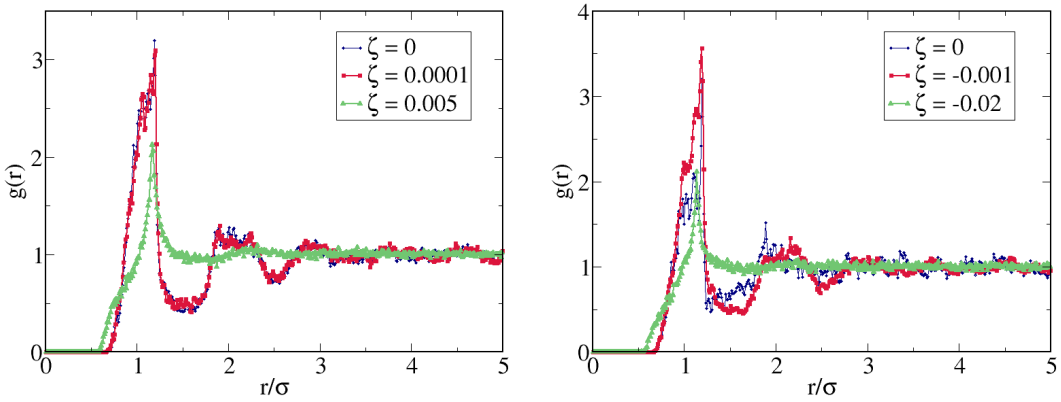

Figure 6.28: Pair distribution function of a system of colloids embedded in an extensile (left) and a contractile (right) nematic liquid crystal that is initialised in the nematic phase. Planar anchoring at the colloidal surface is imposed. Curves for different values of ζ are shown: for small values of ζ spontaneous flow does not affect colloidal structures significantly, while smearing out the signatures of structure at high ζ.

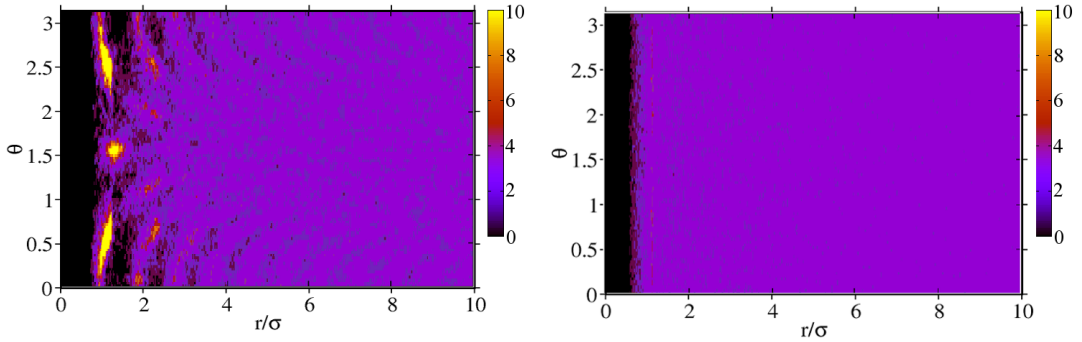

Figure 6.29: Angular pair distribution function for a system of colloids in passive and in contractile ($\zeta = -0.005$) nematics, with planar anchoring. The angle θ is measured in radians and goes from 0 to π.

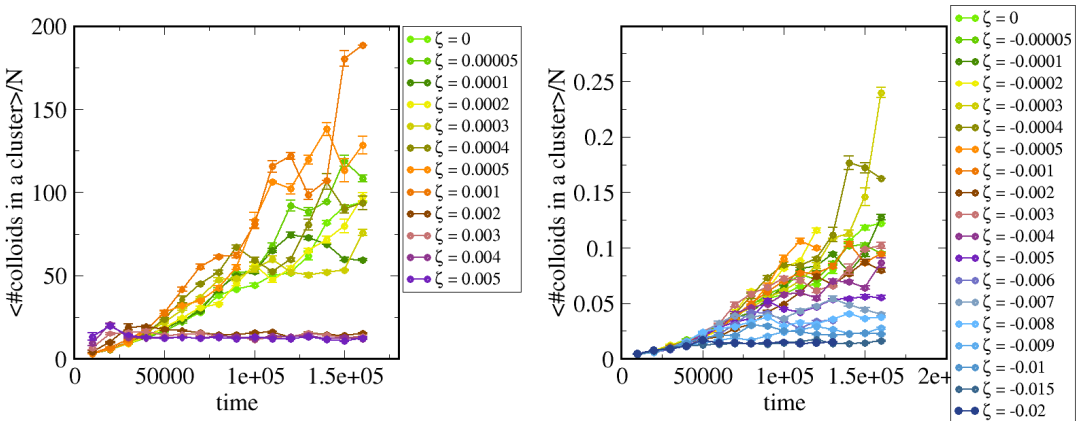

Figure 6.30: Time evolution of the average number of colloids in a cluster (including at least two colloids) in the case of planar anchoring for extensile (left) and contractile (right) nematics. Each points is the average over ten different snapshots and the errors are the associated standard deviations.

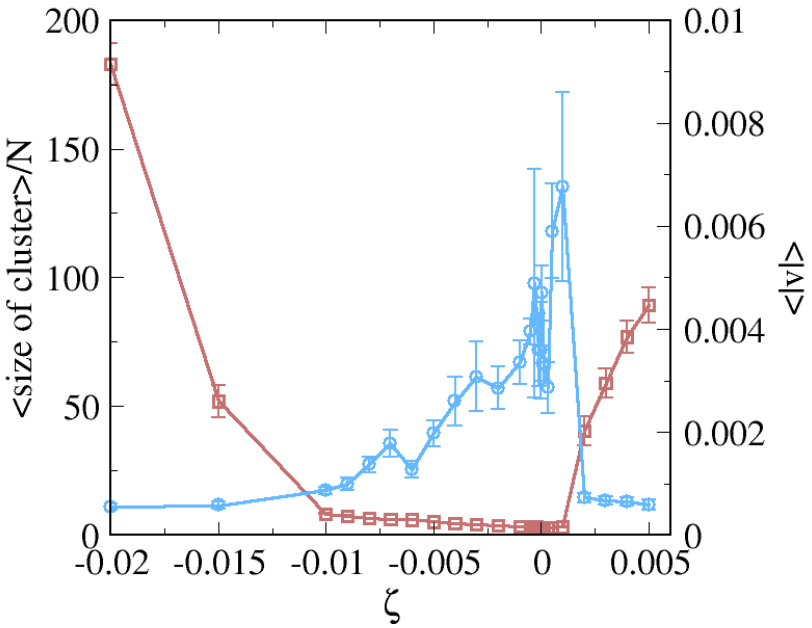

Figure 6.31: This graph shows the correlation between instabilities in the active liquid crystals and the decrease of the average size of a cluster with ζ in the case of planar anchoring.

(right) nematics when planar anchoring is imposed. As in the case of normal anchoring, activity breaks the clusters that form because of the effective, defect-mediated attraction between colloids. Note that for $\zeta > 0$ the appearance of a three-dimensional chaotic flow at $\zeta \gtrsim 0.002$ associates with the flattening of the curves appearing in the left panel of Fig. 6.30, while the breaking of clusters at $\zeta < 0$ (right panel) for increasing $|\zeta|$ is smoother. This is evident in Fig. 6.31, where the average fraction of colloids in a cluster is plotted as a function of ζ, together with the average intensity of the flow. The scenario is very similar to the one presented in Fig. 6.25 for normal anchoring. Again, for small enough $|\zeta|$, the average size of clusters is reduced, according to our definition of a cluster, but spontaneous flow is not strong enough to disrupt the colloidal structure at short distances, as shown by the pair distribution function (see Fig. 6.28). From the stability curve in Fig. 6.31 it is clear that spontaneous flow is characterised by two different regimes: before an intense spontaneous flow sets in at activities comparable with $\zeta^0_{c,contr}$, a non-zero but small fluid velocity is observed for all $\zeta < 0$. This is the region where spontaneous flow stems from defects close to the colloidal surface rather than being a bulk instability, as shown in Fig. 6.14 for the systems in Figures 6.28. We conclude that, when there is a defect-mediated attraction between colloids, the effect of spontaneous flow is to oppose cluster formation, so to favour a more homogeneous distribution of colloids.

Interpretation of the breaking up of clusters in the spontaneous flow regime is two fold. On one side the chaotic character of the flow, that tends to advect colloids in different directions, is responsible for stretching forces on the clusters that must be more important the higher $|\zeta|$ is. However, at small $|\zeta|$, flow stems from defects close to the colloidal surface and is mainly localised there. This is responsible for an effective attraction or repulsion between colloids, additional to the one due to distortions. To study this effect we performed simulations on a system of two colloids in an ordered nematic liquid crystal in quasi-2D. We considered only the cases when the two colloids were oriented either parallel or orthogonally with respect to the far-field director orientation, and initially placed the colloids at a distance comparable to their diameter (equal to 10.6 lattice sites). At this distance we find that in the passive case the attractive forces associated with the elastic distortion of the director field, are not enough to determine a net displacement of the colloids during the observation time. For values of ζ equal to

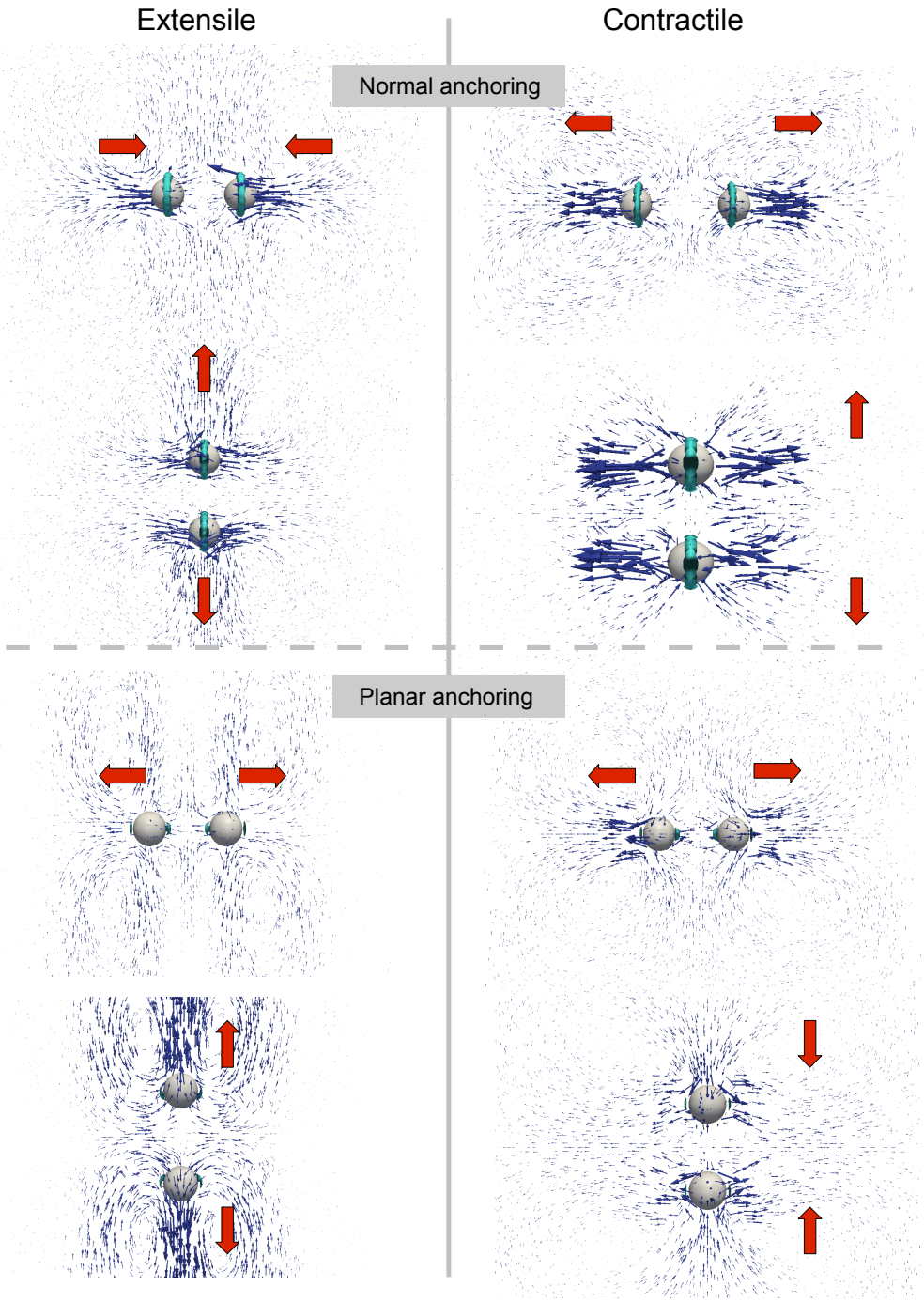

Figure 6.32: Screenshots taken from our simulations of a system of two colloids in active nematics, at $\zeta = 0.005$ and $\zeta = -0.01$ for extensile and contractile nematics respectively.

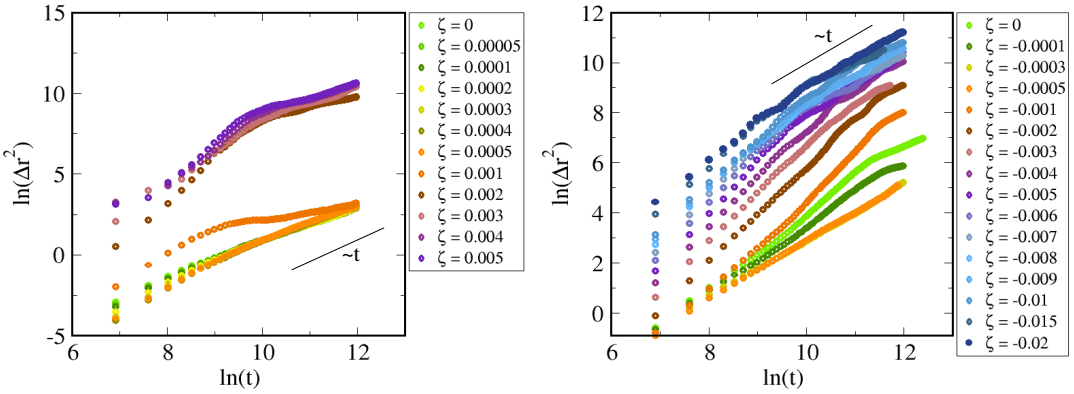

Figure 6.33: Mean squared displacement for a system of colloids embedded in extensile (left) and contractile (right) nematics in the case of planar anchoring.

-0.01 and 0.005 instead, we found that the colloids were either rapidly attracted towards each other or repelled. We did not study this case systematically, and did not try to estimate the force between the colloids, which would have required a separate rheological measurement of the effective viscosity, but we observed that in most cases it is possible to predict the sign of the interaction only on the basis of considerations on the coupling between distortions, active forces, and flow similar to the ones presented in Chapter 4 to explain results on microrheology. Our results are synthesised in Fig. 6.32, where we show the velocity field close to the colloids and use red arrows to indicate whether repulsion or attraction are observed. The colloids attracted only in two of the eight cases considered, one for contractile and one for extensile nematics, meaning that the prevalent effect is a repulsive interaction that we interpret as partly responsible for the slow breaking up of clusters at small $|\zeta|$, that we observe in the presence of anchoring, when the liquid crystal is initialised in the nematic phase.

The MSD of colloids for this case is presented in Fig. 6.33. The comments that we made on spurious velocities for the case of normal anchoring hold also here. For this reason we will focus on the regime of large ζ, where the motion of particles is diffusive. For extensile nematics, the onset of a three-dimensional and chaotic flow appearing at $\zeta \gtrsim 0.002$ clearly affects the MSD, resulting in the two subsets of curves that are visible in the left panel of Fig. 6.33. Also in this case slow-down effects related to a spontaneous flow characterised by vortices at high ζ are visible, especially at $\zeta < 0$, but the effect of collisions is visible on a

much shorter time scale, after which the colloidal displacement becomes diffusive again. This is probably due to the much smaller extent of boojums with respect to the Saturn ring: on average the attraction between colloids is weaker in the case of planar anchoring than in the presence of Saturn.

6.3 Discussion and Conclusions

In this chapter we presented results on a quasi-2D system of spherical colloids embedded in active nematics and studied both the effect of their presence on the stability of the fluid and how their collective properties are affected by the onset of spontaneous flow, in the case of a liquid crystal initially in the nematic phase. (For our choice of parameters this is also the thermodynamically most favoured phase, corresponding to the free-energy minimum.) Our results contribute to the current effort in exploiting activity as a driving force towards colloidal self-assembly [94, 95, 98]. Literature has so far focussed mainly on the aggregation of active, self-propelled particles, while here we considered the instance of passive colloids in active nematics. A similar problem was considered also in [100], where passive beads were embedded in a bacterial suspension and effective attraction was observed and interpreted as the result of a combination of bacterial self-propulsion and of depletion interaction.

Here we consider larger colloidal concentration (we always considered a volume fraction of 15%), so as to be able to observe collective properties of colloids. Moreover, we were able to consider a wide range of activities, thus exploring various regimes. We first characterised the instabilities arising in the active fluid at different ζ and studied how they are affected by the presence of colloids. We started from the case of $w = 0$, which corresponds to colloids that do not directly affect the orientation of the liquid crystal close to their surface, and then considered normal and planar anchoring. We found that the characteristics of spontaneous flow, as well as the critical activity for its onset, are importantly affected by the presence of colloids even at $w = 0$, and also by the type of anchoring when $w > 0$. Colloids play a different role in extensile and contractile nematics. In general they hinder spontaneous flow when $\zeta > 0$, while favouring it when $\zeta < 0$.

When $w > 0$ we only considered the case of strong anchoring ($w = 2.3$).

For small $|\zeta|$ flow stems from the defects located at the colloidal surface due to the anchoring condition. Such flow is not able to affect the colloidal structure significantly, especially at short distances. In this regime the flow stemming from defects does not have a global character, which develops only at larger $|\zeta|$. In the case of normal anchoring that happens for values of ζ larger than $\zeta^0_{c,ext}$ in extensile nematics, while in contractile nematics that happens for a much smaller $|\zeta| < |\zeta^0_{c,contr}|$: again, when the anchoring is normal and a Saturn ring defect surrounds the colloids at their equator, spontaneous flow is hindered in extensile and favoured in contractile fluids. Similar regimes can be observed when the anchoring is planar, but now the onset of a global spontaneous flow is hindered also in the case of contractile nematics, where the critical $|\zeta|$ is slightly larger than $|\zeta^0_{c,contr}|$.

We then tried to understand the effect of activity on colloidal aggregation. We found that colloidal collective properties are strongly affected by the onset of a spontaneous flow, whose effects are very different depending on whether $w = 0$ or a strong anchoring is imposed. When $w = 0$, there is no mechanism bringing the colloids together in a passive system. We find that the onset of spontaneous flow causes a dynamic gathering of colloids and the formation of inhomogeneities in their spatial distribution that can be described with large number fluctuations, corresponding to $\Delta N \sim N^\alpha$, with $\alpha > 0.5$, without phase separation ($\alpha < 1$), although this is instead predicted to take place in two-dimensional systems of active, self-propelled particles [15].

When $w > 0$ defects close to the colloidal surface act as attractive patches between colloids and drive colloidal aggregation. Spontaneous flow opposes that: at small $|\zeta|$, when the flow is only local and non-coherent, this simply results in a reduction of the average size of clusters, but does not affect significantly colloidal structures, at least at short distances, as described by the pair distribution function. A global and coherent flow is responsible for a much more homogeneus distribution of colloids at larger $|\zeta|$, that results in the flattening of the $g(r)$ and in a significant reduction of the average cluster size, despite large clusters still being visible. This holds especially in the case of normal anchoring where the large extent of the Saturn ring is responsible for a stronger attraction between colloids than for the case of planar anchoring.

In conclusion, our study sheds light on the potential role of active fluids in

colloidal self-assembly through a systematic analysis of the interplay between the stability of active nematic liquid crystals and the collective properties of a system of colloids embedded therein. We find that the latter are strongly affected by the onset of spontaneous flow, whose role changes according to the elastic interactions between colloids, that depend on the anchoring strength w. We have already pointed out in previous chapters that the meaning of such a parameter for active suspensions is debatable, and strongly dependent on the type of suspension considered. For example, in the case of a dense bacterial suspension, one can expect that the comparable size of typical colloidal particles used in soft matter and of bacteria would make it difficult to impose a fixed orientation of bacteria at the colloidal surface, so that the case of $w = 0$ might reveal to be the most relevant for such a system.

Also in this case we suggest the system described in [24] as a promising candidate for experiments similar to the ones that we studied here through simulations. Such experiments should in principle be easier to perform than the ones on microrheology, since no external forcing is required once a number of colloids is embedded in the fluid.

Chapter 7

Dependence on Initial Conditions: Performing a Quench

In this chapter we will consider again the problem studied in Chapter 6, but with different initial conditions for the (active) liquid crystal, by performing a quench. This consists in starting from the isotropic phase at values of parameter γ in Eq. 2.4 at which the bulk free energy density has an absolute minimum at $S > 0$, so that the system rapidly goes from the isotropic to the nematic phase. It is interesting to consider also this case since quenching is used in experiments where colloids are included in (passive) liquid crystals. We find that different initial conditions importantly affect the characteristics of spontaneous flow. We will also look at the aggregation properties of colloids and find that they are affected by the onset of spontaneous flow in the way described in Chapter 6.

7.1 Stability and Characteristics of the Flow

One way of incorporating colloids in a liquid crystal in experiments is to insert them in the isotropic phase and then decrease the temperature below the critical point, so that the system relaxes towards a configuration of minimum free energy characterised by orientational order [109]. This procedure can be mimicked in simulations by initialising the liquid crystal in the isotropic phase and choosing the liquid crystal parameters (in our case γ, appearing in Eq. 2.4) so as to produce an abrupt quenching of the system. The relaxation to the nematic phase goes through the formation of defects throughout the bulk.

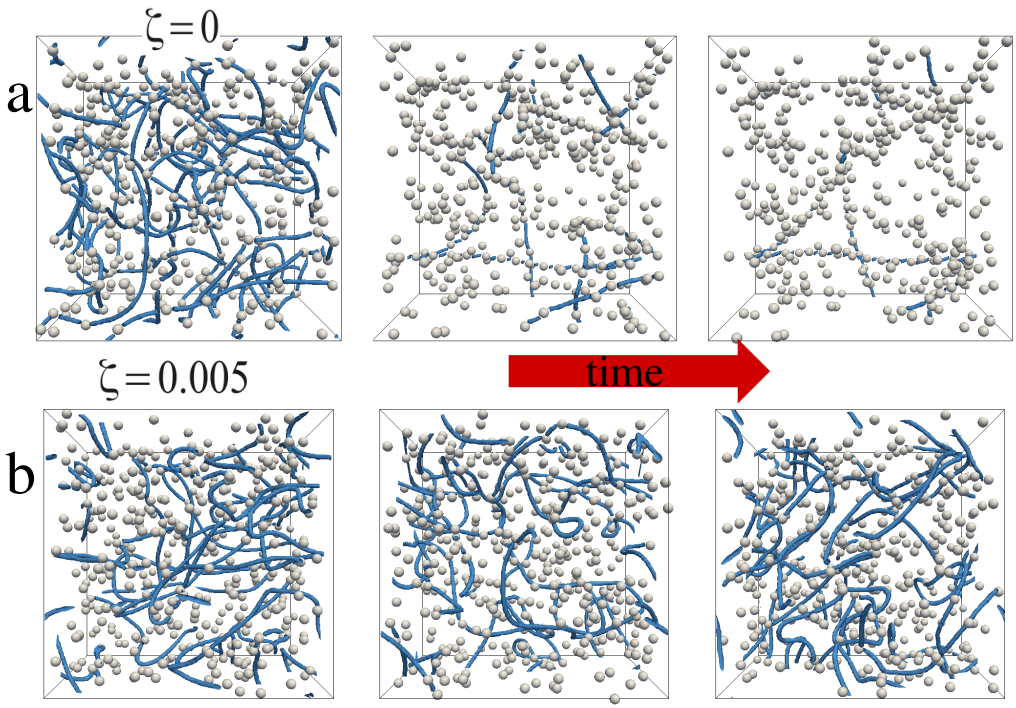

Figure 7.1: Time evolution for a system of colloids embedded in passive (a) and extensile (b) nematics when a quench is performed: in passive liquid crystals the system relaxes to an ordered nematic through the formation of defect lines. Colloids are attracted by defects whose shrinking drives colloidal clustering. At (b) $\zeta = 0.005$, and spontaneous flow hinders relaxation: regions of disorder in the director profile continuously form due to the chaotic character of the flow.

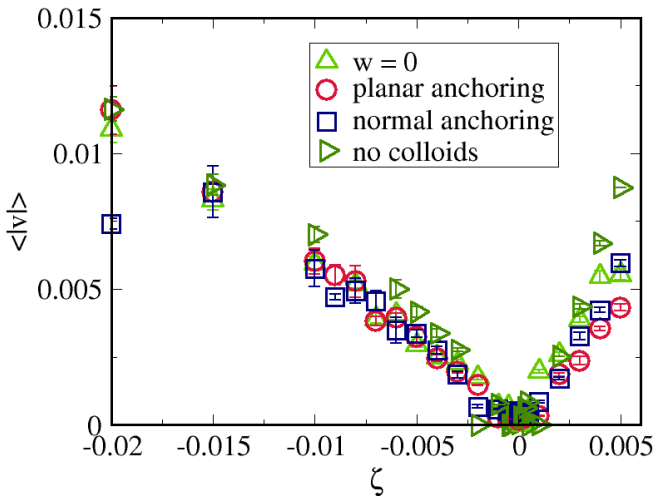

Figure 7.2: The average modulus of the fluid velocity as a function of ζ for active nematics in the absence of colloids, and with 15% colloids volume fraction, at $w = 0$, with normal and planar anchoring (see legend). Averages are computed over a range of configurations once steady state has been achieved. The stability curve is not significantly affected by the presence of colloids, nor by the type of anchoring when $|\zeta| \gtrsim 0.003$.

When colloids are present, they are attracted towards regions of high elastic energy, whose extent they reduce by sitting on top of defects. The shrinking of defects during the process of relaxation in passive liquid crystals brings the colloids together and drives the formation of clusters. This process is illustrated for $w = 0$ in Fig. 7.1 (a) where the mechanism driving colloidal aggregation in the case of $\zeta = 0$ is presented (note that for visualisation purposes the screenshots – and only those – refer to a 3D system). Fig. 7.1 (b) shows instead the case of a spontaneously flowing fluid: the onset of spontaneous flow hinders relaxation and the defects that form at the beginning are advected around.

7.2 Morphology of Spontaneous Flow

We first analyse the stability of the fluid for the values of ζ at which we will later consider the aggregation properties of colloids. A graph showing the dependence of the average modulus of the fluid velocity on ζ, for $|\zeta| \geq 0.0005$ is shown in Fig. 7.2: the onset of spontaneous flow takes place at very small ζ also in the case

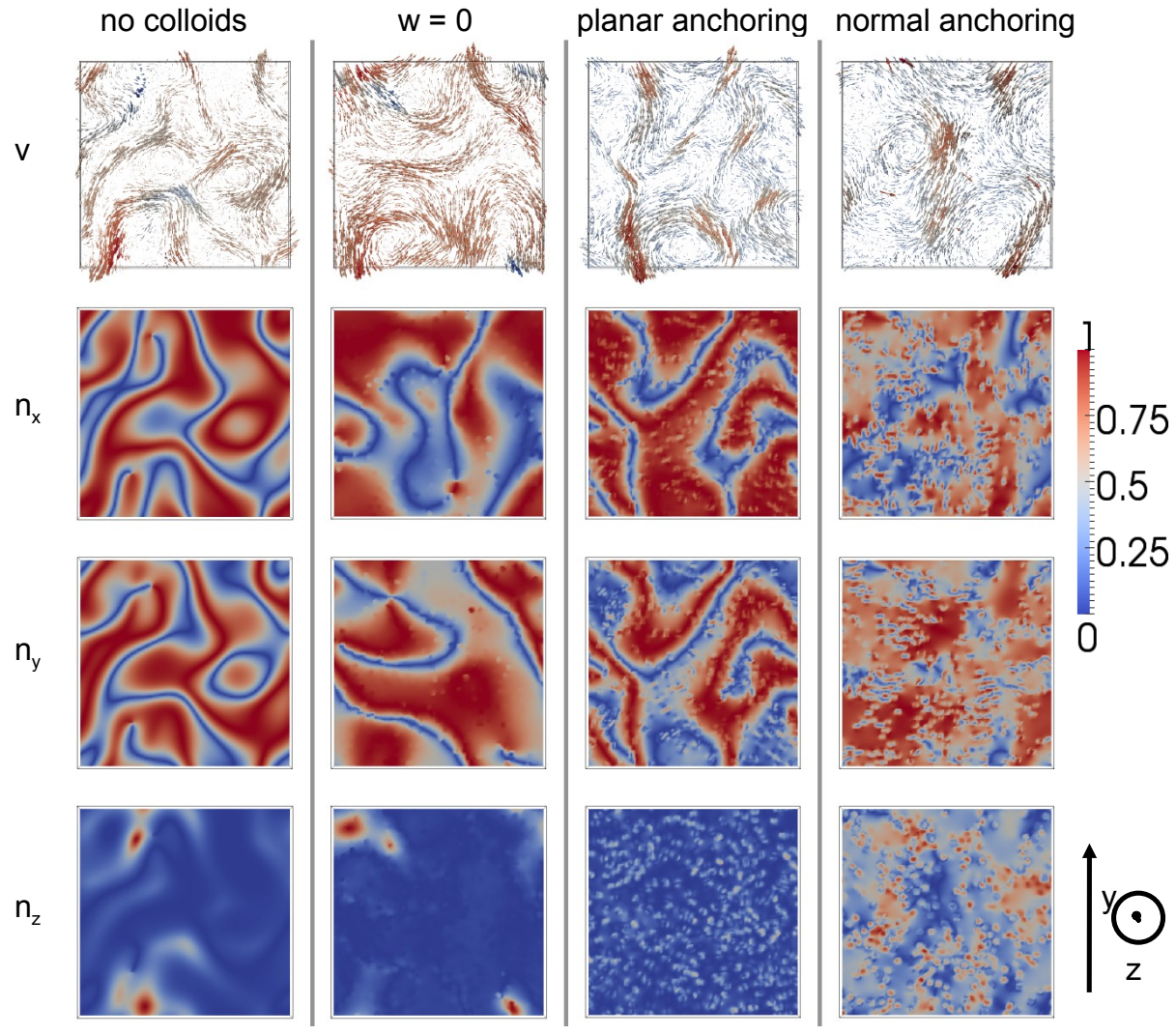

Figure 7.3: Velocity and director profiles in contractile nematics at $\zeta = -0.005$, for all the cases considered in Fig. 7.2. The similarities between their director and velocity profiles are evident.

of contractile nematics where spontaneous flow would set in only at much larger $|\zeta|$ for a bare active liquid crystal initially ordered. What is most striking is that the average fluid velocity is very similar, for all types of anchoring, to that in the absence of colloids, especially in the case of contractile nematics. In order to better understand what goes on in this case, in Fig. 7.3 we compare the velocity and director profiles for $\zeta = -0.005$ for all the four cases considered in Fig. 7.2. It is clear that the characteristics of the flow and of the deformations of the director field are not importantly affected by the presence of colloids or by the type of anchoring. This is true for all $\zeta \leq -0.003$. From these observations we conclude that, interestingly, the anchoring condition does not influence the intensity and the characteristics of spontaneous flow in a large range of activity parameters among the ones considered in our simulations, differently from what was observed in Chapter 6, in the case of an initially ordered director field, where the impact of colloids and of the anchoring condition on the stability of active nematics was significant for all the ζ considered. This is especially true in the case of contractile nematics, where the stability diagram is independent of the anchoring condition, while in extensile nematics small differences can be attributed to the different character of the flow, as will be described later on.

These results suggest that, when a quench is performed, spontaneous flow must be triggered by a different mechanism. While in the previous chapter we were in the regime of small initial perturbations, since a tilt in the director profile was introduced only in a confined region, the initialisation to the isotropic phase rather works as a perturbation on a much larger scale and the system becomes unstable much faster. When this is the case, local flow associated with defects at the colloidal surface plays a minor role compared to the global effect of bulk deformations and flow. As a consequence, the intermediate regime of small, but non-zero $|\zeta|$, that we could observe for $w > 0$ when the active fluid was initialised in the nematic phase and where spontaneous flow only had a local character, is no longer present now that we perform a quench. The spontaneous flow must now originate also from the regions of high orientational disorder that form during the transition to the nematic phase.

From Fig. 7.2, one can see that, for $\zeta \gtrsim -0.003$ and for extensile nematics, the presence of colloids has a large impact on the character of spontaneous flow. To see that, we present the velocity and the director profiles in the absence of

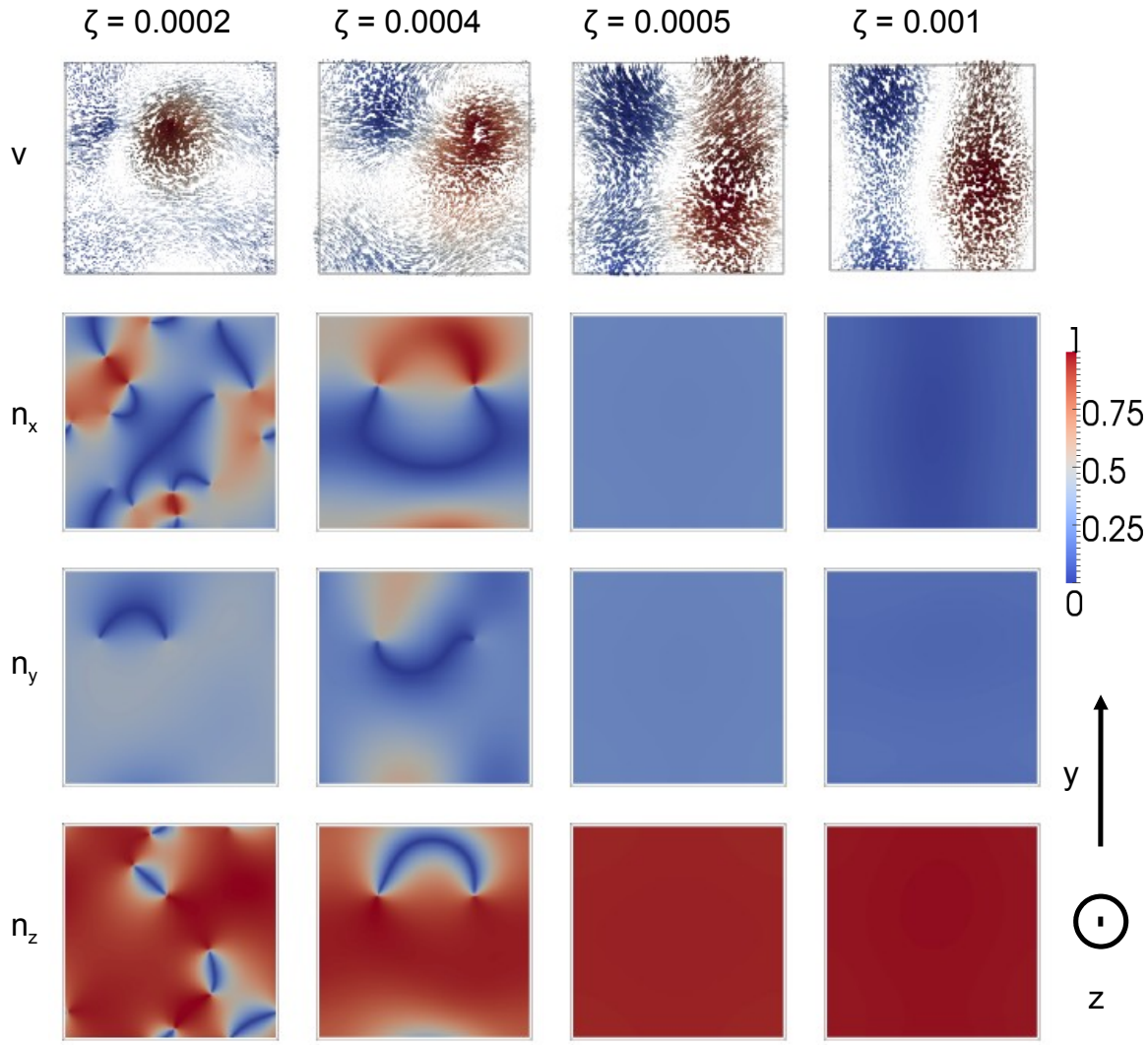

Figure 7.4: Velocity and director profiles in extensile nematics, without colloids, in a regime of spontaneous flow, for ζ between 0.0002 and 0.001. The colour coding for the director profile is as in the legend, while for velocity the colour gives information about the z component: dark blue and dark red refer respectively to the minimum (and therefore negative) and the maximum (positive) component of the velocity field along z.

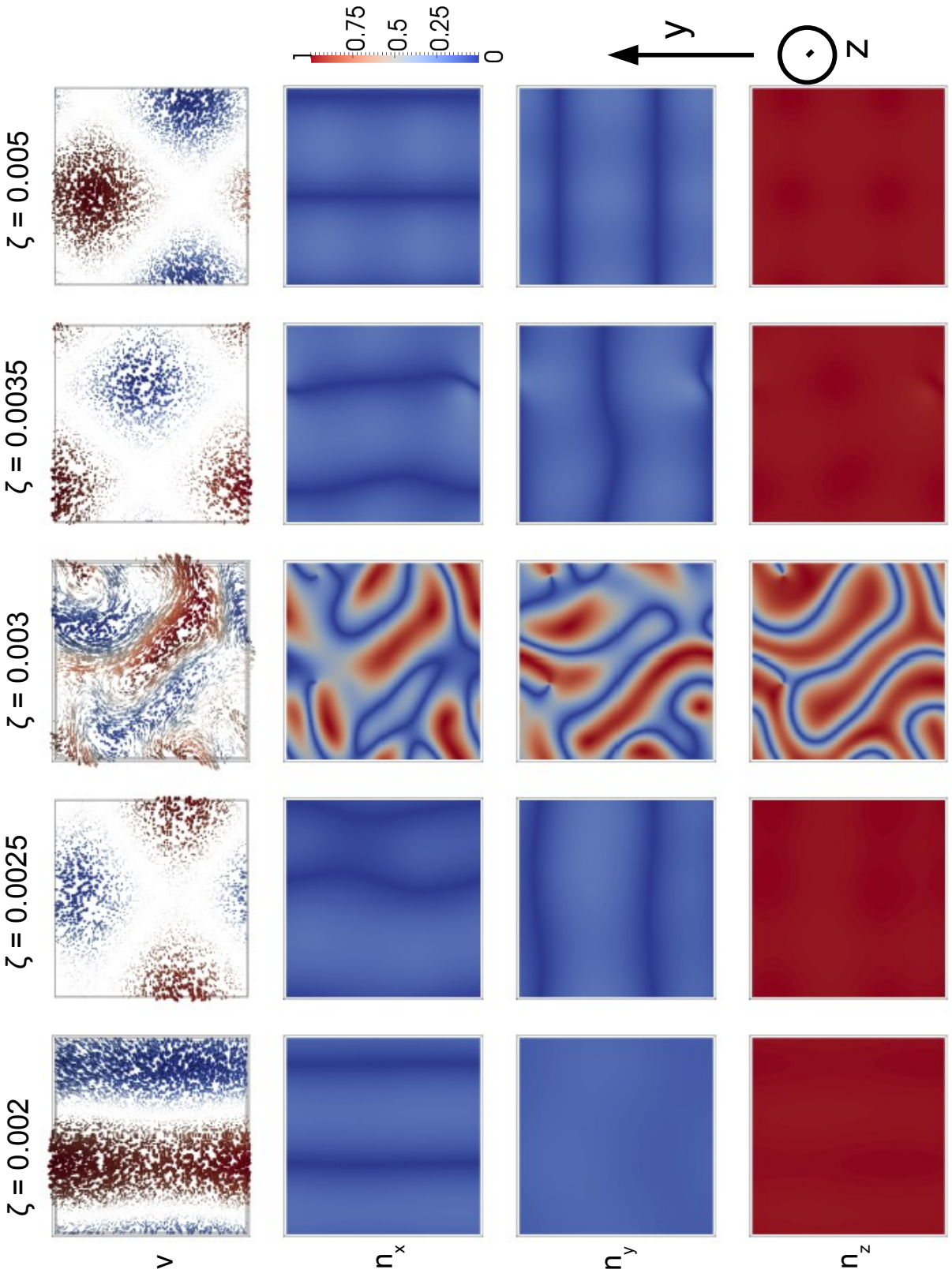

Figure 7.5: Velocity and director profiles in extensile nematics, with a 15% colloidal volume fraction, in a regime of spontaneous flow, for ζ between 0.002 and 0.005. The colour coding for the director profile is as in the legend, while for velocity the colour gives information about the z component: dark blue and dark red refer respectively to the minimum (and therefore negative) and the maximum (positive) component of the velocity field along z.

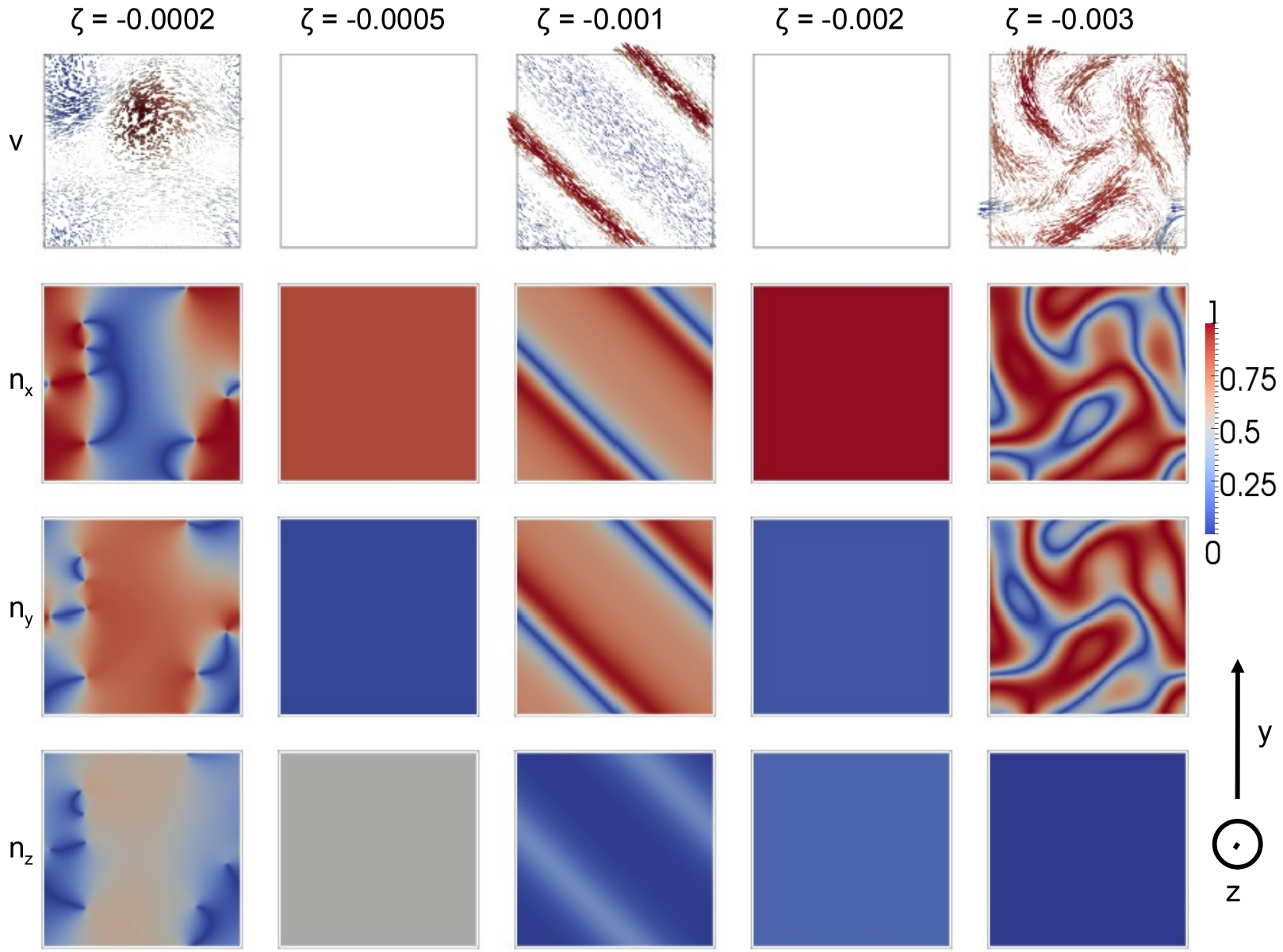

Figure 7.6: Velocity and director profiles in contractile nematics, with a 15% colloidal volume fraction, in a regime of spontaneous flow, for ζ between -0.0002 and -0.003. The colour coding for the director profile is as in the legend, while for velocity the colour gives information about the z component: dark blue and dark red refer respectively to the minimum (and therefore negative) and the maximum (positive) component of the velocity field along z.

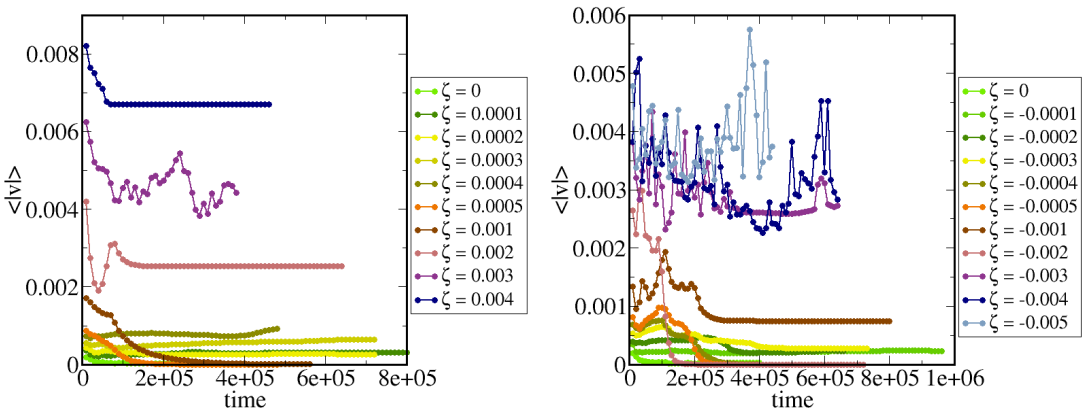

Figure 7.7: Time evolution of the quantity $\langle \vec{v} \rangle$ for extensile (left) and contractile (right) nematics, in the absence of colloids, and for $|\zeta| < 0.005$.

colloids, in Figs. 7.4-7.6, which we will later compare to the corresponding ones in the presence of colloids. It is important to point out that, at very small $|\zeta|$ ($|\zeta| < 0.0005$), the liquid crystal has not achieved complete relaxation yet, despite the long observation time. (The evolution of $\langle |\vec{v}| \rangle$ in time is presented in Fig. 7.7, for some, small $|\zeta|$.) An increase in $|\zeta|$ gives a complete relaxation in a much shorter time (see e.g. $\zeta = -0.0005$), showing that the flow observed at smaller $|\zeta|$ is associated with relaxation and with the presence of disordered regions. For this reason the corresponding values of $\langle |\vec{v}| \rangle$ are not presented in Fig. 7.2.

It is interesting to notice that performing a quench gives access to phases that we did not see when the liquid crystal was initialised in the nematic phase, while there were others that we cannot see any longer. For example, in extensile nematics the flow always develops mainly along the z-axis and never achieves a two-dimensional character before becoming fully three-dimensional and chaotic (at $\zeta = 0.003$). On the other hand, while a flow analogous to the one that we see at $\zeta = 0.002$, characterised by alternating layers of flow in opposite directions, had been observed also in Chapter 6, at $\zeta = 0.0025$ and at $\zeta = 0.0035$ the layers are now replaced by columns of flow, always directed along z, but in alternating directions.

More interestingly, here we see signs of bistability, in both extensile and contractile nematics. For the former, we find that at $\zeta = 0.0025$ and at $\zeta = 0.0035$ the flow is one-dimensional and directed along the z-axis, while at $\zeta = 0.003$ the spontaneous flow is three-dimensional and chaotic. This is a sign of the fact

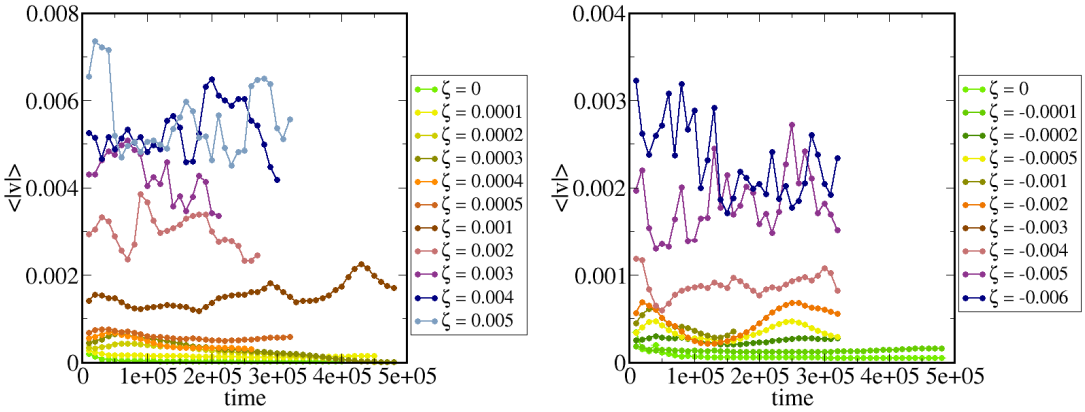

Figure 7.8: Time evolution of $\langle|\vec{v}|\rangle$ for extensile (left) and contractile (right) nematics with a colloidal volume fraction of 15%, in the case of $w = 0$.

that both these two phases are stable in a region of ζ close to 0.003. To verify that we performed simulations with four different initial isotropic configurations at $\zeta = 0.002$, 0.003, 0.004 and 0.005. For all of these values we found that the system could be found either in a one-dimensional flow phase, similar to the ones at $\zeta = 0.002$ or $\zeta = 0.005$ in Fig. 7.5, or in a chaotic flow phase, as the one represented in Fig. 7.5 at $\zeta = 0.003$. We observe something similar for contractile nematics, which are stable at $\zeta = -0.0005$ and at $\zeta = -0.002$, while a one-dimensional flow develops at $\zeta = -0.001$ (see Fig. 7.6). Also in this case we performed several simulations to verify the hypothesis of bistability for $\zeta = -0.001$, -0.002, and -0.003, finding that in all three cases both the regimes of one-dimensional and of a two-dimensional and chaotic flow can be found. [1]

In conclusion, for a bare active liquid crystal, the main effect of a quench is the one of accelerating the transition to a spontaneously flowing phase, that takes place at a much smaller $|\zeta|$ than in an active fluid that is in the nematic phase since the beginning, and the one of giving access to phases that we could not see when the instability was originating from a small tilt along one plane in an ordered nematic.

We now turn to the case where colloids are present, and address the limit of $w = 0$. As in the previous chapter the colloids are spheres with a diameter of 4.6 lattice units and they interact at very close distances through the soft potential

[1] We note here that the values of $\langle|\vec{v}|\rangle$ reported in Fig. 7.2 refer to the phases in Figs. 7.4-7.6.

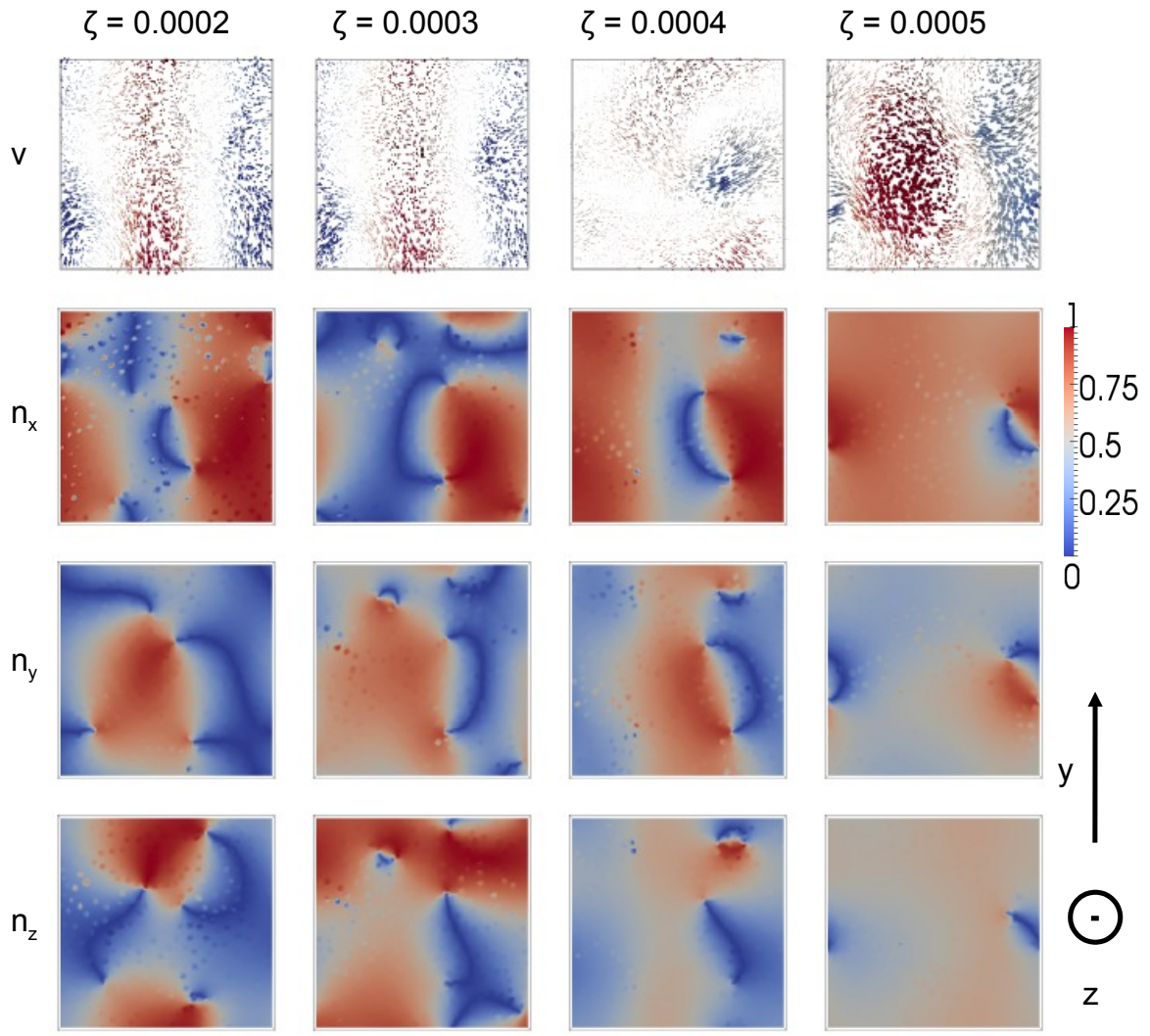

Figure 7.9: Velocity and director profiles in extensile nematics, with a 15% colloidal volume fraction, in a regime of spontaneous flow, for ζ between 0.001 and 0.005. The colour coding for the director profile is as in the legend, while for velocity the colour gives information about the z component: dark blue and dark red refer respectively to the minimum (and therefore negative) and the maximum (positive) component of the velocity field along z.

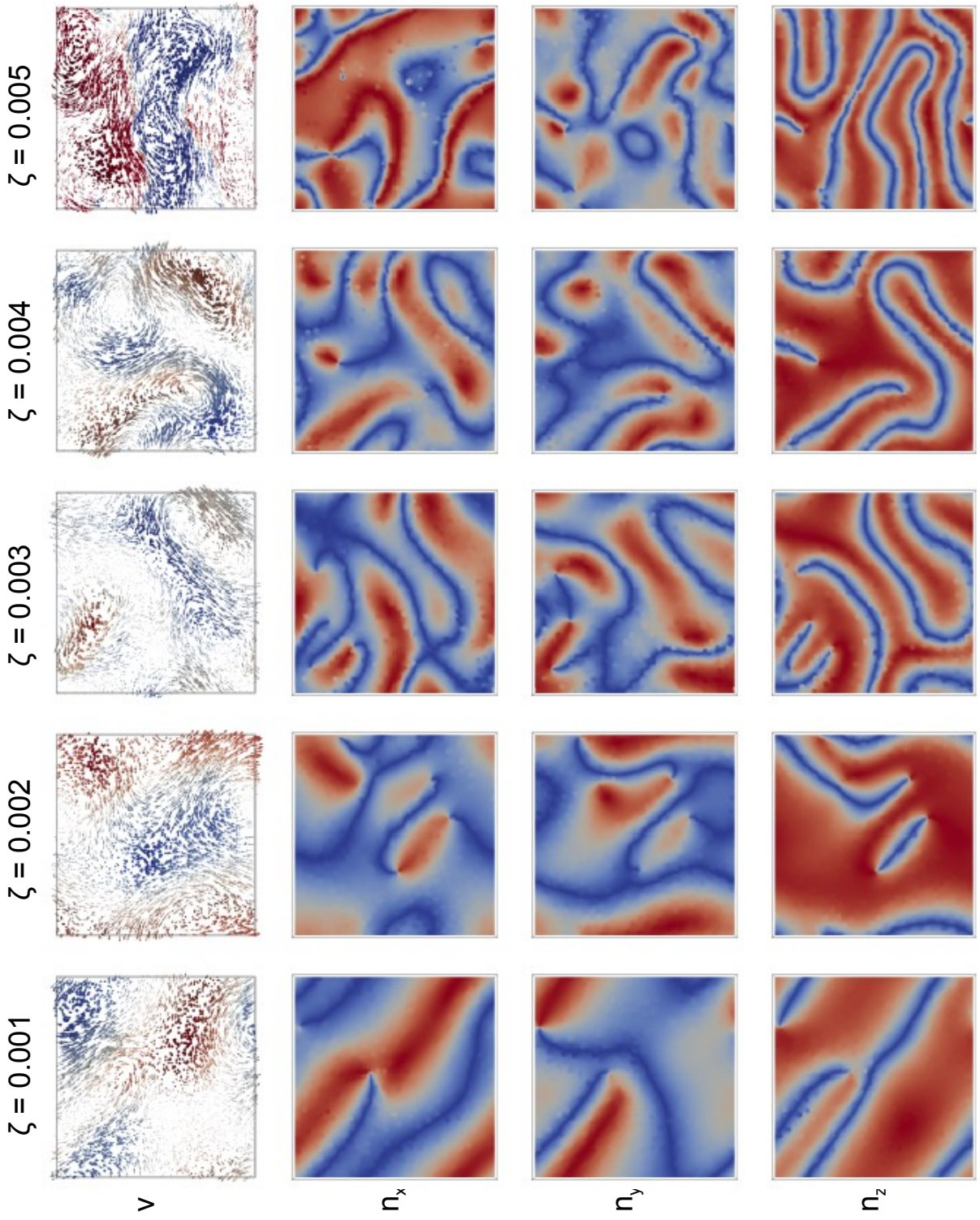

Figure 7.10: Velocity and director profiles in extensile nematics, with a 15% colloidal volume fraction, in a regime of spontaneous flow, for ζ between 0.001 and 0.005. The colour coding for the director profile is as in the legend, while for velocity the colour gives information about the z component: dark blue and dark red refer respectively to the minimum (and therefore negative) and the maximum (positive) component of the velocity field along z.

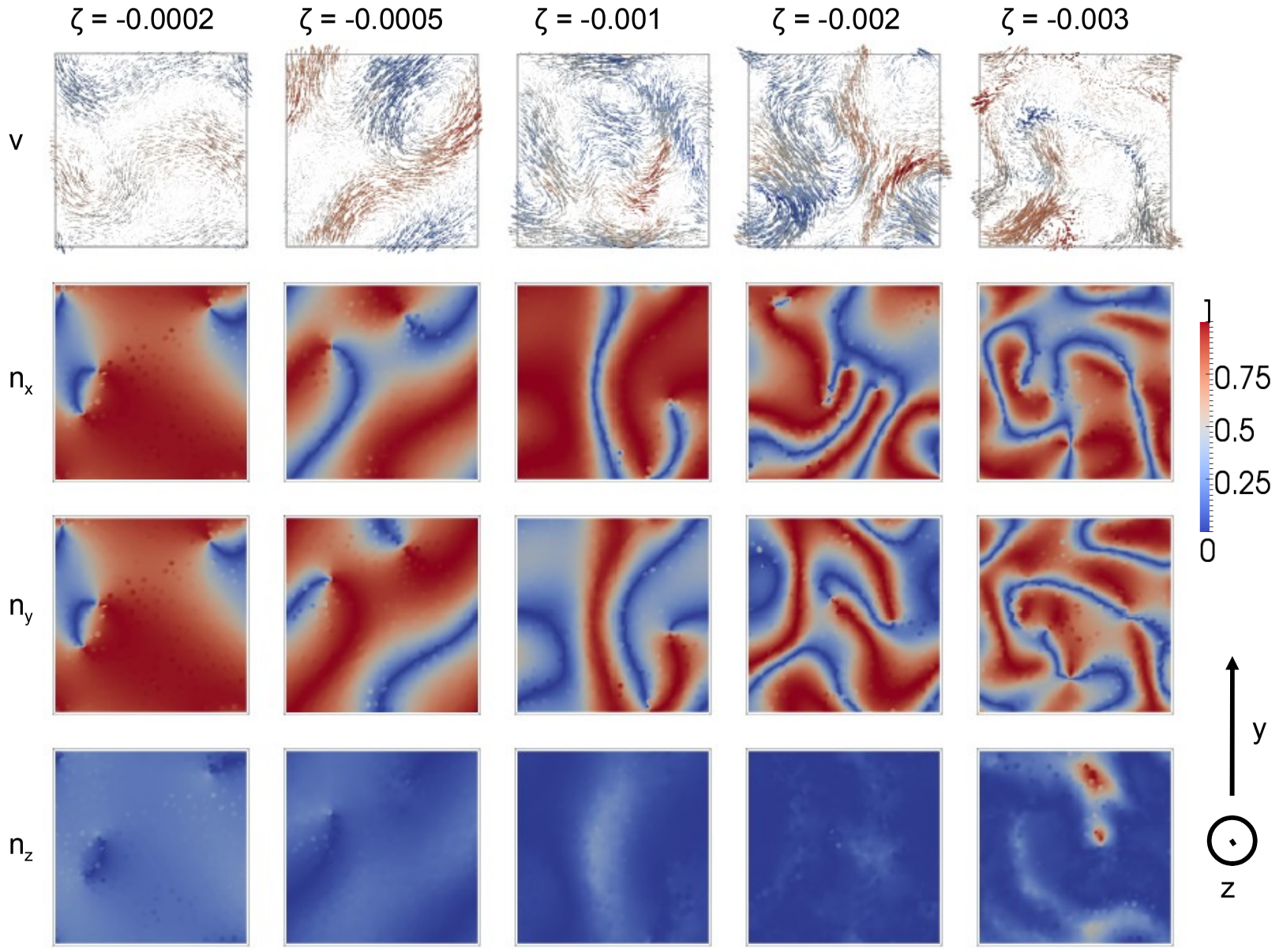

Figure 7.11: Velocity and director profiles in contractile nematics, with a 15% colloidal volume fraction, in a regime of spontaneous flow, for ζ between -0.009 and -0.015. The colour coding for the director profile is as in the legend, while for velocity the colour gives information about the z component: dark blue and dark red refer respectively to the minimum (and therefore negative) and the maximum (positive) component of the velocity field along z.

described in Eq. 6.1 whose aim is to prevent the superposition of spheres. Again, we consider a system of 771 colloids, corresponding to a volume fraction of 15%. The velocity and director profiles corresponding to some representative values of ζ are presented in Fig. 7.9-7.11. As in the absence of colloids, for small, but non-zero $|\zeta|$ a flow originates mainly from the defects that form during the relaxation process, which was not completed during our observation time. The dependence of $\langle|\vec{v}|\rangle$ on time is presented in Fig. 7.8.

The most interesting results are found for larger $|\zeta|$: the main effect of colloids is to enhance the onset of a chaotic flow (which, as in the cases analysed in Chapter 6, develops in three dimensions in extensile nematics, while being mainly confined in the xy-plane in contractile ones). This is true for all $|\zeta| \gtrsim 0.001$. We do not see signs of bistability in this region: as with an initially ordered director profile, colloids tend to favour the onset of a chaotic flow. This happens in extensile nematics and for small $|\zeta|$ in the $\zeta < 0$ region, which is where major differences in the intensity of the flow emerge from Fig. 7.2. We do not present here the full analysis of the flow also in the case of $w > 0$, however the presence of defects, associated with a local flow due to the active nature of the solvent, does not affect the qualitative character of spontaneous flow, which is similar to the one that we described for $w = 0$.

7.3 Aggregation Properties

We now study the characteristics of colloidal aggregation. In order to understand whether the initial condition has an impact on the colloidal structures that form in the presence of anchoring, we can compare the pair distribution functions at $\zeta = 0$ for the different types of anchoring in Fig. 7.12. In all cases we do not aim at describing the final configuration at equilibrium, since the latter might be strongly affected by the soft potential acting at short distances, and by the presence of spurious velocities, which we described in Chapter 3 and which are localised mainly at the defects, and are of the order of 10^{-5}, thus affecting short range interactions. It is however useful to compare the pair distribution functions obtained by averaging over several configurations once $\langle|\vec{v}|\rangle$ has stabilised. Differences in the time interval over which $g(r)$ is measured might be responsible for the difference in the heights of maxima and the depths of

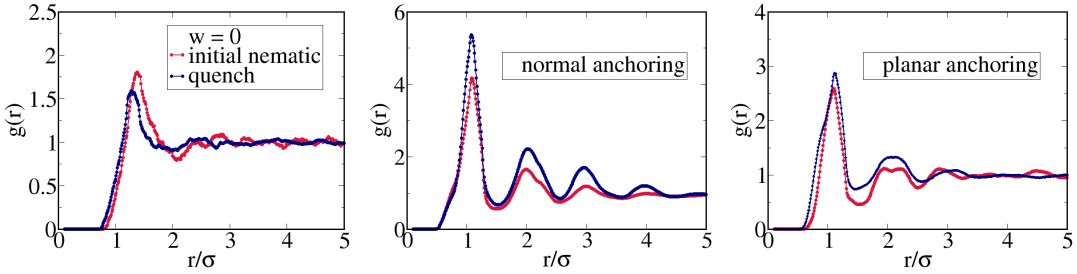

Figure 7.12: Comparison between the pair distribution functions that are obtained with different anchoring conditions, at $\zeta = 0$, in the case of $w = 0$, of normal anchoring and of planar anchoring. The $g(r)$ in the case of a liquid crystal initially in the nematics phase, has been obtained by averaging over the time interval between the times $t = 100000$ and $t = 160000$; for the quench we averaged over the time interval between $t = 200000$ and $t = 260000$.

minima. What is important is that their positions remain unaffected by the initial condition, suggesting that the latter does not affect the colloidal structures forming in passive nematics.

We now address the impact of spontaneous flow on the collective behaviour of colloids. In Fig. 7.13 we show their distribution – and the corresponding director and velocity profiles – at $\zeta = 0$, and at $\zeta = 0.005$, where the fluid is spontaneously flowing. It is clear in this case that spontaneous flow favours an inhomogeneous distribution of colloids. We do not see the formation of stable aggregates, but the colloids are pushed together by the flow, so that regions of larger and smaller colloidal density are continuously formed, in a dynamic way. In Fig. 7.14 we compare $g(r)$ for the passive system with that for a large value of $|\zeta|$, where the spontaneous flow is most intense: its main effect is similar to what we observed when the liquid crystal was initialised in the nematic phase; it decreases the average distance between nearest neighbours (governed by the position of the peak), and increases the height of the main peak.

In Fig. 7.15 we plot the number fluctuations, ΔN, for a system of colloids (15% volume fraction) in extensile and contractile nematics, at $w = 0$. As in the case of a liquid crystal initialised in the nematic phase, we see that the slope of the curve grows with growing ζ. Again, we see large number fluctuations, corresponding to $\Delta N \sim \langle N \rangle^{\alpha}$, with $\alpha > 1/2$. Related to the fact that at $\zeta = 0$ we see $\Delta N \sim \langle N \rangle^{\alpha}$, with $\alpha < 0.5$, as an effect of the finite size of our system, in

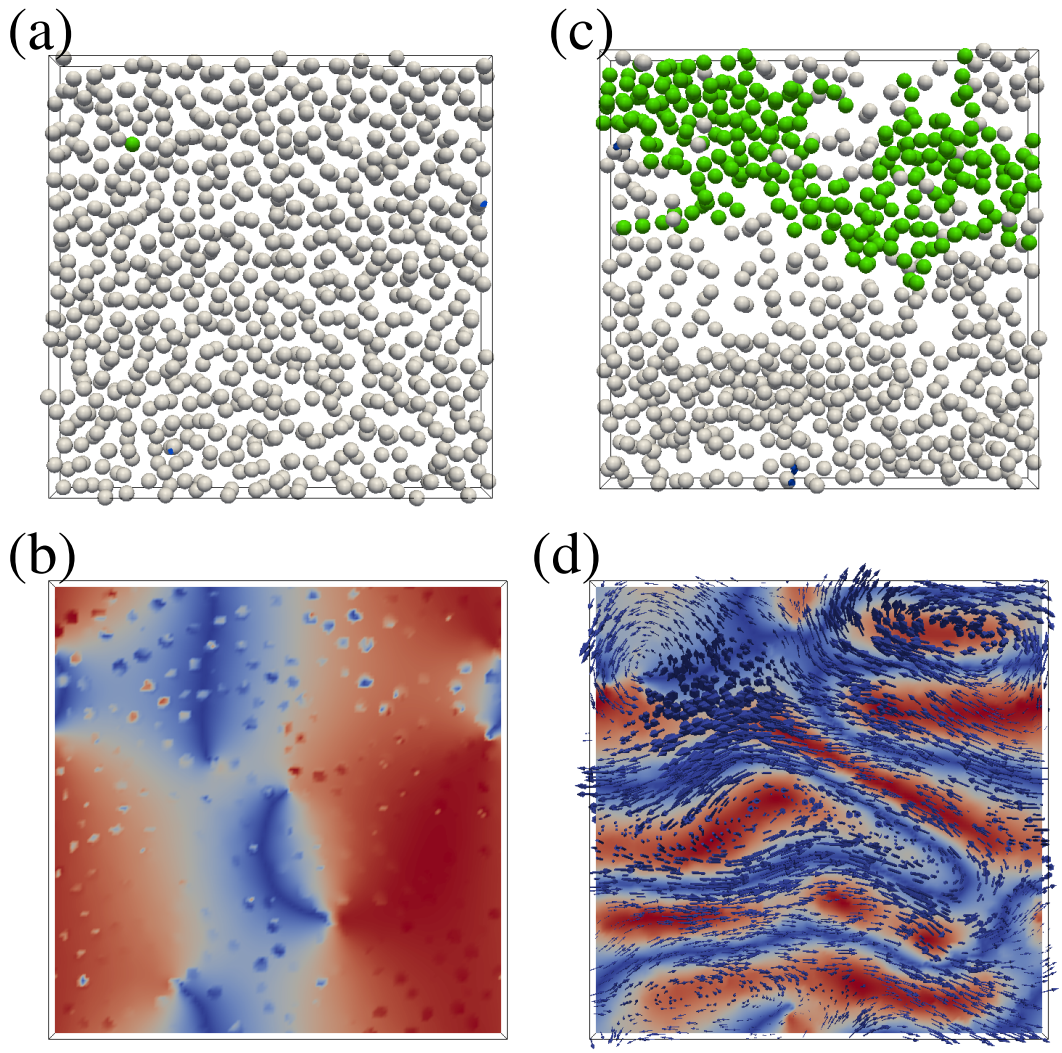

Figure 7.13: Screenshots referring to a system of 771 colloids in extensile nematics at $\zeta = 0$ (a,b) and at $\zeta = 0.005$ (c,d). Aggregates can be found by defining a binding radius, even though what takes place at $w = 0$ is not actual clustering but rather the dynamic formation of inhomogeneities. Here we highlight in green the largest aggregate, defined through a binding radius $r_b = 6.15$. In panels (b) and (d) we show also the director field (background) and the velocity profile (blue arrows). The velocity profile is omitted in panel (b) since relaxation has not been completed yet.

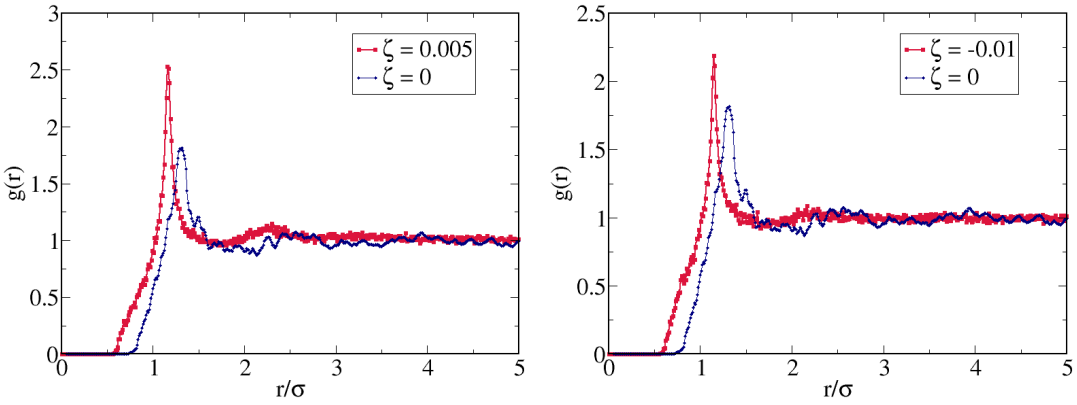

Figure 7.14: Comparison between the pair distribution function for a passive and for a spontaneously flowing nematic liquid crystal in the case of $\zeta > 0$ (left panel) and of $\zeta < 0$ (right panel).

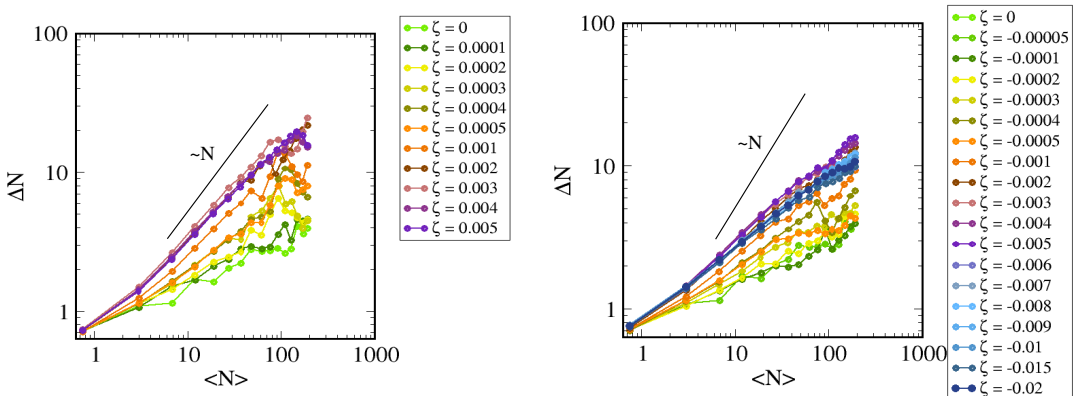

Figure 7.15: Number fluctuations in the cases of an extensile (left) and of a contractile (right) nematic liquid crystal, for $w = 0$ when a quench is performed.

our case α goes from ~ 0.3 to ~ 0.7.

When $w > 0$ an effective attraction between colloids, due to the presence of defects, allows for the formation of clusters. Typical configurations at $\zeta = 0$ and at $\zeta = 0.005$, in the case of normal anchoring, are shown in Fig. 7.16, in panels (a) and (c) respectively, together with the corresponding velocity and director profiles, which are displayed in panels (b) and (d). The role of spontaneous flow is mainly to homogenise the distribution of colloids, as can be seen in panels (a) and (c) in Fig. 7.16. This qualitative observation is made clearer by the pair correlation function, shown in Fig. 7.17, where the panel on the left refers to extensile nematics, and the one on the right to contractile ones.[2] Notice that, in contrast to what we saw in Chapter 6, now the pair distribution function is significantly different from the one at $\zeta = 0$, also for intermediate ζ. This is because when a quench is performed it is no longer possible to find a regime where the flow is localised close to the defects; instead the spontaneous flow always has a global character.

Colloidal aggregation can be studied for $w > 0$ by looking at the average fraction of colloids that are in clusters. This quantity is plotted as a function of time in Fig. 7.18 for the case of normal anchoring. From there one can see that increasing ζ hinders cluster formation, due to the onset of spontaneous flow.

In Figs. 7.19-7.21 we present a similar analysis for the case of planar anchoring. In Fig. 7.19 (a) it can be seen that the colloidal structures formed at $\zeta = 0$ are affected by incomplete relaxation (as is clear from panel (b)). However, the difference between this case and $\zeta = 0.005$ (panels (c) and (d)) is evident: spontaneous flow again loosens the bonds that form due to the presence of defects, and is responsible for a more homogeneous distribution of colloids in space. This is quantified by the pair distribution function in Fig. 7.20. Also in this case, the difference with a liquid crystal initialised in the nematic phase is strongest at intermediate ζ ($\zeta = 0.0001$ and $\zeta = -0.001$ for extensile and contractile nematics respectively), due to the different character of the flow in this range of activities, that we described in Section 7.2. The average size of clusters is presented as a function of time in Fig. 7.21.

The results on colloidal aggregation as a function of ζ are summarised in

[2] At $\zeta = 0$ the system is not equilibrated yet, and the pair distribution function is calculated by averaging over $\sim$60 configurations that are sampled every 1000 steps between time $t = 200000$ and time $t = 260000$.

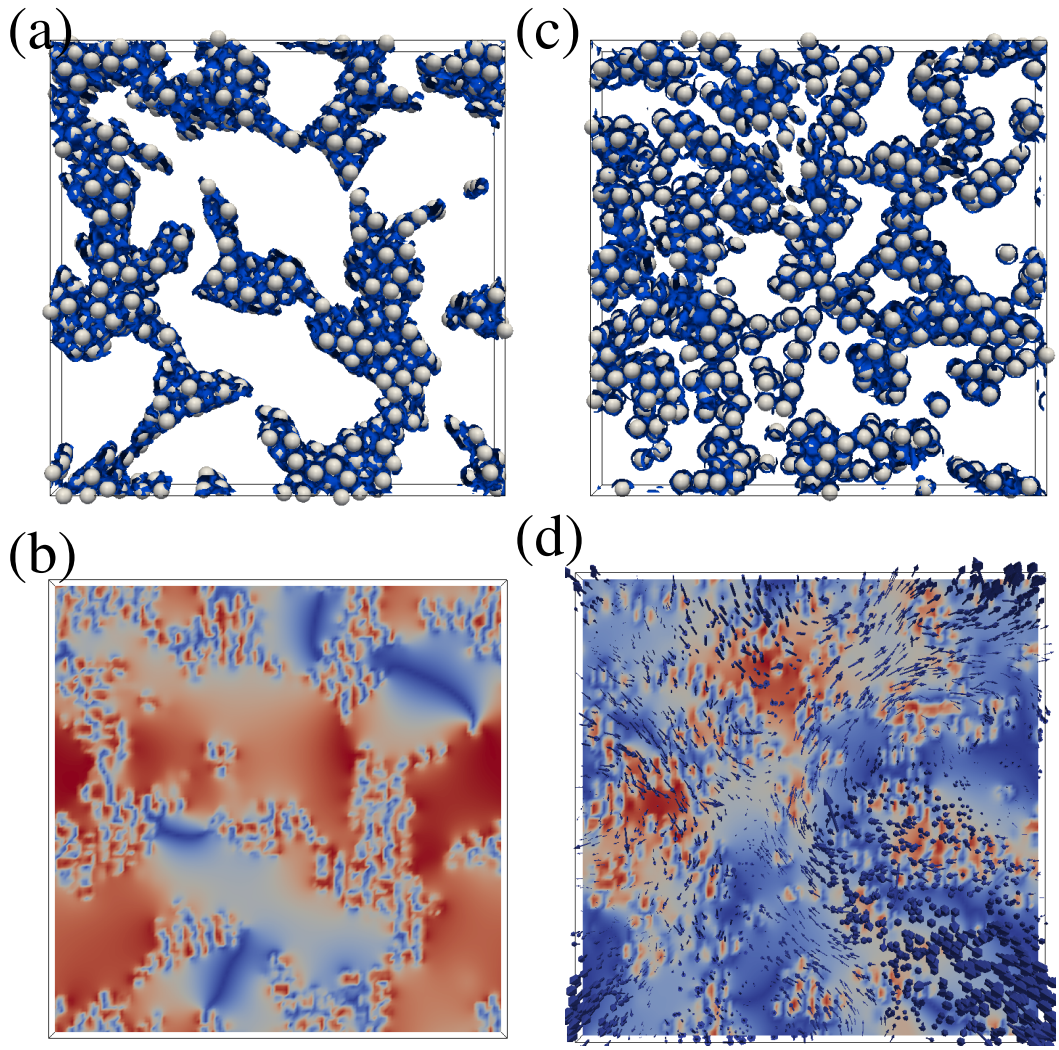

Figure 7.16: Aggregation properties in passive and extensile nematics when normal anchoring is imposed, and a Saturn ring surrounds each spherical colloid. Panels (a) and (c) show the colloidal configurations, and the distribution of defects for a passive system and for an extensile liquid crystal, at $\zeta = 0.005$, respectively. Panels (b) and (d) show the corresponding director (background) and velocity profiles (blue arrows). The colour coding for the director profile is as in the legend, while for velocity the colour gives information about the z component: dark blue and dark red refer respectively to the minimum (and therefore negative) and the maximum (positive) component of the velocity field along z. The flow profile in not shown in panel (b), since it is small and it stems from incomplete relaxation.

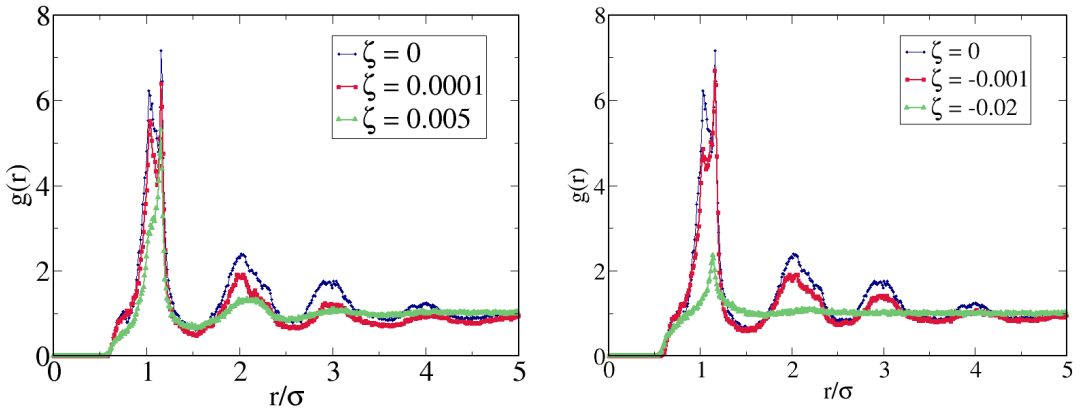

Figure 7.17: Comparison between the pair distribution function for extensile (left) and contractile (right) nematics at different ζ, for normal anchoring.

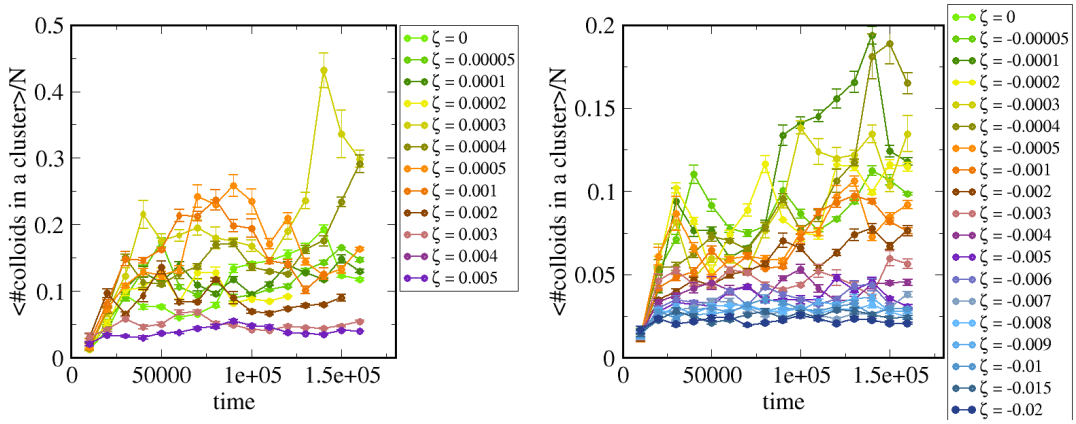

Figure 7.18: Time evolution for the average fraction of colloids in a cluster in the case of extensile (left) and of contractile (right) nematics, for normal anchoring, when a quench is perfomed.

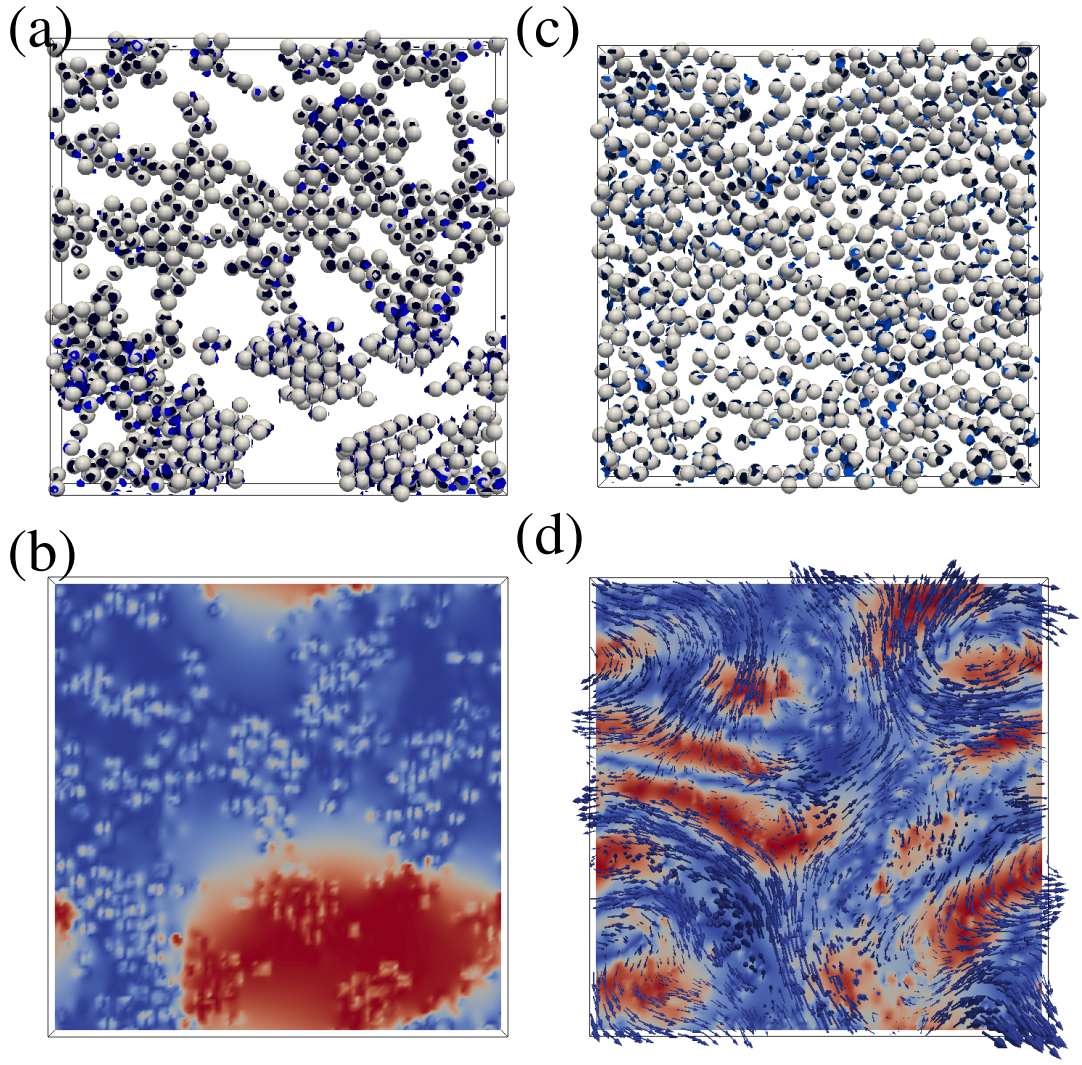

Figure 7.19: Screenshots for passive and extensile nematics when planar anchoring is imposed. Panels (a) and (c) show the colloidal configurations, and the distribution of defects for a passive system and for an extensile liquid crystal, at $\zeta = 0.005$ respectively. Panels (b) and (d) show the corresponding director (background) and velocity profiles (blue arrows). The colour coding for the director profile is as in the legend, while for velocity the colour gives information about the z component: dark blue and dark red refer respectively to the minimum (and therefore negative) and the maximum (positive) component of the velocity field along z. The flow profile is not shown in panel (b), since it is small and it stems from incomplete relaxation.

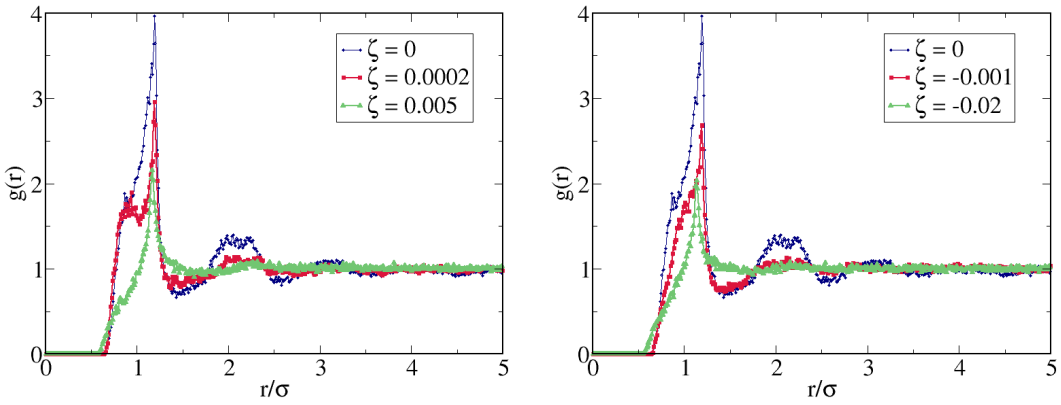

Figure 7.20: Comparison between the pair distribution function for extensile (left) and contractile (right) nematics at different ζ, for planar anchoring.

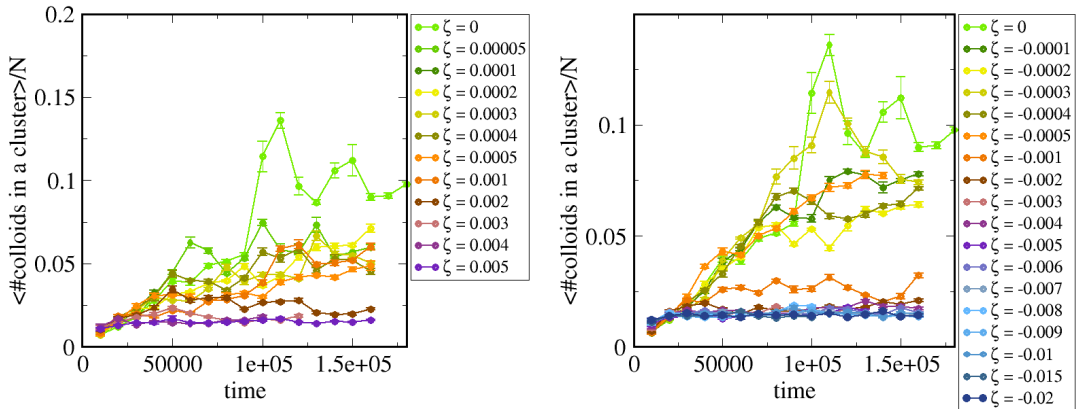

Figure 7.21: Time evolution for the average fraction of colloids in clusters, in the case of extensile (left) and of contractile (right) nematics, for planar anchoring, when a quench is perfomed.

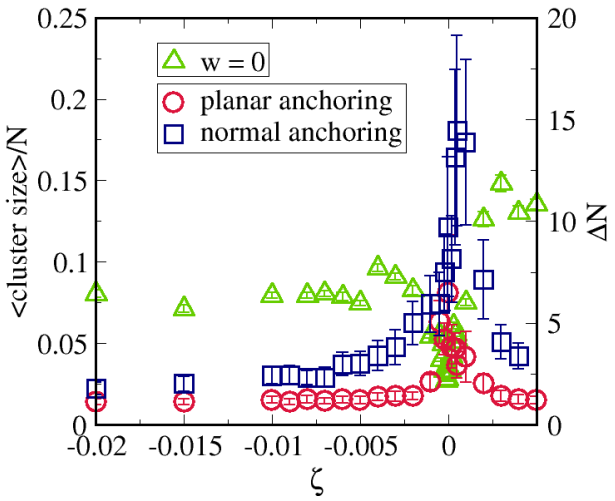

Figure 7.22: The relative average number of colloids in a cluster is studied as a function of ζ for active nematics in the case of 15% colloids volume fraction with normal and planar anchoring (see legend). When no anchoring is imposed ($w = 0$) the quantity to be considered is instead the number fluctuation (ΔN), for which the scale of reference is on the right. A quench is performed and the values showed refer to the steady state. Contrary to the stability of the fluid, the aggregation properties are still affected by the type of anchoring.

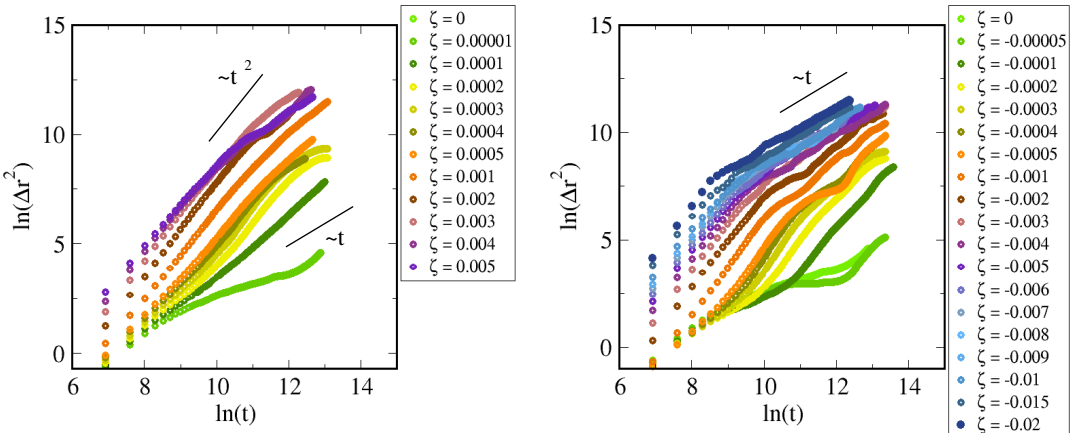

Figure 7.23: Mean squared displacement for a system of colloids embedded in extensile (left) and contractile (right) nematics in the case of $w = 0$.

Fig. 7.22, for normal and planar anchoring, and for $w = 0$. For the latter, colloidal aggregation is quantified by the number fluctuations, ΔN, while for normal and for planar anchoring we instead present the average number of colloids in a cluster, divided by the total number of colloids. When the liquid crystal is initialised in the isotropic phase, spontaneous flow sets in at very small values of the activity parameter, as we showed at the beginning of this chapter, and large number fluctuations can correspondingly be observed already at small $|\zeta|$. Moreover for $w > 0$ the average size of clusters gets significantly reduced.

For completeness, we also show the MSD of colloids for all the different anchorings considered, starting from the case of $w = 0$ in Fig. 7.23. For both planar and normal anchoring the situation is significantly different than in Fig. 6.21: for all $|\zeta| > 0$ colloids do not stop, but rather keep on moving, advected by the flow. The MSD increases continuously for increasing $|\zeta|$, as a direct consequence of the way in which the average modulus of the fluid velocity depends on ζ, as described in Fig. 7.2. Moreover, at all $\zeta \neq 0$ the particles reach a diffusive behaviour at large t. This is true for all types of anchoring (the cases of normal and planar anchoring are presented in Figs. 7.24 and 7.25), as one would expect for particles advected by a chaotic flow.

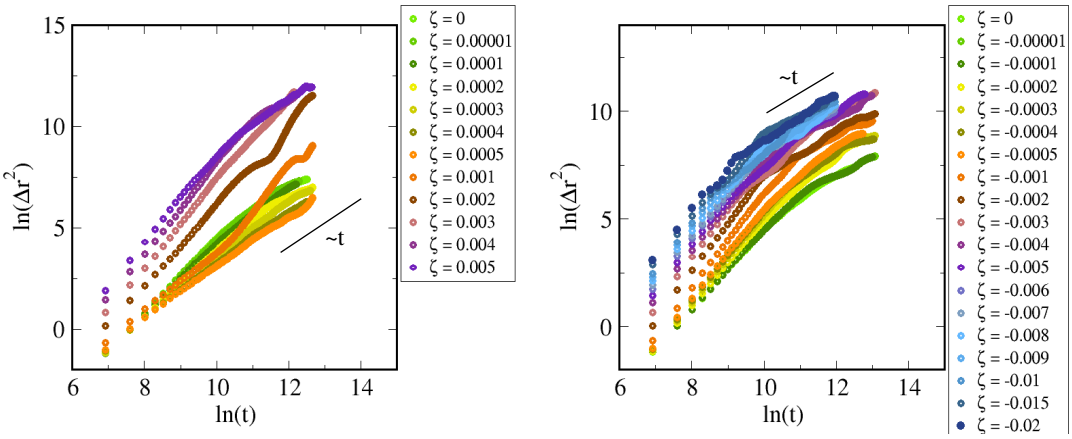

Figure 7.24: Mean squared displacement for a system of colloids embedded in extensile (left) and contractile (right) nematics in the case of normal anchoring.

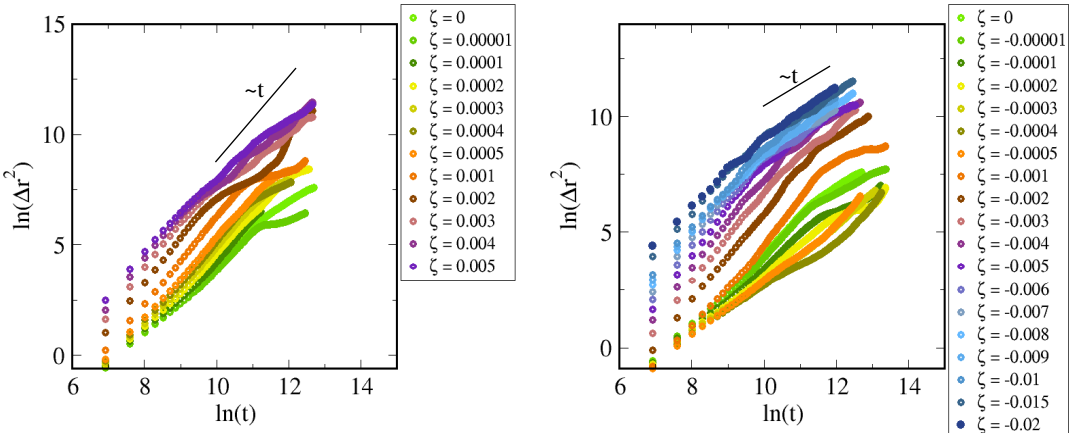

Figure 7.25: Mean squared displacement for a system of colloids embedded in extensile (left) and contractile (right) nematics in the case of planar anchoring.

7.4 Discussion and Conclusions

In this chapter we have presented results that complement Chapter 6, by considering also the case where the liquid crystal is initialised in the isotropic phase, and quenched to the nematic one. An important limitation of our analysis, which is additional to the ones presented in Chapter 6, is that liquid crystal relaxation is very slow and takes a very long time to complete. This translates into long computer times. For this reason most of our simulations at $|\zeta| \lesssim 0.0003$ were not long enough to achieve complete relaxation, and therefore do not offer a raliable picture of the flow (which should be absent, at least in the absence of colloids and at $w = 0$), and of the director profiles. It is also true that the colloidal structures at these ζ are expected to be analogous to the ones described in Chapter 6 and that the most interesting aspects come from the regime of spontaneous flow, where steadiness is reached quickly.

Here we first analysed how the stability of the fluid and the characteristics of spontaneous flow change when a quench is performed. We started from the observation that the stability diagram is not much affected by the presence of colloids, nor by the type of anchoring, once spontaneous flow has set in. This happens at a value of $|\zeta|$ significantly smaller than the critical activity in the case of active liquid crystals initialised in the nematic phase. This is particularly true for contractile nematics, while larger differences in the intensity of the flow (which is quantified by $\langle|\vec{v}|\rangle$) are found in extensile nematics. Our explanation is that, when a quench is performed, the spontaneous flow must originate mainly from the large deformations that are present throughout the bulk while the liquid crystal attempts relaxation to the nematic phase. We presented evidence that in contractile nematics the characteristics of the flow are similar with and without colloids, and for different anchorings, by comparing the velocity and director profiles at $\zeta = -0.005$.

We also presented a detailed analysis of the spontaneous flow developing at those values of ζ for which we later studied the aggregation properties of colloids, for both the bare active liquid crystal, and in the presence of colloids, at $w = 0$. Interestingly we found that, for the bare fluid, performing a quench gives access to some phases that we did not see in Chapter 6, and we also observed evidence of a region of bistability, both in extensile and in contractile nematics, around $\zeta = 0.003$ and $\zeta = -0.001$ respectively. Similar flow and director profiles are

found at $w > 0$, for which we did not present a detailed analysis.

We studied the collective properties of colloids also in this case, by looking at the same quantities that were considered in Chapter 6. Spontaneous flow has a similar role here: when $w = 0$ it causes dynamic inhomogeneities in the distribution of colloids, which relate to large number fluctuations. Differently, when $w > 0$ and an effective attraction drives their clustering at $\zeta = 0$, the role of spontaneous flow is to loosen the bonds between colloids and to make the distribution of colloids in space more homogeneous. The main difference with what was presented in Chapter 6 is to be found at intermediate values of $|\zeta|$, where the quench triggers the onset of spontaneous flow even if the fluid was stable when the liquid crystal was initialised in the nematic phase.

Our results for this type of initial condition might ease the later comparison with experiments, for which we do not know whether it will be easier to include colloids directly in the nematic phase, as studied in Chapter 6, or to perform a quench, as presented in this chapter. Our simulations show that similar results can be expected in the two cases concerning the impact of spontaneous flow on colloidal aggregation. With our studies we have shown that, when passive colloids are embedded in active fluids, activity can either enhance or oppose aggregation, depending mainly on whether or not anchoring is imposed at the colloidal surface.

In conclusion, the study presented in this, as well as in the previous, chapter sheds light on the effect of spontaneous flow on the collective properties of colloids in active liquid crystals. As such, it is part of a wider recent research effort on colloidal self-assembly and, more specifically, on activity-driven self-assembly. Recent studies show that active particles tend to aggregate (see e.g. [14, 15, 47, 98]), which has been explained as stemming from a density-dependent velocity, related to the continuum local energy input, that is intrinsic of active systems [92]. The situation is different when passive colloids are embedded in active fluids. Experiments and simulations presented in [100] suggest that activity is responsible for an effective attraction between passive beads in a bacterial suspension, that is additional to depletion, even though the two effects cannot be studied independently in their case. Our system is again different from the one they considered, since the mechanism bringing colloids together at $w = 0$ is simply advection by spontaneous flow, and there is no direct interaction between the active particles and the colloids. As a consequence, the additional

interaction between colloids is not necessarily attractive, since the flow can both push the colloids together and take them apart. When $w = 0$, this results into dynamic inhomogeneities in the distribution of colloids, rather than into stable aggregates. When an effective attraction between colloids is included, independently of whether a flow is present or not, as in the case of $w > 0$, on average spontaneous flow tends instead to loosen the bonds between colloids and to make their distribution in space more homogeneous than it is in the case of a quiescent active fluid.

Although we considered a wide range for the activity parameter ζ, different anchoring types, and different initial conditions, there are still several aspects that require further investigation. In particular, a more realistic study of the potential value of activity in the design of new materials should consider larger colloidal volume fractions. In the case of liquid crystals the most interesting results are found for volume fractions of $\sim 20\%$ [51], which is when the defect network percolates and the material shows solid-like properties. However, before such studies are performed through simulations, it would be desirable to see laboratory experiments where colloids are introduced into an active liquid crystal. The best candidate at the moment is still the system described in [24].

Chapter 8

Discussion and Conclusions

In this thesis we have presented results from simulations of colloidal systems in active fluids. These were motivated by the fact that active fluids are still unexplored ground, both in terms of fundamental research and in terms of applications. We aimed at filling the gap between the extensive theoretical description and the lack of experimental benchmarking through the use of colloids as a possible link between the two. Spherical colloidal particles are easily available in any soft matter lab, as well as tools for their manipulation as single particles (e.g. optical tweezers) or for their tracking (e.g. optical microscopes). They are therefore widely used to probe the viscoelastic properties of soft materials. Moreover, a high degree of control on the interactions between such particles makes them promising constituents of new materials. The results of our simulations provide a first step to understand the physics of colloids in active fluids, as probes for microrheology experiments, to study the rheological properties of active fluids, and as building blocks for new, composite materials, where active fluids are used as a solvent in colloidal suspensions.

The model that we used is a continuum one and it exploits the strong analogy with nematic liquid crystals, due to the natural tendency of active particles to align along a common direction. As a consequence, our characterisation of active fluids and of colloidal suspensions where they act as a solvent, was always based on the comparison with their passive analogues.

In Chapters 4 and 5 we simulated microrheology experiments where a single, spherical particle is dragged through (passive and) active nematics. In Chapter 4 we also presented results from simulations of macrorheology where the active fluid

was sheared between two walls, for comparison with microrheology results. For both bulk and microrheology we defined an effective viscosity η_{eff}, and analysed its dependence on the size of the system for different anchoring conditions, and on the activity coefficient. By simulating the shearing of active nematics between two walls, we found that, as in the case of passive liquid crystals, the effective viscosity depends strongly on the type of anchoring at the walls. Moreover, in contractile nematics η_{eff} is larger than in passive ones, and the opposite is true for extensile nematics, in agreement with previous results from simulations [40], and from experiments on algal [76] and bacterial [77] suspensions. What is most significant in our results on macrorheology is that we found an important dependence on the distance between the two shearing planes, which is such that η_{eff} diverges, and is therefore ill-defined, in the case of an infinite system.

Our findings on simulations of microrheology presented in Chapter 4 can be summarised as follows: (i) as in the passive case η_{eff} is affected by the anchoring condition at the colloidal surface; (ii) for planar anchoring comparison with the passive case shows that η_{eff} is larger in contractile nematics, and smaller in extensile ones, in agreement with macrorheology, while the opposite is true when normal anchoring is imposed and the colloid is accompanied by a Saturn ring; (iii) in the case of strong anchoring η_{eff} depends strongly on the radius of the probe, R, thus showing that Stokes' law, which describes the drag force acting on a sphere that moves through a simple fluid, and which can be extended to passive nematics [69], does not hold in active fluids. This result remains true when two walls are introduced along one direction in the place of periodic boundaries.

As it might not be clear which anchoring condition applies in active fluids, we also considered the cases of $w = 0$ and of a zero scalar order parameter at the colloidal surface (this is relevant for probes whose size is close to that of active particles). In these cases we found a milder dependence on the size of the probe, and again values of η_{eff} larger than the ones found in passive nematics in the contractile case (and smaller for extensile fluids).

We explained these results with an argument that takes into account the type of deformation produced at the colloidal surface by the anchoring condition, and the flow generated by the associated active stress. Based on this argument, in Chapter 5 we used dimensional analysis to predict a correction to the effective viscosity of active nematics, taking into account the contribution of active stresses.

We showed that such correction is in good agreement with our results, especially in the case of $\zeta < 0$. Strikingly, in this case we found another important result: we predicted the existence of a regime, at large $|\zeta|R^2/K$, characterised by a steady state of *negative drag* and also by bistability in a region of small external forces. This is a counterintuitive effect of the out-of-equilibrium character of active liquid crystals, and it is not there in their passive analogues.

Experimental benchmarking of these results is desirable. According to our description and understanding of the system, the dependence of η_{eff} on R is subject to the existence of nematic order, while the regime of negative drag also requires that a contractile fluid is considered and that planar anchoring is imposed at the colloidal surface. These conditions might be satisfied in a solution of actin filaments, in the presence of myosin motors, but controlling such systems as accurately as required by our predictions is still challenging. At the moment the best candidate for experiments is a system of microtubules and kinesin, which has recently been described in [24], as we mentioned several times when discussing our findings. Such system is however extensile, and therefore not suitable for testing the regime of negative drag, which only applies to contractile nematics. Being able to introduce colloids in the ordered phase for such system, would anyway allow to perform microrheology experiments whose results could be directly compared to ours.

In Chapters 6 and 7 we considered a quasi-two dimensional system of colloids in active nematics. We systematically changed the activity coefficient ζ, both in the contractile and in the extensile regions, and applied different anchoring conditions ($w = 0$, (strong) planar and normal anchorings), keeping the colloidal volume fraction fixed and equal to 15%.

Different initial conditions for the liquid crystal were chosen in Chapters 6 and 7; in the former the (active) liquid crystal was in the nematic phase from the onset, and the transition to spontaneous flow was triggered by a small tilt of $\pm 10^\circ$ with respect to the x-axis, introduced along the xy-plane. In Chapter 7 a quench was performed. In both cases we characterised the spontaneous flow with and without colloids for $w = 0$. In Chapter 6 we also analysed in detail the impact of the anchoring condition. Our main aim was to study the collective properties of colloids and how the latter are affected by spontaneous flow. The main findings of Chapter 6 can be summarised as follows: (i) the onset of spontaneous flow

at $w = 0$ renders the distribution of colloids inhomogeneous; (ii) when $w > 0$ spontaneous flow opposes the formation of clusters that would otherwise take place in the passive system thanks to the defect-mediated effective attraction between colloids.

Concerning point (i), at $w = 0$, rather than forming stable clusters, colloids gather dynamically, as they are pushed together and driven apart by the flow. We quantified this aggregation phenomenon through number fluctuations, which we found to be increasing for increasing $|\zeta|$, in strong correlation with the onset of spontaneous flow. At $w > 0$ and small $|\zeta|$ the flow stems mainly from the defects close to the colloidal surface, and does not have a large impact on the colloidal structure. For larger $|\zeta|$ the flow becomes global and it tends to loosen the bonds between colloids, promoting their more homogeneous distribution over the simulation box.

The case of a quench was studied in Chapter 7. We found that the initial condition has a significant impact on the onset and on the character of spontaneous flow. The quick transition from the isotropic to the nematic phase is responsible for the formation of defects, that in the case of a passive liquid crystal slowly disappear during the relaxation process. When $|\zeta| > 0$ defects are associated with a local flow, additional to the passive backflow. Defects then act as seeds for the onset of spontaneous flow, whose character, at large enough $|\zeta|$ ($|\zeta| \gtrsim 0.003$) is largely independent of the presence of colloids, and on the anchoring condition at their surface. Therefore the initial condition does not have a large impact on the collective properties of colloids. The results presented in Chapters 6 and 7 scan a wide range of parameters, which should ease the comparison with future experiments. Once more, the best candidate to achieve this is the system described in [24].

Main limitations to our simulations are that noise is not included, and the use of a soft repulsive potential between colloids, that might play a role at large times and short range, in the clustered phase. This regime is also the most affected by the presence of spurious velocities, which originate close to the colloidal surface, and which are intrinsic to lattice Boltzmann simulations for liquid crystals whenever colloids are introduced [67, 68]. However, the regime we aimed at describing, and where our results are most interesting, is the one characterised by the onset of a global flow. In this regime the velocity of the fluid

is such that advection renders all these drawbacks negligible, as we discussed extensively at the end of Chapters 6 and 7. We expect therefore that the findings summarised at point (i) and (ii) are valid despite the limitations of our study.

We note here that in the case of colloidal suspensions in passive nematics, the most interesting properties of the material as a whole were found at volume fractions $\gtrsim 20\%$. We therefore suggest that a further step towards the design of new, composite active materials should explore a range of volume fractions larger than the one we considered, and we hope that our study will open the way to further investigations, both with simulations and experiments.

Appendix A

Hasimoto Corrections To The Effective Viscosity

As we have explaind extensively in Chapter 4, our results on the microrheology of active (and passive) nematics were corrected according to [82] in order to take into account the hydrodynamic interactions of the probe particle with its own copies in neighbouring cells of the periodic simulation box, mediated by the simple fluid. We report here shortly how the corrections presented in [82] were applied to our case. We refer here to [63], where the original calculation was reviewed in the context of numerical simulations of colloids with periodic boundary conditions.

A sphere of radius R, dragged through a simple fluid with viscosity η by a constant force F, so that its limit velocity is v, obeys Stokes' law (Eq.1.10). When such particle interacts with its periodic copies, the drag coefficient $\xi = F/v$ is such that the ratio between Stokes' drag ($6\pi\eta R$) and ξ is:

$$\frac{6\pi\eta R}{\xi} = \left(1 - 2.837\frac{R}{L} + 4.19\left(\frac{R}{L}\right)^3 - 27.4\left(\frac{R}{L}\right)^6\right). \tag{A.1}$$

This result can be interpreted by saying that the particle obeys Stokes' law, where η is substituted by η^*, corrected according to Eq. A.1:

$$\eta^* = \frac{\xi}{6\pi R}\left(1 - 2.837\frac{R}{L} + 4.19\left(\frac{R}{L}\right)^3 - 27.4\left(\frac{R}{L}\right)^6\right). \tag{A.2}$$

In Chapters 4 and 5 we applied Eq. A.2 to calculate η_{eff} from the values of the equilibrium velocity v of the probe particle and of the applied force F.

Appendix B

Macrorheology in Active Fluids: Analytical Predictions in One Dimension

In Chapter 4 we have compared our numerical results with analytical predictions obtained from the linearisation of Eqs.2.11 and 2.7. The whole calculation was performed by Dr. A. Morozov. Here we present the linearised equations and their solution.

Assuming that the flow is in the y-direction, the linearised form of Eqs. 2.11 and 2.7 is:

$$\Gamma K \delta Q''_{yz}(z) + \frac{\alpha}{2} u'_y(z) = 0, \tag{B.1}$$

$$\eta u''_y(z) - \zeta \delta Q'_{yz}(z) - K s \delta Q'''_{yz}(z) = 0, \tag{B.2}$$

where $\delta Q_{yz}(z)$ and $u_y(z)$ are the deviations of the order-parameter tensor and the velocity from their rest values due to the applied shear; prime denotes the derivative with respect to z. Here,

$$\alpha = \xi - 1 \qquad s = \frac{2\xi + S(\xi - 3)}{3}, \tag{B.3}$$

for the planar anchoring, and

$$\alpha = \xi + 1 \qquad s = \frac{2\xi + S(\xi + 3)}{3}, \tag{B.4}$$

for the normal anchoring. The linear reponse of the system to the applied shear, satisfying the boundary conditions $u_y(0) = -v_0$, $u_y(L) = v_0$, and $\delta Q_{yz}(0) = \delta Q_{yz}(L) = 0$, is given by

$$u_y(z) = v_0 \frac{\sinh \lambda z}{\sinh \frac{\lambda L}{2}}, \tag{B.5}$$

$$\delta Q_{yz}(z) = \frac{\alpha\, v_0}{2\Gamma K \lambda \tanh \frac{\lambda L}{2}} \left(1 - \frac{\cosh \lambda z}{\cosh \frac{\lambda L}{2}}\right), \tag{B.6}$$

where

$$\lambda = \sqrt{\frac{\zeta s}{2\eta\Gamma K + K s^2}}. \tag{B.7}$$

Note that here ζ appears with its sign under squared root: for extensile nematics λ is a real quantity, while it becomes complex when $\zeta < 0$. The apparent viscosity is calculated by dividing the total shear stress by the shear rate $2v_0/L$ which yields

$$\eta_{\text{eff}} = \frac{L\lambda}{2 \tanh \frac{\lambda L}{2}} \left[\eta + \frac{s^2}{2\Gamma}\right]. \tag{B.8}$$

Appendix C

How Colloids Affect Spontaneous Flow: The Case of Planar Anchoring

We present here the detailed analysis of the characteristics of the flow and director profiles that characterise the onset of spontaneous flow when planar anchoring is imposed at the colloid surface. At low and positive ζ, the flow is at first very localised and we do not see the onset of one-dimensional and two-dimensional flows as in the case of $w = 0$. This is shown in Fig. C.1 where key cases are presented, corresponding to $\zeta = 0.001$, 0.002 and 0.005. For $\zeta \lesssim 0.001$ the flow is localised and not directed along one precise direction. Also, its is not strong enough to deform the director profile significantly: from the snapshots presented in Fig. C.1 for the director profile, it is clear that at $\zeta = 0.001$ the bulk director is aligned along the x axis, as from the initial conditions. Deformations are only due to the presence of colloids and to the anchoring condition. Once again the critical ζ for the onset of a global flow in extensile nematics is between 0.001 and 0.002. At $\zeta = 0.002$ a global flow develops in three dimensions, with a chaotic character able to disrupt the nematic order. Differently from the case of $w = 0$ and of a bare fluid, the onset of spontaneous flow is abrupt and does not pass through a flow restricted to only one or two dimensions. The case of a contractile fluid is similar and shown in Fig. C.2: a two-dimensional chaotic flow, able to disrupt nematic order and similar to the one observed in the absence of colloids at very large $|\zeta|$ develops for $|\zeta| \gtrsim 0.015$, which is remarkably larger than the critical

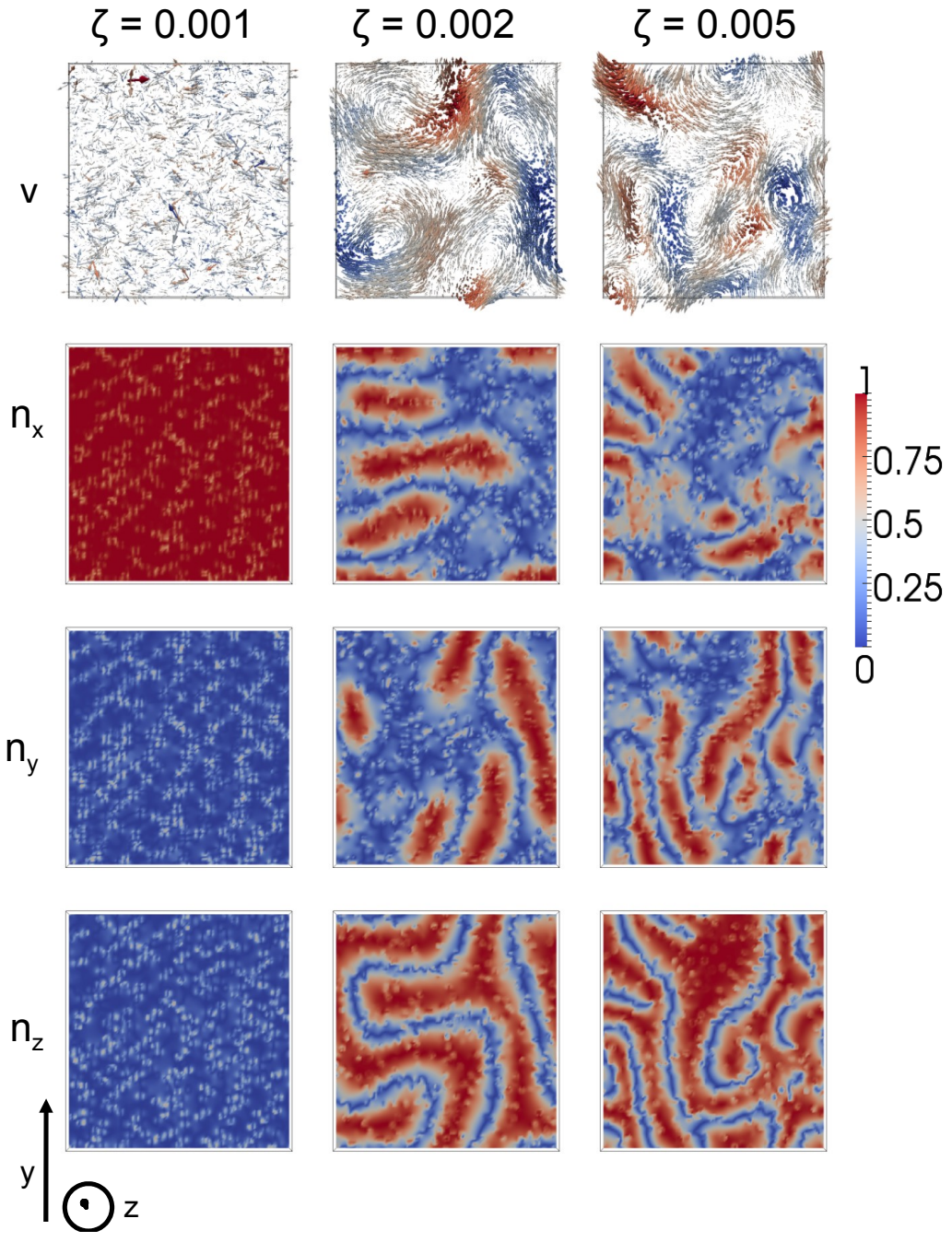

Figure C.1: Velocity and director profiles developing in extensile nematics, with a 15% colloidal volume fraction, in a regime of spontaneous flow, for ζ between 0.001 and 0.005. The anchoring is planar. The color coding for both the velocity and the director is as in Fig. 6.2. These snapshots refer to time $t = 160000$.

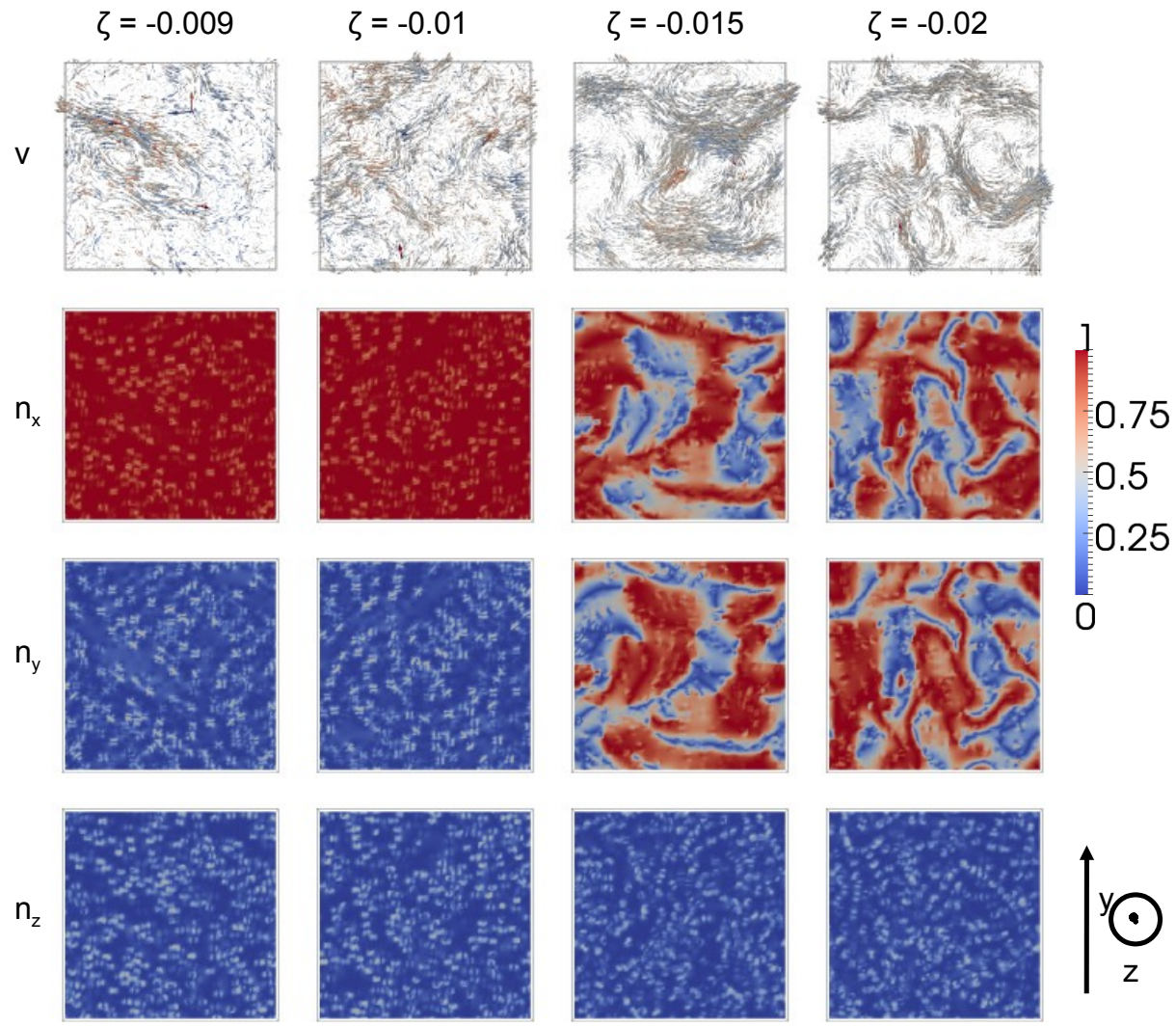

Figure C.2: Velocity and director profiles developing in contractile nematics, with a 15% colloidal volume fraction, in a regime of spontaneous flow, for ζ between -0.009 and -0.015. The anchoring is planar. The color coding for both the velocity and the director is as in Fig. 6.2. These snapshots refer to time $t = 160000$.

ζ at $w = 0$, in contrast with respect to what we saw for normal anchoring. It is worth noting that a coherent flow is visible also for $\zeta > -0.015$, but it is not large enough to affect nematic order.

Bibliography

[1] J. S. Lintuvuori, D. Marenduzzo, K. Stratford, and M. E. Cates. *J. Mater. Chem.*, 20 (2010), 10547.

[2] M. Miesowicz. *Nature*, 158 (1946), 261.

[3] M. Cates, S. Fielding, D. Marenduzzo, E. Orlandini, and J. Yeomans. *Phys. Rev. Lett.*, 101 (2008), 068102.

[4] G. Foffano, J. S. Lintuvuori, A. N. Morozov, K. Stratford, M. E. Cates, and D. Marenduzzo. *Europhys. J. E*, 35 (2012), 98.

[5] L. Onsager. *Ann.N.Y.Acad.Sci.*, 51 (1949), 627.

[6] P. de Gennes and J. Prost. *The Physics of Liquid Crystals.* Oxford University Press (1995).

[7] L. D. Landau and E. M. Lifshitz. *Theory of Elasticity.* Butterworth-Heinemann, Oxford, UK (1986).

[8] M. Kléman. *Rep. Prog. Phys.*, 52 (1989), 555.

[9] D. C. Wright and N. D. Mermin. *Rev. Mod. Phys.*, 61 (1989), 385.

[10] F. Chandrasekhar. *Liquid Crystals.* Second Edition, Cambridge University Press (1992).

[11] M. Mermin. *Rev. Mod. Phys.*, 51 (1979), 591.

[12] T. C. Lubensky, D. Pettey, N. Currier, and H. Stark. *Phys. Rev. E*, 57 (1998), 610.

[13] H. Stark. *Phys. Rep.*, 351 (2001), 387.

[14] S. Ramaswamy. *Annu. Rev. Condens. Matter Phys.*, 1 (2010), 323.

[15] V. Narayan, S. Ramaswamy, and N. Menon. *Science*, 317 (2007), 105.

[16] J. Palacci, B. Abécassis, C. Cottin-Bizonne, C. Ybert, and L. Bocquet. *Phys. Rev. Lett.*, 104 (2010), 138302.

[17] I. Buttinoni, G. Volpe, F. Kümmerl, G. Volpe, and C. Bechinger. *J. Phys. Condens. Matt.*, 24 (2012).

[18] J. Toner and Y. Tu. *Phys. Rev. Lett.*, 75 (1995), 4326.

[19] H. Gruler, U. Dewald, and M. Eberhardt. *Europhys. J. B*, 11 (1999), 187.

[20] M. Cates, O. Henrich, D. Marenduzzo, and K. Stratford. *Soft Matter*, 5 (2009), 3791.

[21] Y. Hatwalne, S. Ramaswamy, M. Rao, and R. Simha. *Phys. Rev. Lett.*, 92 (2004), 118101.

[22] N. D. Mermin and H. Wagner. *Phys. Rev. Lett.*, 17 (1966), 1133.

[23] T. Vicsek, A. Cziròk, E. Ben-Jacob, I. Cohen, and Shochet. *Phys. Rev. Lett.*, 75 (1995), 4326.

[24] T. Sanchez, D. T. N. Chen, S. J. De Champ, M. Heymann, and Z. Dogic. *Nature*, 491 (2012), 431.

[25] M. C. Marchetti, J. F. Joanny, S. Ramaswamy, T. B. Liverpool, J. Prost, M. Rao, and R. Aditi. *Rev. Mod. Phys.*, 85 (2013), 1143.

[26] J. Toner and Y. Tu. *Phys. Rev. Lett.*, 80 (1998), 4819.

[27] J. Toner and Y. Tu. *Phys. Rev. E*, 58 (1998), 4828.

[28] N. Shimoyama, K. Sugawara, T. Mizuguchi, Y. Hayakawa, and M. Sano. *Phys. Rev. Lett.*, 76 (1996), 3870.

[29] E. M. Purcell. *Am. J. of Phys.*, 45 (1977), 3.

[30] J. R. Blake. *J. of Theor. Biol.*, 64 (1977), 697.

[31] K. Drescher, J. Dunkel, L. H. Cisneros, S. Ganguly, and R. E. Goldstein. *Proc. Natl. Acad. Sci. USA*, 108 (2011), 10940.

[32] J. S. Hyams and G. G. Borisy. *J. Cell Sci.*, 33 (1978), 235.

[33] M. Polin, I. Tuval, K. Drescher, J. P. Gollub, and R. E. Goldstein. *Science*, 325 (2009), 487.

[34] M. Lenz, T. Thorensen, M. L. Gardel, and A. R. Dinner. *Phys. Rev. Lett.*, 108 (2012), 238107.

[35] S. Ramaswamy and M. Rao. *New Jour. of Phys.*, 9 (2007), 423.

[36] R. Voituriez, J. F. Joanny, and J. Prost. *Europhys. Lett.*, 70 (2005), 404.

[37] C. Dombrowski, L. Cisneros, S. Chatkaew, R. E. Goldstein, and J. O. Kessler. *Phys. Rev. Lett.*, 93 (2004), 098103.

[38] D. Marenduzzo, E. Orlandini, M. Cates, and J. Yeomans. *Phys. Rev. E*, 76 (2007), 031921.

[39] I. Tuval, L. Cisneros, C. W. Dombrowski, C. W. Wolgemuth, J. O. Kessler, and R. E. Goldstein. *Proc. Natl. Acad. Sci. USA*, 102 (2004), 2277.

[40] S. M. Fielding, D. Marenduzzo, and M. E. Cates. *Phys. Rev. E*, 83 (2010), 041910.

[41] P.-G. de Gennes. Soft matter (nobel lecture). *Angew. Chem. Int. Ed. Engl.*, 31 (1992), 842845.

[42] G. M. Whitesides and M. Boncheva. *Proc. Natl. Acad. Sci. USA*, 99 (2002), 4769.

[43] Y. Gi-Ra, D. J. Pine, and S. Sacanna. *J. Phys.: Condens. Matter*, 25 (2013), 193101.

[44] S. Sacanna, M. Korpics, K. Rodriguez, Colón-Meleéndez, S.-H. Kim, D. J. Pine, and Y. Gi-Ra. *Nature Comms*, 4 (2013), 1688.

[45] C. Bae, J. Moon, H. Shin, and M. M. Sung. *J. Am. Chem. Soc.*, 129 (2007), 14232.

[46] S. Sacanna, L. Rossi, and D. J. Pine. *J. Am. Chem. Soc.*, 134 (2012), 6112.

[47] J. Palacci, S. Sacanna, A. P. Steinberg, D. J. Pine, and P. M. Chaikin. *Science*, 339 (2013), 936.

[48] P. F. Damasceno, M. Engel, and S. C. Glotzer. *Science*, 337 (2012), 453.

[49] S. Sacanna, T. M. Irvine, P. Chaikin, and D. J. Pine. *Nature*, 464 (2010), 575.

[50] P. Poulin, H. Stark, T. C. Lubensky, and D. A. Weitz. *Science*, 275 (1997), 1770.

[51] T. Wood, J. S. Lintuvuori, A. B. Schofield, D. Marenduzzo, and W. C. K. Poon. *Science*, 334 (2011), 79.

[52] M. Ravnik and S. Zumer. *Soft Matter*, 5 (2009), 269.

[53] A. Beris and B. Edwards. *Thermodynamics of Flowing Systems*. Oxford: Oxford University Press (1994).

[54] F. Frank. *Discuss. Faraday Soc.*, 25 (1958), 19.

[55] P. M. Chaikin and T. C. Lubensky. *Principles of Condensed Matter Physics*. Cambridge University Press (1995).

[56] C. Denniston, E. Orlandini, and J. M. Yeomans. *Europhys. Lett.*, 52 (2000), 481.

[57] R. Simha and S. Ramaswamy. *Phys. Rev. Lett.*, 89 (2002), 058101.

[58] T. B. Liverpool and M. C. Marchetti. *Phys. Rev. Lett.*, 90 (2003), 138102.

[59] S. Chen and G. Doolen. *Annu. Rev. Fluid Mech*, 30 (1998), 329.

[60] P. Bhatnagar, E. Gross, and M. Krook. *Phys. Rev. Lett.*, 94 (1954), 511.

[61] N.-Q. Nguyen and A. J. C. Ladd. *Phys. Rev. E*, 66 (2002), 046708.

[62] A. J. C. Ladd. *J. Fluid. Mech.*, 271 (1994), 285.

[63] A. J. C. Ladd. *J. Fluid. Mech.*, 271 (1994), 211.

[64] C. Denniston, D. Marenduzzo, E. Orlandini, and J. M. Yeomans. *Philosophical Transactions: Mathematical, Physical and Engineering Sciences*, 362 (2004), 1745.

[65] R. Courant, E. Isaacson, and M. Rees. *Comm. Pure Appl. Math.*, 5 (1952), 243255.

[66] J.-B. Fournier and P. Galatola. *Europhys. Lett.*, 72 (2005), 403.

[67] A. J. Wagner. *Int. J. Mod. Phys. B*, 17 (2003), 193.

[68] O. Henrich, D. Marenduzzo, K. Stratford, and M. E. Cates. *Computers and Mathematics with Applications*, 59 (2010), 2360.

[69] J. Loudet, P. Hanusse, and P. Poulin. *Science*, 306 (2004), 1525.

[70] H. Stark and D. Ventzki. *Europhys. Lett.*, 57 (2002), 60.

[71] H. Stark and D. Ventzki. *Phys. Rev. E*, 64 (2001), 031711.

[72] M. Skarabot and I. Musevic. *Soft Matter*, 6 (2010), 5476.

[73] F. Mondiot, J. Loudet, O. Mondait-Monval, and P. Snabre. *Phys. Rev. E*, 86 (2012), 010401(R).

[74] J. S. Lintuvuori, K. Stratford, M. E. Cates, and D. Marenduzzo. *Phys. Rev. Lett.*, 105 (2010), 178302.

[75] T. B. Liverpool and M. C. Marchetti. *Phys. Rev. Lett.*, 97 (2006), 268101.

[76] S. Rafai, L. Jibuti, and P. Peyla. *Phys. Rev. Lett.*, 104 (2010), 098102.

[77] A. Sokolov and I. S. Aranson. *Phys. Rev. Lett.*, 103 (2009), 14810.

[78] G. Foffano, J. S. Lintuvuori, K. Stratford, M. E. Cates, and D. Marenduzzo. *Phys. Rev. Lett.*, 109 (2012), 028103.

[79] D. Mizuno, C. Tardin, C. Schmidt, and F. C. MacKintosh. *Science*, 315 (2007), 370.

[80] A. Lau, B. D. Hoffman, A. Davies, J. C. Crocker, and T. C. Lubensky. *Phys. Rev. Lett.*, 91 (2003), 198101.

[81] D. T. N. Chen, A. W. C. Lau, L. A. Hough, M. F. Islam, M. Goulian, and T. C. Lubensky. *Phys. Rev. Lett.*, 99 (2007), 148302.

[82] H. Hasimoto. *J. Fluid. Mech.*, 5 (1959), 317.

[83] B. Rubinstein, M. F. Fournier, K. J. Jacobson, A. B. Verkhovsky, and A. Mogilner. *Biophys. J.*, 97 (2009), 1853.

[84] E. Tjhung, M. E. Cates, and D. Marenduzzo. *Soft Matter*, 7 (2011), 7453.

[85] T. A. Waigh. *Rep. Prog. Phys*, 68 (2005), 685.

[86] M. S. Silva and *et al. Proc. Natl. Acad. Sci. USA*, 108 (2011), 9408.

[87] J. Howard. *Annu. Rev. Biophys.*, 38 (2009), 217.

[88] R. Bernal, P. A. Pullarkat, and F. Melo. *Phys. Rev. Lett.*, 99 (2007), 018301.

[89] K.-H. Lin, J. C. Crocker, V. Prasad, A. Schofield, D. A. Weitz, T. C. Lubensky, and A. G. Yodh. *Phys. Rev. Lett.*, 85 (2000), 1170.

[90] F. Romano and F. Sciortino. *Nature Materials*, 10 (2011), 171.

[91] P. Poulin. *Current Opinion in Colloid & Interface Science*, 4 (1999), 66.

[92] J. Tailleur and M. E. Cates. *Phys. Rev. Lett.*, 100 (2008), 218103.

[93] M. E. Cates, D. Marenduzzo, I. Pagonabarraga, and J. Tailleur. *Proc. Natl. Acad. Sci. USA*, 107 (2010), 11715.

[94] Y. Fily and M. C. Marchetti. *Phys. Rev. Lett.*, 108 (2012), 235702.

[95] G. S. Redner, M. F. Hagan, and A. Baskaran. *Phys. Rev. Lett.*, 110 (2013), 055701.

[96] L. Berthier and J. Kurchan. *Nature Physics*, 9 (2013), 310.

[97] J. Bialké, T. Speck, and H. Löwen. *Phys. Rev. Lett.*, 108 (2012), 168301.

[98] I. Buttinoni, J. Bialké, F. Kummel, H. Löwen, C. Bechinger, and T. Speck. *Phys. Rev. Lett.*, 110 (2013), 238301.

[99] X.-L. Wu and A. Libchaber. *Phys. Rev. Lett.*, 84 (2000), 3017.

[100] L. Angelani, C. Maggi, M. L. Bernardini, A. Rizzo, and R. Di Leonardo. *Phys. Rev. Lett.*, 107 (2011), 138302.

[101] J. S. Lintuvuori, K. Stratford, M. E. Cates, and D. Marenduzzo. *Phys. Rev. Lett.*, 107 (2011), 267802.

[102] J. S. Lintuvuori, A. C. Pawsey, K. Stratford, M. E. Cates, P. S. Clegg, and D. Marenduzzo. *Phys. Rev. Lett.*, 110 (2013), 187801.

[103] S. Zumer, M. Ravnik, T. Porenta, G. Alexander, and J. M. Yeomans. Blue phases as templates for 3d colloidal photonic crystals. *SPIE*, (2010).

[104] O. Lavrentovich. *Proc. Natl. Acad. Sci. USA*, 108 (2011), 5143.

[105] P. Poulin, V. Cabuil, and D. Weitz. *Phys. Rev. Lett.*, 79 (1997), 4862.

[106] M. Yada, J. Yamamoto, and H. Yokoyama. *Phys. Rev. Lett.*, 92 (2004), 185501.

[107] C. M. Noël, G. Bossis, A.-M. Chaze, F. Giulieri, and S. Lacis. *Phys. Rev. Lett.*, 96 (2006), 217801.

[108] K. Takahashi, M. Ichikawa, and Y. Kimura. *J. Phys.: Condens. Matter*, 20 (2008), 075106.

[109] S. P. Meeker, W. C. K. Poon, J. Crain, and E. M. Terentjev. *Phys. Rev. E*, 61 (2000), R6083.

[110] H. Stark. *Europhys. J. B*, 10 (1999), 311.

[111] J. Fukuda, M. Yoneya, and H. Yokoyama. *Eur. Phys. J. E*, 13 (2004), 87.

[112] O. Guzman, E. B. Kim, S. Grollau, N. L. Abbott, and J. J. de Pablo. *Phys. Rev. Lett.*, 91 (2003), 235507.

[113] M. Ravnik, M. Skarabot, S. Zumer, U. Tkalec, I. Poberaj, D. Babic, N. Osterman, and I. Musevic. *Phys. Rev. Lett.*, 99 (2007), 247801.

[114] I. Musevic and M. Skarabot. *Soft Matter*, 4 (2008), 195.

[115] T. Araki and H. Tanaka. *Phys. Rev. Lett.*, 97 (2006), 127801.

[116] M. R. Mozaffari, M. Babadi, J.-i. Fukuda, and E. M. R. *Soft Matter*, 7 (2011), 1107.

[117] M. Tasinkevych, N. M. Silvestre, and M. M. Telo da Gama. *New J. Phys*, 14 (2012), 073030.

[118] I. I. Smalyukh, O. D. Lavrentovich, A. N. Kuzmin, A. V. Kachynski, and P. N. Prasad. *Phys. Rev. Lett.*, 95 (2005), 15701.

[119] E. Kim, K. Stratford, R. Adhikari, and M. E. Cates. *Langmuir*, 24 (2008), 6549.

[120] M. Ravnik and J. M. Yeomans. *Phys. Rev. Lett.*, 110 (2013), 026001.

[121] L. Giomi, M. J. Bowick, X. Ma, and M. C. Marchetti. *Phys. Rev. Lett.*, 110 (2013), 228101.

[122] D. Marenduzzo and E. Orlandini. *Soft Matter*, 6 (2010), 774.

Publications

G. Foffano, J. S. Lintuvuori, K. Stratford, M. E. Cates, and D. Marenduzzo. Colloids in active fluids: anomalous microrheology and negative drag. In *Phys. Rev. Lett.*, 2012.

G. Foffano, J. S. Lintuvuori, A. N. Morozov, K. Stratford, M. E. Cates, and D. Marenduzzo. Bulk Rheology and Microrheology of Active Fluids. In *Europhys. J. E*, 2012.

G. Foffano, J. S. Lintuvuori, K. Stratford, M. E. Cates, and D. Marenduzzo. Collective properties of colloids in active fluids (*In preparation*).